

**RESEARCH  
IN  
APPLIED GEOPHYSICS**

**No. 42**

**1988**

**The Effects  
of Inhomogeneities on  
Magntotellurics**

**Ross W. Groom**

**GEOPHYSICS LABORATORY  
DEPARTMENT OF PHYSICS  
UNIVERSITY OF TORONTO**

THE EFFECTS OF INHOMOGENEITIES  
ON MAGNETOTELLURICS

*by*

Ross W. Groom

*Department of Physics  
University of Toronto*

A Thesis submitted in conformity with  
the requirements of the degree of  
Doctor of Philosophy at the  
University of Toronto

©1988 by Ross W. Groom

## ABSTRACT

The magnetotelluric (MT) method is a low-frequency, electromagnetic (EM), geophysical method which is widely used for investigating the conductivity structure of the Earth's crust and upper mantle. Although MT often seeks to determine the gross conductivity structure and the variation of conductivity with depth, it suffers from the ubiquitous presence of EM scatterers of all scales. The thesis advances the understanding of the effects of multiple and small-scale inhomogeneities on the MT impedance tensor.

One of the most pressing difficulties at present in MT are distortions of the EM fields by small-scale, 3-D inhomogeneities which are often found near the surface of the Earth. The thesis investigates the effects of these inhomogeneities on the observed impedance tensor. These studies show that for a great many cases the impedance tensor conforms to a particular factorization, each part of which is related either to the local inhomogeneities or to the large scale structure. Each factor is associated with a different physical effect. This factorization is used to explain the necessary requirements for a useful parametrization of the data contained within the impedance tensor. The development of such a complete, useful decomposition is begun with a method for dealing with the most significant effect of small-scale surface bodies; namely galvanic or frequency-independent distortion of the horizontal electric fields.

In addition, analytic and statistical solutions are provided to a number of relevant low-frequency EM scattering problems which model the response of inhomogeneities. An analytic solution for two semi-infinite slabs over a basement is developed in the thesis. This extends existing solutions to this problem so as to include all frequencies and arbitrary basement conductivities. For the particular case of an insulating or perfectly-conducting basement, the above method is extended to provide the EM response for a model of a quasi-anisotropic layer. This model was used to study the benefits of extensive spatial sampling of the electric field in complex media and the presence of fictitious conducting layers when data due to large lateral inhomogeneities are interpreted one-dimensionally. The study showed, for this particular model, that the use of large electrode spacing could be beneficial if used with care. The anisotropy model was also employed to investigate the question of what bulk properties the MT method samples. A statistical technique is used for investigating the response of very fine-bedding in MT demonstrating that such structures can have a relatively significant effect of up to ten degrees on the impedance phase. These results are corroborated by a deterministic model.

## ACKNOWLEDGEMENTS

I would like to express my gratitude to the following people for their contributions to this thesis.

To the members of my supervising committee: Richard Bailey, whose ideas, insights and suggestions have not only helped to make this work stimulating for me but they have also made a large contribution towards its success. To Dick Peltier, for scrutinizing the manuscript and for the suggestions he made early in the work which contributed to the direction of the research. To Nigel Edwards, for stimulating discussions which helped to develop my physical intuition towards the electromagnetic scattering problem.

To the other examiners: Gordon West for scrutinizing the manuscript, for many helpful suggestions and discussions and for the significant contribution he has made towards my understanding of electromagnetics. To John Weaver for his very thorough reading and examination of the thesis and to R. A. Ross, not only for his willingness to be part of the examining committee but also for the contributions he has made to my mathematical education.

I would also like to thank Peter Walker who was a constant source of help and ideas especially at the difficult stages in the development of the theory. I am especially indebted to Richard Smith who was always available to listen and help with any oral presentations. I am thankful to Gerry Mitrovica, Richard Smith, Marianne Mareschal, and Donna-Maria DeCaires who read the manuscript, Tony Cavaliere would provided the experimental data and to Ron Kurtz and Alan Jones for their suggestions and encouragement in the development of the decomposition. Some of the figures were hand drafted by Khader Khan and Raul Cunha. Computer plotting was accomplished with TPLOT, written by Dave Boerner.

The friendship and comradeship I have found within the Geophysics group at the University of Toronto has meant a great deal to me. The support and encouragement which I have been given here is in no small way a part of the reason why I was able to complete this work.

I am deeply grateful to my son, Rubin, for his constant support and love throughout this endeavor, to Maria for her patience and help through the difficult time of preparing the manuscript and, of course, to my parents Harrold and Isabel Groom for their constant encouragement and confidence in me.

# CONTENTS

Abstract . . . . .	i
Acknowledgements . . . . .	ii
Table of Contents . . . . .	iii
<b>Chapter 1 Introduction . . . . .</b>	<b>1</b>
<b>Chapter 2 The Effects of Stochastic Fine Bedding in 1-D Structures . . . . .</b>	<b>18</b>
§ 2.1 Introduction . . . . .	18
§ 2.2 A Statistical Approach for Induction in a Medium with Fine Vertical Structure . . . . .	20
§§ 2.2.1 Introduction . . . . .	20
§§ 2.2.2 Stochastic Variables . . . . .	21
§§ 2.2.3 Stochastic Differential Equations . . . . .	21
§§ 2.2.4 Solutions to Stochastic Differential Equations . . . . .	22
§§ 2.2.5 Application to One-Dimensional Induction . . . . .	26
§§ 2.2.6 Estimation of Solutions . . . . .	28
§§ 2.2.7 Examples and Conclusions . . . . .	31
§ 2.3 A Deterministic Approach . . . . .	35
§ 2.4 Summary . . . . .	41
<b>Chapter 3 H-Polarization Induction in Two Semi-Infinite Slabs . . . . .</b>	<b>43</b>
§ 3.1 Introduction . . . . .	43
§ 3.2 The Boundary Value Problem . . . . .	44
§ 3.3 Separability and Eigenfunctions . . . . .	48
§ 3.4 The Solution . . . . .	56
§ 3.5 The Layered Solution . . . . .	59
§ 3.6 The Uniqueness of the Solution . . . . .	60
§ 3.7 The Fourier Coefficients and Convergence . . . . .	63
§ 3.8 Comparisons to Other Solutions . . . . .	67
§ 3.9 Summary . . . . .	77
<b>Chapter 4 A Study of the Effects of Multiple Horizontal Inhomogeneities . . . . .</b>	<b>80</b>
§ 4.1 Introduction . . . . .	80
§ 4.2 The Effects of a Finite Number of Vertical Dikes . . . . .	82
§ 4.3 The Effects of an Infinite Periodic Array . . . . .	87
§ 4.4 Investigation of the Bulk Properties of the Model . . . . .	88
§ 4.5 The Frequency Response of the Model . . . . .	90
§ 4.6 Experimental Evaluation of the Bulk Parameters . . . . .	95
§ 4.7 Summary . . . . .	99

Chapter 5	<b>The Effects of Small-Scale Surface Inhomogeneities</b>	101
§ 5.1	Introduction	101
§§ 5.1.2	The Galvanic Distortion Operator	103
§ 5.2	Distortions Due to a Hemisphere	106
§§ 5.2.1	Electrostatic Distortion Due to a Hemisphere	107
§§ 5.2.2	The Channelling Tensor, $C$	112
§§ 5.2.3	Effects on Magnetotelluric Interpretation	116
§§ 5.2.4	Effects in a One-Dimensional Environments	128
§ 5.3	Summary of the Effects of Small-Scale Surface Inhomogeneities	130
Chapter 6	<b>A Decomposition of the Magnetotelluric Tensor Which is Useful in the Presence of Current Distortion</b>	133
§ 6.1	Introduction	133
§ 6.2	The Ideal Distortion Model of the Impedance Tensor	136
§ 6.3	A Useful Factorization of the Distortion Operator	141
§ 6.4	Uniqueness and Existence of the Factorization	146
§ 6.5	The Decomposition of the Impedance Tensor	152
§ 6.6	A Comparison of Interpretation Methods	158
§ 6.7	Indicators of Three-Dimensional Induction, Parameter Error Estimation, Methodology	165
§ 6.8	An Example with Experimental Data	168
§§ 6.8.1	Constrained Decompositions	174
§ 6.9	Interpretation and Modelling	183
§ 6.10	Summary	184
Chapter 7	<b>Conclusions</b>	185
References		189
Appendix 1	<b>A Propagation Matrix Method for 1D Forward Modelling</b>	195
Appendix 2	<b>The Magnetic Field of a Conducting Hemisphere</b>	198
Appendix 3	<b>Other Decompositions</b>	206

## CHAPTER 1

### INTRODUCTION

#### Review

In the quest to understand the structure and evolution of the Earth, scientists for centuries have attempted to determine its physical properties. Since, all but a small fraction of the Earth is unreachable, indirect methods must often be used to measure these properties. Electrical conductivity is one such physical parameter which can be observed to great depths via measurements of electromagnetic fields on or near the surface of the Earth. The electrical conductivity of rocks and minerals has a very wide range of values. This variation is caused by a large number of physical parameters such as rock porosity, temperature, lithology, fluid and electrolyte content. The amount of variation and the causes of the variation in the electrical conductivity mean electromagnetic techniques yield valuable information but these variations can also be the source of severe difficulties. It is the purpose of this thesis to investigate some of those difficulties in the magnetotelluric method which are currently recognized as obstacles to further progress.

The magnetotelluric method (MT) is an electromagnetic (EM) geophysical technique which utilizes natural source fields generated by lightning, ionospheric and magnetospheric currents. The large horizontal spatial extent of the MT source field over a broad frequency band allows examination of the conductivity structure deep into the Earth via surface measurements of the resulting electric and magnetic fields. Determination of the deep conductivity structure of the Earth is important to understanding the evolution of the crust and the properties of the upper mantle. Other geophysical methods (*e.g.* seismology) are not as sensitive to such important characteristics of the lower crust as porosity, fluid content and salinity.

Although earlier workers (*e.g.* Tikhonov, 1950) investigated the potential of using natural electromagnetic fields, the MT method was essentially established in 1953 when Cagniard published his seminal paper. Cagniard assumed that the Earth was horizontally stratified and excited by plane, monochromatic, electromagnetic waves. He then showed that the ratio of horizontal electric and magnetic fields is a function only of the layered structure and the frequency of the source field, and is not significantly dependent on the source field strength or the angle of incidence of the source field at the Earth's surface. The theory for the MT method has progressed in generalizing the conductivity structure but the assumption of a plane wave source has generally remained. Although early in the history of the MT method there were doubts (Wait 1954, Price 1962) concerning the application of plane wave theory for the source, Madden and Nelson (1964) have shown this to be a reasonable approximation in most instances.

The actual conductivity distribution in the Earth's crust is much more complex than the one-dimensional structure that was originally investigated. Although the Earth's conductivity generally varies with depth, as the temperature and pressure increase, superimposed on this broad one-dimensional average structure are large features such as dikes, coast lines, subduction zones and fold belts. These superimposed structures are, electrically, often effectively two-dimensional over much of the utilized frequency band. That is, they are long enough in one horizontal direction to be considered infinite. As well, there are many inhomogeneities present which must be considered three-dimensional, and these can have scale-lengths from fractions of a metre up to hundreds of kilometers. It is essential to understand the effects on the EM fields of both the two and three-dimensional features even if the structures causing the effects are not of primary interest. These effects must be quantified if one hopes to determine correctly the nature of the upper-crust and thus to determine the approximately one-dimensional structure of the lower crust and upper mantle.

The magnetotelluric method suffers from a very significant impediment to

attaining the above goals. Since the source field is produced high above the Earth's surface by processes which are not fully understood, one has no means of knowing the strength and precise spatial character of the source field without obtaining more extensive simultaneous measurements than are practical. This is unlike most controlled source EM techniques where the source field is known extremely well. An additional restriction is that the plane wave character of the source provides no means, via source-field spatial characteristics, for selectively exciting parts of the Earth's conductivity structure as a means for determining horizontal variations in conductivity.

Horizontal variations in conductivity can have many different and significant effects on the MT method. Just as the measured fields in MT are affected by the conductivity over great depths, so too is the conductivity sampled over large horizontal extents by the measured fields. To investigate lateral variations in conductivity, a number of magnetotelluric measurement sites are located over a large area. Two and three dimensional numerical methods or experimental scale model studies are then generally used to simulate the response of the inhomogeneities as a function of the horizontal coordinates.

Since both the strength and polarization of the MT source field vary randomly as functions of time, it is customary to express the Earth's electromagnetic response in terms of a frequency-dependent, linear transfer function or impedance tensor. The impedance tensor expresses the linear relation between the horizontal components of the electric and magnetic fields. When the conductivity structure is two-dimensional, the impedance tensor contains two intrinsic complex impedances<sup>1</sup>. Each impedance is associated with one of the two-dimensional polarizations (E or H). For two-dimensional structures, the impedance tensor also contains the information required to obtain the horizontal rotation angle (strike) from the measurement coordinates to the natural structural coordinates. Swift (1967) has shown explicitly how to retrieve the two impedances and the strike direction when the conductivity structure is at

---

<sup>1</sup> see the Notation and Basic Theory section of this chapter for details

most two-dimensional. The assumption of a two-dimensional structure is often inadequate and so there have been a number of attempts to extend Swift's work to the more general case of an arbitrary three dimensional conductivity structure (*e.g.* Eggers (1982), LaTorraca *et al* (1986), Yee and Paulson (1984)). These have not yet met with general acceptance in the magnetotelluric community. The acquisition of a deeper understanding of this particular problem and the provision of partial solutions are two of the primary objectives of this thesis.

### The Problem

The complexity and cost of obtaining magnetotelluric measurements require that the number of measurement sites be small and this results in an inability to resolve the details of complex or small-scale inhomogeneities. The complex near-surface conductivity structure, for example, is more amenable to investigation by controlled source electrical or EM techniques which offer more precise knowledge of the source field and an ability to vary the source field characteristics. The plane wave character of the natural source field, on the other hand, makes the MT method more useful in the study of the large scale properties and the deep structure of the crust rather than the delineation of small-scale structure.

It is nevertheless necessary to understand the effects of the small-scale structure on MT measurements for two reasons. First, it is important to know how complex small-scale inhomogeneities contribute to the determination of the bulk or large-scale properties, and second it is important to understand how the proximity of small-scale structures may distort the estimates of bulk properties. Since the natural source field excites a very large area, it is extremely difficult and often intractable to investigate via numerical modelling methods the effects of inhomogeneities which are either extremely complex or have the same scale as the measurements. There has not been a great deal of investigation into these problems although some work has been done on the scattering of the

fields by small-scale surface inhomogeneities (*e.g.* Berdichevsky and Dmitriev 1976, Bahr 1985).

Usually in MT, the most significant effects from nearby inhomogeneities, are distortions of the horizontal electric fields which are controlled by the bulk material properties. These distortions, even for small structures, can be large if the conductivity contrast is great. Although these telluric effects were recognized prior to the first use of the magnetotelluric method (Migaux, 1946), the investigation of these problems is still primarily done by numerical modelling methods. Two-dimensional modelling programs, although rapidly executed, do not provide the ability to include small, three-dimensional, near-surface structures. Such features are almost ubiquitous and constitute a pressing source of difficulty in magnetotelluric interpretation. Three-dimensional modelling programs are not only slow and costly to employ but also suffer from the inability to include complex structures, especially in models containing both large and small-scale features. This inability is not only due to practical (time and cost) but also to numerical (stability) limitations.

The limitations of numerical modelling studies and the lack of available analytic solutions have led to attempts to decompose each impedance tensor into a minimum set of diagnostic parameters. The resulting parameters are then intended to be interpreted using analytic solutions and model studies to determine the conductivity structure. Interpretation of the parameters is restricted because there is not a complete understanding of the information which is contained in the impedance tensor when the conductivity structure is three-dimensional. It would seem desirable therefore to separate those parts of the data due to the large-scale structure which need to be fitted to a model, from those due to the small-scale features which are usually not of interest. Explanations as to how this information can be separated and recovered is limited.

Apart from the problem of determining what structure can be resolved, there is also the question of what bulk properties can be determined. If one

investigates conductivity in the Earth, one finds that the measured values of conductivity vary dramatically from point to point and from scale to scale. Thus, any determination of conductivity structure from electromagnetic methods determines some bulk material properties which depend on the scale of the measurements. It is not clear how this determination relates to the intrinsic physical properties. In what sense are the determined properties an average and how can the correct dimensions of the bulk structure be obtained?

The principal purpose of this thesis is to examine the effects, on the impedance tensor, of small-scale inhomogeneities which, as discussed above, are not usually amenable to modelling studies. In other words, to try to determine the extent to which modelling, both two and three dimensional, and one-dimensional inversion can be effective in light of the ubiquitous presence of small-scale inhomogeneities. In particular, via a number of different types of studies, various kinds of small scale and multiple electromagnetic scatterers will be characterized by their effects on the magnetotelluric impedance relation.

## Outline

Analytic solutions provide insight into the effects of inhomogeneities and are also useful for checking numerical methods. The H-polarization response of two semi-infinite conducting slabs, in contact, over a basement of arbitrary conductivity, is sought in Chapter 3. This problem was the subject of the first published analytic solution in MT involving lateral heterogeneity (d'Erceville and Kunetz 1962) but the original solution was restricted in its range of applicability to only two particular basement conductivities (zero and infinity). Subsequently, this problem has also been attempted for cases in which the frequency is sufficiently low that the semi-infinite slabs can be considered to behave as thin sheets (Bailey 1977, Dawson and Weaver 1979). A new broad band frequency domain solution is obtained in this thesis which is valid for arbitrary basement conductivities and which is exact on the surface of the model that represents the Earth's surface but approximate elsewhere. This new solution is

compared to the previous analytic solutions that are restricted to special cases, and to solutions obtained using two different numerical modelling techniques.

Conductivities in the Earth often vary by orders of magnitude laterally as well as vertically. The electromagnetic response to these variations generally involves an interaction between inductive and charge effects, with the most dramatic variations occurring in the electric field. The two-dimensional H-Polarization mode is a relatively simple, but still useful, model as it maintains the two physical effects, their interaction and the dramatic influence which they exact on the electric field. Chapter 4 extends an available analytic solution (Rankin 1962) for a vertical inhomogeneity over a basement of infinite or zero conductivity to include multiple structures. The extended solution can include either a finite number of vertical structures or an infinite periodic array of vertical structures. The inhomogeneities are therefore small in one horizontal coordinate and infinite in the other. This study investigates the effects of such a structure on the impedance tensor and shows that the impedance response is a function of, among others things, the electrode separation and placement and the inhomogeneity resistivity-thickness product. Important conclusions are derived with regard to spatial sampling of the electric field. The results indicate that correct bulk resistivity values can be determined by a judicious measurement of the average electric field. Long electrode spacing, however, will not always produce meaningful results. As well, an intuitive assertion is verified that the EM fields in this polarization sense the depth extent of the complex media as if the bulk conductivity were the inverse of the spatially averaged resistivity. The chapter also shows that lateral inhomogeneities can masquerade as one-dimensional structure.

The next two chapters (Chapters 5 and 6) of this thesis together constitute an attack on the problem of 3-D inhomogeneities which are near-surface and small in scale. Small-scale, for these purposes, means that the scatterers cause negligible secondary electric fields to be generated by induction. Near-surface inhomogeneities that have a size comparable to the scale of the measurements

have been a constant cause of difficulties in interpretation. This is arguably (Vanyan, 1987) the most important problem in magnetotellurics at present. Some recent contributions to the resolution of this problem have been made by Larsen (1975,1977), Bahr (1985), and Zhang *et al* (1987). Bahr (1985) made an initial study of the physics of the general problem although this work has not yet reached the journal stage. Larsen (1975,1977) and Zhang *et al* (1987) made quite specialized assumptions. These authors have nevertheless established the principles to be employed in the present work. The important principle elucidated in these papers is that the most significant effect of the small bodies on the electric fields is a frequency-independent or *galvanic* distortion of the frequency-dependent electric fields produced by both inductive and galvanic excitation in a large-scale structure. (Large-scale, here, means that the structure is sufficiently large to generate significant secondary fields by induction processes which are necessarily frequency-dependent.) The galvanic distortion (sometimes called *static* distortion) is caused by charges on conductivity boundaries or gradients. These charge effects are often termed *current channelling* because currents tend to be drawn into regions of high conductivity and repelled by regions of low conductivity.

Chapter 5 is devoted to the study of the way in which small-scale 3D inhomogeneities effect the regional (large-scale) electromagnetic fields. In this chapter, the galvanic distortion of the regional electric field is first analytically determined for a particular simple small-scale scatterer (embedded conducting hemisphere). This analytic solution clearly shows the manner in which a small scatterer causes the horizontal components of the measured electric field to become position-dependent mixtures of the regional electric field components. As well, the analytic model is employed to describe the electrostatic distortion of the magnetic field and thus to show how such scatterers can distort the measured impedance phases purely through non-inductive scattering effects.

The simple analytic model is then used to investigate the galvanic effects of such bodies on the impedance tensor. For example, if the regional structure

is at most 2-D, the impedance tensor  $\mathbf{Z}$ , in the principal coordinates of the regional structure, can be approximately expressed as

$$\mathbf{Z} = \mathbf{C} [\mathbf{I} - \mathbf{Z}_2 \mathbf{D}] \mathbf{Z}_2. \quad (1.1)$$

Here  $\mathbf{Z}_2$  is the impedance tensor for the regional structure when the distorting inhomogeneities are not present,  $\mathbf{C}$  describes the galvanic effects on the electric fields and  $\mathbf{D}$  describes the galvanic effects on the magnetic field.

This analytic model is also useful for explicitly investigating parameterizations or decompositions of the impedance tensor in the presence of such inhomogeneities. With the aid of this analytic model and a two-dimensional modelling program, the effects of such scatterers on the commonly used two-dimensional interpretation of Swift (1967) are examined. As additional illustration of the usefulness of the analytic model, two of the more recent decompositions (Eggers 1982, Bahr 1985) are examined in Appendix 3.

The development of the analytic model and the ideas discussed above provided the motivation for an extension of the factorization of (1.1). This factorization can incorporate the effects of galvanic distortion of the electric and magnetic fields by 3D scatterers, weak 3D induction (not interacting with the galvanic), as well as the influence of the large-scale 2-D structure.

The factorization developed in Chapter 5 gives insight into a concept for a useful parameterization or interpretation of the measured impedance tensor. The aim of the concept is to provide a decomposition of the measured impedance data which separates the regional parameters from the local. Previous authors have worked on various decomposition methods of this type for certain particular models. Larsen (1975,1977) provided a means for dealing with weak 3D local effects when the regional structure is one-dimensional. Zhang *et al* (1987) provided a method for dealing with up to 2-D structure when the local galvanic effects were also 2-D. Bahr (1985) provided the first fundamental analysis for 3D local structure with 2-D regional structure. The decomposition developed here provides a method which accommodates both the models of

Larsen and Zhang *et al*, reduces to the original method of Swift(1967) when his model is appropriate and extends the allowed models to include strong 3D galvanic scattering in a one or two-dimensional regional structure. The development of the factorization was influenced by a desire to provide a useful parameterization or decomposition which allows a) unambiguous data presentation b) straightforward formulation of fitting methods c) investigation of uniqueness d) incorporation of as large a set of physical situations as possible and e) provision of concepts for extension to additional physical effects.

In chapter 6, a decomposition of the measured impedance tensor is developed which incorporates the most significant effect of small-scale, near-surface inhomogeneities; namely that of galvanic or frequency-independent distortion of the horizontal electric fields. The decomposition is based on the assumption that the source field excites a large-scale structure which is at most two-dimensional together with small-scale, three-dimensional structures which cause static distortion only of the electric fields. The principal aim is to recover, as closely as possible, the correct two-dimensional information from which standard two-dimensional techniques can determine the large-scale conductivity structure. The decomposition method, in fact, obtains the correct regional strike and “static-shifts” of the true two-dimensional impedances. That is, the recovered impedances are the true impedances but multiplied by unknown frequency-independent, real constants. The scaling of the impedances must be determined by some independent method (*i.e.* resistivity or controlled source EM). Some information which characterizes the local three-dimensional structure is also obtained in two distortion parameters termed twist and shear. The method was applied to both synthetic and field data.

An analysis of the effects of fine irregularities in a layered medium is discussed. This work was undertaken because of the extensive amount of study that is done on the 1-D MT inverse problem. Because of the diffusive nature of the problem, if the conductivity structure is simply a function of depth, it is intuitively expected that the surface impedance will be a function merely

of the average conductivity at a depth appropriate to the frequency being utilized. Chapter 2 investigates this assumption and the extent to which it is true. It is important to know what effects fine layered structure can have on the measured fields so that the effects are not incorrectly attributed to lateral structure. For this investigation two techniques were developed for studying fine-bedding structure; one statistical, the other deterministic. Although, the conclusions of both methods agree that the assumption concerning the vertical spatial averaging of the conductivity is generally correct, the results show that discrepancies can occur. The magnitudes of these discrepancies in the surface impedance are discussed as are the conditions under which such effects are present.

### Context with Previous Work

Table 1.1 provides a means of summarizing the thesis and placing it in the context of previous work. The regional (large-scale) and local (small-scale) structure are each divided into 1, 2 or 3-D models. Categories will be referred to by these divisions. For instance, category 31 will be 3-D local with 1-D regional structure.

Table 1.1 :

<i>LOC</i> \ <i>REG</i>	<i>1D</i>	<i>2D</i>	<i>3D</i>
<i>1D</i>	<u><i>G</i></u>	<i>S</i>	<i>numerical modelling</i>
<i>2D</i>	<i>Z, <u>G</u></i>	<i>Z, <u>G</u></i>	
<i>3D</i>	<i>BD, H, W B, L, P, <u>G</u></i>	<i>B, <u>G</u></i>	<i>P</i>

### Synopsis of Research

B:Bahr (1985), BD:Berdichevsky and Dmitriev (1976), G:Groom (1987,1988)  
 H:Hermance (1982), L:Larsen (1977), P:Park (1985), S:Swift(1967),  
 W:Wannamaker *et al* (1984), Z:Zhanget *al* (1987)

Category 11 was, of course, first introduced by Cagniard (1953) but is now principally studied as an inverse problem. The forward treatment of this category is extended in this thesis to the case of strong random variations (Chapter 2). Category 12, has the classic decomposition due to Swift (1967) and is now presently dealt with by 2-D numerical modelling and inversion techniques. The parameterization method developed in this thesis reduces to the same parameters as Swift's method for this model. As well, analytic solutions provided in the thesis have implications for this category (Chapter 3 and 4). Models in category 13 are principally studied via 3-D numerical modelling programs.

Zhang (1987) developed a decomposition method for categories 21 and 22. The decomposition method developed here is appropriate to these categories as well. As well, new analytic solutions are provided for both these categories in the thesis (Chapters 3 and 4). To this author's knowledge, there has been no work published which is specific to category 32. 3-D numerical methods should however provide estimates for specific models in this category.

A great deal of work has been generated which is specific to category 31. Berdichevsky and Dmitriev (1976) studied this problem with a specific model for the 3-D body and a general model for the 1-D structure. Hermance (1982) and Wannamaker *et al* (1984) have investigated this problem numerically for specific simple models, as has Park (1985). Larsen (1975,1977) has provided a parameterization method for models of this type when the 3-D scattering is weak. The method developed in this thesis accounts for these models even when the scattering is strong (Chapter 6) and shows that there can be effects on the magnetic field (Chapter 5). Bahr (1985) has provided some insight into this category and the next category 32. Chapter 6 provides a more complete solution to the parameterization problem for this category. The method ac-

counts for electrostatic distortion of the electric fields and also provides a basis for incorporation of the electrostatic effects on the magnetic field. Finally, category 33 has been investigated only by numerical techniques (*e.g.* Park, 1985). As mentioned earlier the general eight parameter, mathematically based decompositions of course apply to all categories but do not attempt to physically separate local and regional effects.

### Notation and Basic Theory

A brief summary of the basics of MT theory is required to introduce the notation used.

Macroscopically, electromagnetic fields are governed by Maxwell's equations

$$\nabla \times \vec{H} = \vec{J} + \frac{\partial \vec{D}}{\partial t} + \vec{J}^s \quad (1.2a)$$

$$\nabla \times \vec{E} = -\frac{\partial \vec{B}}{\partial t} \quad (1.2b)$$

$$\nabla \cdot \vec{B} = 0 \quad (1.2c)$$

$$\nabla \cdot \vec{D} = \rho_f, \quad (1.2d)$$

together with constitutive relations

$$\vec{D} = \epsilon \vec{E} \quad (1.3a)$$

$$\vec{B} = \mu \vec{H} \quad (1.3b)$$

$$\vec{J} = \sigma \vec{E}. \quad (1.3c)$$

$\vec{H}$  is the magnetic field,  $\vec{B}$  is the magnetic induction field,  $\vec{E}$  is the electric field,  $\vec{D}$  is the electric displacement field,  $\vec{J}$  is the current density, and  $\vec{J}^s$  is the source current density. The characteristics of the medium,  $\epsilon$ ,  $\mu$  and  $\sigma$ , are the permittivity, magnetic permeability and electric conductivity, respectively.  $\rho_f$  is free charge density.

Maxwell's equations (1.2) simplify somewhat as a consequence of the normal magnetotelluric assumptions. The source, being high above the Earth's surface, is removed from the problem and the source field will be assumed uniform over any plane parallel to the Earth's surface. Secondly the magnetic permeability,  $\mu$  is assumed constant everywhere as the permeability of free-space,  $\mu_0$ .

The source field has a statistical nature and noise is present. Weighted signal stacking is therefore required to obtain estimates of the impedance tensor which contains the "physics" of the problem. Since stacking of impedance estimates is simple and straightforward in the frequency domain as opposed to the time domain and since there is no more available information in the time domain, the frequency domain is utilized. In this domain, all fields have a  $e^{i\omega t}$  dependence. Also, the magnetic effects of displacement currents are neglected (the quasi-static approximation). The reason for the validity of this can be seen by applying Maxwell's equations (1.2) in the frequency domain to a homogeneous medium. The magnetic and electric fields obey the wave equation

$$\nabla^2 \phi = k^2 \phi \quad (1.4)$$

where the wavenumber,  $k$ , is given by

$$k^2 = \mu\omega^2\epsilon + i\mu\omega\sigma. \quad (1.5)$$

Thus, the fields both propagate and decay through the medium. The fields, for typical frequencies and Earth characteristics, decay to negligible amplitudes over distances much smaller than a free-space wave-length. In other words, in the Earth

$$|\mu\omega^2\epsilon| \ll |i\sigma\mu\omega|.$$

The MT problem is therefore studied as a diffusion problem as opposed to a propagation problem. In summary, Maxwell's equations for the magnetotelluric method reduce to

$$\nabla \times \vec{H} = \sigma \vec{E} \quad (1.6a)$$

$$\nabla \times \vec{E} = -i\mu_0\omega \vec{H} \quad (1.6b)$$

$$\nabla \cdot \vec{H} = 0 \quad (1.6c)$$

$$\nabla \cdot \vec{E} = \frac{\rho_f}{\epsilon} \quad (1.6d)$$

In addition, since charge is conserved

$$\nabla \cdot \vec{J} = -\frac{\partial \rho_f}{\partial t} \quad (1.7)$$

However, the charge density reaches its equilibrium value in an extremely short time ( $t \approx \frac{\epsilon}{\sigma}$ ) (Grant and West 1965). Thus,

$$\nabla \cdot \vec{J} = 0, \quad (1.8)$$

or the normal component of current density is continuous across any interface.

Because of the uniform spatial character of the source field, if the conductivity structure is one-dimensional, the electric and magnetic fields have only a horizontal component. These then both obey, everywhere, the differential equation

$$\frac{\partial^2 \phi}{\partial z^2} = k^2 \phi \quad (1.9)$$

where, now  $k^2 = i\mu\omega\sigma$ . The  $z$ -axis is taken to point down, normal to the Earth's surface, and the  $x$  and  $y$ -axes are parallel to the Earth's surface and orthogonal to each other. The magnetic field can be determined from the electric field. The ratio of the single component electric field to the magnetic field is a complex scalar in the frequency domain having the units of electrical impedance and is appropriately a function of frequency.

If one assumes that the conductivity and the current source spatial dependences are two-dimensional, (*e.g.* both independent of  $y$ ) then all quantities become independent of  $y$ . In this two-dimensional problem Maxwell's equations (1.6), in a region containing no sources, become (*e.g.* Jones and Price, 1970)

$$\frac{\partial}{\partial z} E_x - \frac{\partial}{\partial x} E_z = -i\mu_0\omega H_y \quad (1.10a)$$

$$\frac{\partial}{\partial x} H_y = \sigma E_z \quad (1.10b)$$

$$-\frac{\partial}{\partial z} H_y = \sigma E_x \quad (1.10c)$$

$$\frac{\partial}{\partial z} H_x - \frac{\partial}{\partial x} H_z = \sigma E_y \quad (1.11a)$$

$$\frac{\partial}{\partial x} E_y = -i\mu_0\omega H_z \quad (1.11b)$$

$$-\frac{\partial}{\partial z} E_y = -i\mu_0\omega H_x \quad (1.11c)$$

These equations separate into two polarizations, each characterized by orthogonal field components. Eqns. 1.11a, 1.11b, and 1.11c involve only  $E_y, H_x$ , and  $H_z$ . This polarization is termed the E-polarization, H perpendicular to strike or the TE (transverse electric) polarization. Eqns. 1.10a, 1.10b and 1.10c involve only  $H_y, E_x$  and  $E_z$ . This polarization is called H-polarization, E perpendicular to strike or the TM (transverse magnetic) polarization. Since the two sets of equations involve independent sets of fields, one can solve the systems independently. For example, in the TE mode utilizing Eqns. 1.11b and 1.11c in Eqn. 1.11a one obtains the appropriate diffusion equation in a uniform medium

$$\frac{\partial^2 E_y}{\partial x^2} + \frac{\partial^2 E_y}{\partial z^2} = i\sigma\mu_0\omega E_y = k^2 E_y \quad (1.12)$$

and in the TM mode substituting Eqns. 1.10b and 1.10c in 1.10a one obtains for a uniform medium

$$\frac{\partial^2 H_y}{\partial x^2} + \frac{\partial^2 H_y}{\partial z^2} = k^2 H_y. \quad (1.13)$$

Note that the TM mode has an associated vertical electric field  $E_z$  while the TE mode has a vertical magnetic field  $H_z$ .

In each of the two-dimensional polarizations, there is only one horizontal component in both the electric and magnetic fields. Thus, each polarization has a characteristic impedance which is the ratio of horizontal electric to magnetic

field. In this thesis

$$Z_{\parallel} = \frac{E_y}{H_x} \quad (1.14)$$

is termed the parallel or E-polarization impedance. While

$$Z_{\perp} = \frac{E_x}{H_y} \quad (1.15)$$

is termed the perpendicular impedance or H-polarization impedance. Both of these impedances are complex scalars and are functions of frequency. If the horizontal coordinate system is not aligned with the natural coordinate system of the two-dimensional structure then the rotation angle about the vertical axis between the two coordinate systems is termed the strike direction.

This summary provides all the basic physics and notation required by the reader. Any additional material is developed when needed.

## CHAPTER 2

### THE EFFECTS OF STOCHASTIC FINE BEDDING IN 1-D STRUCTURES

#### 2.1 Introduction

Even in sedimentary basements where the upper portion of the Earth consists of essentially horizontal structures, conductivity well logs reveal that the conductivity can vary dramatically within any geological layer from the mean conductivity of that layer. This variation generally appears quite random with large variations repeatedly occurring over short distances. It is the purpose of this chapter to investigate whether these variations can alter the EM fields from those which are due to the mean material. Although the results are not particularly profound, the study serves to clarify the problem of fine layering in MT, to indicate that statistical field techniques can be of use in MT and to set the stage for the more complex two and three-dimensional problems which follow in later chapters.

It initially will be assumed that the conductivity in the Earth is only a function of depth and that the MT source produces a plane, spatially uniform and vertically propagating wave. Typically the polarization of the source field will change randomly and so an impedance tensor is measured at the surface of the Earth via the relation

$$\vec{E}(\omega) = \mathbf{Z}(\omega)\vec{H}(\omega) \quad (2.1).$$

The horizontal fields,  $\vec{E}$  and  $\vec{H}$ , each have two components, both parallel to the earth's surface. With the source and conductivity structure assumptions described above, this impedance tensor will have the form

$$\mathbf{Z}(\omega) = \begin{pmatrix} 0 & Z_0(\omega) \\ -Z_0(\omega) & 0 \end{pmatrix}. \quad (2.2)$$

The impedance tensor element,  $Z_0$  is the ratio of horizontal electric field component to perpendicular horizontal magnetic field component.  $Z_0(\omega)$  is used in the 1-D magnetotelluric inverse problem to infer the variation of resistivity with depth (Parker 1980, Weidelt 1972, Oldenburg *et al* 1984).

Since magnetotelluric data are collected at low frequencies, the propagation of the electromagnetic fields in the conducting Earth is studied as a diffusion process. That is, the decay and phase rotation of the fields through the medium is studied. If the conductivity structure is only a function of depth and the electric and magnetic fields are parallel to the layering, then it is expected that it will be the average structure which determines the impedance,  $Z_0$ , at the surface. That is, any fine bedding or layering is expected to produce an impedance which has negligible variations from that which would be produced by a more homogeneous conductive structure having the same average vertical conductivity. Although the differences may be expected to be small, this chapter investigates the effects of random fine layered structure. One would like to know explicitly when the effects of fine bedding are significant and how large the effects can be on the measured surface impedance,  $Z_0$ .

A differential equation is derived here which describes propagation in such randomly varying material. Although the results are not particularly surprising, this equation indicates that there are differences between the fields due to the random material and those caused by the mean material. The solutions to the differential equation indicate the conditions under which significant differences may occur.

## 2.2 A Statistical Approach for Induction in a Medium with Fine Vertical Structure

### 2.2.1 Introduction:

Rock conductivity is primarily a function of porosity, permeability, fluid content and dissolved electrolytes, rather than the properties of the actual rock matrix. Rock conductivity can therefore vary dramatically even over short distances. The effects of these small-scale variations are difficult to investigate from a deterministic standpoint for a broad set of conditions. Such complexity in the case of wave scattering is often investigated by means of statistical techniques (Aki and Richards, 1980). Such an approach will be used for the case of low frequency, quasi-static electromagnetic propagation.

If one studies measurements of conductivities  $\sigma(\vec{r})$  of rock samples collected in a volume, the conductivities will vary from sample to sample. This variation will generally appear to be random and will be described by a probability density  $f(\vec{r})$ . If this distribution were known then one could obtain the mean, variance and other statistical properties of  $\sigma(\vec{r})$ . However, if one assumes that the conductivity have stationary statistics ( i.e. the averages of quantities like  $[\sigma(\vec{r})\sigma(\vec{r}_1)]$  are functions of the distance  $|\vec{r} - \vec{r}_1|$ ) then one can possibly obtain estimates of the magnitudes and smoothness of the electromagnetic field amplitudes and phases as functions of position.

Sections 2.2.1 to 2.2.4 review a method (van Kampen 1975) for statistical field problems. This method will then be applied to obtain the solution for low frequency induction in a medium which has conductivity variations which are functions of depth, alone.

**2.2.2 Stochastic Variables:**

A stochastic function or variable  $\nu(x, \xi)$  is a function of a simple variable  $x$  and a random outcome  $\xi$ .  $\nu$  might be a conductivity perturbation for example where  $x$  represented depth.  $\Omega$  is the set of all outcomes. Subsets  $A$  of  $\Omega$  called random events are described by a probability measure  $P(A)$  (Papoulis,1965). In more common terms,  $\nu(x, \xi)$  is an ensemble of functions of  $x$  in which each one is identified by an event label  $\xi$ . The ensemble of functions is called a stochastic process.

Averages are evaluated by integrating over  $\Omega$ . Thus

$$\langle \nu(x_1) \dots \nu(x_n) \rangle = \int_{\Omega} \nu(x_1; \xi) \dots \nu(x_n; \xi) dP(\xi) \quad (2.3)$$

To make the problem tenable, it is common in physical applications (Aki and Richards 1980, van Kampen 1975) to assume the variable  $\nu(x, \xi)$  to be fully stationary, meaning that all averages, as in the equation above, are dependent only on differences in  $x$ . Assuming that the stochastic variables are fully ergodic (*i.e.* statistical averages can be obtained from spatial averages), which is not a severe additional restriction, then stochastic averages become spatial averages which are useful quantities in geophysical problems.

**2.2.3 Stochastic Differential Equations:**

A non-stochastic ordinary differential equation of order  $n$  can always be written as a set of  $n$  coupled differential equations

$$\frac{\partial \vec{u}}{\partial x} = \vec{F}(x, \vec{u}) \quad (2.4)$$

where  $\vec{F}$  and  $\vec{u}$  are vectors in  $n$ -space. On the other hand a stochastic differential equation has the form

$$\frac{\partial \vec{u}}{\partial x} = \vec{F}(x, \vec{u}; \xi) \quad (2.5)$$

Homogeneous linear equations of the form

$$\frac{\partial \vec{u}}{\partial x} = [A_0 + \alpha A_1(x; \xi)] \vec{u} \quad (2.6)$$

will be considered where  $A_0$  is a sure (i.e. not statistical) matrix independent of  $x$ ,  $\alpha$  is a parameter determining the size of the fluctuations and  $A_1(x; \xi)$  is a stochastic function assumed stationary. Therefore  $\langle A_1(x) \rangle$  is independent of  $x$  and thus can be incorporated with  $A_0$  and  $\langle A_1(x) \rangle$  taken to be zero. Although it is assumed that  $A_1(x; \xi)$  is known fully in a statistical sense, it is obviously difficult to have this knowledge in most physical problems.

Differential equations of this sort are readily realizable in electromagnetics where the electromagnetic parameters of a medium may vary in a random manner even on the macroscopic level and thus Maxwell's equations are still obeyed in the medium. A simple example is one dimensional propagation in a medium with a random refractive index ( $\nu$ ). This process is described by the differential equation

$$\frac{d^2 \psi}{dx^2} + \frac{\omega^2}{c^2} \{ \nu_0^2 + \alpha \nu_1^2(x; \xi) \} \psi = 0 \quad (2.7)$$

which with  $u_1 = \psi$ ,  $u_2 = \frac{d\psi}{dx}$  allows the equation to be written in the form of equation (2.4). This example demonstrates what occurs if a total physical system is divided into a basic state or environment plus a random field of fluctuations. In attempting to establish a set of differential equations for the random field, the influence of the basic state give rise to random coefficients in the differential equations.

#### 2.2.4 Solutions to Stochastic Differential Equations:

A solution to a stochastic differential equation is a stochastic function  $u(x; \xi)$  which for each  $\xi$  satisfies the differential equations with appropriate initial or boundary conditions. To obtain a useful solution one must obtain the statistics of the stochastic solution. In other words, one would desire the moments of the random solution.

As an example consider the differential equation

$$\frac{\partial u}{\partial z} = -i \{ \nu_0 + \alpha \nu_1(z; \xi) \} u \quad (2.8)$$

with the boundary condition

$$u(0, \xi) = a. \quad (2.9)$$

This differential equation models a number of physical problems including a harmonic oscillator with fluctuating frequency and one-dimensional monochromatic propagation in which the environmental parameters vary.

The solution to equation (2.8) is

$$u(z; \xi) = a \exp \left\{ -i\nu_0 z - i\alpha \int_0^z \nu_1(x'; \xi) dx' \right\} \quad (2.10)$$

and thus

$$\langle u(z) \rangle = a e^{-i\nu_0 z} \langle \exp \left\{ -i\alpha \int_0^z \nu_1(x'; \xi) dx' \right\} \rangle. \quad (2.11)$$

To evaluate the average of the exponential (the characteristic function of the integral in 2.11) the concept of cumulants is used. The integral

$$I(\xi) = \int_0^z \nu_1(x'; \xi) dx' \quad (2.12)$$

is a stochastic quantity. The cumulants  $\kappa_m$  of the characteristic functions of a stochastic quantity are defined by

$$\langle e^{-i\alpha I} \rangle = \exp \left\{ \sum_{m=1}^{\infty} \frac{(-i\alpha)^m}{m} \kappa_m \right\} \quad (2.13)$$

where the cumulants are defined in terms of the moments of  $I$ . For these purposes  $\kappa_1, \kappa_2$  were taken to be sufficient and the remaining terms small.

$$\kappa_1 = \langle I \rangle \quad (2.14)$$

$$\kappa_2 = \langle I^2 \rangle - \langle I \rangle^2. \quad (2.15)$$

This assumption is equivalent to stating that the statistics of  $\nu_1$  are completely determined by its first two moments. In other words,  $\nu_1(z)$  is Gaussian and higher order cumulants are exactly zero. Therefore,

$$\kappa_1 = 0 \quad (2.16)$$

$$\kappa_2 = \int_0^z \int_0^z \langle \nu_1(z_1)\nu_1(z_2) \rangle dz_1 dz_2. \quad (2.17)$$

Here the fact that the mean of the perturbations is zero has been utilized.

This method (van Kampen) assumes that there exists a correlation-distance  $\tau_c$  such that  $[\nu_1(z_1), \nu_1(z_2)]$  are statistically independent if  $|z_1 - z_2| > \tau_c$ . Therefore the integrand in  $\kappa_2$  vanishes when  $|z_1 - z_2| > \tau_c$  and  $\kappa_2$  is integrated over an area of  $\tau_c z$ . The second term in the expansion in equation (2.13) is of order  $(\alpha\tau_c)\alpha z$ . Thus the criterion of validity for the expansion of (2.13) is also that

$$\alpha\tau_c \ll 1. \quad (2.18)$$

If the Gaussian assumption were not made, higher order terms would be of order  $(\alpha\tau_c)^{m-1}(\alpha z)$ .

The solution for the first moment of the solution function is then

$$\langle u(z) \rangle = ae^{-i\nu_0 z} \exp \left\{ -\alpha^2 \int_0^z \int_0^{z_1} \langle \nu_1(z_1)\nu_1(z_2) \rangle dz_2 dz_1 \right\}. \quad (2.19)$$

The last expression is due to the stationarity of  $\nu_1$  with the result that the average in the integrand is therefore a function of the difference  $(z_1 - z_2)$  alone. Thus  $\langle u(z) \rangle$  satisfies the non-stochastic or sure differential equation

$$\frac{d\langle u(z) \rangle}{dz} = \left\{ -i\nu_0 - \alpha^2 \int_0^z \langle \nu_1(z)\nu_1(z_2) \rangle dz_2 \right\} \langle u(z) \rangle \quad (2.20)$$

Recalling that the integrand in the above equation differs from zero only when  $|z_2 - z| < \tau_c$  it can be shown that

$$\int_0^z \langle \nu_1(z)\nu_1(z_2) \rangle dz_2 \approx \int_0^\infty \langle \nu_1(0)\nu_1(\tau) \rangle d\tau = c_0 \quad (2.21)$$

where  $c_0$  is now independent of  $z$ . Thus, one has the solution to equation (2.20) with this approximation as

$$\langle u(z) \rangle = A \exp \{ -i\nu_0 - \alpha^2 c_0 \} z \quad (2.22)$$

when  $z > \tau_c$ .

For the case of a harmonic oscillator or monochromatic propagation the fluctuations give rise to a damping in the amplitude which can be seen as a loss of phase coherence between individual solutions for different  $\xi$ . In the induction problem  $\nu = \frac{\gamma}{4}$  where  $\gamma$  is the square root of  $i\sigma\mu\omega$ . The result gives an increase in amplitude damping with  $z$  and a decrease in the rate of phase rotation with  $z$  due to the fluctuations. This will be seen more explicitly below.

To consider propagation or induction where the propagation constant or induction parameter varies significantly within a wavelength or skin-depth, one needs to consider the problem

$$\frac{\partial \vec{u}}{\partial z} = [A_0 + \alpha A_1(z; \xi)] \vec{u} \quad (2.23)$$

where now  $\vec{u}$  has more than one component and  $A_0$  and  $A_1$  are matrices.

To utilize the results previously obtained one makes the transformations (van Kampen)

$$\vec{u}(z) = e^{A_0 z} \vec{v}(z) \quad (2.24)$$

$$e^{-A_0 z} A_1(z; \xi) e^{A_0 z} = V(z; \xi) \quad (2.25)$$

and thus (2.23)

$$\frac{\partial \vec{v}(z)}{\partial z} = \alpha V(z; \xi) \vec{v}(z) \quad (2.26)$$

and

$$\vec{v}(0) = \vec{a} \quad (2.27)$$

The solution to equation (2.26) is

$$\vec{v}(z) = \vec{a} \exp \left\{ \alpha \int_0^z V(t) dt \right\}. \quad (2.28)$$

Assuming  $\langle A_1(z; \xi) \rangle = 0$ , as before, and utilizing the same methods as above gives

$$\langle \vec{v}(z) \rangle = \vec{a} \exp \left\{ \alpha^2 \int_0^z dz_1 \int_0^{z_1} \langle V(z_1)V(z_2) \rangle dz_2 \right\}. \quad (2.29)$$

Letting

$$K(z_1) = \int_0^{z_1} \langle V(z_1)V(z_2) \rangle dz_2 \quad (2.30)$$

gives the differential equation

$$\frac{d\langle \vec{v}(z) \rangle}{dz} = \alpha^2 K(z) \langle \vec{v}(z) \rangle \quad (2.31)$$

and on substitution for the original variables gives

$$\frac{d\langle \vec{u}(z) \rangle}{dz} = \left\{ A_0 + \alpha^2 \int_0^z \langle A_1(z)e^{A_0(z-t)} A_1(t)e^{-A_0(z-t)} \rangle dt \right\} \langle \vec{u}(z) \rangle. \quad (2.32)$$

Which after a transient distance  $\tau_c$  (2.21) gives

$$\frac{d\langle \vec{u}(z) \rangle}{dz} = \left\{ A_0 + \alpha^2 \int_0^\infty \langle A_1(z)e^{A_0\tau} A_1(z-t)e^{-A_0\tau} \rangle d\tau \right\} \langle \vec{u}(z) \rangle \quad (2.33)$$

This is the fundamental result obtained by van Kampen. The unperturbed matrix  $A_0$  is modified by an additional term due to the fluctuations in the coefficients.

### 2.2.5 Application to One-Dimensional Induction:

We will now obtain, using the previous analysis, the solution for quasi-static induction in a medium in which the fluctuations vary only with depth and which is excited from above by a wave of infinite wave-length ( the MT problem ).

With a time variation  $e^{i\omega t}$ , Maxwell's equations become

$$\frac{dE_y}{dz} = i\mu\omega H_x \quad \text{and} \quad \frac{dH_x}{dz} = \sigma E_y. \quad (2.34)$$

Therefore, using the basic differential equation

$$\frac{d\vec{u}}{dz} = [A_0 + \alpha A_1(z; \xi)] \vec{u} \quad (2.35)$$

where  $\sigma = \sigma_0 + \alpha\sigma_1(z; \xi)$  and  $u = (E_y, H_x)$  we have

$$A_0 = \begin{pmatrix} 0 & i\mu\omega \\ \sigma_0 & 0 \end{pmatrix}, \quad A_1 = \begin{pmatrix} 0 & 0 \\ \sigma_1 & 0 \end{pmatrix}. \quad (2.36)$$

The general solution to the unperturbed problem is

$$\vec{u} = e^{A_0 z} \vec{c} = \begin{pmatrix} \cosh \gamma z & \frac{1}{\beta} \sinh \gamma z \\ \beta \sinh \gamma z & \cosh \gamma z \end{pmatrix} \vec{c} \quad (2.37)$$

where  $\beta = \frac{\sigma_0}{\gamma}$ . ( $\gamma = \sqrt{i\sigma_0\mu\omega}$ ). Utilizing this result in the integral in equation (2.33) gives for that integral

$$\frac{\alpha^2}{\beta^2} \int_0^\infty \langle \sigma_1(z)\sigma_1(z-\tau) \rangle \begin{pmatrix} 0 & 0 \\ \beta \sinh \gamma z \cosh \gamma z & -\sinh^2 \gamma z \end{pmatrix} d\tau. \quad (2.38)$$

Let

$$c_1 = \int_0^\infty \langle \sigma_1(z)\sigma_1(z-\tau) \rangle \sinh(\gamma\tau) \cosh(\gamma\tau) d\tau \quad (2.39)$$

$$c_2 = \int_0^\infty \langle \sigma_1(z)\sigma_1(z-\tau) \rangle \sinh^2(\gamma\tau) d\tau \quad (2.40)$$

where  $c_1, c_2$  are complex constants. Thus (2.33) and (2.38) result in the differential equations for the average or mean fields

$$\frac{d\langle E_y \rangle}{dz} = i\mu\omega \langle H_x \rangle \quad (2.41)$$

and

$$\frac{d\langle H_x \rangle}{dz} = \sigma_0 \langle E_y \rangle + \frac{\alpha^2}{\beta} c_1 \langle E_y \rangle - \frac{\alpha^2}{\beta^2} c_2 \langle H_x \rangle. \quad (2.42)$$

From (2.41) and (2.42), the differential equations can be obtained to describe the low-frequency propagation of the mean fields in the random medium. Thus the mean electric field in the random material satisfies the sure second order ODE

$$\frac{d^2 \langle E_y \rangle}{dz^2} = i\mu\omega \left( \sigma_0 + \frac{\alpha^2}{\beta} c_1 \right) \langle E_y \rangle - \frac{\alpha^2}{\beta^2} c_2 \frac{d\langle E_y \rangle}{dz} \quad (2.43a)$$

and  $\langle H_x \rangle$  satisfies a similar equation. For comparison the mean field in the average material obeys

$$\frac{d^2 \langle E_y \rangle}{dz^2} = i\mu\omega \sigma_0 \langle E_y \rangle \quad (2.43b)$$

and thus (2.43a) contains an additional first-derivative term and a modification in the constant multiplying  $\langle E_y \rangle$ .

The importance of the differences in the governing differential equation (2.43a) from the differential equation for the mean material (2.43b) is dependent on the magnitudes of the average conductivity ( $\sigma_0$ ), the fluctuation parameter ( $\alpha$ ), and the constants  $c_1$  and  $c_2$ . In general, however, there is additional amplitude damping and a variation in phase rotation with depth. These results are common to problems of fields propagating through a one-dimensional material with random parameters.

### 2.2.6 Estimation of Solutions

Solutions of (2.43) are dependent upon the constants  $c_1$  and  $c_2$  which are determined from the autocorrelation function of the random variations. This function may be estimated by conductivity well logs or a statistical analysis of the conductivity in sedimentary rocks combined with a knowledge of the sedimentary sequence. However, in the present analysis, some assumptions will be made to obtain the two constants ( $c_1, c_2$ ) and thus to determine estimates of the coefficients in (2.43) and then the form of the solutions to this equation.

Recall for  $E = E_y, H = H_x$  that

$$\frac{d^2 \langle E \rangle}{dz^2} = i\mu\sigma_0\omega \langle E \rangle + i\mu\omega \frac{\alpha^2}{\beta} c_1 \langle E \rangle - \frac{\alpha^2}{\beta^2} c_2 \frac{d \langle E \rangle}{dz} \quad (2.43)$$

where  $\beta = \frac{\gamma}{\lambda}$ ,  $\lambda = i\mu\omega$  and  $\gamma^2 = i\sigma_0\mu\omega$  and

$$c_1 = \int_0^\infty \langle \sigma_1(z)\sigma_1(z-\tau) \rangle \sinh(\gamma\tau) \cosh(\gamma\tau) d\tau$$

and

$$c_2 = \int_0^\infty \langle \sigma_1(z)\sigma_1(z-\tau) \rangle \sinh^2(\gamma\tau) d\tau.$$

The autocorrelation function of the random conductivity is given by

$$\langle \sigma_1(z)\sigma_1(z_\tau) \rangle = R(\tau) \approx \frac{1}{D} \int_0^D \sigma_1(z)\sigma_1(z-\tau) d\tau \quad (2.44)$$

where  $D$  is the thickness of the stochastic structure. That is, one assumes the random structure is confined vertically to a thickness  $D$ .

Let us assume that  $\sigma_1$  is scaled to be of order  $\sigma_0$  so that one can define

$$R(\tau) = \sigma_0^2 \quad \text{if} \quad \tau < \tau_c \quad (2.45)$$

and zero otherwise in order to estimate the coefficients in the differential equation. With the assumption that the correlation distance  $\tau_c$  is a fraction of the skin-depth in the average medium

$$c_1 = \sigma_0^2 \int_0^{\tau_c} \sinh(\gamma\tau) \cosh(\gamma\tau) d\tau \approx \frac{1}{2} \gamma \sigma_0^2 \tau_c^2 \quad (2.46)$$

to first order in  $\gamma\tau$  and

$$c_2 = \sigma_0^2 \int_0^{\tau_c} \sinh(\gamma\tau) \sinh(\gamma\tau) d\tau \approx -\frac{1}{3} \gamma^2 \sigma_0^2 \tau_c^3 \quad (2.47)$$

to second order in  $\gamma\tau$ .

Thus, the differential equation (2.43) becomes

$$\frac{d^2 \langle E \rangle}{dz^2} = i\mu\sigma_0\omega \langle E \rangle + (i\mu\sigma_0\omega)^2 \alpha^2 \left( \frac{\tau_c^2}{2} \right) \langle E \rangle + (i\mu\sigma_0\omega)^2 \alpha^2 \frac{\tau_c^3}{3} \frac{d \langle E \rangle}{dz}. \quad (2.48)$$

Since  $\sigma_0\mu\omega = \frac{2}{\delta^2}$  this can be written as

$$\frac{d^2 \langle E \rangle}{dz^2} = i \frac{2}{\delta^2} \langle E \rangle - \frac{4}{\delta^4} \alpha^2 \frac{\tau_c^2}{2} \langle E \rangle - \frac{4}{\delta^4} \alpha^2 \frac{\tau_c^3}{3} \frac{d \langle E \rangle}{dz}. \quad (2.49)$$

Then writing the correlation length

$$\tau_c = a\delta$$

in terms of  $\delta$ , the skin-depth in the average medium, one obtains a particularly simple expression for the differential equation governing the mean electric field:

$$\frac{d^2 \langle E \rangle}{dz^2} = \frac{2}{\delta^2} (i - \alpha^2 a^2) \langle E \rangle - \frac{4}{3\delta} \alpha^2 a^3 \frac{d \langle E \rangle}{dz}. \quad (2.50)$$

The general solution for the mean electric field is therefore

$$\langle E \rangle = e^{-pz} (Ae^{qz} + Be^{-qz}) \quad (2.51)$$

where

$$p = \frac{2}{3} \frac{\alpha^2 a^3}{\delta} \quad (2.52)$$

and

$$q^2 = p^2 + \frac{2}{\delta^2} (i - \alpha^2 a^2). \quad (2.53)$$

The constants  $A$  and  $B$  are determined by the boundary values. The solution of the mean magnetic field can be found from 2.51 via 2.41.

The solution demonstrates directly that there is additional amplitude decay due to the random material, as expected. However, (2.52) and (2.53) express explicitly when this additional decay occurs. Equation (2.53) shows that the phase rotation is modified as well by the random material.

Now, compare more closely the solution (2.51-2.53) with the homogeneous results where the material has no random fluctuations in conductivity. In the homogeneous solution, the parameter  $p$  is identically zero and  $q^2$  is simply  $\frac{2}{\delta^2}i$ . On the other hand, for the stochastic result both  $p$  and  $q$  are dependent on the fluctuation parameter,  $\alpha$  which describes the extent to which the conductivity varies about the mean. When  $\alpha = 0$ ,  $p$  and  $q$  reduce to the values in the homogeneously conducting problem. Second, the correlation length  $\tau_c = a\delta$  affects the stochastic solution. For a fixed frequency, as  $\tau_c$  decreases then the parameter  $a$  in (2.52, 2.53) decreases and the solution eventually reduces to the uniform problem. In other words, if the variations do not correlate over significantly large distances then no variation from the homogeneous case will be observed. Thirdly, the effects of the random variations change with frequency. In particular, the anomalous response diminishes to zero as frequency decreases (2.51). In the stochastic model, for a fixed correlation length ( $\tau_c$ ),  $a$  decreases as frequency decreases since the skin-depth ( $\delta$ ) increases. Thus  $p$  (2.52) approaches zero as frequency decreases and  $q$  (2.53) approaches its value for the average conducting layer. Finally, the average conductivity of the random layer

also affects the stochastic solution. As the average conductivity of the random layer increases, the skin-depth  $\delta$  decreases and thus for fixed frequency and correlation length, the effects of the random layer increase (2.51-2.53) as  $p$  and  $q$  become more modified from their sure solutions.

### 2.2.7 Examples and Conclusions

An examination of equations (2.51-2.53) indicates that for reasonable physical parameters one would not expect very large effects on the amplitude of the resulting fields but may well expect some reasonably significant effect in the complex phase angle of the solution. To investigate this a numerical routine was developed which utilized the sure differential equations (2.41, 2.50) to obtain a solution for the mean fields. However, before these results can be shown, reasonable values for the fluctuation parameter ( $\alpha$ ) must be discussed.

One difficulty with this formulation of the problem is that whatever excursions in conductivity above the mean are allowed an equal excursion below the mean is equally probable. Because of the estimate of the autocorrelation function (2.45), any values for  $\alpha$  above 1 indicate a sixteen percent probability of negative conductivity. However, restricting  $\alpha$  to be less than one would not allow for reasonable excursions above the mean. An examination of the propagation matrix (Appendix 1) for a thin layer shows that, for small layers, the electric field is propagated through a layer of negative conductivity with a value approximately equal to the value obtained when propagated through layer of equal thickness but with a positive conductivity of the same magnitude. The magnetic field on the other hand is not propagated correctly. Thus, both mean fields are determined by first obtaining the mean electric fields via (2.50 - 2.53) and then obtaining the mean magnetic field from (2.41).

The model employed to investigate the effects of the random material on the surface impedance consists of a stochastic layer over a uniform half-space. The approximation of (2.45) was used for the autocorrelation function of the conductivity variations. It is realized, of course, that this is an overestimation.

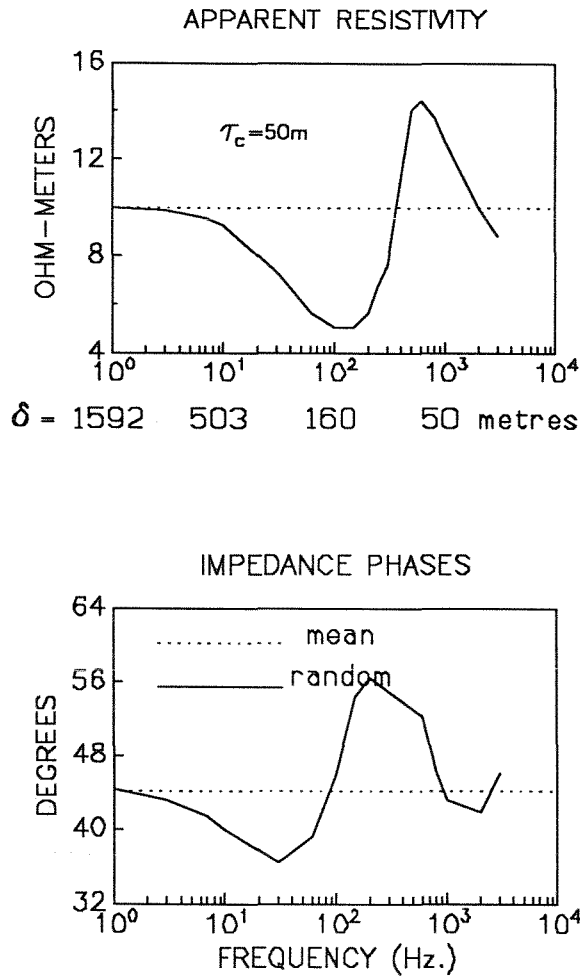
Also, since the differential equation (2.50) is only correct when  $z$  is more than one correlation length  $\tau_c$  within the random layer, the homogenous solution is used for the upper autocorrelation length in the random layer. This of course is incorrect but conservative, as the effects of the random layer are underestimated by this assumption and the results at lower frequencies will not be significantly affected.

Figure 2.1 are examples of the surface impedance,  $Z_0$ , as a function of frequency for such a model as discussed above. Here  $Z_0$  is the ratio of the mean electric field to the mean magnetic field. The magnitude of the impedance is represented as the conventional apparent resistivity

$$\rho_a = \frac{1}{\mu_0 \omega} |Z_0|^2. \quad (2.54)$$

The phase angle of  $Z_0$  is termed the impedance phase.

In the first example (Figure 2.1a), the average conductivity is uniform (.1 S/m) everywhere below the Earth's surface. The random layer had a thickness of 1700m and an average conductivity of .1 S/m. The characteristic frequency of this layer is .9 Hz since at this frequency, for the average conductivity, the thickness (1700m) is approximately one skin depth. In other words, the layer is a thick layer relative to the frequencies to be utilized. The correlation length was taken to be 50m. Thus the stochastic results for frequencies greater than about 200 Hz must be held suspect as the characteristic frequency of this length is 1000 Hz. The random layer overlies a uniform half-space of conductivity .1 S/m. Thus, the response of the average material would be constant with frequency with an apparent resistivity  $10\Omega m$  and an impedance phase of 45 degrees. The fluctuation parameter ( $\alpha$ ) was chosen to be 5 and thus a negative conductivity has about a forty-two percent chance of occurring. The differential equation (2.50) is only correct for this model when  $z > \tau_c$  and thus the region  $z < \tau_c$  was estimated as uniform ( $10\Omega m$ ). Note, the impedance approaches the uniform halfspace result as frequency decreases to 1 Hz. This is not the effect of the lower half-space since the fields have not significantly penetrated the lower half space until about 1 Hz. Similar curves to those in Figure 2.1a



**Figure 2.1a:** The effects on surface impedance of a 1700m random layer of average conductivity .1 S/m are plotted as solid lines. Beneath the random layer is a homogenous half-space of resistivity 10  $\Omega m$ . A uniform layer of 50m and resistivity 10 $\Omega m$  overlies the random layer. The surface impedance due to the average structure is given by the dotted lines for comparison. The skin-depth ( $\delta$ ) is given in metres for the average material at the beginning of each decade of frequency.

for varying  $\tau_c, \alpha$  and average conductivity confirm the conclusions previously stated in this section.

As a second example, a thin (150 m) random layer was used with a smaller fluctuation parameter ( $\alpha = 2.5$ ). The average structure is again .1

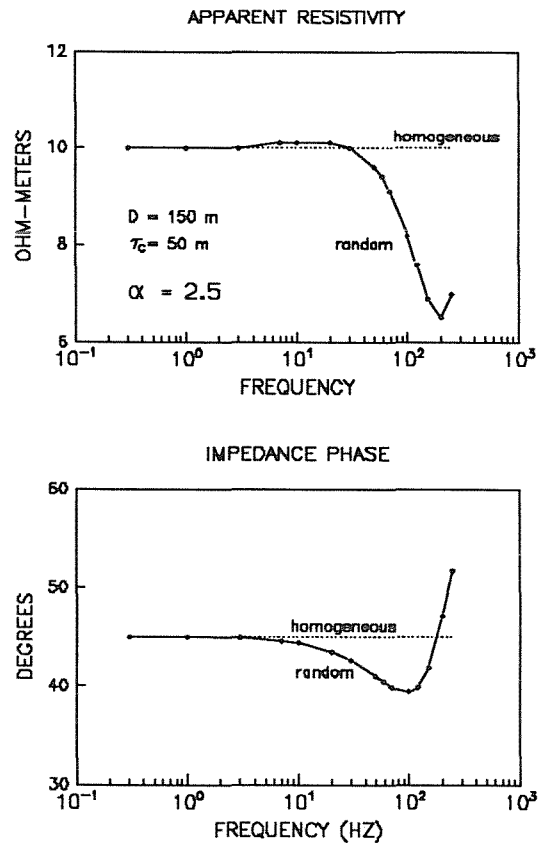


**Figure 2.1b:** The effects on surface impedance of a 150m random layer of average conductivity .1 S/m. Beneath the random layer is a homogenous half-space of resistivity  $10 \Omega m$ . A uniform layer of 50m and resistivity  $10 \Omega m$  overlies the random layer.

S/m throughout with a uniform top 50m layer.

As stated previously it is probable that the possibility of negative conductivities is not a serious drawback. This is because it is the mean electric field which is determined from the stochastic results and the magnetic field is determined from the electric field. The electric field is in fact propagated approximately correctly through two thin layers; one of positive conductivity and the other with an equivalent but negative conductivity. However to check this assertion, a deterministic method was also studied.

### 2.3 A Deterministic Approach

In this section, fine bedding effects on the MT one-dimensional surface impedance are studied with a deterministic or non-statistical model. This provides results for comparison with the statistical analyses of the previous section (Section 2.2).

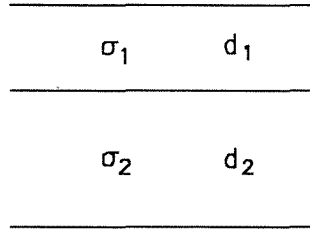


**Figure 2.2:** A doublet of two conducting layers which have conductivities  $\sigma_1$  and  $\sigma_2$  and thicknesses  $d_1$  and  $d_2$ .

Consider a pair of uniformly conducting layers which have conductivities  $(\sigma_1, \sigma_2)$  and thicknesses  $(d_1, d_2)$  respectively (Figure 2.2). Now, let

$$\frac{d_2}{d_1} = R \quad , \quad \frac{\sigma_2}{\sigma_1} = r \quad \text{and} \quad L = d_1 + d_2. \quad (2.55)$$

The average conductivity of the doublet is

$$\sigma_{\text{ave}} = \frac{\sigma_1 d_1 + \sigma_2 d_2}{d_1 + d_2}. \quad (2.56a)$$

Substitution of (2.55) in (2.56a) gives:

$$\sigma_{\text{ave}} = \sigma_1 \left( \frac{1 + rR}{1 + R} \right). \quad (2.56)$$

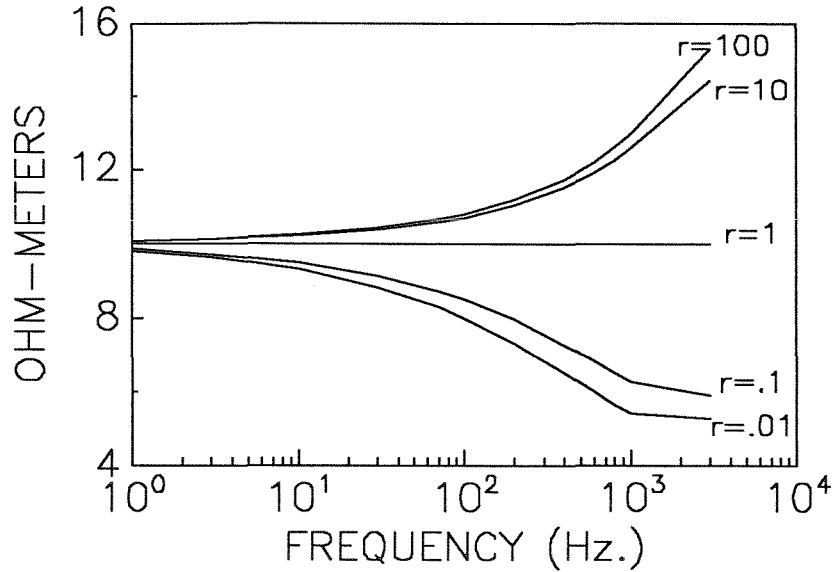
To verify the previous sections results a model was developed of fine structure and a numerical method for determining the surface impedance due to this model. The physical model consists of a stack of  $n$  doublets of the type illustrated in Figure 2.2 with the variable parameters,  $r, R$  and  $L$ . The parameter  $L$  is analogous to the correlation length  $\tau_c$  in the stochastic problem and  $r$  is

equivalent to the fluctuation parameter  $\alpha$ . For example, from (2.56) and (2.55),  $r = 1$  is equivalent to  $\alpha = 0$  (2.51). From the statistical results, the largest effects are expected from the fine structure to occur for high  $\sigma_{\text{ave}}, \omega, L$  and either large  $r$  or small  $r$ . The next figures (Figures 2.3,2.5) show this is indeed correct for the parameters  $L$  and  $r$ . The effect of the average conductivity was verified but the results are not shown here.

To obtain the electromagnetic solutions for these models accurately, I utilized a propagator matrix technique for determining solutions to the forward one-dimensional problem. This method, which is discussed in Appendix 1, allows one to determine quickly and accurately the electromagnetic fields due to a large number of fine layers bounded below by a homogeneous half-space. (The uniform half-space below is no restriction since if an infinitely thick fine structured material is required; it is sufficient to place the half-space at sufficient depth that the fields will not significantly penetrate it.) If desired, a uniform layer of arbitrary thickness and conductivity can be added above the fine structure material to remove any possibility of effects on the surface impedance from the first doublet.

From the results of the previous study, it is expected that the most significant effects on the impedance will occur when  $r$  (ratio of conductivities) is either small or large or when there is a high conductivity contrast between top and bottom layers in the doublets. Figure 2.3 contains a comparison of surface impedance for various values of  $r$ . The conductivity structure used is a half-space of uniform average conductivity .1S/m but buried at 10m is a 1700m layer of fine bedding. This will be the structure assumed for the remainder of the analyses but with different values for the parameters  $r, R$  and  $L$ . Any deviation from an apparent resistivity of  $10\Omega m$  and an impedance phase of 45 degrees is an anomalous response due to the fine bedding. The doublet thickness was 50m and  $R = 3$  for Figure 2.3. This figure shows clearly that the effects of fine bedding increase with conductivity contrast as in the statistical analyses. Figure 2.4 is a study of the effects of the parameter  $R$ , the ratio of

APPARENT RESISTIVITY (Comparison of  $r$ )



IMPEDANCE PHASES

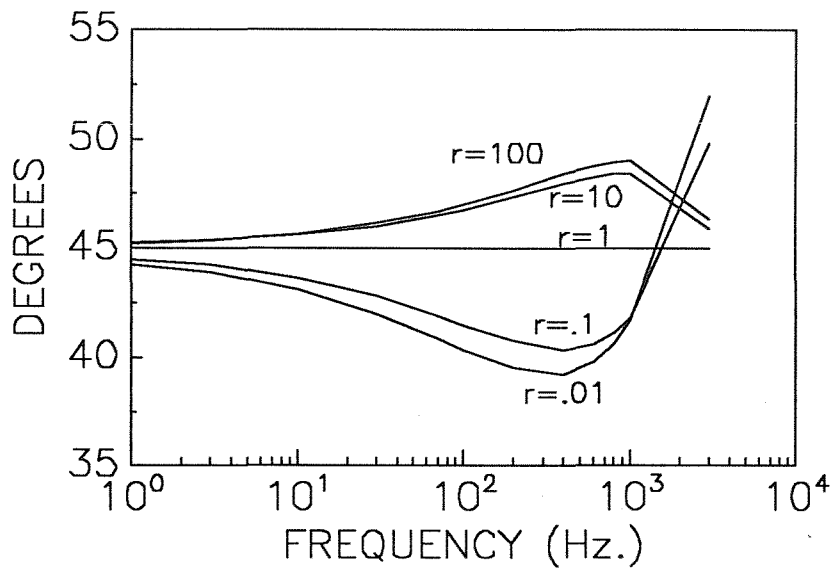
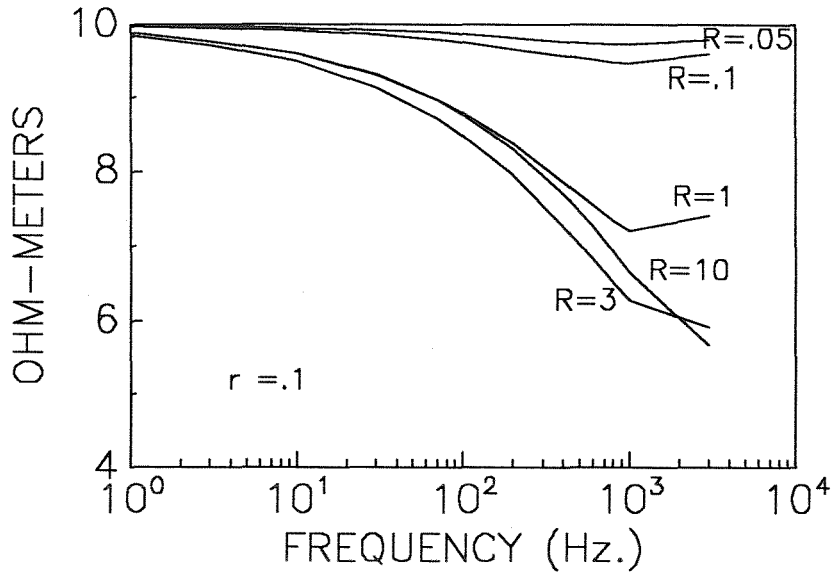


**Figure 2.3:** A comparison of anomalous impedance response for the parameter  $r$  (2.55). The structure is a half-space of average conductivity .1 S/m but buried at 10m is a 1700m layer of fine bedding with a doublet thickness,  $L$ , of 50m.  $R$  (2.55) is fixed at 3.

APPARENT RESISTIVITY (Comparison of  $R$ )



IMPEDANCE PHASES

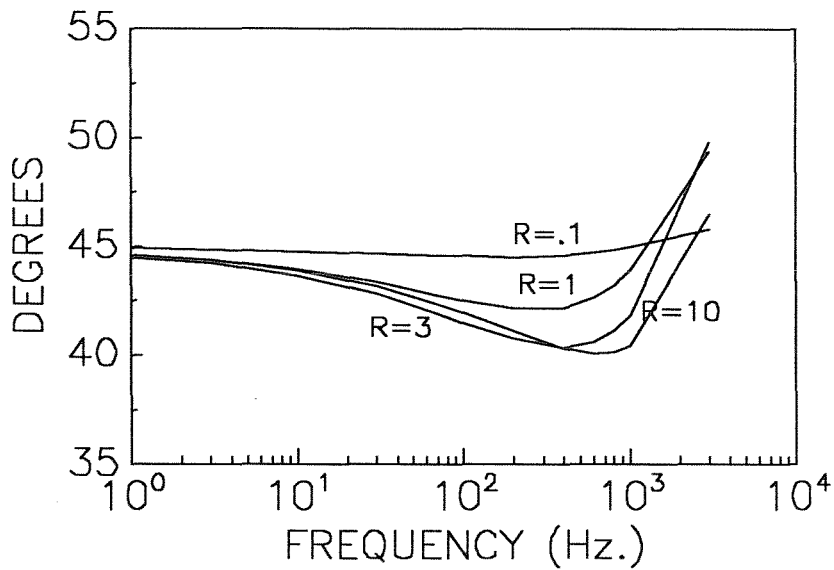


**Figure 2.4:** A comparison of anomalous response for the parameter  $R$ . The structure is the same as in Figure 2.3, above but now  $r$  is fixed at .1 and  $R$  is varied.

thicknesses. Equations 2.56 and 2.55 show that as  $R$  becomes small, the top conductivity ( $\sigma_1$ ) approaches the average conductivity and the bottom layer becomes a very thin but highly resistive layer. Thus as expected, intuitively, the anomalous response decreases as  $R$  becomes small. However, notice that the maximum anomalous response occurs when  $R = 3$  not when  $R$  is largest.

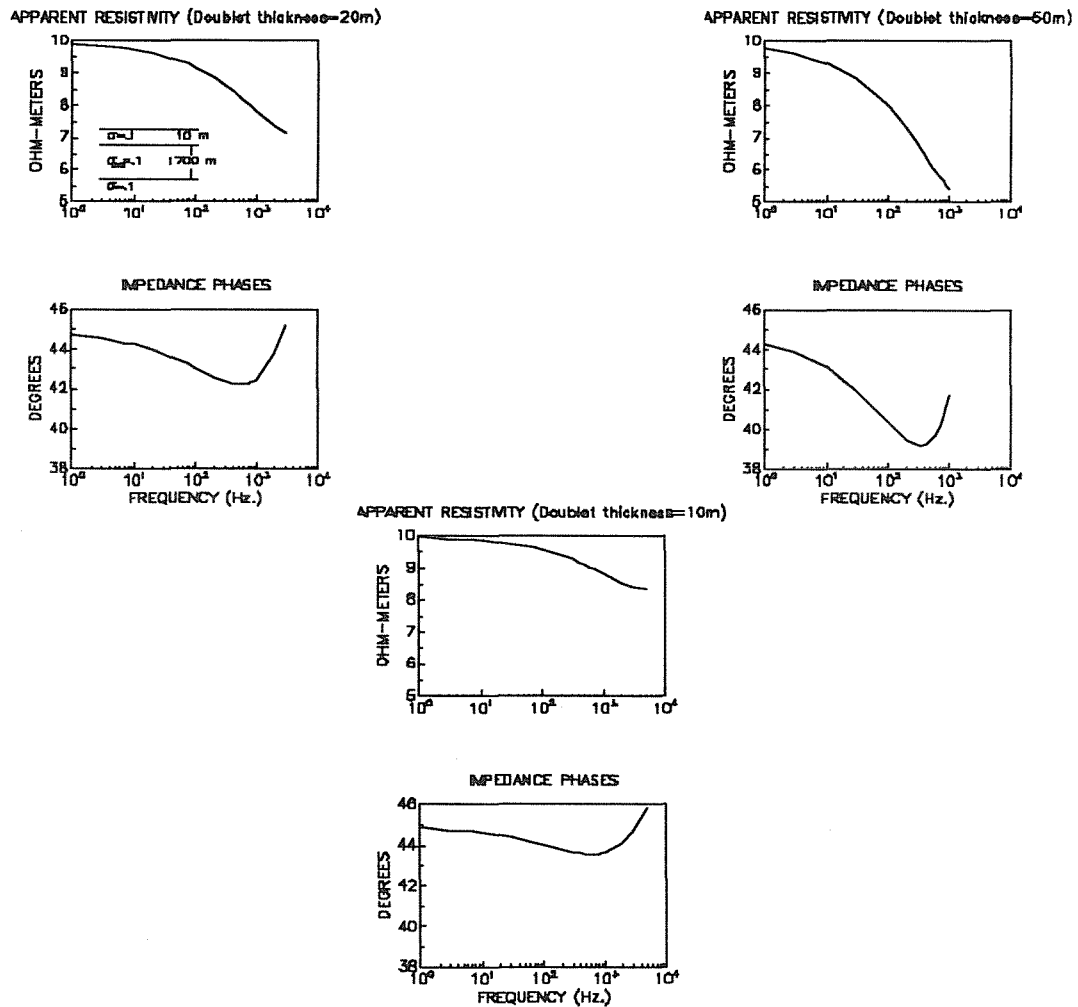


**Figure 2.5:** The effects on impedance of fine layered structure: apparent resistivities and impedance phases as functions of frequency for three doublet thicknesses (10,20 and 50m). The average conductivity of each doublet is  $.1S/m$ . 1700m of the fine structure is buried 10m below the surface in a homogeneously conducting half-space of the same conductivity (.1).

To study the effects of the total doublet thickness and frequency; a fine layering model was used with  $R = 3$  and  $r = .01$  where, according to the previous figures, a significant anomalous response was expected. The same structure was used as in the previous figures but  $L$  was varied. In Figure 2.5, the impedances are shown for three doublet thicknesses,  $L = 10, 20$  and  $50m$ . Recall that for a uniform half-space of the same average conductivity the apparent resistivity would be constant at  $10\Omega m$  while the impedance phase would be constant at 45 degrees. Thus, any variations from these constants indicates a difference between the effective conductivity and the response of the average medium.

Two tables are included to help the reader scrutinize the results of Figure 2.5. Table 2.1 contains the thicknesses and resistivities of each layer in the doublet for the three doublet total thickness,  $L$ . Table 2.2 contains a sampling of relevant skin-depths in the average medium and the top and the bottom layers at 4 frequencies. These tables are included to show that the

Table 2.1:

$L(m)$	$d_1(m)$	$\rho_1(\Omega m)$	$d_2(m)$	$\rho_2(\Omega m)$
10	2.5	2.57	7.5	257
20	5	2.57	15	257
50	12.5	2.57	37.5	257

Layer Depths and Resistivities for 3 Doublet Thicknesses ( $L$ )

Table 2.2:

$\rho(\Omega m)$	3000Hz	1000Hz	500Hz	100Hz
10	29	50	71	159
2.57	15	26	36	80
257	147	255	360	806

Skin Depths(m)

thicknesses of the layers are small compared to skin-depths at the frequencies presented.

The statistical results for the effect of correlation length or doublet thickness is corroborated by Figure 2.5. The decreasing effect of the fine structure with decreasing frequency is also corroborated by this study. First note that the anomalous response, both in magnitude and phase, decreases as the frequency decreases in all curves in Figure 2.5. This is not the effect of the uniform half-space below the fine layering, since 1700 m. is one skin-depth in the average medium at about .9 Hz. A comparison of the responses for the three doublet thicknesses (Figure 2.5) shows that the anomalous response decreases with doublet thickness. Recall that the doublet thickness,  $L$ , in the deterministic model is equivalent to the correlation length,  $\tau_c$  in the statistical model.

Generally, the most significant anomalous responses are the impedance phases, since variations in apparent resistivity of even up to fifty percent are not usually considered important in the study of the Earth's crust. It should however be noted that variations in phase of up to ten degrees were obtained from fine layered structure of this type. This may be relevant in considering that applications of one-dimensional inversion methods often assume errors with phases much less than seen here. It is interesting to note that the maximum anomalous phase response moves up in frequency as the doublet thickness decreases. Also, it is interesting to note that the maximum phase excursion for the 50 m doublet thickness occurs between 300 and 400 Hz. In this frequency range both layers of the doublet are extremely thin compared to a skin-depth in the respective layer (Tables 2.1 and 2.2). Even at a decade less (30-40 Hz.) there is still a significant anomalous impedance response for the 50 m doublet.

## 2.4 Summary

In this chapter, the effects of fine structure in a layered medium has been studied via two methods. Principally these studies were done with the use of a stochastic model but a simple deterministic model was also examined to show that the effects observed are fundamentally those of fine layers, not of their stochastic nature. Both methods confirm that variations in impedance magni-

tude, caused by such fine structure, are probably not normally very significant for studies of the Earth's conductivity structure. However, the impedance phase variations should be considered. These phase variations occur, most significantly, at high frequencies, with large correlation lengths, high average conductivity and when there are high contrasts in conductivity between the beds. The results show that fine bedding can produce an impedance phase response differing from the uniform case by as much as 10 degrees. The effects on the apparent resistivities are less significant. They vary from the uniform model by at most a factor of two.

A conclusion, not surprisingly, of this chapter is that it seems very difficult to make the problem of one-dimensional inversion difficult by introducing irregularities in the conductivity distribution. The concept of an effective bulk medium is a valid one for the one-dimensional problem. One must look elsewhere for real obstacles to the MT technique.



## CHAPTER 3

### H-POLARIZATION INDUCTION IN TWO SEMI-INFINITE SLABS

#### 3.1 Introduction

Although there are a number of efficient two-dimensional modelling programmes available for calculation of electromagnetic induction responses to uniform source fields, analytic solutions to particular problems are always valuable. The effects on the Earth's natural electromagnetic field of vertical contacts of infinite length between two regions of different conductivity are the most studied analytic problem in magnetotellurics ( d'Erceville and Kunetz, 1962, Rankin, 1962, Weaver, 1963, Parker, 1968, Weidelt, 1971, Schmucker, 1970, Bailey, 1977, Dawson and Weaver, 1979). There are a number of important reasons why this is so. The solutions of such problems are of significant geophysical interest when describing changes in apparent resistivity across conductivity discontinuities which reach near or to the Earth's surface. These solutions, for example, are important in explaining the coast effect on geomagnetic variations. Numerical solutions may not be sufficient, in all cases, because of numerical inaccuracies. Thus analytic solutions are essential and also provide an important means for checking numerical programmes.

The H-polarization solution, for a vertical contact between two different homogeneous conducting media, underlain by a half-space of arbitrary but uniform conductivity and excited by a uniform source field, is sought in this chapter (Figure 3.1). The very first analytic solution obtained in magnetotellurics (d'Erceville and Kunetz, G , 1962) was for just this problem, for the particular cases in which the conducting substratum was either a perfect conductor or a perfect insulator. Rankin (1962) adapted this solution to obtain the effects of a conducting inhomogeneity in the shape of a rectangular prism of infinite strike length. These two solutions (d'Erceville and Kunetz, Rankin) have been

used extensively to check the accuracy of numerical methods. However, they are of limited use for this purpose since the theoretical result is restricted to substratum conductivities which are either zero or infinite. More recently, Bailey (1977) and Dawson and Weaver (1979) have studied the same problem when the two semi-infinite slabs could be considered thin sheets (Schmucker, 1970). The remainder of the analytic solutions (Weaver, 1963, Parker, 1968, Schmucker, 1970, Weidelt, 1971) are for the other two-dimensional polarization (E-Polarization). Thus, previous solutions to the inhomogeneity problem addressed in this chapter were restricted to unrealistic basement conductivities (*i.e.* zero or infinite) or to the approximate solution at very low frequencies (*i.e.* thin sheet).

For solutions at the surface of the earth, the d'Erceville and Kunetz solution is adequate for higher frequencies, while the Dawson and Weaver solution is adequate at frequencies low enough that the slabs may be considered thin sheets. This chapter, however, contains an analytic solution for the complete frequency range for any desired lower half-space conductivity. The analyses also provide a more complete proof of the first solution (d'Erceville and Kunetz, 1962) for the case of an infinitely resistive basement. As well, the proof shows that below the Earth's surface the original solution of d'Erceville and Kunetz is not exactly correct in the case of a perfectly conducting substratum since from a rigorous point of view this substratum conductivity also contains a contribution due to a continuous spectrum. The uniqueness of the solution is discussed as well as the nature of its inadequacies. Comparisons to numerical solutions are shown and some interesting geophysical implications are also discussed.

### 3.2 The Boundary Value Problem

The model to be considered is shown in Figure 3.1. The earth's surface ( $z = 0$ ) is taken to be a flat boundary between the atmosphere (considered insulating), and the conducting earth. The earth is assumed to consist of two

semi-infinite slabs of different conductivities ( $\sigma_1, \sigma_2$ ) contacting at  $x = 0$  and bounded below, at  $z = D$ , by a half-space of arbitrary conductivity,  $\sigma_b$ . The magnetic permeability is assumed constant, throughout all space with a value equal to the permeability of free space,  $\mu_0$ .

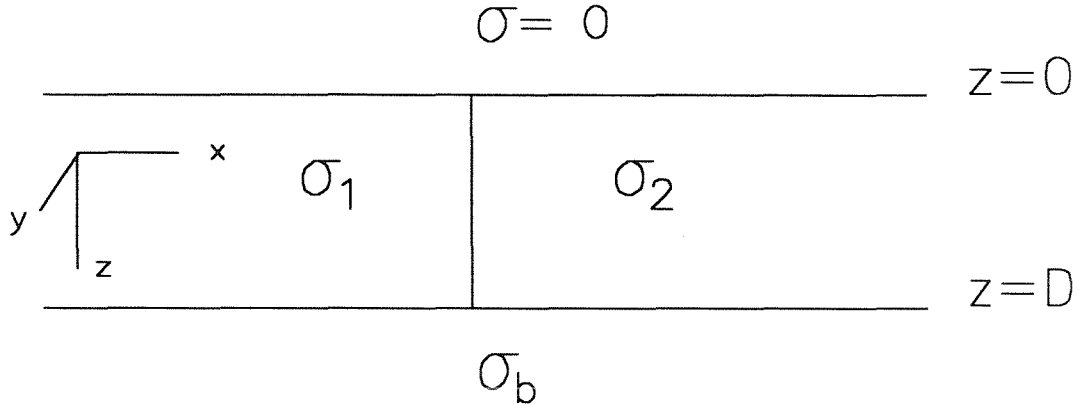


**Figure 3.1:** The Model. Two semi-infinite conducting slabs, over a half-space of arbitrary conductivity under a perfect insulator. The conductivities of the slabs are neither zero nor infinite.

All the physical parameters are thus independent of the coordinate  $y$ . If the electromagnetic source field is also independent of  $y$ , this boundary value problem decouples into two independent modes, which are termed the E and H-Polarizations (Jones and Price, 1970). In the H-polarization mode, the magnetic field has only one component,  $(H_y \hat{y})$  while the electric field has components  $(E_x \hat{x}, E_z \hat{z})$ .

If the magnetic field,  $H_y$ , is sinusoidally varying in time then

$$H_y(x, z) = H(x, z)e^{i\omega t} \quad (3.1)$$

and thus, trivially  $\nabla \cdot \vec{H} = 0$  everywhere. The electric fields, in a region of constant conductivity, are determined from  $H_y$  by the differential form of Ampere's law as

$$\nabla \times H_y \hat{y} = \sigma \vec{E} = \sigma(E_x, 0, E_z) = \left(-\frac{\partial H}{\partial z}, 0, \frac{\partial H}{\partial x}\right), \quad (3.2)$$

where the magnetic effects of displacement currents have been neglected. Utilizing (3.2) and Faraday's law,  $H$  satisfies the Helmholtz equation in the conducting regions

$$\nabla^2 H = \left(\frac{\partial^2}{\partial x^2} + \frac{\partial^2}{\partial z^2}\right) H = i\sigma\mu\omega H = \alpha^2 H. \quad (3.3)$$

Further, if the effects on the magnetic field at the surface of the earth of displacement currents in the air are neglected then from (3.2)

$$\text{when } z = 0, \quad \frac{\partial H}{\partial x} = 0, \quad -\infty < x < \infty.$$

This is obtained from the vanishing of normal current density across the earth's surface. Therefore, at the surface of the earth  $H$  is a constant,

$$H(x, 0) = H_0 \quad (3.4).$$

Since, the effects of the contact on the electromagnetic fields must become zero at infinite distances from the contact

$$H(x, z) \rightarrow H_1^0(z), \quad x \rightarrow -\infty \quad (3.5a)$$

$$H(x, z) \rightarrow H_2^0(z), \quad x \rightarrow +\infty, \quad (3.5b)$$

where  $H_i^0(z)$  are the magnetic fields due only to the layer over the half-space on the respective sides of the contact. Equations (3.1-3.5) are the accepted governing equations and boundary conditions for the H-Polarization.

To obtain a solution I follow the method of d'Erceville and Kunetz (1962) but with modifications and clarifications. Thus, let

$$H_i(x, z) = H_i^0(z) + P_i(x, z), \quad i = 1, 2, \quad (x, z) \in \mathcal{D}_i \quad (3.6)$$

where

$$\mathcal{D}_1 = \{(x, z), -\infty < x \leq 0, 0 \leq z \leq D\} \quad (3.7a)$$

$$\mathcal{D}_2 = \{(x, z), 0 \leq x < \infty, 0 \leq z \leq D\}. \quad (3.7b)$$

Since, both  $H_i$  and  $H_i^0$  satisfy the Helmholtz equation (3.2) inside their respective regions, then from (3.3) and (3.6)

$$\nabla^2 P_i(x, z) = \alpha_i^2 P_i, \quad i = 1, 2. \quad (3.8)$$

From (3.4, 3.5) and (3.6)

$$P_i(x, 0) = 0, \quad i = 1, 2, \quad \forall x \quad (3.9)$$

and from (3.5)

$$P_i(x, z) \rightarrow 0 \quad \text{as} \quad |x| \rightarrow \infty. \quad (3.10)$$

The vertical electric field must also go to zero as  $|x|$  becomes infinite. Thus, both  $P_i$  and its normal derivative are specified at infinity. The boundary is closed (Morse and Feshbach, 1953, Chapter 6), in the terms of the theory of partial differential equations, since the domain of  $z$  is finite, the domain of  $x$  is semi-infinite, and the value and normal derivatives are specified at infinity in  $x$ .

One also requires additional electromagnetic boundary conditions at the contact interface ( $x = 0$ ). The continuity of tangential magnetic field requires (3.6)

$$P_1(0, z) - P_2(0, z) = H_2^0(z) - H_1^0(z) \quad , \quad 0 \leq z \leq D \quad (3.11a)$$

while the continuity of tangential electric fields requires from (3.2)

$$\frac{1}{\sigma_1} \frac{\partial P_1}{\partial x} = \frac{1}{\sigma_2} \frac{\partial P_2}{\partial x} \quad , \quad \text{for} \quad x = 0 \quad 0 \leq z \leq D. \quad (3.11b)$$

The continuity of normal current across the contact is trivially satisfied. To see this, note that by (3.2) the continuity of normal current density requires

the continuity of vertical derivative of the total magnetic field. Since the total magnetic field is continuous for all  $z$  on the contact, the vertical derivative must also be continuous across the contact except possibly at the intersection  $(0,D)$ . At  $z = D$ , for most cases the vertical derivative does not actually exist.

The Helmholtz operator (3.8) is elliptic and thus for a closed boundary with constant  $\alpha_i$ , either Dirichlet (value specified) or Neumann (slope specified) boundary conditions give a unique and stable solution. Cauchy boundary conditions (slope and value specified) will overspecify the solution (Morse and Feshbach, pg 706). From equations (3.9-11), note that there is a mixture of boundary conditions. At  $|x| = \infty$ , Cauchy boundary conditions apply, at  $z = 0$  Dirichlet conditions (3.9) apply while at  $x = 0$  there is (3.11) a modification of Cauchy conditions. Except for the two cases when the basement conductivity is either zero or infinite or unless one satisfies the problem in the lower half-space, there are no boundary conditions which can be applied at  $z = D$  (except at the endpoints,  $x = 0$  and  $|x| = \infty$ ). This is because the fields are unknown on this boundary. I will now proceed to outline a method for obtaining solutions which does not require solving the problem in the basement. The adequacy of these solutions will then be investigated.

### 3.3 Separability and the Eigenfunctions

No theoretical guide was found to the boundary value problem which has been described above. Problems with semi-bounded domains and mixed boundary conditions are not generally available. A comprehensive theory therefore had to be developed for the general problem as well as the particular solution needed here. This section is somewhat more broad than the problem at hand as it develops the general theory for the required solution.

Solutions are sought, within the domains  $\mathcal{D}_i$ , for the differential equations

$$\frac{\partial^2 P_i}{\partial x^2} + \frac{\partial^2 P_i}{\partial z^2} - \alpha_i^2 P_i = 0, \quad i = 1, 2 \quad (3.12)$$

where  $\alpha_i$  is constant in region  $i$ . These differential equations are separable in rectangular coordinates (Morse and Feshbach, pp. 498), and since the surface

$z = 0$  is a *nodal surface* ( $P_i = 0$ ) this is also an appropriate coordinate system for solution (M and F, pp. 497).

A separable solution has the form

$$\chi_i = X_i(x)Z_i(z) \quad (3.13)$$

Substitution of (3.13) in (3.12) leads to

$$\frac{1}{X_i} \frac{d^2 X_i}{dx^2} + \frac{1}{Z_i} \frac{d^2 Z_i}{dz^2} - \alpha_i^2 = 0 \quad (3.14)$$

if  $\chi_i$  is bounded and non-zero. (The solution of (3.12) will be bounded within each region but not necessarily at boundaries.) Since the first term is a function of  $x$  only, while the second term is a function of  $z$  only and the third is a constant, the above equation implies that each term in the equation is independent of position (constant) and that their sum is zero. That is

$$\frac{1}{Z_i} \frac{d^2 Z_i}{dz^2} = -\lambda^2 \quad (3.15a)$$

$$\frac{1}{X_i} \frac{d^2 X_i}{dx^2} = \alpha_i^2 + \lambda^2 = \beta^2 \quad (3.15b)$$

or

$$\frac{1}{Z_i} \frac{d^2 Z_i}{dz^2} = \alpha_i^2 + \lambda^2 = \beta^2 \quad (3.15c)$$

$$\frac{1}{X_i} \frac{d^2 X_i}{dx^2} = -\lambda^2 \quad (3.15d)$$

where  $\lambda^2$  is termed the separation constant. The family of separable solutions consists of products of solutions of (3.15a) and (3.15b) where each product has a different separation constant. The general solution of (3.12) can be expressed as a linear combination of elements from the set of separable solutions (M and F, pp.498). The eigenfunctions and eigenvalues of (3.15) which contribute to the solution (the *spectrum*), must now be determined. The spectrum may be either a continuous set of points (continuous spectrum) or a set of discrete points (point spectrum) or contain both a continuous and a point-spectrum

(Titchmarsh,1962). If the spectrum is discrete, there may be either a finite or an infinite number of points in the spectrum.

To determine the eigenfunctions and spectrum, let us consider the analogous problem of a membrane which satisfies the Helmholtz equation on a box (Figure 3.2). Recall that for the elliptic operator and a closed boundary, Dirichlet boundary conditions uniquely determine a solution. Therefore, there exists a unique solution to the following boundary value problem,

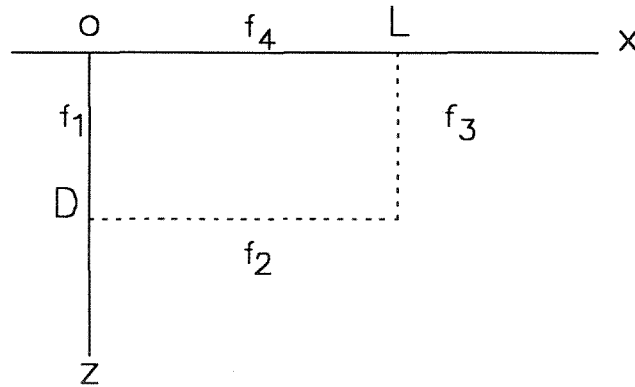


Figure 3.2: An analogous problem on a box.

$$u_{xx} + u_{zz} = k^2 u, \quad 0 < z < D, 0 < x < L \quad (3.16a)$$

$$u(z, 0) = f_1(z), \quad 0 < z < D \quad (3.16a)$$

$$u(D, x) = f_2(x), \quad 0 < x < L \quad (3.16b)$$

$$u(z, L) = f_3(z), \quad 0 < z < D \quad (3.16c)$$

$$u(0, x) = f_4(x), \quad 0 < x < L. \quad (3.16d)$$

The solution can be given by separation of variables (3.15) as

$$u(z, x) = u_1(z, x) + u_2(z, x) + u_3(z, x) + u_4(z, x) \quad (3.17)$$

where

$$u_1(z, x) = \sum_{n=1}^{\infty} c_n^{(1)} \sin \frac{n\pi z}{D} \sinh \beta_n (L - x), \quad c_n^{(1)} = \frac{2}{D \sinh \beta_n L} \int_0^D f_1(s) \sin \frac{n\pi s}{D} ds \quad (3.18a)$$

$$u_2(z, x) = \sum_{n=1}^{\infty} c_n^{(2)} \sin \frac{n\pi x}{L} \sinh \beta_n z, \quad c_n^{(2)} = \frac{2}{L \sinh \beta_n D} \int_0^L f_2(s) \sin \frac{n\pi s}{L} ds \quad (3.18b)$$

$$u_3(z, x) = \sum_{n=1}^{\infty} c_n^{(3)} \sin \frac{n\pi z}{D} \sinh \beta_n x, \quad c_n^{(3)} = \frac{2}{D \sinh \beta_n L} \int_0^D f_3(s) \sin \frac{n\pi s}{D} ds \quad (3.18c)$$

$$u_4(z, x) = \sum_{n=1}^{\infty} c_n^{(4)} \sin \frac{n\pi x}{L} \sinh \beta_n (D - z), \quad c_n^{(4)} = \frac{2}{L \sinh \beta_n D} \int_0^L f_4(s) \sin \frac{n\pi s}{L} ds \quad (3.18d)$$

where by (3.15)  $\beta_n^2 = k^2 + (\frac{n\pi}{D})^2$  in (3.18a) and (3.18c) and  $\beta_n^2 = k^2 + (\frac{n\pi}{L})^2$  in (3.18b) and (3.18d). The solution satisfies (3.16) and thus is the unique solution in the set of solutions which can be represented as an infinite sum (3.18). For example, in the one-dimensional problem the Fourier expansion can adequately approximate a function if there is a finite number of discontinuities in the interval and if the function is bounded. In the same sense, one would expect such a solution (3.18) to satisfy the boundary value problem (3.16). With the elliptic operator, infinite discontinuities decay rapidly from single points and thus such a representation (3.18) would adequately express the function except at or near a finite number of discontinuities or singularities.

Let us examine the membrane problem (3.16) as the domain of  $x$  increases to infinity. Let  $f_4(x) = 0$ , as in the electromagnetic problem being considered when  $P_i = 0$  at the Earth's surface. This requires

$$c_n^{(4)} = 0, \quad \forall n. \quad (3.19)$$

Second, let us assume that

$$f_2(L) \rightarrow 0 \quad \text{as} \quad L \rightarrow \infty \quad (3.20)$$

and furthermore that, beyond some value for  $x$ ,  $f_2$  decays exponentially. (This is a reasonable assumption for the secondary magnetic field.) Actually, for the

next result this requirement can be weakened, as it is merely required that the inner products of  $f_2$  with the sine eigenfunctions remain bounded

$$\lim_{L \rightarrow \infty} \left| \int_0^L f_2(s) \sin \frac{n\pi s}{L} ds \right| < \infty$$

and therefore by (3.18b)

$$c_n^{(2)} \rightarrow 0, \quad L \rightarrow \infty, \quad \forall n. \quad (3.21)$$

Also, note that even as  $L \rightarrow \infty$

$$\left| \sin \frac{n\pi x}{L} \right| \leq 1, \quad \forall x$$

and it would appear that

$$u_2(z, x) \rightarrow 0, \quad \forall (z, x) \quad \text{as } L \rightarrow \infty. \quad (3.22)$$

This would imply that the lower boundary condition does not influence the solution! However, as will be shown later, (3.22) is not always correct. The significance of the contribution due to  $u_2$  will be discussed more fully below.

Now combine (3.18a) and (3.18c) to give

$$\begin{aligned} u_1(z, x) + u_3(z, x) &= \frac{1}{2} \sum_{n=1}^{\infty} \sin \frac{n\pi z}{D} \\ &\times \left[ (c_n^{(1)} e^{\beta_n L} - c_n^{(3)}) e^{-\beta_n x} - (c_n^{(1)} e^{-\beta_n L} - c_n^{(3)}) e^{\beta_n x} \right]. \end{aligned} \quad (3.23)$$

It can be shown that only one term actually remains in (3.23) as the domain of  $x$  is extended to infinity (*i.e.*  $L \rightarrow \infty$ ) if it is required that  $f_3(z) \rightarrow 0$  as  $L$  goes to infinity as in the EM problem. Thus, as  $L \rightarrow \infty$

$$|c_n^{(3)} e^{\pm \beta_n L}| \leq \frac{2}{D} \int_0^D |f_3(s)| ds \rightarrow 0, \quad \forall n \quad (3.24)$$

and therefore the two terms containing  $c_n^{(3)}$  go to zero in (3.23). Considering the two terms containing  $c_n^{(1)}$ ;

$$|c_n^{(1)} e^{-\beta_n L} e^{\beta_n x}| \leq |c_n^{(1)}| \rightarrow 0, \quad \forall n \quad (3.25)$$

by (3.18a) under the reasonable assumption that  $f_1(z)$  is singular only on a set of measure zero (*i.e.* singular only at a finite or infinite number of discrete points).

However,

$$c_n^{(1)} e^{\beta_n L} e^{-\beta x} = \frac{4e^{-\beta_n x}}{D(1 - e^{-2\beta_n L})} \int_0^D f_1(s) \sin \frac{n\pi s}{D} ds \quad (3.26a)$$

$$\xrightarrow{L \rightarrow \infty} \frac{4e^{-\beta_n x}}{D} \int_0^D f_1(s) \sin \frac{n\pi s}{D} ds. \quad (3.26b)$$

Therefore by (3.19, 3.21) and (3.23-3.26)

$$u(z, x) = \sum_{n=1}^{\infty} c_n \sin \frac{n\pi z}{D} e^{-\beta_n x} \quad (3.27)$$

where

$$c_n = \frac{2}{D} \int_0^D f_1(s) \sin \frac{n\pi s}{D} ds. \quad (3.28)$$

It follows then, that as  $L$  is extended to infinity a set of discrete eigenvalues (3.15a) or spectrum (*i.e.*  $n(\frac{\pi}{D})$ ) is retained.

Although

$$u(z, x) \rightarrow 0 = f_3(z), \quad \text{as } x \rightarrow \infty \quad (3.29a)$$

$$u(0, x) = 0 = f_4(x), \quad (3.29b)$$

$$u(z, 0) = f_1(z), \quad (3.29c)$$

as required, when  $z = D$

$$u(D, x) = \sum_{n=1}^{\infty} c_n \sin(n\pi) e^{-\beta_n x} = 0 \neq f_2(x)$$

and the solution will not necessarily satisfy the lower boundary condition. This implies that the solution cannot always be represented correctly with only a point-spectrum as the domain of  $x$  increases to infinity. The question then arises as to how a continuous set of eigenvalues (continuous spectrum) arises and what is the nature of the error when it is neglected.

Returning to look at equation (3.17), it was shown that  $u_4 = 0$ , everywhere (3.18d). While from the previous analysis,  $u_1 + u_3$  is adequately represented by a discrete spectrum and thus by (3.27). Upon closer investigation of  $u_2$ , one notices (3.18b) that as the domain of  $x$  goes to infinity the spectral density becomes continuous as  $\frac{n\pi}{L} \rightarrow 0$  while  $c_n^{(2)} \rightarrow 0$  (3.21). Thus, the error in the solution is exactly  $|u_2(z, x)|$ . However,

$$u_2(0, x) = 0, \quad \forall x \tag{3.30a}$$

$$u_2(z, 0) = 0, \quad \forall z \tag{3.30b}$$

$$u_2(z, x) \rightarrow 0 \quad x \rightarrow \infty \tag{3.30c}$$

independent of  $L$  and thus the solution is correct and unique on the surface of the earth, at the contact and as  $|x| \rightarrow \infty$ . Note also that in the case of a perfectly insulating basement,  $f_2$  will be exactly zero and thus so will  $u_2$ . Therefore, in this case, there is no need for a continuous spectrum. This is one of the substrata considered by d'Erceville and Kunetz (1962).

One can analyse more exactly the magnitude of  $u_2$  and thus the error. In principle, if  $u_2$  is known on  $z = D$  then it is known everywhere. From (3.18a), for finite  $L$

$$u_2(z, x) = \sum_{n=1}^{\infty} \sin \frac{n\pi x}{L} \frac{\sinh \beta_n z}{\sinh \beta_n D} \frac{2}{L} \int_0^L f_2(s) \sin \frac{n\pi s}{L} ds. \tag{3.31}$$

Note again that  $u_2$  is zero on the surfaces  $z = 0, x = 0$  and  $x = L$ . As a function of  $z$ ,  $|u_2(x)|$  has its maximum at the boundary  $z = D$  since  $|\sinh \beta_n z|$  is an increasing function of  $z$ .

To examine  $u_2$  when  $L$  is infinite, an informative example is the case where the solution decays exponentially along the bottom surface. That is,

$$f_2(x) = u(D, 0)e^{-\alpha x} = u(D, x). \tag{3.32}$$

Then, using (3.31) for  $L$  finite:

$$u_2(D, x) = 2\pi u(D, 0) \sum_{n=1}^{\infty} \sin \frac{n\pi x}{L} \frac{n(1 - e^{-\alpha L})}{\alpha^2 L^2 + n^2 \pi^2}$$

$$= \frac{2}{\pi} u(D, 0) \sum_{n=1}^{\infty} \sin q_n x \frac{q_n}{\alpha^2 + q_n^2} (1 - e^{-\alpha L}) q_0$$

where  $q_0 = \frac{\pi}{L}$ ,  $q_n = nq_0$ . Now letting  $L \rightarrow \infty$ ,  $u_2$  can be expressed as a sine transformation:

$$u_2(D, x) = \frac{2}{\pi} u(D, 0) \int_0^{\infty} \sin(qx) \frac{q}{\alpha^2 + q^2} dq. \quad (3.33)$$

This is obviously the transformation of  $\frac{q}{\alpha^2 + q^2}$ , which is itself the sine transform of  $u_2(D, x)$ . In general, the error in the semi-unbounded problem (*i.e.*  $L = \infty$ ) is given by

$$u_2(z, x) = \frac{2}{\pi} \int_0^{\infty} \sin(qx) \frac{\sinh \beta(q)z}{\sinh \beta(q)D} \hat{u}_2(D, q) dq \quad (3.34)$$

where  $\beta(q) = \sqrt{q^2 + k^2}$  and  $\hat{u}_2(D, q)$  is the sine transform of  $u_2(D, x)$  or  $u(D, x)$ . Therefore, if  $u_2(D, x)$  is known, the complete solution can be found from (3.34).

It is now possible to consider the second case solved by d'Erceville and Kunetz (1962). In this instance, the basement is considered infinitely conducting and therefore the normal derivative of the secondary magnetic field is zero on the boundary,  $z = D$  but the magnetic field is not zero.  $u_2$  is therefore not zero and the contribution of the continuous spectrum is not obviously zero as was assumed by d'Erceville and Kunetz.

The appropriateness of the Fourier solution is of course dependent on the nature of the discontinuities and singularities in the function one wishes to represent. The function is required to be continuous except at a finite number of points (piecewise continuous). As well, the Fourier solution can only approximately represent the solution at singularities. No singularities are expected in the EM problem except possibly in the derivatives at the intersections  $(0, 0)$  and  $(D, 0)$  (Dawson and Weaver, 1979).

### 3.4 The Solution

I wish now to obtain the solution to the original electromagnetic problem utilizing only the point or discrete spectrum but keeping in mind the nature of the error by not including the continuous spectrum. That is, the solution is exact at the surface,  $z = 0$  but has an error as  $z$  increases. From the considerations of the previous sections, the perturbed magnetic field is expressed as

$$P_i(x, z) = \sum_{n=1}^{\infty} [A_{in} \sin(\lambda_n z)] e^{\pm \beta_{in} x}, i = 1, 2 \quad (3.35a)$$

where  $\beta_{in}^2 = \alpha_i^2 + \lambda_n^2$ . The secondary electric fields are given by (3.2)

$$E_{s,i}^x(x, z) = \frac{-1}{\sigma_i} \sum_{n=1}^{\infty} \lambda_n [A_{in} \cos(\lambda_n z)] e^{\pm \beta_{in} x} \quad (3.35b)$$

$$E_i^z(x, z) = \frac{\pm 1}{\sigma_i} \sum_{n=1}^{\infty} \beta_{in} [A_{in} \sin(\lambda_n z)] e^{\pm \beta_{in} x} \quad (3.35c)$$

but only if the derivatives can be obtained by term by term differentiation.

Now, reconsider the eigenvalues  $\lambda_n$  and thus the periodicity of  $P_i$ . Since all the perturbed electromagnetic fields are to be obtained by a Fourier expansion, the problem of convergence must be considered. As well, a means to estimate the function  $u_2$  which comes from the continuous spectrum is desired. Especially at the end points of the domain of expansion, continuity of the perturbed magnetic field is required. This will ensure that the expansion (3.35a) converges uniformly in  $z$  throughout the interval. Uniform convergence is essential so that one may obtain the vertical derivative of the perturbed magnetic field, and therefore the secondary horizontal electric field, by differentiation everywhere in the interval of expansion. That is, if (3.35a) converges uniformly throughout its period then the sum of the term by term derivatives of (3.35b) with respect to  $z$  will also converge. It is also required that the vertical derivative of  $P_i$  be continuous at the endpoints. If the vertical derivative were discontinuous, then there would be inaccuracies near the discontinuity, overshoots or undershoots at the corners (Gibbs' phenomenon) and the perturbed

horizontal electric field will converge, at  $z = 0$ , but only to the mean of the values at the two endpoints of the  $z$ -domain. Since one wishes to evaluate the fields correctly at the Earth's surface to obtain the impedance, this continuity is essential. It is important to note that convergence of the expansion for the vertical derivatives of the  $P_i$  is ensured but not uniform convergence. Thus, discontinuities in the derivatives of  $P_i$  will cause Gibbs' effects in the secondary horizontal electric field. However, it is ensured that there are no such effects at the surface  $z = 0$ . This is essential since this is the surface on which MT measurements are made. It is therefore required that

$$P_i(x, 0) = P_i(x, T) \quad , \quad i = 1, 2 \quad (3.36a)$$

$$\frac{\partial P_i}{\partial z} \Big|_{(x,0)} = \frac{\partial P_i}{\partial z} \Big|_{(x,T)} \quad , \quad i = 1, 2 \quad (3.36b)$$

where  $T$  is the periodicity.

$P_i(x, z)$  must be extended to a larger domain, in  $z$ , than  $(0, D)$  in order to obtain an expansion that ensures (3.36). This was done by d'Erceville and KUNETZ, possibly unknowingly, in the case of the perfectly conducting basement. The above requirements (3.36) are satisfied if the perturbed magnetic field,  $P_i$ , is periodic in  $4D$  ensuring (3.36a) and antisymmetric about  $z = 2D$  ensuring (3.36b). Thus, extending the entire problem to  $z \in [0, 4D]$  with the layered or primary fields ( $H_i^0$ ) being antisymmetric about  $z = 2D$  ensures the required results. The boundary conditions at the contact and at infinity are the same as for the smaller domain (3.5, 3.11). Therefore, the eigenfunctions of (3.35a) have the form,

$$\sin\left(\frac{n\pi z}{2D}\right). \quad (3.37)$$

The boundary value problem is summarized in (3.46a-e).

In the cases of a perfectly conducting or insulating substratum, the present formulation of the boundary value problem reduces to the formulations used by d'Erceville and KUNETZ in their original solutions. The problem of convergence of the perturbed magnetic field and the correct convergence of its vertical derivative were never considered by these authors. It was fortunate that their

considerations of the boundary conditions at the interface of the lower half-space gave the continuity which was required. Note that if only even values of  $n$  are used (3.37) then the solution is that of (3.18) and necessarily  $P_i = 0$  at  $z = D$  and thus one has completely neglected the error function  $u_2$  (3.31). However, the inclusion of odd  $n$  allows us to estimate the contribution due to continuous spectra. Remember of course that the contribution of the continuous spectrum is zero at the surface  $z = 0$  and the odd point-spectrum does not contribute here.

The Fourier coefficients  $A_{in}$  are obtained by applying electromagnetic boundary conditions at the contact  $x = 0$  (3.11). The continuity of the tangential magnetic field  $H$  and the tangential electric field  $E_z$  across the interface  $x = 0$  results in the equations

$$H_1^0(z) + \sum_n A_{1n} \sin\left(\frac{n\pi z}{2D}\right) = H_2^0(z) + \sum_n A_{2n} \sin\left(\frac{n\pi z}{2D}\right) \quad (3.38)$$

and

$$\frac{1}{\sigma_1} \sum_n \beta_{1n} A_{1n} \sin\left(\frac{n\pi z}{2D}\right) = -\frac{1}{\sigma_2} \sum_n \beta_{2n} A_{2n} \sin\left(\frac{n\pi z}{2D}\right) dz, \quad (3.39)$$

for  $z \in [0, 4D]$ .

Utilizing these equations and the orthogonality of the sine functions, from (3.38)

$$c_n = \frac{1}{2D} \int_0^{4D} (H_1^0(z) - H_2^0(z)) \sin\left(\frac{n\pi z}{2D}\right) dz = A_{2n} - A_{1n} \quad (3.40)$$

and from (3.39)

$$\frac{\beta_{1n} A_{1n}}{\sigma_1} = -\frac{\beta_{2n} A_{2n}}{\sigma_2}. \quad (3.41)$$

Thus, (3.40,3.41) imply:

$$A_{1n} = \frac{-\sigma_1 c_n}{\sigma_2 \frac{\beta_{1n}}{\beta_{2n}} + \sigma_1} \quad (3.42a)$$

$$A_{2n} = \frac{\sigma_2 c_n}{\sigma_1 \frac{\beta_{2n}}{\beta_{1n}} + \sigma_2}. \quad (3.42b)$$

The continuity of normal  $\vec{J}$  is ensured at the contact since

$$H_1(0, z) = H_2(0, z) \quad , \quad 0 \leq z \leq 4D \quad (3.43a)$$

and by (3.2), the horizontal current density (normal to the contact) is the negative of the vertical derivative of the total magnetic field. Therefore

$$\frac{\partial H_1}{\partial z} \Big|_{(0,z)} = \frac{\partial H_2}{\partial z} \Big|_{(0,z)}, \quad 0 \leq z < 4D. \quad (3.43b)$$

### 3.5 Layered Solutions

If a layer of conductivity  $\sigma_i$  and thickness  $D$  overlies a half-space of conductivity  $\sigma_b$ , where neither  $\sigma_i$  nor  $\sigma_b$  are zero or infinite, the magnetic and electric fields in the upper layer can be expressed as

$$H_i^0(z) = H_0 \frac{[\kappa_i e^{\alpha_i z} + e^{-\alpha_i z}]}{\kappa_i + 1}, \quad 0 \leq z \leq D, \quad (3.44a)$$

$$E_{x_i}^0(z) = H_0 \frac{\alpha_i [-\kappa_i e^{\alpha_i z} + e^{-\alpha_i z}]}{\sigma_i (\kappa_i + 1)} \quad (3.44b)$$

where

$$\kappa_i = \zeta_i e^{-2\alpha_i D} \quad , \quad \zeta_i = \frac{R_i - 1}{R_i + 1} \quad , \quad R_i = \sqrt{\frac{\sigma_b}{\sigma_i}} \quad \text{and} \quad H_i^0(0) = H_0. \quad (3.45)$$

These expressions (3.44,3.45) are suitable for basement conductivities of either zero or infinity. For it can be shown that the limits of (3.44a) and (3.44b) as  $\sigma_b \rightarrow 0$  or  $\sigma_b \rightarrow \infty$  exist and are equal to the above expressions when  $\zeta_i = -1$ , ( $R_i = 0$ ) or  $\zeta_i = 1$ , ( $R_i = \infty$ ).

To extend the problem to the larger domain  $(0, 4D)$ , the normal (layered solution) magnetic fields are continued analytically via (3.44a) to the domain  $z \in [0, 2D]$  and then via antisymmetry to  $z \in [0, 4D]$ . Therefore one can obtain the Fourier coefficients,  $c_n$  (3.40).

### 3.6 The Uniqueness of the Solution

As mentioned earlier, no theoretical framework was found for this boundary value problem with the particular type of boundary conditions required here. It must therefore be verified that the solution obtained is unique. It must be ensured that not merely a solution was found but that *the* only solution was obtained.

The solution space is the set of bounded, differentiable functions with bounded derivatives. The solution given by (3.35a) is obviously bounded and differentiable on the given domains,  $\mathcal{D}_i$ . The completeness of the solution space is given by Fourier theory and the theory of partial differential equations in separable co-ordinates. That is, the sequence of functions formed by finite sums of Fourier components converges to a solution within the space of bounded and differentiable functions. In fact, the solution is unique up to discrete spectra in the solution space, as will be proven below.

$P_i(x, z)$  ,  $i = 1, 2$ , must satisfy the conditions

$$P_1 \rightarrow 0, x \rightarrow -\infty \quad P_2 \rightarrow 0, x \rightarrow +\infty \quad , \quad (3.46a)$$

$$P_i(x, 0) = 0 \quad , \quad i = 1, 2 \quad (3.46b)$$

$$\nabla^2 P_i = \alpha_i^2 P_i \quad , \quad i = 1, 2 \quad (3.46c)$$

$$P_1(0, z) - P_2(0, z) = H_2^0(z) - H_1^0(z) \quad , \quad 0 \leq z \leq D \quad (3.46d)$$

$$\frac{1}{\sigma_1} \frac{\partial P_1}{\partial x} = \frac{1}{\sigma_2} \frac{\partial P_2}{\partial x} \quad , \quad x = 0 \quad 0 \leq z \leq D \quad (3.46e)$$

Suppose the solution is not unique. Then there exists solutions  $\hat{P}_i$  of the above equations such that

$$\hat{P}_i(x, z) = P_i(x, z) + h_i(x, z) \quad (3.47)$$

where  $P_i$  is the solution given by the above method and  $h_i(x, z) \neq 0$  somewhere in the domain  $\mathcal{D}_i$ .

Upon substitution of (3.47) in (3.46), it can be shown that

$$h_1 \rightarrow 0, x \rightarrow -\infty \quad h_2 \rightarrow 0, x \rightarrow +\infty \quad (3.48a)$$

$$\nabla^2 h_i = \alpha_i^2 h_i \quad , \quad i = 1, 2, \quad (3.48b)$$

$$h_i(x, 0) = 0 \quad , \quad i = 1, 2 \quad (3.48c)$$

$$h_1(0, z) = h_2(0, z) \quad , \quad 0 \leq z \leq D, \quad (3.48d)$$

$$\frac{1}{\sigma_1} \frac{\partial h_1}{\partial x} = \frac{1}{\sigma_2} \frac{\partial h_2}{\partial x} \quad , \quad x = 0 \quad , \quad 0 \leq z \leq D. \quad (3.48e)$$

Suppose that the functions  $h_i$  are bounded. Then, the boundary value problem for the  $h_i$  are separable and  $h_i$  has a solution of the form

$$h_i(x, z) = \sum_n \chi_{in}(x) \phi_{in}(z) \quad , \quad i = 1, 2 \quad (3.49)$$

such that

$$\frac{1}{\chi_{in}} \chi_{in}'' + \frac{1}{\phi_{in}} \phi_{in}'' = \alpha_i^2 \quad (3.50)$$

where  $'$  implies differentiation with respect to the appropriate variable.  $\chi_{in}$  and  $\phi_{in}$  satisfy the differential equations

$$\frac{1}{\chi_{in}} \chi_{in}'' = -\lambda_n^2 \quad (3.51a)$$

$$\frac{1}{\phi_{in}} \phi_{in}'' = (\alpha_i^2 + \lambda_n^2) = \beta_{in}^2. \quad (3.51b)$$

Since  $\phi$  is defined over a finite domain then there exists an infinitely denumerable set of solutions to (3.51a) such that

$$\phi_{in}(z) = a_{in} \cos(\lambda_n z) + b_{in} \sin(\lambda_n z) \quad n = 1, \infty. \quad (3.52)$$

The boundary condition as  $x \rightarrow \pm\infty$  requires for all  $n$

$$\chi_{1n}(x) = A e^{\beta_{1n} x} \quad (3.53a)$$

and

$$\chi_{2n}(x) = B e^{-\beta_{2n} x}. \quad (3.53b)$$

The square root of  $\beta_{1n}^2$  is chosen such that as  $\lambda_n \rightarrow \infty$  then  $\beta_{1n} \rightarrow +\lambda_n$ .

Thus, the solutions for the  $h_i$  are

$$h_1(x, z) = \sum_{n=1}^{\infty} [a_{1n} \cos(\lambda_n z) + b_{1n} \sin(\lambda_n z)] e^{\beta_{1n} x} \quad (3.54a)$$

and

$$h_2(x, z) = \sum_{n=1}^{\infty} [a_{2n} \cos(\lambda_n z) + b_{2n} \sin(\lambda_n z)] e^{-\beta_{2n} x}. \quad (3.54b)$$

Applying the condition that  $h_1 = h_2$  along the contact and using the orthogonality of the sinusoidal functions implies that

$$a_{1n} = a_{2n} \quad \text{and} \quad b_{1n} = b_{2n} \quad (3.55)$$

Utilizing this result and the continuity of the vertical electric field across the contact one concludes that

$$\frac{\beta_{1n}}{\sigma_1} a_{1n} = -\frac{\beta_{2n}}{\sigma_2} a_{1n} \quad , \quad (3.56a)$$

$$\frac{\beta_{1n}}{\sigma_1} b_{1n} = -\frac{\beta_{2n}}{\sigma_2} b_{1n} \quad . \quad (3.56b)$$

Thus, if  $a_{1n} \neq 0$  or  $b_{1n} \neq 0$ , then

$$\frac{\beta_{1n}}{\sigma_1} = -\frac{\beta_{2n}}{\sigma_2} \quad , \quad n = 1, \infty \quad (3.57a)$$

or

$$\frac{\sqrt{i\sigma_1\mu\omega + \lambda_n^2}}{\sigma_1} = -\frac{\sqrt{i\sigma_2\mu\omega + \lambda_n^2}}{\sigma_2} \quad (3.57b)$$

which clearly is false if  $\sigma_1 \neq \sigma_2$ . Therefore,

$$a_{1n} = a_{2n} = b_{1n} = b_{2n} = 0 \quad , \quad n = 1, \infty \quad (3.58)$$

and  $h_1$  and  $h_2$  are zero everywhere, and the solution is unique in the set of bounded, differentiable functions. If the function is nondifferentiable and/or unbounded, the closest estimate in the solution space will be obtained in the sense of an integral metric or distance. The electromagnetic fields are expected

to be well-behaved (*i.e.* differentiable and bounded) except possibly at single points.

In the cases of the infinitely resistive and conducting basements, no mention was made by d'Erceville and Kunetz of the presence of singularities in the electromagnetic fields in or on the boundaries of the finite conducting slabs. They assumed that the true fields are contained within the solution space and thus expected the accuracy of the answer to depend only on the number of Fourier terms.

### 3.7 The Fourier Coefficients and Convergence

The Fourier coefficients will now be determined to ensure that the solutions in fact converge and the rate in which they converge. This will allow for evaluation of the solution by computer and investigation of accuracy when only a finite sum of terms are used. These considerations are important since the rate of convergence of the solution with a basement conductivity which is neither zero nor infinite is much slower than for either of these two unphysical basement conductivities.

The Fourier coefficients,  $c_n$ , for the difference of the layered magnetic field, from which the coefficients of the perturbed magnetic field are obtained, are given by

$$c_n = \frac{2}{4D} \int_0^{4D} \Delta H^0(z) \sin\left(\frac{n\pi z}{2D}\right) dz \quad (3.59a)$$

$$= \frac{1}{D} \int_0^{2D} \Delta H^0(z) \sin\left(\frac{n\pi z}{2D}\right) dz \quad (3.59b)$$

where

$$\Delta H^0(z) = H_1^0(z) - H_2^0(z). \quad (3.60)$$

Using (3.44a) for the layered magnetic fields and performing the integration gives

$$c_n = g_{1n} - g_{2n} \quad (3.61)$$

where

$$g_{in} = \frac{2n\pi}{n^2\pi^2 + (2D\alpha_i)^2} H_0 \left[ 1 + (-1)^{n+1} \frac{\zeta_i e^{\alpha_i D} + e^{-\alpha_i D}}{\zeta_i e^{-\alpha_i D} + e^{\alpha_i D}} \right]. \quad (3.62)$$

Recall from (3.45) that

$$\zeta_i = \frac{R_i - 1}{R_i + 1} \quad \text{where} \quad R_i = \sqrt{\frac{\sigma_b}{\sigma_i}}.$$

As a check, note that the results are equivalent to d'Erceville and Kunetz for the limiting substrata,  $\sigma_b = 0$  or  $\sigma_b = \infty$ . For if the the basement is an insulator then  $R_i = 0$ ,  $\zeta_i = -1$ ,  $i = 1, 2$  and thus

$$c_n = \begin{cases} 0 & , \text{ if } n = 2m + 1 \\ \frac{2m\pi D^2 H_0 (\alpha_2^2 - \alpha_1^2)}{(m^2\pi^2 + D^2\alpha_1^2)(m^2\pi^2 + D^2\alpha_2^2)} & , \text{ if } n = 2m. \end{cases} \quad (3.63)$$

Therefore

$$H_i(x, z) = H_i^0(z) + \sum_{m=1}^{\infty} A_{i2m} \sin\left(\frac{m\pi z}{D}\right) e^{\pm\beta_{i2m} x} \quad (3.64)$$

as in the d'Erceville and Kunetz solution. Note that the expansion is only in even terms which ensures that

$$P_i(x, D) = 0 \quad , \quad \forall x \quad (3.65)$$

and thus from the layered solution  $H_i^0(z)$  the total magnetic field is zero at the interface with the insulating basement.

Similarly, if the basement is infinitely conducting then  $\zeta_i = 1$  and

$$c_n = \begin{cases} 0, & \text{if } n = 2m \\ \frac{16n\pi D^2 H_0 (\alpha_2^2 - \alpha_1^2)}{(n^2\pi^2 + 4D^2\alpha_1^2)(n^2\pi^2 + 4D^2\alpha_2^2)}, & n = 2m + 1 \end{cases} \quad (3.66)$$

and thus

$$H_i(x, z) = H_i^0(z) + \sum_{n=1,2}^{\infty} A_{in} \sin\left(\frac{n\pi z}{2D}\right) e^{\pm\beta_{in} x} \quad (3.67)$$

again as in the d'Erceville and Kunetz solution. The horizontal electric field is given by

$$E_{xi} = -\frac{1}{\sigma_i} \left[ \frac{\partial H_0^i(z)}{\partial z} \pm \sum_{n=1,2}^{\infty} \left( \frac{n\pi}{2D} \right) A_{in} \cos\left(\frac{n\pi z}{2D}\right) e^{\pm\beta_{in}x} \right] \quad (3.68)$$

and

$$E_{xi}(x, D) = 0 \quad (3.69)$$

as required.

Let us now consider the convergence of the eigenfunction solutions. The eigenfunction coefficients for the fields,  $A_{in}$ , are linearly related (3.42) to the Fourier coefficients,  $c_n$ , of the difference of the primary magnetic field at the contact (3.40). Consider the convergence rate of the coefficients,  $c_n$ ,

$$c_n \rightarrow \infty = \begin{cases} \frac{2DH_0(\alpha_2^2 - \alpha_1^2)}{m^3\pi^3}, & n = 2m & \sigma_b = 0 ; \\ \frac{16DH_0(\alpha_2^2 - \alpha_1^2)}{n^3\pi^3}, & n = 2m + 1 & \sigma_b = \infty ; \\ \frac{2H_0(-1)^{n+1}(\xi_1 - \xi_2)}{n\pi}, & & 0 < \sigma_b < \infty \end{cases} \quad (3.70)$$

where  $\alpha_i^2 = i\sigma_i\mu\omega$  and

$$\xi_i = \frac{\zeta_i e^{\alpha_i D} + e^{-\alpha_i D}}{\zeta_i e^{-\alpha_i D} + e^{\alpha_i D}}. \quad (3.71)$$

To analyse the convergence of the solutions for the fields, write from (3.35)

$$P_i(z, x) = \sum_{n=1}^{\infty} B_{in} \sin\left(\frac{n\pi z}{2D}\right) \quad (3.72)$$

where

$$B_{in} \rightarrow \infty \propto c_n e^{-\left(\frac{n\pi}{D}\right)|x|}. \quad (3.73)$$

Therefore, as  $n$  becomes large

$$|B_{in}| \leq |c_n|.$$

Since  $\Delta H_0$  is guaranteed to converge (section 3.4), the perturbed magnetic fields  $P_i$  are guaranteed to converge at least as fast. For the electric fields, write

$$E_{s_i}^x(z, x) = \frac{-1}{\sigma_i} \sum_1^{\infty} C_{in} \cos\left(\frac{n\pi z}{2D}\right) \quad (3.74)$$

and

$$E_i^z(z, x) = \frac{\pm 1}{\sigma_i} \sum_1^{\infty} D_{in} \sin\left(\frac{n\pi z}{2D}\right) \quad (3.75)$$

where

$$\begin{aligned} C_{in}, D_{in} \\ n \rightarrow \infty \end{aligned} \propto \frac{n\pi}{2D} c_n e^{-n\left(\frac{n\pi}{2D}\right)|x|}. \quad (3.76)$$

Therefore, as  $n$  becomes large, the rate of convergence for the horizontal and vertical electric fields are the same. In particular,

$$|C_{in}|, |D_{in}| \leq \frac{n\pi}{2D} |c_n|.$$

In fact,  $\frac{n\pi}{2D} c_n$  are the coefficients in the expansion of  $\frac{\partial \Delta H^0(z)}{\partial z}$  (3.40). The convergence of the vertical derivative of  $\Delta H^0$  is guaranteed by the expansion to  $z = 4D$  except at the discontinuity in this function at  $z = 2D$  (section 3.4). Therefore, the convergence of the eigenfunction expansions for the electric fields is guaranteed in the required domain,  $z \in (0, D)$ .

The nature of the convergence of the solution can be studied by considering a simpler extension to  $z = 4D$  than the extension described in section 3.4. If one takes  $H_i$  to be symmetric about  $z = D$  and antisymmetric about  $z = 2D$ , then  $P_i$  and  $\Delta H^0$  are continuous in  $z$  through the whole domain,  $z \in [0, 4D]$ . The convergence of the term by term derivative of  $\Delta H^0$  is guaranteed except at points of discontinuity of the derivative ( $z = D$ ). The Fourier coefficients,  $c_n$ , in this expansion decay as  $\frac{1}{n^2}$ . The vertical derivative at  $z = D$  converges to the mean of the limits from either side. This mean is in fact zero. In this case, there is no tangential electric field at the boundary  $z = D$ . There is very little difference between the solution obtained in this manner from the one above, except near the lower boundary,  $z = D$ . The difference is in the contribution

due to the odd spectra (*i.e.*  $n$  odd). Both this expansion and the expansion utilized (3.35) are attempts to approximate the contribution to the solution due to the continuous spectrum. There are twice the number of discrete spectra as are required to represent the contribution of only the point-spectrum (3.27, 3.28). There are, however, no differences in the solution at the surface  $z = 0$  for either expansion.

It must be remembered that the vertical derivative of the perturbed magnetic field does not actually exist at the surface  $z = D$  since it is discontinuous at this point. This can be seen from (3.2) and the fact that the tangential electric field is continuous across this surface. Whereas, the vertical derivative of the magnetic field is the horizontal current density,  $J_x$ , which is not continuous across the surface  $z = D$ . There is, in fact, a step discontinuity in the derivative across this surface. Therefore any solution should attempt to determine the limit of the derivative as  $z \rightarrow D$  rather than the derivative on that surface. A fairly accurate estimate of the electric field at  $z = D$  should then be obtained by this expansion.

### 3.8 Comparisons with Other Solutions.

It is now possible to assess directly the limits of validity of 2-D numerical methods with non-pathological basements. This is something which has not yet been possible except in the asymptotic limits of high or low frequencies.

As a check on the numerical implementation of the solution, comparisons were made in the cases of highly conducting or highly insulating basements to the appropriate limit solutions, first provided by d'Erceville and Kunetz (1962). The results were as expected and no examples are shown here.

Since it is expected that any 2-D modelling programme will have difficulty with highly conducting or resisting basements, unless the programme was not specifically designed for these limits, a model with a more moderate basement conductivity was selected. In the following figures (Figures 3.3-3.8), the model consisted of a relatively resistive slab (15,000  $\Omega$ -metres) against a more con-

ducting slab of ( $300 \Omega\text{m}$ ) with a moderately conducting basement ( $10 \Omega\text{m}$ ). The depth to basement is 9 km. A diagram of this particular model is included in Figure 3.3.

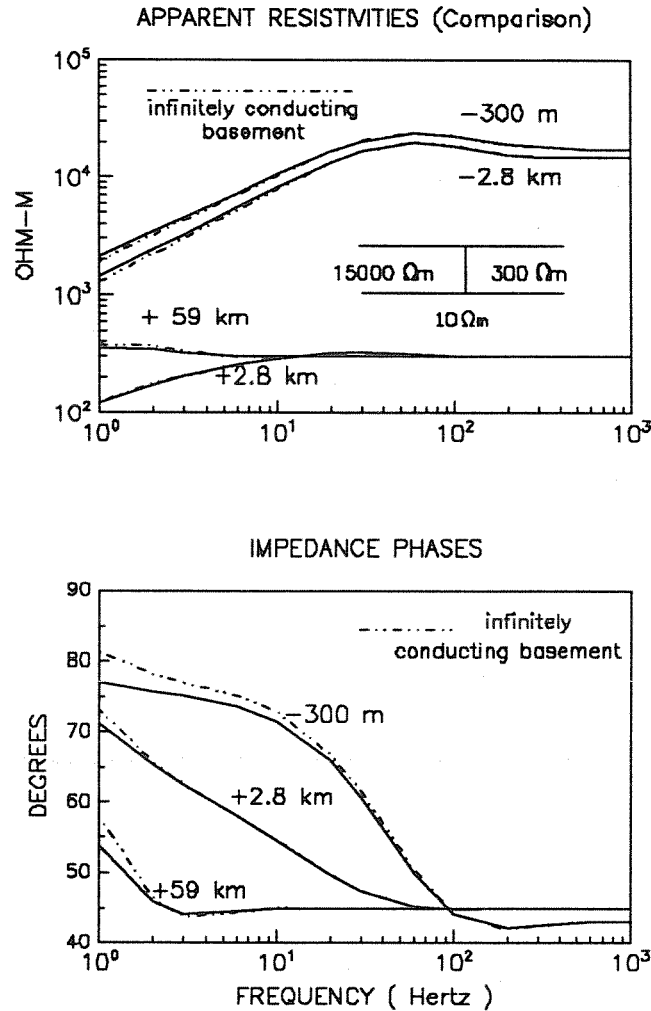


**Figure 3.3:** A comparison of the full solution versus d’Erceville and Kunetz’s (1962) solution for a perfectly conducting substratum. The apparent resistivities and impedance phases at four positions on the surface are presented. The model is given in the top diagram. Solid lines represent the solution presented here while the dashed line is the solution by d’Erceville and Kunetz for an infinitely conducting substratum.

The first test with the above model was to compare the solution by the

method of this chapter, to the solution for the perfectly conducting basement. Surface impedances are compared for the two solutions in Figure 3.3. As expected the two are identical at high frequencies where the substratum has little or no effect. Also as expected, the two solutions begin to separate significantly at frequencies when the depth to basement is comparable to the electromagnetic skin-depth. In the more conducting slab, the depth to basement (9 km.) corresponds to 1 skin-depth when the frequency is approximately 1 Hz, while in the resistive slab, this correspondence occurs at approximately 38 Hz. The comparison is given in Figure 3.3 at four measuring positions on the earth's surface ( $z = 0$ ). Two measuring positions are to the left of the contact (-300m. and -2.8 km.), while the other two are to the right of the contact (2.8 km. and 59 km.). The magnitude of the impedance

$$Z(\omega) = \frac{E_x}{H_y} \quad (3.77)$$

is given in terms of apparent resistivity (top figure) as:

$$\rho_a = \frac{1}{\mu\omega} |Z|^2. \quad (3.78)$$

The phase difference between the horizontal electric and magnetic fields is given as the phase of the complex impedance (bottom figure).

Examination of Figure 3.3 shows that on the resistive side (-2.8 km, -300m), the apparent resistivities are essentially identical to about 10-20 Hz while on the conducting side (2.8 km, 59 km) they remain identical almost to 1 Hz. The phases begin to split on the resistive side between 40-50 Hz and on the conductive side at about 3 Hz. These results corroborate the high frequency solutions on the top surface ( $z = D$ ).

I turn now to comparisons of numerical methods. Figure 3.4 contains comparisons of the solution for the same model as used in Figure 3.3 but for a broader range of frequencies. The first numerical programme used for comparison was written at M.I.T and utilizes an electrical circuit analogy (Madden and Thompson, 1965). Eight measuring positions on the top surface are compared.

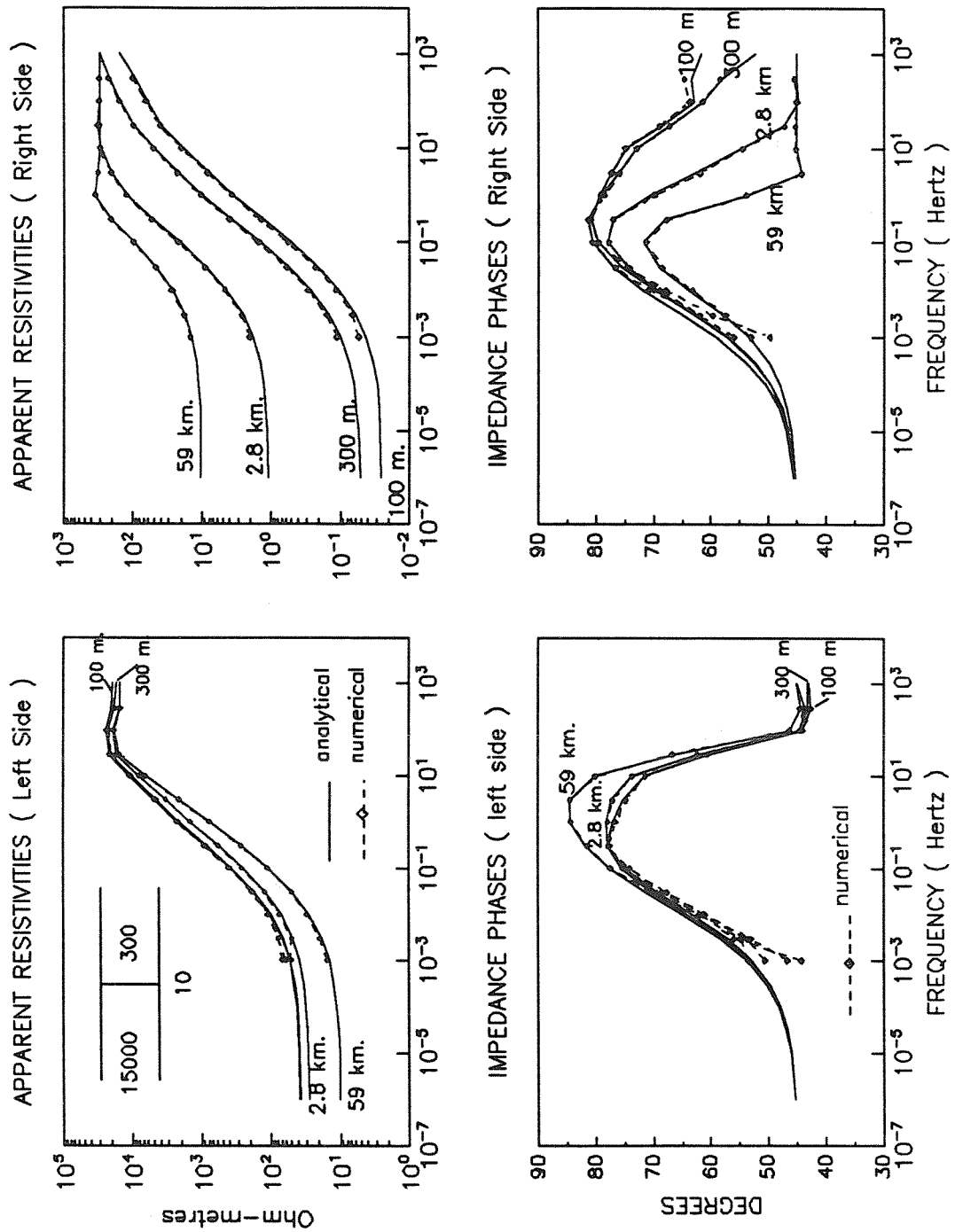


Figure 3.4: A comparison of the analytic solution to a numerical solution by circuit analogy. Apparent resistivities and phases are presented at the top surface ( $z = 0$ ) at eight different positions. The analytical solutions are given by solid lines while numerical solutions are dashed with diamonds.

Four of these positions are to the left of the contact (59 and 2.8 km., 300 and 100m) and four to the right (100m, 300m, 2.8km, 59km). Apparent resistivities and impedance phases are shown in the figure. I am now principally interested in the frequency range from about 100 Hz. and less, since the high frequencies were verified above (Fig. 3.3). We see from the figure that the apparent resistivities are very comparable but begin to differ at about 700 seconds in period. The impedance phases are also very comparable in the medium frequencies but there are drastic differences below a period of 20 seconds. That the numerical phase results are in error in the low frequencies is evident from the extreme irregularity in the results. This is difficult to see in Figure 3.4 because of the number of curves but examination of individual phase curves indicates erratic results in the low frequencies ( $< .1Hz$ ). The analytic solution has smoother solutions but this does not in itself prove that they are correct. A remarkable correspondence has been shown in the middle frequencies where the numerical results should be most reliable. Another numerical programme is used to check the low frequency solutions.

Comparison was then made to a finite difference method which has been developed at the University of Victoria (Brewitt-Taylor and Weaver, 1976). The programme requires significantly more time and effort to calculate multiple frequencies than the previous numerical method. It was used at five frequencies to check the shape of the low-frequency results (Figure 3.5). The frequencies used range from 1Hz. to .0001 Hz. See from Figure 3.5 that the comparison is exceptionally good. In particular, the low frequency asymptotes agree for both phase and apparent resistivity.

Although, as discussed above, my solution is exactly correct for the electric and magnetic fields at the top surface, I have also considered its accuracy below the surface. The following three figures (Fig. 3.6-3.8) are comparisons of the analytic solution as a function of depth to the numerical techniques of Madden and Brewitt-Taylor and Weaver. The model used is the same as that in the above figures (3.4 and 3.5) and is illustrated again in Figure 3.6. A frequency of

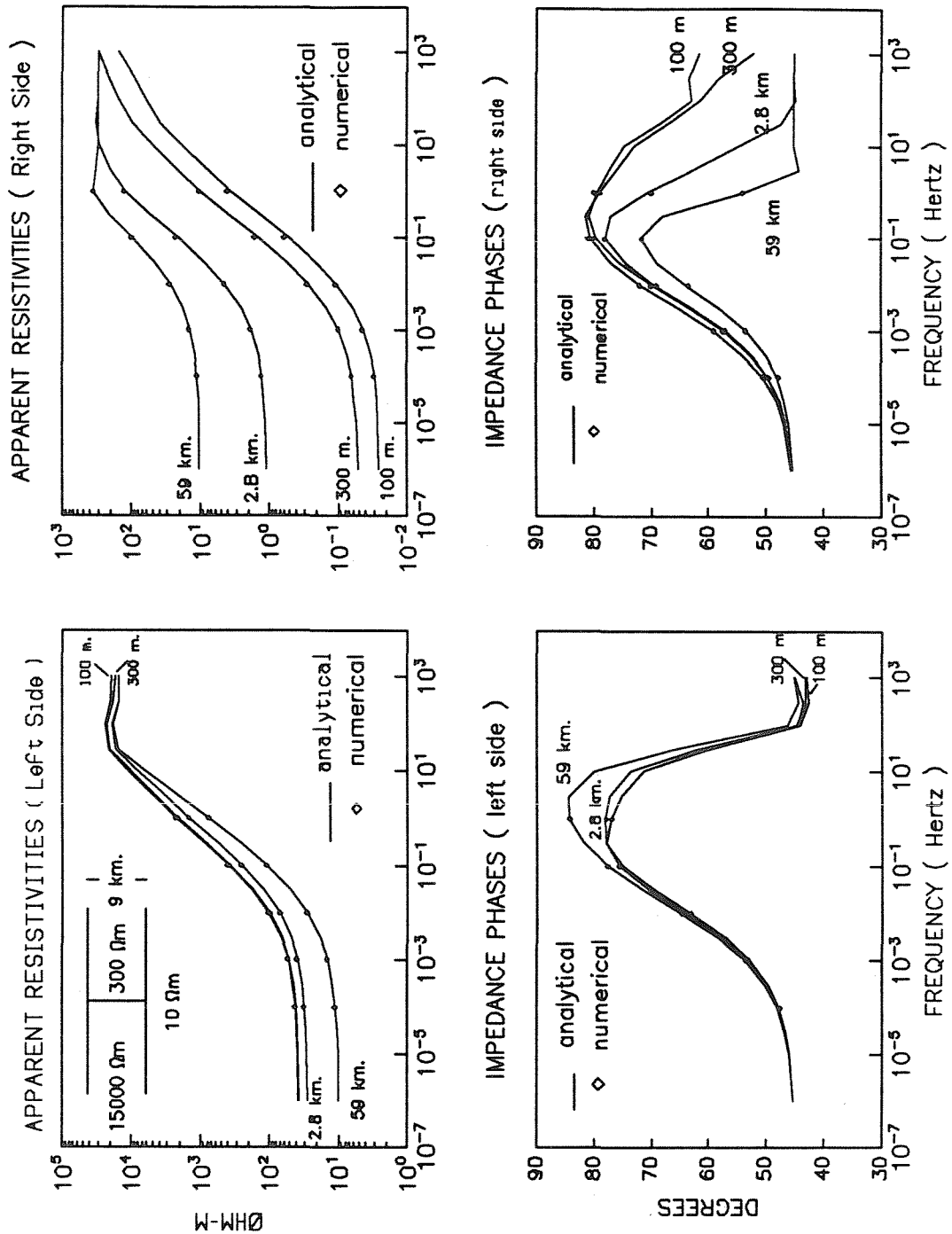
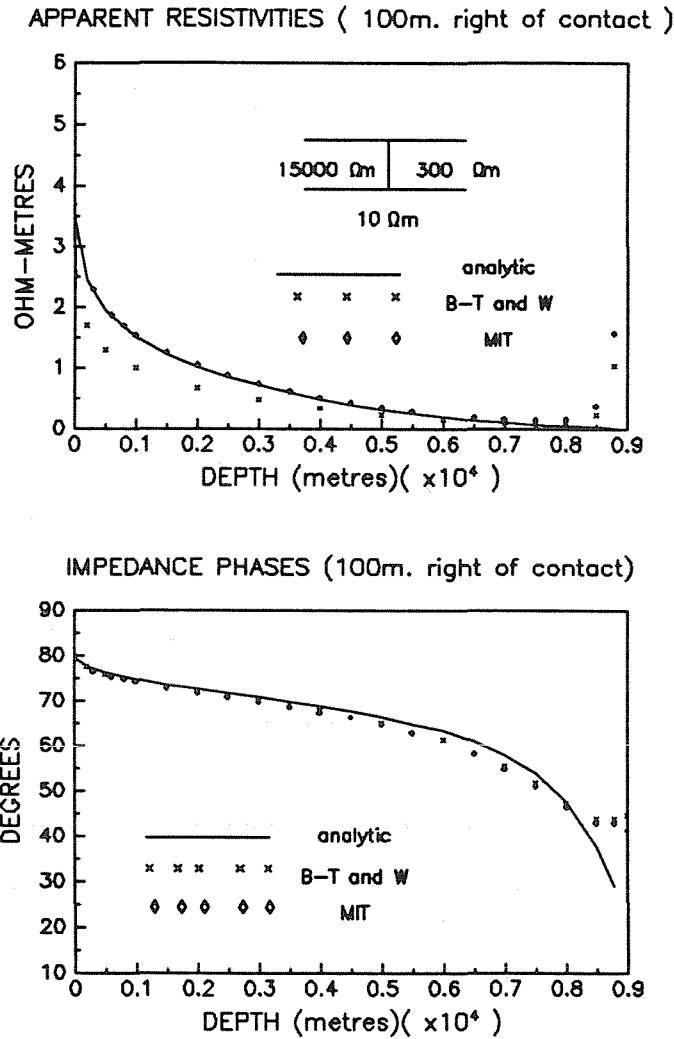


Figure 3.5: A comparison of the analytic solution to a numerical solution by an integral equation technique (Brewitt-Taylor and Weaver). Apparent resistivities and phases are given at the same measuring positions, as in the previous figure (3.4). Numerical solutions are represented by diamonds.

1 Hz was used, since at this frequency the three methods gave very comparable results.



**Figure 3.6:** Investigation of the solution as a function of depth. The analytic solution is compared to the two numerical solutions at positions 100m to the right of the contact. The top figure is the impedance magnitude, as apparent resistivity, while the complex angle of the impedance is at bottom. The crosses represent the numerical solutions due to Brewitt-Taylor and Weaver while the diamonds are the solutions due to Madden. The skin depth at 1 Hz in the right slab is about 8.72 km. while in the substratum it is approximately 1.6 km.

The first comparison is at a lateral position 100m to the right of the contact

in the more conducting slab. Figure 3.6 compares the apparent resistivity and impedance phases as functions of depth through the slab to the two numerical methods. As remarked above, the solution of this chapter should be exactly correct on the top surface ( $z = 0$ ) and on the contact ( $x = 0$ ). Thus, the analytic results should be quite accurate at this lateral position except possibly near the basement contact. The comparison of impedance phases (bottom figure), shows that the three methods give very comparable results down to about 8 km. The difference between the analytic solution and the M.I.T. result for apparent resistivity is very small to about 8 km. There are large discrepancies between the analytic and finite difference method (B-T and W). The reader should note that the apparent resistivity and phase given in Figure 3.6 at  $z = 0$  by the integral equation method do not agree with the results given in Figure 3.5 by the same programme. This is probably because the electric fields are calculated by central differences schemes from node point values of the magnetic field. This particular programme (B-T and W) seems to correct this problem by interpolation when apparent resistivities and phases are given for the surface. (In fact, the program used was an old one (Weaver, private communication) and the author assures me that their new version provides solutions which are in very good agreement with the analytic solution.) Note the agreement between all three methods at about 8 km.. The numerically derived apparent resistivity values rise near the basement and approach  $10 \Omega\text{m}$  which is the basement conductivity. Also, all the phases are much flatter as a function of depth than are the impedances. The impedance is a ratio of the electric and magnetic fields and these two fields are calculated in different ways at the node points. The impedance phase, at this frequency is dominated especially near surface, by the phase of the electric field. The phases calculated, numerically, approach 45 degrees as  $z \rightarrow D$  which is the impedance phase for a half-space. The numerical impedances at the basement contact may be suspect as they seem too close to the half-space values as if there were no lateral inhomogeneity. This may be due to boundary conditions placed on the numerical solution at the bottom of the numerical grid. This is seen again in

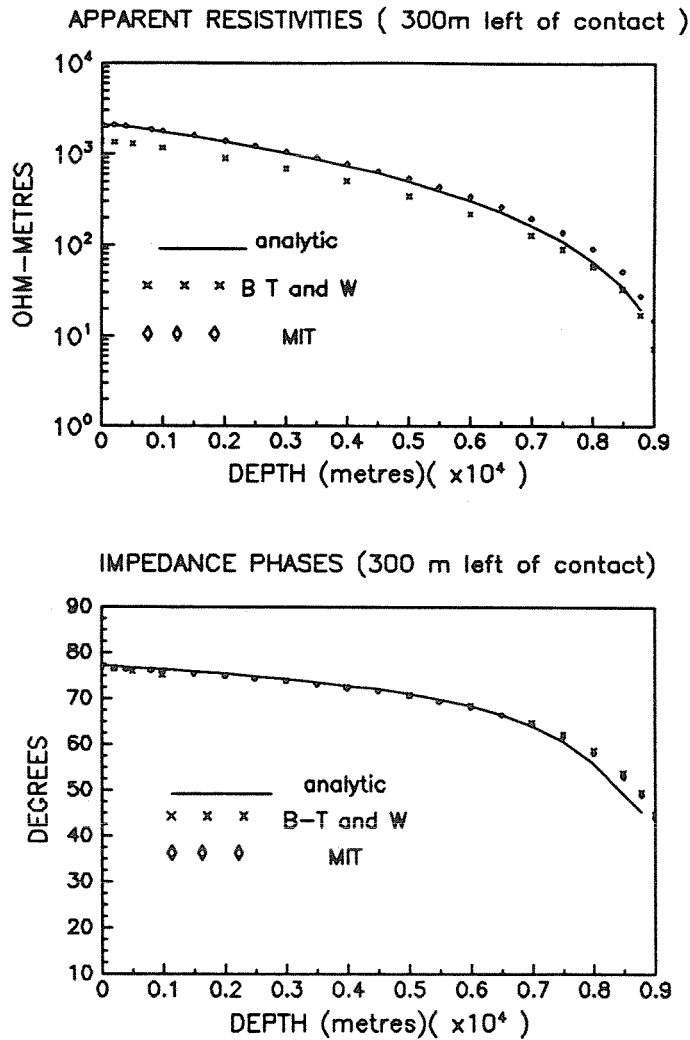


Figure 3.7: Investigation of the solution as a function of depth at positions 300 m. to the left of the contact in the more resistive slab. The same conductivity model is used as in the previous figures. The skin depth at this frequency (1 Hz) is approximately 61.5 km.

the next two examples (Figures 3.7 and 3.8).

Figure 3.7 is a comparison similar to the above figure (3.6) but at a lateral position of 300m to the left of the contact in the more resistive slab. The apparent resistivities are greater here and are thus plotted in  $\log \rho_a$ . Again a discrepancy is seen, near surface, between the integral equation results and

their own surface apparent resistivities on one hand and both the other numerical method and the analytic solution on the other. (Weaver has redone these calculations with the new University of Victoria code and found very good agreement with the MIT and analytic results). Nevertheless, the integral equation results approach very closely the other two solutions (analytic and circuit analogy) near the basement contact where grid spacing is small. The phases differ by very little, for all three methods, except by a few degrees near the basement. Again it must be noted that the numerical results approach very closely the half-space solutions at the basement as if there was no conductivity contrast laterally above the uniform half-space.

Both of the two previous comparisons as functions of depth were relatively close to the contact where the error is expected to be small. Finally, we look at the results as a function of depth much further from the contact (2.8 km) but not so far that the solutions have decayed close to the layered solution. The results are for the same model, at 1 Hz. and in the more conducting slab. At 1 Hz., 2.8 km. is about .3 skin-depths in the conducting medium. The comparisons are given in Figure 3.8.

The integral equation results for apparent resistivity again differ from either the electrical circuit analogy results or the analytic results and approach the analytic results at the basement. The impedance phase results agree well for all three methods until a depth of about 5 km. and then the analytic results diverge from the numerical results. The numerical results for impedance phase at the contact are again 45 degrees for both methods. It is not obvious which result is correct since the numerical results have converged at  $z = D$  to the half-space values ( $\rho_{app} = 10\Omega m$ , phase = 45degrees) independent of position on the bottom surface. That is, the numerical results on the bottom surface do not indicate the presence of a lateral inhomogeneity.

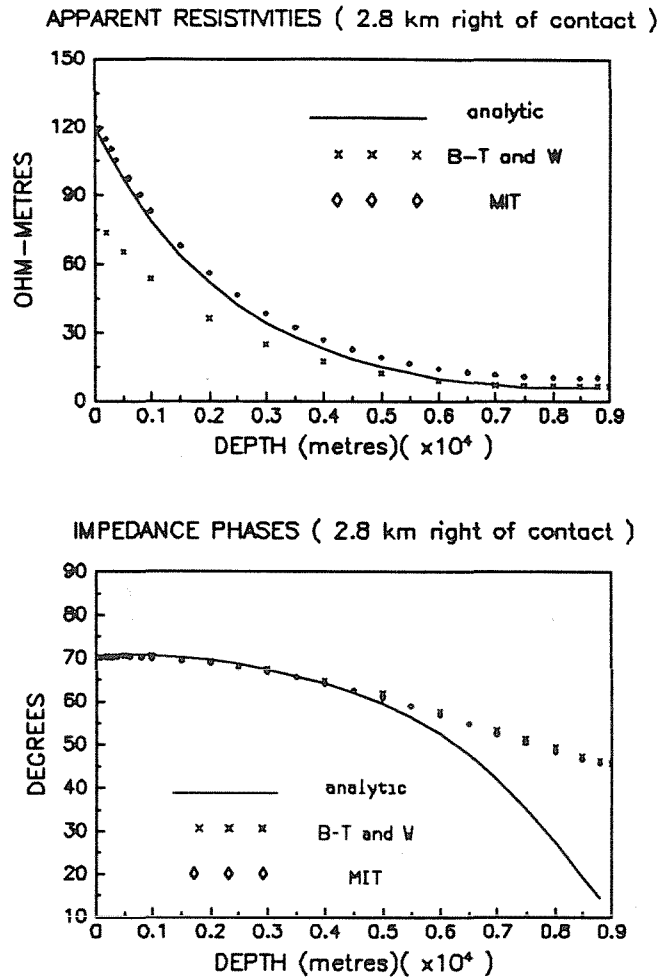


Figure 3.8: A comparison of solutions as a function of depth at 2.8 km. to the right of the contact. Again the same conductivity model is used.

### 3.9 Summary

In summary, I have provided a solution method for H-Polarization induction in two semi-infinite slabs. This solution is neither limited to high frequencies nor to low frequencies. The solution, although excluding continuous spectra, is exactly correct at all points on the earth's surface ( $z = 0$ ) and at the contact ( $x = 0$ ) except at possible singularities which may occur at the triple point  $(x, z) = (0, D)$ . The solution error at depth (below the Earth's surface) has been described and estimated. In fact, the accuracy of the solu-

tion with depth has been shown to be good until near the bottom of the slabs. This has been corroborated by comparisons with numerical solutions. The solution attained here is a unique solution and the rate of convergence for the eigenfunction series has been characterized.

The solution is incomplete not only in its exclusion of continuous spectra but in its inability to represent completely unbounded functions if they occur. It was shown why the solution for a perfectly insulating basement does not require continuous spectra and the possible presence of an error, albeit small, in the original solution for a perfectly conducting basement by disregarding the contribution due to a continuous spectrum.

This solution, apart from providing a more complete and useful model for numerical testing, has provided some physical insights. A significant new contribution is an analytic result for the low frequency behaviour for a realistic substratum. The solution has verified the intuitively expected result that the low frequency asymptote (Figure 3.5) for the surface impedance phases is 45 degrees, independent of position, when the substratum conductivity is neither infinite nor zero. That is, the impedance phases approach the phase for a half-space with the conductivity of the substratum. There has been no explicit analytic demonstration of this result prior to this solution. The low frequency asymptotes for the apparent resistivities (Fig. 3.5) are however a function of position and are not, except in the extreme lateral positions, the half-space solution. The low-frequency responses are what is termed "statically shifted" from the layered solution. This shifting is often thought to be due only to small-scale inhomogeneities. In the following chapters I will discuss the effects of small-scale three-dimensional (Chapter 5) and narrow two-dimensional (Chapter 4) inhomogeneities. The static shifting in these examples will be shown to be quite different from such effects due to small-scale three-dimensional scatterers. The principal difference is that small lateral changes in measuring position do not appreciably alter the impedances in the case of large-scale inhomogeneities, whereas such changes in measuring position cause

dramatic differences in impedance in the case of 3D small-scale structure.

Although, in principle, measurements of the E-Polarization impedance would exclude the possibility of interpreting such data in terms of a 1-D model, it is of interest to see that the apparent resistivity and phase curves calculated for the model here (Figure 3.5) can be inverted for a one-dimensional structure. These produce, for example, to the right of the contact, a conductivity at depth which is nearly three orders of magnitude higher than the actual substratum conductivity! The effect of the vertical contact is therefore to produce, in the one-dimensional model, a false conducting region at depth. Note however, if the contact was not infinite in the strike length, at some sufficiently low frequency, current would flow around the sides of the contact and the apparent resistivities would begin to rise, as frequency decreases, to the basement conductivity. Therefore the apparent basement conductor of infinite depth in the 2-D case would have a vertically bounded extent in the finite strike length case. One can see (Figure 3.5) from the spatial extent of these effects that even if the contact was buried beneath the Earth's surface, these effects would still be seen. The argument here is meant to impress again on the reader that large-scale lateral inhomogeneities can, if the interpreter is not careful, masquerade as high conducting layers at depth. Small changes in the measuring position, in such physical situations, will not drastically alter the results.



## CHAPTER 4

### A STUDY OF THE EFFECTS OF MULTIPLE HORIZONTAL INHOMOGENEITIES

#### 4.1 Introduction

Conductivities within the Earth often vary by orders of magnitude laterally as well as vertically. The electromagnetic response of these variations generally involves an interaction between inductive and charge effects with the most dramatic variations occurring in the electric fields. The two-dimensional H-polarization mode is a relatively simple but still useful model as it maintains the two physical effects, their interaction and the marked effects on the electric field.

This chapter provides an analytic solution, in the H-polarization mode, to the effects of multiple vertical conducting slabs (dikes) embedded in a host medium. The solution is also extended to an infinite periodic array to model an anisotropic layer. Extreme electrical anisotropy can be developed by these models.

The study provides some insight into the influences of multiple horizontal, laterally bounded, inhomogeneities on magnetotelluric (MT) sounding curves. The solution method can be utilized to study the effects of such complicated media on the surface impedance, the effective bulk parameters of these media and the information that can be recovered by magnetotellurics. This is a particularly useful model to study, as one is able to examine two important problems which are presently of interest in MT. The first problem being how such quasi-anisotropic structures mislead conventional one-dimensional interpretation. Such structures have already been invoked to explain magnetotelluric results (Schmucker 1986). Second, one can study an experimentally topical

problem; that of obtaining adequate spatial sampling of the electric field. One would like to know what sorts of effects can arise from too small or misplaced electrodes over such structure.

Rankin (1962) adapted the solution of d'Erceville and Kunetz (1962) to produce an analytic solution in the H-polarization mode for a bounded domain. His solution was for a vertical dike of infinite length embedded in a host layer underlain by a basement of infinite or zero conductivity. In this chapter, Rankin's solution is modified to provide a solution which can include either multiple dikes or an infinite array of dikes in a host material. The analytic solutions are used to produce computer solutions for the electromagnetic fields of particular models. Wait and Spies (1984) proposed extending the Rankin model to multiple dikes. However, after providing some of the more obvious mathematical development for multiple structures with a perfectly insulating basement, restricted their results to the case of only one dike. Wait and Spies provided normalized responses as functions of position across the single dike.

In the case of an infinite array, an analysis was done here to determine effective bulk medium parameters for such structures. With the aid of the computer solutions, the analysis which determines the effective bulk parameters was justified. Both from this analysis and from the computer solutions one can distinguish the important parameters and their effect on the MT sounding curves. These parameters include the host resistivity, the resistivity of the inhomogeneities, the resistivity-thickness product of the inhomogeneities, the basement depth and conductivity, and the measuring position. The frequency-dependence of a parameter is usually important. As well as varying from the laterally homogeneous response, the surface response can vary dramatically from position to position.

It is shown that the thickness of the anisotropic layer can be correctly determined by MT sounding curves if the layer is taken to have a uniform resistivity which is equal to its effective resistivity. As well, with correct spatial sampling of the electric field, one can obtain the correct effective resistivity by

the MT method. However, it is also shown, for such elongated structures, incorrect sampling of the electric field could produce apparent resistivities which are extremely different from the effective bulk resistivity. The results show the MT method to be an effective method for determining both the appropriate bulk conductive parameters and the correct thicknesses of significantly inhomogeneous media. This will be especially true if the complex material is buried at some depth.

Lateral structures can masquerade as one-dimensional structure. For example, the H-polarization response, obtained over a conducting host which contains resistive dikes, seems to indicate a conducting layer at depth when this data is interpreted one-dimensionally. A change in measuring position or long electrode spacings will not always help, for in some structures even large changes in measuring position will not detect the lateral structure.

#### 4.2 The Effects of a Finite Number of Vertical Dikes:

Rankin (1962) adapted the Fourier technique of d'Erceville and Kunetz for a single vertical contact (discussed in Chapter 3) to obtain the H-polarization solution for a vertical conducting rectangular prism of infinite length embedded in a host material. Here, the method of Rankin (1962) is first extended to obtain the solution for multiple vertical structures or dikes. In particular, I initially chose to study the problem of a sequence of  $N$  dikes of horizontal thickness  $d$  and resistivity  $\rho_d$  embedded in a host medium of resistivity  $\rho_h$ . Each dike is separated by a distance  $h$  and the inhomogeneity structure has a depth  $D$ . The general model is illustrated in Figure 4.1. The model here will be restricted to only two basement resistivities ( $\rho_B$ ), zero and infinity. Since the basics of the theory are included in Chapter 3, only a sketch of the previous theoretical analysis will be provided. The reader is referred to Chapter 3 and the previously cited literature for further information.

Recall from Chapter 3 that for the H-polarization mode

$$\vec{H} = H(x, z)e^{i\omega t}\hat{y} \quad (4.1a)$$

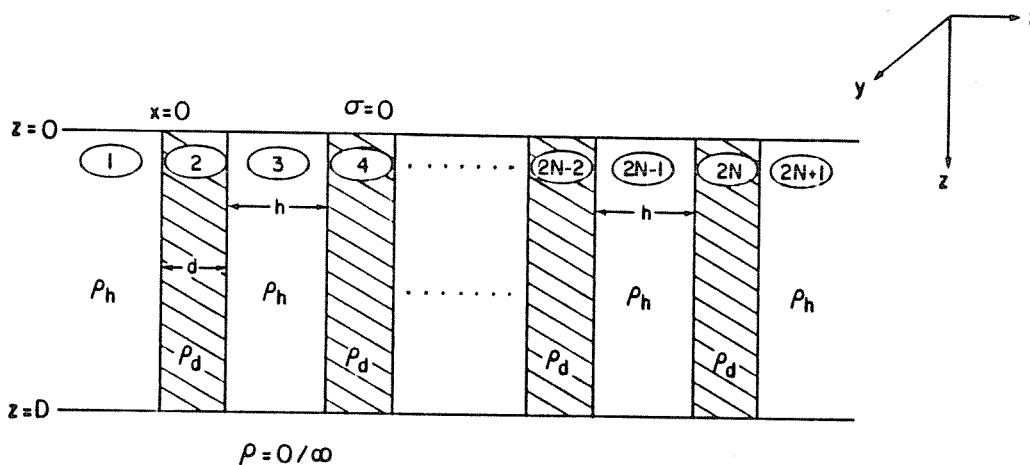


**Figure 4:1** An illustration of the  $N$  dykes 2D model for horizontal anisotropy. The dykes have thickness  $d$  and are separated by a distance  $h$ . The resistivity of the dykes is  $\rho_d$  and that of the host,  $\rho_h$ . The inhomogeneity structure has a depth of  $D$  metres. The upper resisting half-space represents the Earth's atmosphere.

$$\nabla^2 H = i\sigma\mu_0\omega H = \alpha^2 H \quad (4.1b)$$

$$\sigma E_x = -\frac{\partial H}{\partial z} \quad (4.1c)$$

$$\sigma E_z = \frac{\partial H}{\partial x}. \quad (4.1d)$$

Following Rankin, in any region labelled  $i$  (Figure 4.1), let

$$H_i(x, z) = H_i^0(z) + P_i(x, z), \quad i = 1, 2N + 1 \quad (4.2)$$

where  $H_i^0(z)$  is the layered solution for region  $i$  and  $P_i(x, z)$  is the secondary magnetic field in the same region. Each perturbation function satisfies the two dimensional Helmholtz equation

$$\nabla^2 P_i = \alpha^2 P_i \quad (4.3)$$

in each homogeneous rectangle. The differential equation (4.3) is separable (Chapter 3) and thus the perturbed solutions have the form

$$P_i(x, z) = \sum_{n=1}^{\infty} f_{in}(x) \sin \lambda_n z \quad (4.4)$$

where  $\lambda_n = \frac{n\pi}{D}$  if  $\rho_B = \infty$  and if  $\rho_B = 0$ ,  $\lambda_n = \frac{n\pi}{2D}$ . From (4.4) and (4.3)

$$f_{in}(x) = a_{in} e^{\sqrt{\lambda_n^2 + \alpha^2} x} + b_{in} e^{-\sqrt{\lambda_n^2 + \alpha^2} x}. \quad (4.5)$$

If the basement is perfectly conducting then  $f_{in} = 0$  when  $n$  is even to ensure that the horizontal electric field is zero at the interface  $z = D$ . Also

$$b_{1n} = 0, \quad \forall n \quad (4.6a)$$

$$a_{2N+1,n} = 0, \quad \forall n \quad (4.6b)$$

which ensures that the fields decay to zero correctly as the lateral position increases to infinity. The remainder of the coefficients are obtained in a similar manner as in the solution for a vertical contact solution (Chapter 3). If  $x_i$  is a vertical contact, then equating the horizontal magnetic field at all depths,  $z$ , results in

$$P_i(x_i, z) - P_{i+1}(x_i, z) = H_{i+1}^0(z) - H_i^0(z) = \Delta H_i^0(z) = \sum_{n=1}^{\infty} b_{in} \sin \lambda_n(z). \quad (4.7)$$

Then, using the orthogonality of the sine functions,

$$f_{in}(x_i) - f_{i+1,n}(x_i) = b_{in}, \quad \forall n, \quad i = 1, 2N. \quad (4.8)$$

The Fourier coefficients  $b_{in}$  are determined simply from (4.7) since they are the coefficients of a known function ( $\Delta H_i^0$ ). A similar relation between the  $f_{in}$  are obtained by equating the tangential component of the electric field (vertical field) at each conductivity contrast contact. In this way, a system of  $4N$  linear equations with  $4N$  complex coefficients ( $a_{in}, b_{in}$ ) is developed for each Fourier component. The  $4N$  coefficients ( $a_{in}, b_{in}$ ) describing the perturbed fields are

then found by solving this complex matrix equation. A computer programme was written to obtain these solutions by the LU decomposition method.

The computation to calculate the set of coefficients can be quite lengthy, since a  $4N \times 4N$  system of equations must be solved for each Fourier component and a large number of Fourier coefficients may be needed if the series (4.4) is slow to converge. Thus, it was necessary to investigate precisely the convergence of the Fourier expansion. The accuracy of the finite Fourier expansion was found to be a predictable function of the model and the frequency. Details will not be given here, as the arguments and results are analogous to the case of a single contact given in the previous chapter (3), section 7. This allowed the inclusion of software routines to obtain any desired accuracy without excessive computation.

Figure 4.2 is an example of the surface impedances ( $\frac{E_z}{H}$ ) from such a model. This particular model consisted of 5 relatively conducting dikes ( $\rho_d = 10\Omega m, d = 500m$ ) separated by a distance of 500m in a host ( $\rho_h = 1000\Omega m$ ). The depth of the structures is 1000m and the impedances were calculated at a frequency of 100Hz. This example was chosen as it shows intermediate behaviour between the high frequency response which sees only the very local material and the low frequency response which is considerably effected by the basement conductivity. At this frequency, the skin-depth in the resistive material exceeds the width of the resistive structures whereas the skin-depth in the conducting material is less than the width of the conducting structures. The choice of basement resistivity is not relevant here since at this frequency the depth of the structure is much larger than skin-depth in either the host or the dikes.

The impedances in this figure (4.2) are presented as a function of position along the top surface of the structure ( $z = 0$ ). Only the central region of the multiple structures is shown (1000m – 3000m). The entire structure begins at 0 and ends at 5000m. Impedances are expressed as apparent resistivities and phases.

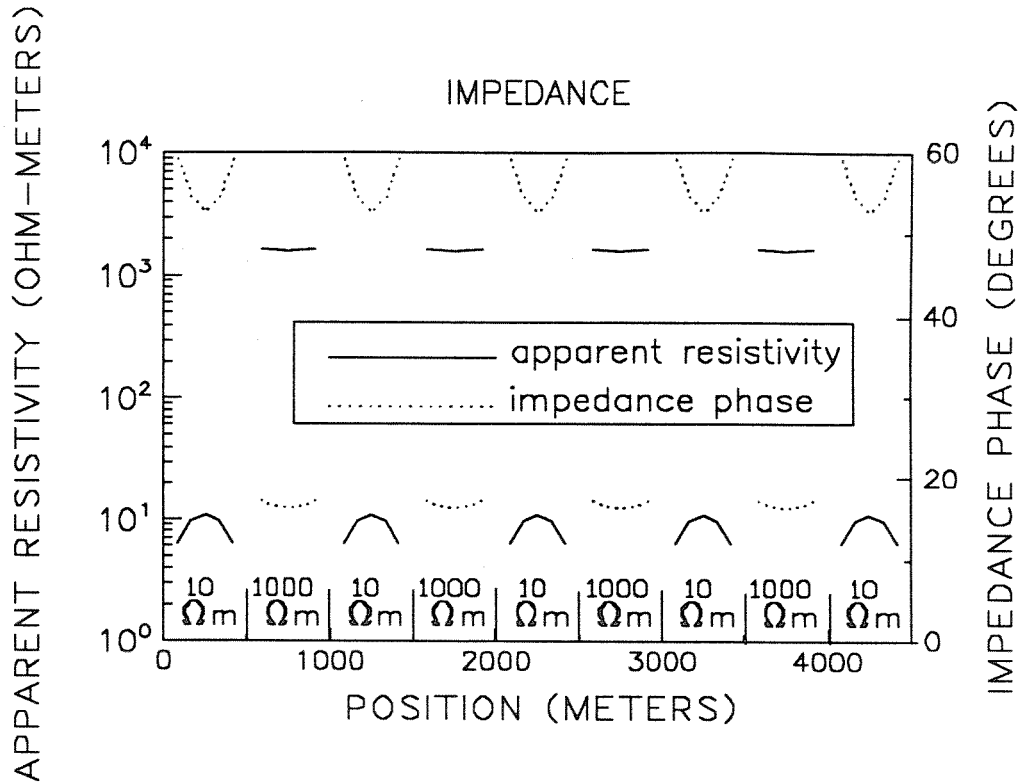


**Figure 4.2:** Surface impedance across 5 vertical pairs in terms of apparent resistivity and phase at 100 Hz. The parameters are  $h = d = 500m$ ,  $\rho_d = 10$  and  $\rho_h = 1000\Omega m$ . The half-space is perfectly resisting and at a depth of 1000m.

A number of effects can be seen from this example (Fig. 4.2). Firstly, one sees that the apparent resistivity is suppressed over the relatively conductive dikes while it is enhanced (slightly) over the resistive host. Secondly, the impedances are sometimes a function of position (*e.g.* over the conductive dikes). The effect of the lateral structure is significant only when the distance to the nearest vertical contact is less than one skin depth in that medium. As frequency decreases to a point where the entire width of the structure is significantly less than a skin-depth, the impedance over a particular vertical structure (whether host or dike) becomes independent of position (*e.g.* over the resistive host - Fig. 4.2). The suppression of the apparent resistivities over the conductive material was found to be a function both of frequency and

resistivity-thickness product of the resistive material.

### 4.3: The Effects of an Infinite Periodic Array

In the center of the structure containing 5 dikes, the impedances are essentially periodic with a period of 1000m. Noting this leads to a computationally more efficient but still informative model. Rather than a set of  $N$  dikes in a host, the model used was an infinite periodic sequence of vertical structures of alternating resistivity,  $\rho_d$  and  $\rho_h$ , and widths  $d$  and  $h$ . In this manner, a model for an anisotropic layer over a half-space is developed. The solution follows from the solution for multiple dikes but with modifications.

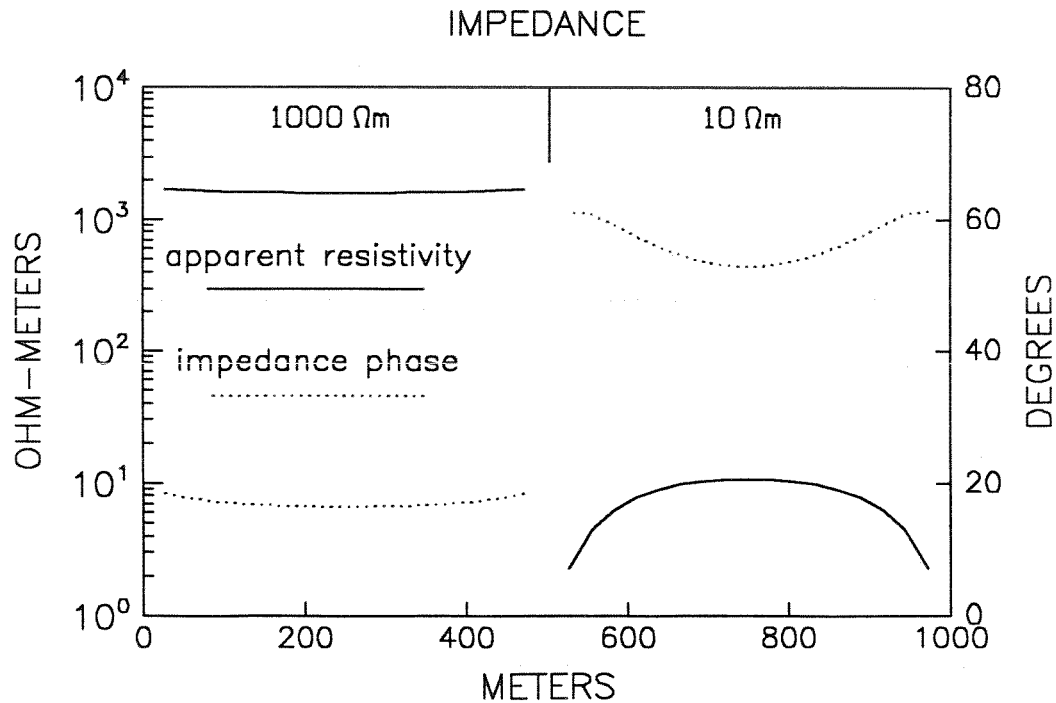


**Figure 4.3:** The impedances across a vertical doublet in a periodic array which has a structure comparable to the finite number of dykes in Figure 4.2. Each vertical structure is 500m across. The resistive host is on the left while the conducting dyke is on the right.

One significant advantage of the periodic model is that the fields for this

type of structure are much quicker to solve numerically and thus the model provides a means for more rapid study. Since the structure is entirely periodic over all values of  $x$  then the fields at the left of these vertical doublets must equal the fields at the right. In this way only 4 complex coefficients are required for each Fourier component and thus only a  $4 \times 4$  linear system must be solved to obtain each of the components. In addition, for high order Fourier components there are approximations for the coefficients and the numerical solution can be obtained even more rapidly. This model also allows one to readily obtain the charge on the interfaces utilizing the continuity of normal current density (1.8) and Gauss' Law (1.6d). This can be useful since the suppression and enhancement of the electric field which causes the variation in the apparent resistivities is due effectively to gross polarization of the medium. Charge develops on the vertical interfaces and this charge produces a secondary field which either increases the electric field (in the resistive material) or decreases the electric field (in the conducting material).

Figure 4.3 is provided to show just how similar the solutions are for the two models. This figure utilizes the equivalent structure, for this type of model, as that used for Figure 4.2. The modified structure now consists of alternating conducting ( $\rho_d = 10\Omega m$ ) and resistive ( $\rho_h = 1000\Omega m$ ) vertical dikes of width 500m.. The depth of this complex layer is that of the model for Figure 4.2, namely 5000m.

#### 4.4 Investigation of the Bulk Properties of the Model

The alternating periodic dike structure enables one to analyse the bulk properties of this extremely electrically anisotropic layer. Here the effective conductivity for horizontal current flow is quite different from that for vertical flow. As frequency decreases, the horizontal electric fields at any given depth, in such a structure, will eventually become essentially constant as a function of horizontal position within each member of the pair. The entire field is then nearly entirely horizontal and decays with depth. At such frequencies one can

investigate the anisotropic layer as a bulk medium. This occurs when the skin depth in both of the vertical structures becomes significantly larger than the widths in the respective material. This can be verified by evaluating the horizontal fields as a function of depth with this solution.

Assume the effective resistivity of the medium is merely the spatially averaged resistivity

$$\rho_{\text{eff}} = \frac{d\rho_d + h\rho_h}{d + h}. \quad (4.9)$$

It will be shown that this is, in fact, true for such structure. (The concept that one vertical structure, in the pair, is the dike while the other the host is retained.) Since current density is continuous across all these vertical interfaces,  $\vec{J}_x$  will be constant as a function of  $x$ . Thus one can define an effective or average electric field

$$J = \frac{1}{\rho_{\text{eff}}} E_{\text{ave}} \quad (4.10)$$

Therefore the electric fields in each region can be described in terms of this average electric field. In the dike

$$E_d = \rho_d J = \frac{\rho_d}{\rho_{\text{eff}}} E_{\text{ave}} \quad (4.11)$$

while in the host

$$E_h = \rho_h J = \frac{\rho_h}{\rho_{\text{eff}}} E_{\text{ave}}. \quad (4.12)$$

From voltage considerations

$$dE_d + hE_h = (d + h)E_{\text{ave}}. \quad (4.13)$$

Therefore from equations 4.11-4.13

$$E_{\text{ave}} = \frac{1}{d + h} \left[ d + h \frac{\rho_h}{\rho_d} \right] E_d = \beta(d) E_d \quad (4.14a)$$

$$= \frac{1}{d + h} \left[ h + d \frac{\rho_d}{\rho_h} \right] E_h = \beta(h) E_h. \quad (4.14b)$$

Therefore, the apparent resistivity over the dike is given by

$$\rho_{\text{app}}(d) = \frac{1}{\beta^2(d)} \rho_{\text{eff}} \quad (4.15)$$

while over the host

$$\rho_{\text{app}}(h) = \frac{1}{\beta^2(h)} \rho_{\text{eff}}. \quad (4.16)$$

If the dikes are resistive then  $\frac{\rho_h}{\rho_a} < 1$ . Therefore,  $\beta(d) < 1$  and  $\beta(h) > 1$  and thus the obvious conclusion is reached that

$$\rho_{\text{app}}(d) > \rho_{\text{eff}} \quad (4.17a)$$

$$\rho_{\text{app}}(h) < \rho_{\text{eff}}. \quad (4.17b)$$

The variations from the effective resistivity are not only dependent on the ratio of resistivities but the ratio of the widths. For example, a thin dike produces, in the case of a resistive dike, a relatively large increase in apparent resistivity over the dike. Whereas, a thick resistive dike produces a large decrease in apparent resistivity over the host. Obviously, if the dikes are conducting these relations are reversed.

#### 4.5 The Frequency Response of the Model

The results of the above analysis indicate a low-frequency behaviour for the medium which may not be surprising to the reader. At the same time, the high frequency result is obvious as the apparent resistivity will approach the resistivity of the local material. However, this model enables another aspect of magnetotelluric behaviour to be studied; namely the response in the transitional frequency range between the low and high frequency behaviour. In particular, to study whether the impedance response can be modelled one-dimensionally and if so whether false conducting or resistive layers appear when the data is so interpreted. To argue that a one-dimensional interpretation would never be applied to such 2-D structure is not correct. As will be seen in the following chapter, if the large-scale structure is 2-D, small-scale 3-D inhomogeneities will often cause a mixing of the E and H-polarization impedances. This will occur when the measured impedances are modelled simply two-dimensionally as in the conventional method of Swift (1967). Conducting dikes might well reduce

the apparent resistivity for the E-polarization mode to sufficiently low levels that, in the presence of small-scale electric field distortion, the E-polarization parameters could be just versions of the H-polarization parameters but shifted by a frequency-independent parameter (“static shift”). The interpreter might then be lead to interpret the data with a one-dimensional model. The problem of the effects of small-scale surface structure will be studied more closely in the following chapter (5).

Figure 4.4 is an example computed with the program which will be used to illustrate the effects of such horizontally laminated structure. A plot (Fig. 4.4) is given of apparent resistivity versus frequency at points over both the resistive region and the conducting region. In this example, which models a set of resistive dikes in a more conducting host,  $d = 50m$ ,  $\rho_d = 1000\Omega m$ ,  $h = 550m$  and  $\rho_h = 10\Omega m$ . The depth of the structure was chosen to be 15 kilometers to more clearly illustrate the effects. There are a number of things to observe from this figure (4.4). First, note that over the resistive dike, at all frequencies, the apparent resistivity is enhanced above the resistivity of the dike while over the relatively conducting host, the apparent resistivity is suppressed. The points for measurement were taken to be exactly in the middle of each member of the doublet structure.

One can see the frequency dependent effect of the structure. At high frequencies, each member of the structure is seen individually. As frequency decreases, a transition to seeing the bulk properties is made and finally at low frequencies the basement resistivity dominates. The results are shown for both zero and infinitely resistive basements. In the low frequencies the apparent resistivities sweep upwards for the infinitely resistive basement and sweep downwards for the infinitely conducting basement.

It is important to note that, as frequency decreases, the apparent resistivities reach the bulk effective resistivities *prior* to significant effects due to the basement resistivity. This is important as it means that the truncation of the anisotropic layer by the lower half-space has not interfered with the observa-

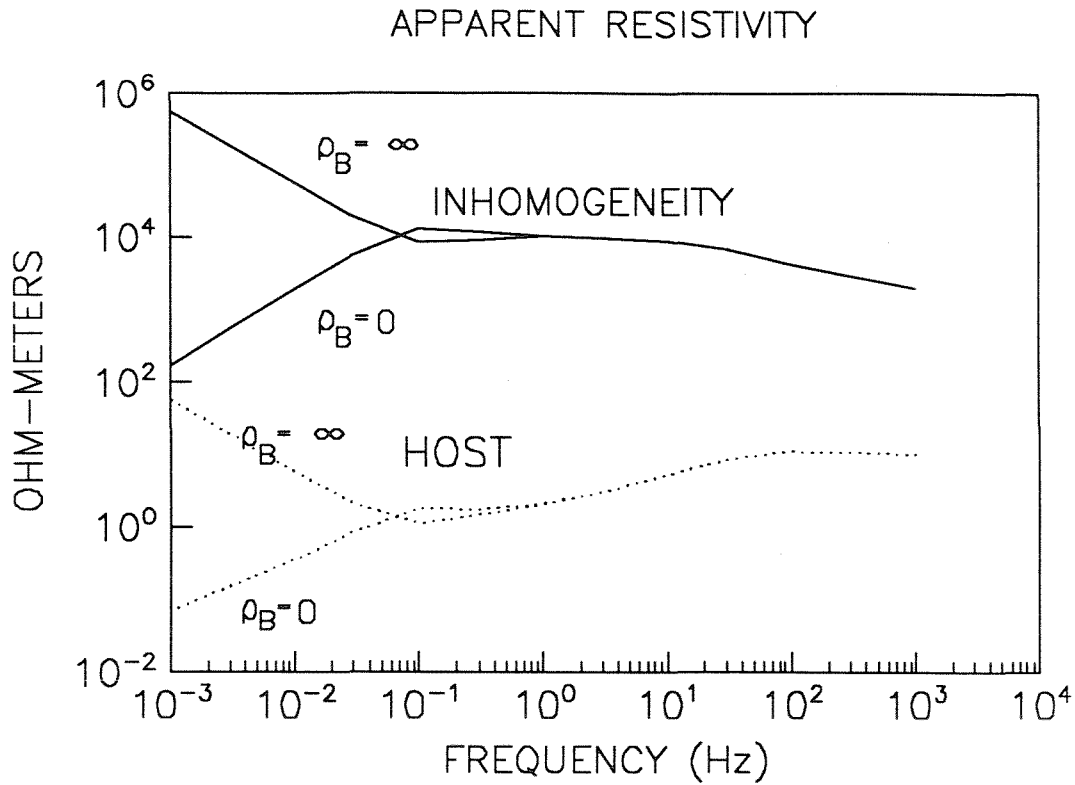


**Figure 4.4:** Surface apparent resistivity as a function of frequency at two sites. One site at the center of resistive inhomogeneity ( $d = 50m, \rho_d = 1000\Omega m$ ) while the other is at the center of conducting host ( $h = 550m, \rho_h = 10\Omega m$ ). The depth of the anisotropic layer is 15km.

tion of the transition of the anisotropic layer's response from its high frequency response to that of a bulk medium. The bulk effective resistivity (4.9) for this model is  $92.5 \Omega m$ . Equations 4.14-4.16 predict the apparent resistivities when the anisotropic layer is acting as a bulk medium and the basement has negligible effect. Over the conducting region, these equations predict that by .1 Hz the apparent resistivity should be  $1.08 \Omega m$  while over the resistive region it should be  $1.8 \times 10^4$  ohm-meters. Figure 4.4 shows that the apparent resistivities level off very close to these values before being swung upwards or downwards at still lower frequencies by the basement resistivity. The results of Chapter 3, which solves for a contact over an arbitrary basement conduc-

tivity, indicates that, even if the basement is neither perfectly conducting nor insulating, this enhancement and suppression will still be maintained into the extreme low frequencies.

Now consider how the basement is revealed by the impedance response in Figure 4.4. The frequency at which the apparent resistivities begin to change rapidly to approach the basement resistivity is .1 Hz. This frequency is that at which the fields just penetrate to the basement and thus contains information about the apparent depth to basement. If the material were homogeneous this would happen at a frequency where the thickness of the layer was approximately one skin-depth. At .1 Hz., the skin-depth in a material having a resistivity equal to that of the effective resistivity (92.5) would be approximately 15 km. Whereas 15 km is approximately one skin depth at 1 Hz. in the resistive dikes and one skin depth at .01 Hz. in the conducting host. Thus one can conclude that at this frequency the anisotropic layer is acting like a bulk material having a resistivity equal to that of the effective resistivity. In particular, the correct thickness can be determined if the effective bulk resistivity is utilized. However, the shift of the apparent resistivities up or down from the effective resistivity is so severe as a function of position that considerable averaging over measuring sites or possibly very long telluric lines would be required to evaluate it. The fact that the apparent resistivities over the dike and host can be predicted from bulk considerations also indicates that the layer is acting as a bulk material. Consideration of how to evaluate the effective bulk resistivity will be considered below.

Finally, note that over the conducting host, the thin resistive dikes have the effect of producing what appears to be a conducting layer at depth when the curves are interpreted only one-dimensionally. Interpretation of the other polarization (E-polarization) would indicate an electrical anisotropy at depth. The question that then arises concerns whether the response is due to 2 or 3-D structure or 1-D anisotropy. The 1-D anisotropic model in fact may be important, in practice. Schmucker (1986) observes such quasi-anisotropy in

the crust or upper mantle under West Germany and attributes it to a series of highly conducting dikes. R. Kurtz (private communication) also has data which may indicate deep anisotropy in the mantle under Ontario.

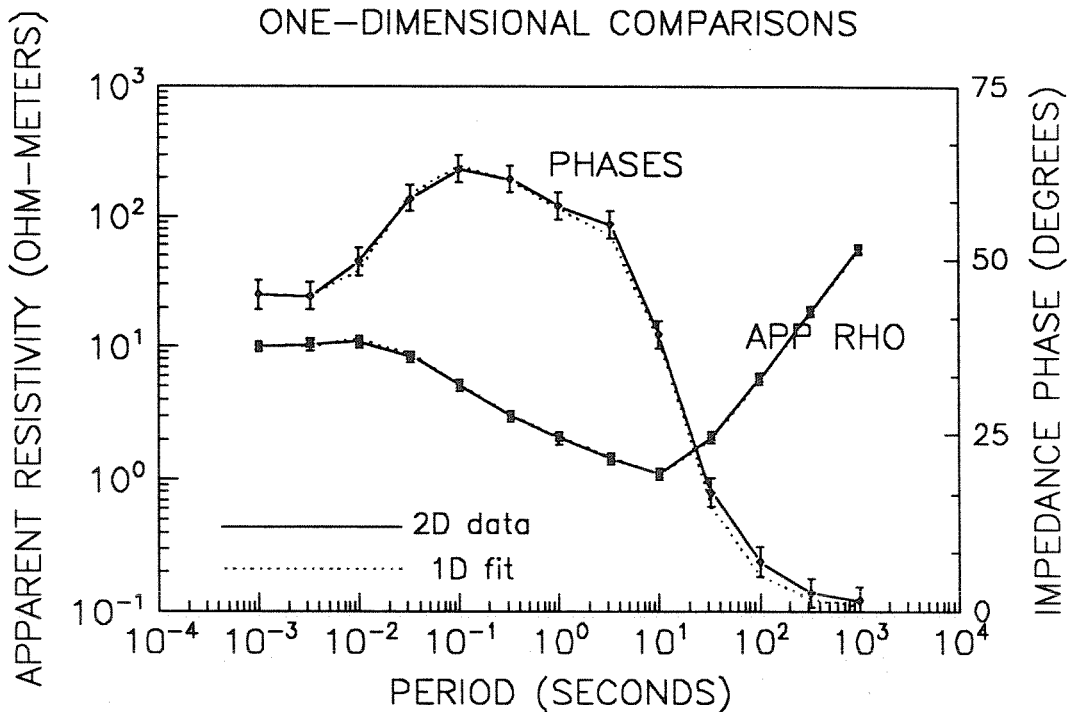


**Figure 4.5:** 1D inversion of 2D data. The data is that of the previous model (Figure 4.4) from the site over the conducting host. The inversion model is two layers over a half-space. The 1D model parameters are  $d_1 = 192m$ ,  $d_2 = 1707m$ ,  $\rho_1 = 10\Omega m$ ,  $\rho_2 = 1.14\Omega m$ ,  $\rho_B = 10^6\Omega m$ .

The impedance phases for these results do not contradict a one-dimensional interpretation. That is, the apparent resistivities and phases can be inverted together to obtain exceptionally good fits with one-dimensional models. As an example of how well this type of data can be modelled one-dimensionally, the sounding data over the conducting region from the previous model (Figure 4.4) is inverted and the fit to data shown in Figure 4.5. The inversion of data for the resistive basement was chosen to be displayed here. The 1D model chosen was two layers over a half-space with the resistivity of the top layer constrained

to be  $10\Omega m$ . Arbitrarily two degrees of phase error and a ten percent apparent resistivity error were added to simulate real data with low noise. The resulting model parameters which were forward modelled to obtain the impedance curves of Figure 4.5 are  $d_1 = 192m$ ,  $d_2 = 1707m$ ,  $\rho_1 = 10\Omega m$ ,  $\rho_2 = 1.14\Omega m$  and  $\rho_B = 10^6\Omega m$ . The inversions were done with both basement resistivities to compare the results. Except for the basement resistivity in the one-dimensional model, the 1D parameters for the two basement conductivities are very comparable, indicating the basement conductivity was not a factor in the parameters for the false conducting layer. For the conducting basement at the same site, the best fitting model parameters are  $d_1 = 188m$ ,  $d_2 = 1919m$ ,  $\rho_1 = 10\Omega m$ ,  $\rho_2 = 1.2\Omega m$  and  $\rho_B = 10^{-6}\Omega m$ . Thus, for this particular model, the apparent resistivities and phases at the host measuring position produce one-dimensional models which have a false conducting layer of depth.

#### 4.6 Experimental Evaluation of the Bulk Parameters

The question then arises as to how one should actually determine the correct bulk parameters. We have learned that the MT sounding curves can give approximately the right thickness if the correct bulk resistivity is known. In other words, the thickness of structure in the apparent resistivity curves is determined correctly, in terms of the effective resistivity. However if one never correctly measures the effective bulk resistivity then one would incorrectly determine the thickness. The solution is to correctly measure the average electric field (4.10). Two scales for the inhomogeneities are to be considered. In one case, the widths of the dikes are significantly less than the electrode spacing while in the other the dike widths are about the electrode spacing.

Figure 4.6 illustrates how dipole placement, for measuring the electric field, determines the apparent resistivity obtained. The model in Figure 4.6 is taken from a numerical study done by the Geological Survey of Canada for a region in eastern Newfoundland. In this model  $d = h = 1km$ ,  $\rho_d = 10$  and  $\rho_h = 1000$  ohm-metres. The depth of the structure is 5 km. and the basement

resistivity is zero. Equation 4.9 tells us that the effective resistivity is 505 ohm-meters while (4.15) indicates the apparent resistivity of the conducting dikes is  $.2\Omega m$  while over the resistive host it is 1980 ohm-meters. Figure 4.6 shows the apparent resistivities and phases for 5 different electrode placements. The electrode lengths are 1000m for all cases. The placements range from the electrode being entirely over the conducting region ( $0 \times 1000$ ), through three quarters over it ( $250 \times 750$ ), half ( $500 \times 500$ ), one-quarter ( $750 \times 250$ ), to entirely over the resistive region ( $1000 \times 0$ ).

It can be seen from Figure 4.6, that correct sampling ( $500 \times 500$ ) of the electric fields can give the correct bulk resistivity ( $505\Omega m$ ). This occurs when one samples equally over both structures. The results can give misleading bulk parameters if the electrodes are incorrectly placed. The misleading effects, as can be seen from the impedance phases, occur mostly in the apparent resistivities except in the case when there is no sampling of the electric field over the resistive part of the structure. The resulting apparent resistivities are shifted from those of the bulk response by frequency independent factors. The phase responses on the other hand are virtually identical except in the case where the electric field was sampled simply over the conducting material. In this case, the impedance phase is significantly different from the bulk response.

A very recent method (EMAP, Bostick 1986) for spatial sampling of the electric field in MT has emerged which has been utilized primarily by the oil industry. In this method, the spatial sampling is typically done with very long arrays of electrodes having lengths of the order of a kilometer. Thus the conclusions from this study are that although this method can help, in cases of elongated structure, the method must be used with care. Also, this study has given some indications as to the way in which such long electrodes determine bulk properties. Finally, note that at 5 Hz. one skin-depth in the bulk material ( $505 \Omega m$ ) is 5058 m. This is just the frequency that the model begins to significantly turn downwards towards the basement resistivity (zero).

Finally, a different scale of inhomogeneity is studied where the electrode

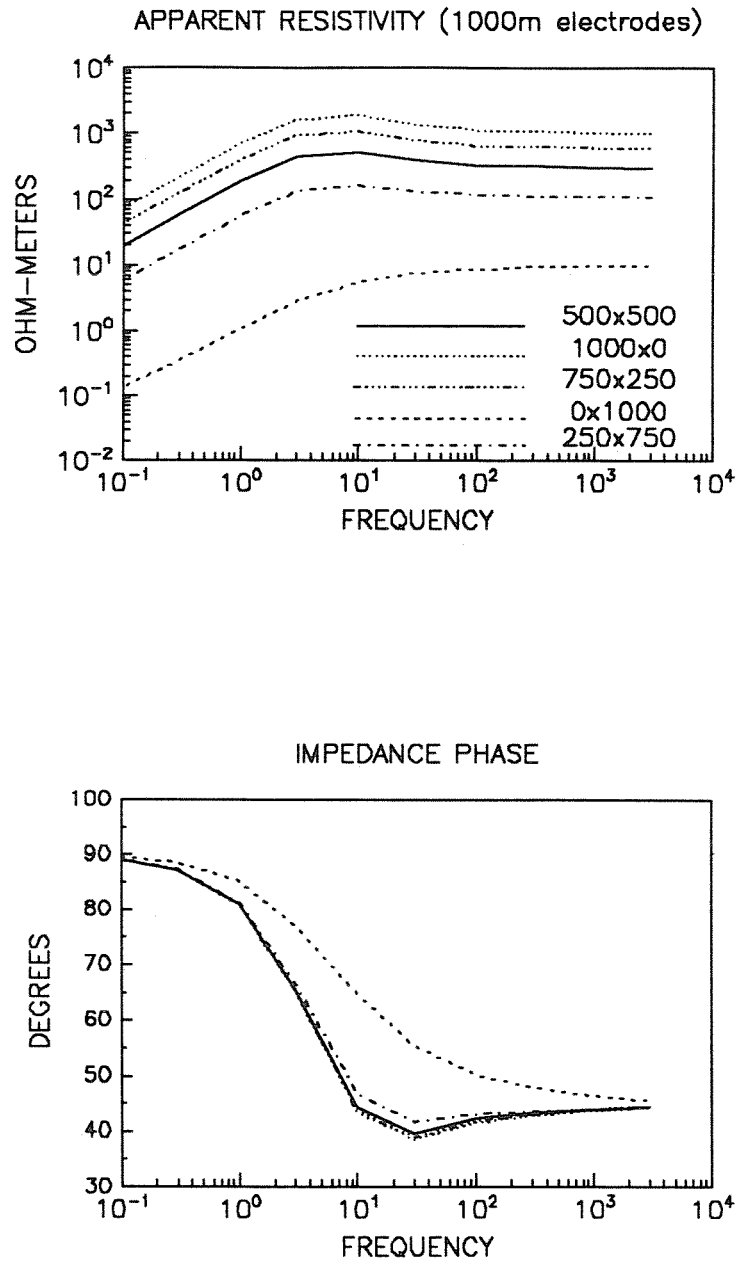


**Figure 4.6:** A study in the use and abuse of long electrodes to measure the electric field. In this model,  $d = h = 1km$ , while  $\rho_h = 1000\Omega m$  and  $\rho_d = 10\Omega m$ .  $D = 5km$  and the effective bulk resistivity ( $\rho_{eff}$ ) is 505 ohm-meters. The electrode length is 1km, and the surface impedances are shown for 5 different electrode placements.

separation covers multiple structures. This, to some extent, models inhomogeneous

geneities which are small compared to the electrode length. The resistivity contrast is again the same as in the previous models (10-1000 $\Omega m$ ). The thickness of the dikes is 10m and they are separated from each other by 10m of host. The depth of the anisotropic layer is 2000m. Again the effective resistivity is 505 ohm-meters (4.9).

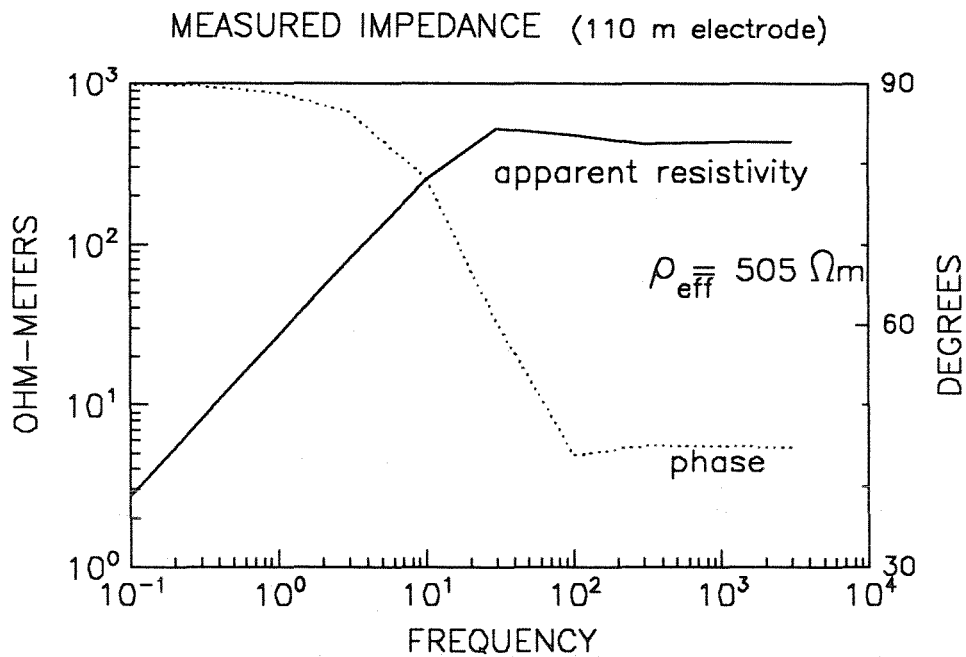


**Figure 4.7:** Fine structure impedance with 110m electrode. In this model  $d = h = 10m$  while again  $\rho_h = 1000\Omega m$  and  $\rho_d = 10\Omega m$ . The electrode covers 5 doublet pairs and one more conducting structure.

With averaging over several structures one expects reasonable estimates of bulk parameters. Figure 4.7 presents the impedances when the electrode length is 110 meters. With a fixed electrode spacing, the impedances are only slightly functions of positioning. For this reason, the response of only one particular placement of the electrodes was plotted. In this case the electrode covered 5 doublet pairs and then extended 10 meters onto the conducting host. For an electrode of this length this layout is expected to have the largest variation from the effective resistivity. One sees however, from Figure 4.7, that this electrode

layout determines very close to the correct bulk resistivity. The skin depth in 505 ohm-meter material is 2064 meters at 30 Hz. This is the frequency at which the basement begins to significantly effect the apparent resistivity. Thus, in this case, the spatial sampling of the electric field has produced both an apparent resistivity which is appropriate to the material (the effective resistivity) and the correct thickness of the layer when the correct bulk parameter is used.

#### 4.7 Summary

For the first time, a solution has been provided for the MT H-polarization impedance over a strong horizontally anisotropic structure which models the frequency dependence of the transition from the influence of the individual media to that of the bulk medium.

For structures of this type it is shown that for sufficiently low frequencies, the material behaves as a bulk material. The correct bulk resistivity is its effective resistivity (4.9). The model has indicated that for elongated structures MT can obtain useful parameters if the electric field is sampled correctly. However, incorrect sampling can produce erroneous results. These erroneous results are dependent upon frequency, the host resistivity, the depth of the inhomogeneous layer and the resistivity-thickness product of the inhomogeneities. A haphazard use of long electrodes will not necessarily produce useful results. As well, it is shown that in the presence of resistive dikes, impedance curves obtained over the more conducting host can produce false conducting layers if the curves are interpreted only one-dimensionally. Experimentally, these false interpretations can be difficult to avoid as will be discussed in detail in the following chapter. The H-polarization solution for a contact over an arbitrary basement of the previous chapter allows the interesting extension to models containing finite non-zero resistivities.

A conducting layer overlying such a structure will have the same effects as a long electrode. That is the electric fields over the two structures will become averaged upon diffusing through an upper layer. The amount of averaging will

depend upon the thickness of the layer versus the widths of the structure. If the overlying structure is sufficiently thick, the electric fields measured on the Earth's surface should be the averaged electric field. Thus, even in such extreme cases of inhomogeneities as the models of this chapter when the material is buried at sufficient depth, magnetotellurics perceives the structure in a reasonable manner. However, the results would indicate that if resistive dikes do not reach the surface a false conducting layer could be indicated on the sounding curves without any surface signature for the dikes. This will occur when the overlying layer is not electromagnetically thick and the distances between the contacts are relatively large compared to electrode spacing.



## CHAPTER 5

### THE EFFECTS OF SMALL-SCALE NEAR-SURFACE INHOMOGENEITIES

#### 5.1 Introduction

Magnetotelluric data are normally presented in the frequency domain as impedance tensors which map the measured horizontal components of the magnetic field at the earth's surface to the horizontal electric fields. The linear relation

$$\vec{E}(\vec{r}, \omega) = \mathbf{Z}(\vec{r}, \omega) \vec{H}(\vec{r}, \omega) \quad (5.1)$$

is often termed the fundamental assumption of magnetotellurics (MT). The impedance tensor  $\mathbf{Z}(\vec{r}, \omega)$ , which varies with position  $\vec{r}$  and frequency  $\omega$ , reflects the earth's conductivity distribution. Implicit in the MT method is the assumption that the impedance tensor is independent of source. Although experience has demonstrated that such a linear relationship (5.1) is often true, there is no complete proof of its validity in all possible conductivity distributions nor is there an exhaustive explanation of the exact way in which it reflects the earth's conductivity distribution.

$\mathbf{Z}(\vec{r}, \omega)$  is a rank two, complex tensor

$$\mathbf{Z}(\vec{r}, \omega) = \begin{pmatrix} Z_{11} & Z_{12} \\ Z_{21} & Z_{22} \end{pmatrix}.$$

For an arbitrary earth structure, there is no obvious and clear means for interpreting the raw impedance data. The desirable step subsequent to the experimental determination of such impedance data is the extraction of parameters from the data which have some physical significance. These parameters must have some interpretable meaning in terms of the actual conductivity distribution within the earth. In the case of a 2-D earth structure (*i.e.* uniform along one horizontal axis), Maxwell's equations (Chapter 1) show the electromagnetic fields decouple into two distinct polarizations. These polarizations

correspond to the horizontal electric field accompanied by its perpendicular horizontal magnetic field being polarized parallel or perpendicular to the strike axis of the structure. When the coordinate axes (measurement axes) correspond to the principal axes (*i.e.* natural axes), the impedance tensor has the form

$$\mathbf{Z}_2 = \begin{pmatrix} 0 & a \\ -b & 0 \end{pmatrix}. \quad (5.2)$$

The components of the tensor,  $a$  and  $b$ , are the intrinsic surface impedances of the medium; one is associated with current flow parallel to the strike and the other with the magnetic field solely parallel to the strike. (If the structure is one dimensional then  $a = b$ .) If the measurement axes are not aligned with the principal axes of the structure then the measured impedance tensor is derived from the intrinsic impedance tensor (5.2) via the standard transformation of a linear mapping to a rotated coordinate frame;

$$\mathbf{Z}_m = \mathbf{R} \mathbf{Z}_2 \mathbf{R}^t \quad (5.3)$$

where  $\mathbf{R}$  is a rotation operator,

$$\mathbf{R} = \begin{pmatrix} \cos\theta & \sin\theta \\ -\sin\theta & \cos\theta \end{pmatrix}.$$

$\theta$  is the angle between the coordinate, or measurement frame and the principal, or natural frame.

If the structure is truly two-dimensional, the angle  $\theta$  can be easily shown to be

$$\theta = \frac{1}{2} \tan^{-1} \left( \frac{Z_{22} - Z_{11}}{Z_{12} - Z_{21}} \right) \pm \frac{\pi}{2} \quad (5.4)$$

where  $Z_{ij}$  are elements of the measured impedance tensor.  $\mathbf{Z}_m$  can then be rotated by  $\theta$  to obtain the intrinsic impedance tensor  $\mathbf{Z}_2$  and the correct principal impedances then obtained. However, in the presence of measurement noise, equation (5.4) is not a stable method for obtaining the 2-D strike angle. Swift(1967) has shown that minimizing the functional

$$|Z_{11}|^2 + |Z_{22}|^2 \quad (5.5)$$

as a function of rotation angle is a stable and accurate method in practise for obtaining the strike angle.

There is no decomposition whose parameters are readily interpretable when the MT impedance tensor is produced from arbitrary three-dimensional conductivity distributions. Initially and even at present, interpreters hoped that the effects of small three-dimensional structures would not have significant impact on the derivation of correct large-scale conductivity parameters by the two-dimensional model of the impedance tensor (5.3). The present chapter develops an analytic model of a small-scale surface inhomogeneity by which to investigate the effects of such bodies on the measured impedance tensor. This model is not intended to represent all the possible effects of small-scale scatterers on the measured impedance tensor. Rather, the model is used to 1) demonstrate the nature of the limitations of the conventional or two-dimensional method of interpretation, 2) derive an expansion of the measured impedance tensor which includes two-dimensional effects, three-dimensional galvanic effects and weak three-dimensional induction, 3) give motivation for an analytic decomposition of the measured impedance tensor which includes galvanic three-dimensional effects (Chapter 6), and 4) discuss two other theoretical decompositions which have been presented in the last decade (Appendix 3).

### 5.1.2 The Galvanic Distortion Operator:

Some work has been done to include the effects of three dimensional bodies which have primarily a galvanic or direct current (charge distribution) effect with a very weak inductive response.

In 1976, Berdichevsky and Dmitriev provided some insights into the problem of small-scale inhomogeneities. They considered a body (Figure 5.1) embedded in a host conductivity structure which was simply a function of depth. Their intention was to investigate the distorting effect on the impedance tensor of surface inhomogeneities using this model as an example. The distort-

ing body has an elliptical cross-section and a thickness equal to that of the top layer. The dimensions of the body are considered small with respect to any spatial variations of the primary electromagnetic field produced by the one-dimensional structure. To estimate the effects of the inhomogeneity, they considered the electric fields of the one-dimensional solution to be distorted by a  $2 \times 2$ , real (implying frequency independent) distortion matrix which they termed  $F$ . That is

$$\vec{E}(\omega) = F\vec{E}_0(\omega) \quad (5.6)$$

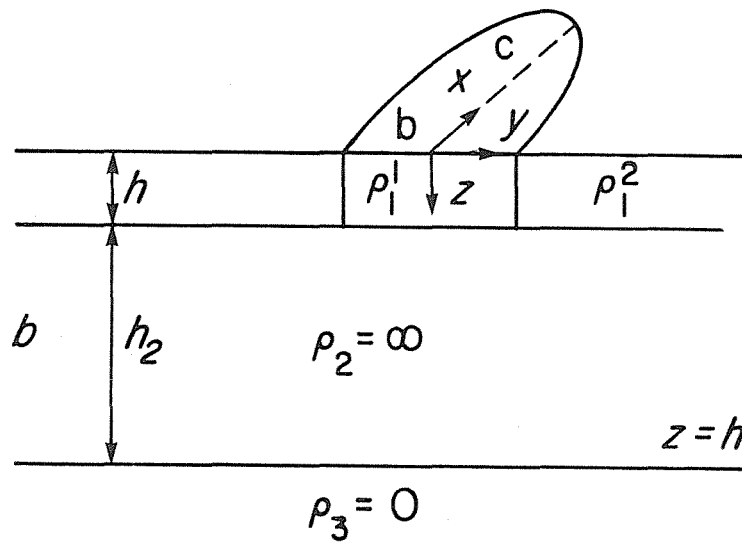


**Figure 5.1:** The distortion model of Berdichevsky and Dmitriev, 1976

where  $\vec{E}_0 = (E_x^0, E_y^0)$  are the components of the primary electric field. For the purposes of this and the next chapter, primary field will always refer to the field of the large scale structure.

Recall the assumption that, in the frequency domain, the electric fields tangential to the earth's surface are related to the tangential magnetic fields via a transfer function,  $Z(\vec{r}, \omega)$ . It will henceforth be implicit that  $\vec{E}, \vec{H}$  and  $Z$  are functions of frequency and position. Thus,

$$\vec{E} = Z\vec{H}.$$

If the regional or large-scale conducting structure is one-dimensional then

$$\mathbf{Z} = \begin{pmatrix} 0 & Z_0 \\ -Z_0 & 0 \end{pmatrix} = \mathbf{Z}_0. \quad (5.7)$$

and therefore combining (5.6) and (5.7)

$$\vec{E} = \mathbf{F} \vec{E}_0 = \mathbf{F} \mathbf{Z}_0 \vec{H}_0 = \mathbf{Z} \vec{H} \quad (5.8)$$

where  $\vec{H}_0$  is the primary magnetic field and  $\vec{H}$  is the total horizontal magnetic field.

Berdichevsky and Dmitriev determined the distortion matrix,  $\mathbf{F}$ , by considering the first layer to be a thin sheet and then calculating the electrostatic effect of the inhomogeneity. Estimating the anomalous magnetic field ( in effect, an upper bound was determined ) due to the presence of the body via the Biot-Savart law, they then determined the resulting impedance tensor,  $\mathbf{Z}$ .

However, upon representing the problem in this manner, they determined the resulting impedance tensor and thus the distortion tensor only at a measurement site on one of the principal axes of the ellipse. On these axes, the electric distortion tensor  $\mathbf{F}$  is diagonal and thus the resulting effect of the body is solely that of anisotropy. That is , at such sites, the impedance tensor,  $\mathbf{Z}$ , is given by

$$\mathbf{Z} = \mathbf{F} \mathbf{Z}_0 = \begin{pmatrix} F_{11} & 0 \\ 0 & F_{22} \end{pmatrix} \begin{pmatrix} 0 & Z_0 \\ -Z_0 & 0 \end{pmatrix} = \begin{pmatrix} 0 & F_{11}Z_0 \\ -F_{22}Z_0 & 0 \end{pmatrix} \quad (5.9)$$

ignoring the perturbing effects on the magnetic field. The complex phases of the principal impedances ( i.e. the off-diagonal elements of the impedance tensor ) remain unchanged, since the elements of  $\mathbf{F}$  are real, but the principal impedances have been multiplied by scaling factors  $F_{11}$  and  $F_{22}$  which are generally different. Over those frequencies where the inhomogeneity has only a galvanic effect, the principal impedances are “split” by a constant factor but have identical phase angles. This effect has become known by interpreters of magnetotelluric data as “static shift”.

Although the effect of anisotropy is one effect of small bodies, the analyses which follow shows that Berdichevsky and Dmitriev's choice of the measuring position was unfortunate, and is an oversimplified view of the problem of small-scale inhomogeneities in magnetotellurics.

A more realistic model will be presented, with a more complete solution, to illustrate more fully the effects of such surface inhomogeneities. With the use of this model, the effect of such inhomogeneities on the conventional interpretation or decomposition (Swift, 1967) of the impedance tensor can be discussed. This analysis is meant to demonstrate the need for a more complete decomposition of the impedance tensor which can take into account more comprehensively the effects of such inhomogeneities. Such a decomposition will be presented later in this thesis (Chapter 6).

## 5.2 Distortions Due to a Hemisphere

The following illustration does not attempt to explain or express all the effects of small-scale inhomogeneities, but rather to dispel some common misconceptions, and illustrate some of the characteristics of the phenomena. Also it is used to justify the need for the decomposition which is presented later.

To study the effects of small-scale surface inhomogeneities, consider a conductive hemisphere of uniform conductivity,  $\sigma_2$ , embedded in a medium of conductivity  $\sigma_1$ . The conducting media are enclosed above by an insulating half-space to represent the fact that the earth's atmosphere is approximately an insulator at magnetotelluric frequencies. The radius,  $R$ , of the hemisphere is much less than either the electromagnetic wavelength or the skin-depths at the relevant frequencies in both media. This assumption allows us to consider the inhomogeneity to be excited by a uniform electric field when the body is sufficiently removed from any inhomogeneities in the medium in which it is embedded. In addition, the flux of the time-varying magnetic field through the hemisphere is considered to be sufficiently small to neglect any induced secondary electric fields. The electromagnetic problem thus reduces to the

electrostatic distortion by a hemisphere when excited by a uniform electric field.

### 5.2.1 Electrostatic Distortion Due to a Hemisphere

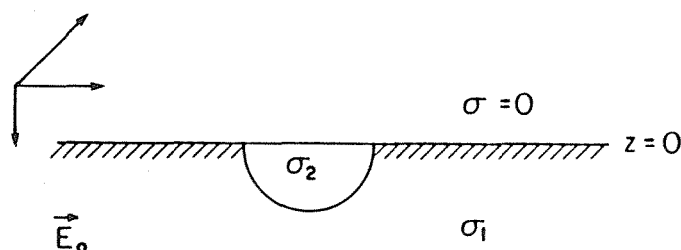


**Figure 5.2:** Conducting hemisphere excited by a uniform electric field embedded in a homogeneous conducting half-space.

To begin this illustration, consider the electrostatic effect of a conducting hemisphere in a uniformly conducting half-space (Figure 5.2) excited by a uniform static electric field,  $E_0\hat{x}$ . The upper half-space is an insulator. Maxwell's equations in the conducting medium thus become

$$\nabla \times \vec{E} = 0 \tag{5.10a}$$

$$\nabla \times \vec{H} = \sigma \vec{E} \tag{5.10b}$$

everywhere and

$$\nabla \cdot \vec{E} = 0 \tag{5.10c}$$

except at boundaries. Thus, the electric field can be determined by a potential function,  $\phi$ , such that

$$\vec{E} = -\nabla\phi \tag{5.11}$$

and therefore from (5.10c),  $\phi$  satisfies Laplace's equation:

$$\nabla^2 \phi = 0 \quad (5.12)$$

except at boundaries. As well, there are the additional boundary constraints that

- 1)  $\phi$  is continuous across all boundaries.
- 2)  $\sigma \frac{\partial \phi}{\partial n} = J_n$  is continuous across all boundaries.
- 3)  $\frac{\partial \phi}{\partial z} = 0$  at  $z = 0$ .
- 4)  $-\nabla \phi \rightarrow E_0 \hat{x}$  as  $r \rightarrow \infty$

where  $\hat{n}$  is the unit normal vector to the surface.

The second boundary condition is the requirement that normal current density be continuous, while the third is due to the lack of current in the insulator, combined with boundary condition 2.

The solution is extracted by symmetry from the electrostatic problem of a uniformly conducting sphere, in a homogeneous medium, excited by a constant static field (Ward, 1967). In a spherical co-ordinate system the solution is expressible as

$$\phi_i(r, \theta, \phi) = \left( -E_0 + \frac{P}{R^3} \right) r \sin \theta \quad (5.13)$$

within the inhomogeneity and

$$\phi_e(r, \theta, \phi) = \left( -E_0 r + \frac{P}{r^2} \right) \sin \theta \quad (5.14)$$

outside the hemisphere but within the conducting half-space.

$$P = \frac{\sigma_2 - \sigma_1}{\sigma_2 + 2\sigma_1} E_0 R^3$$

is the induced electric dipole moment of the hemisphere.

That (5.13) and (5.14) satisfy the boundary conditions, 1-4, can be easily checked. Both solutions,  $(\phi_i, \phi_e)$ , are clearly solutions of Laplace's equation. Since Laplace's equation has a unique solution for given boundary conditions,

the above solution is the required one. It is to be noted, for an equal source, that the primary electric field and therefore all electric fields are twice those for the similar problem of a sphere in a whole-space.

The total electric fields are therefore given by (5.11, 5.13)

$$\vec{E}_i(x, y, z) = E_0 \left( \frac{3\sigma_1}{\sigma_2 + 2\sigma_1}, 0, 0 \right) \quad (5.15)$$

within the hemisphere, and outside the hemisphere and within the conducting medium, ( $z \leq 0$ ), by (5.11, 5.14)

$$\vec{E}_e(x, y, 0) = \left( E_0 + P \frac{(2x^2 - y^2)}{r^5}, \frac{3Pxy}{r^5}, \frac{3Pxz}{r^5} \right). \quad (5.16)$$

The magnitude of the secondary electric fields fall off as  $\left(\frac{R}{r}\right)^3$ . If the measurement site is a distance  $2R$  outside the hemisphere, the magnitude of secondary electric field is less than four percent of that of the primary electric field. Recall the assumption that the radius of the hemisphere is very small compared to the electromagnetic skin-depth. It is clear that at low frequencies the scattered electric fields die off due to geometric effects long before there is significant phase rotation or amplitude loss due to diffusion in the host medium. The implications here are two-fold. The first is that such small-scale bodies must be near-surface for them to have any significant effect on the electric fields measured at surface. Secondly, it is not necessary to consider phase rotations of the fields when measuring at low frequencies near the distorting bodies.

The previous solution for the distorted electric fields due to the hemisphere provides the means for determining the effects of the hemisphere on the magnetic field. The source of this anomalous electrostatic magnetic field is the anomalous current density,  $\vec{J}_a$ , within all of the conducting half-space including the conducting hemisphere. The anomalous magnetic field at any field point is given by

$$\vec{H}_a(x_0, y_0, z_0) = \frac{1}{4\pi} \int \frac{\vec{J}_a(x, y, z) \times \hat{r}}{r^2} dV \quad (5.17)$$

where  $\vec{r} = r\hat{r}$  is the vector from  $\vec{J}_a dV$  to the field point  $(x_0, y_0, z_0)$  and the integral is over the half-space  $z < 0$ .

At the surface of the conducting medium, the total horizontal magnetic field,  $\vec{H}_h^a$ , can be written as <sup>1</sup>

$$\vec{H}_h^a = \vec{H}_H^y + \vec{H}_e^2 + \vec{H}_e^1 \quad (5.18)$$

where each term can be expressed as an integral. The first term,  $\vec{H}_H^y$ , is due to the anomalous currents in the hemisphere:

$$\vec{H}_H^y(x_0, y_0, 0) = \frac{\beta}{2\pi} \int_{V_H} \frac{z}{r^3} dV \vec{y} \quad (5.19)$$

where

$$\beta = \frac{\sigma_1(\sigma_2 - \sigma_1)}{\sigma_2 + 2\sigma_1} E_0$$

and the integral is over the volume of the hemisphere. In the spherical coordinate system  $r^2 = r_s^2 + r_0^2 - 2r_0r_s \cos(\phi - \phi_0)\sin\theta$ ,  $r_s^2 = x^2 + y^2 + z^2$  and  $r_0^2 = x_0^2 + y_0^2$ .

To determine the magnetic field due to the anomalous current outside the hemisphere a vector identity (Lee, 1975) is used:

$$\begin{aligned} \frac{\vec{J}_a(x, y, z) \times \hat{r}}{r^2} &= \nabla_0 \left( \frac{1}{r} \right) \times \vec{J}_a(x, y, z) = \nabla_0 \times \left( \frac{\vec{J}_a}{r} \right) \\ &= \frac{\nabla \times \vec{J}_a(x, y, z)}{r} - \nabla \times \left( \frac{\vec{J}_a(x, y, z)}{r} \right) \end{aligned}$$

where again  $\hat{r} = \frac{\vec{r}}{r}$  is the unit vector pointing from the source point  $(x, y, z)$  to the field point  $(x_0, y_0, z_0)$ ,  $\nabla_0$  is an operator with respect to the field points and  $\nabla$  is an operator with respect to source points. The first term in the above identity is identically zero since only static (*i.e.* galvanic) effects are considered. Volume integrals over the second term can be transformed into integrals over

<sup>1</sup> The details of the discussion which follows are contained in Appendix 2

the surface of the volume. Thus, the second term,  $\vec{H}_e^2$  is due to an integral over the surface of the hemisphere:

$$\vec{H}_e^2(x_0, y_0, z_0) = \frac{-\beta R^2}{4\pi R} \int_0^{2\pi} \int_{\frac{\pi}{2}}^{\pi} \frac{\cos\theta \sin^3\theta}{r(\theta, \phi)} d\theta d\phi \hat{y}, \quad (5.20)$$

where  $r^2(\theta, \phi) = R^2 + r_0^2 - 2r_0 R (\cos\theta \cos\theta_0 + \cos(\phi - \phi_0) \sin\theta \sin\theta_0)$ .

$\vec{H}_e^1$  contains the only contribution to the magnetic field parallel to the exciting electric field. This term is obtained by an integral over the surface of the conducting medium outside the hemisphere.

$$\begin{aligned} \vec{H}_e^1(x_0, y_0, z_0) = & \frac{\beta R^3}{4\pi} \int_R^\infty \frac{1}{\rho^2} \left\{ \int_0^{2\pi} \frac{3\cos\phi \sin\phi}{r} d\phi \hat{x} \right. \\ & \left. - \int_0^{2\pi} \frac{2\cos^2\phi - \sin^2\phi}{r} d\phi \hat{y} \right\} d\rho \end{aligned} \quad (5.21)$$

where  $r^2(\theta, \phi) = \rho^2 + r_0^2 - 2r_0\rho (\cos(\phi - \phi_0) \sin\theta_0)$  and  $\rho^2 = x^2 + y^2$ .

The total electrostatically magnetic field can now be evaluated via these integrals. However, for the purposes of this thesis an estimation of this magnetic field in the proximity of the hemisphere is all that is required. How this anomalous magnetic field modifies the measured impedance tensor and the order of magnitude of the effects is what is desired, not the exact determination of the anomalous magnetic field.

The total electrostatic magnetic field can be easily evaluated at the centre of the hemisphere on the surface ( $z = 0$ ) (A2.14,A2.19,A2.22,A2.24)

$$\vec{H}_a(0, 0, 0) = \frac{-\beta R}{2} \vec{y}. \quad (5.22)$$

As well, the total field can be approximated on the surface inside the hemisphere ( $\frac{r_0}{R} < 1$ ) as (A2.15,A2.18,A2.21,A2.23)

$$\vec{H}_a(x_0, y_0, 0) \approx -\beta R \left[ \frac{1}{2} \vec{y} - \frac{3}{128} \left( \frac{r_0}{R} \right)^2 \sin 2\theta_0 \vec{x} \right] \quad (5.23)$$

In general, the horizontal magnetic field can be expressed as

$$\vec{H}_a(x_0, y_0, 0) = -E_0 (\alpha \vec{y} + \gamma \vec{x}). \quad (5.24)$$

The anomalous magnetic field has its most significant effect in the proximity of the hemisphere. In the region of the hemisphere (A2.26)

$$\alpha = O(\sigma_1 R) \quad [\sigma_1 \neq \sigma_2] \quad (5.25)$$

and  $\gamma$  is approximately two orders of magnitude smaller. If the conductivities of the host and inhomogeneity are not sufficiently different, the effect of the anomalous magnetic field is even less significant and need not be considered.

In conclusion, the electrostatic anomalous magnetic field is proportional to the primary electric field. The proportionality constants are of course frequency independent geometric factors. These geometric factors are at most of order  $(\sigma_h L)$  where  $\sigma_h$  is the conductivity of the host and  $L$  is a characteristic scale length of the inhomogeneity. The electrostatic anomalous magnetic field falls off sufficiently rapidly due to geometric effects to neglect diffusion loss and phase variation.

### 5.2.2 The Channelling Tensor , C

The total electric field at the surface of the conducting medium is of interest, since magnetotelluric measurements are made on the surface of the earth. If the primary electric fields are approximately uniform over the hemisphere the above model gives a reasonable solution for the effects of the hemisphere. Here the primary electric field is the field which would exist if the hemisphere were not present.

For a primary electric field  $E_0 \hat{x}$  (5.15)

$$\vec{E}_i(x, y, z) = E_0 \left( \frac{3\sigma_1}{\sigma_2 + 2\sigma_1}, 0, 0 \right)$$

within the hemisphere and outside on the surface ( $z = 0$ ) of the conducting medium (5.16)

$$\vec{E}_e(x, y, 0) = E_0 \left( 1 + P \frac{(2x^2 - y^2)}{r^5}, \frac{P3xy}{r^5}, 0 \right);$$

where now

$$E_0 P = \frac{\sigma_2 - \sigma_1}{\sigma_2 + 2\sigma_1} R^3 E_0 \quad (5.26)$$

is the induced electric dipole moment of the hemisphere.

By superposition and symmetry, for an arbitrary but uniform exciting field which contains no vertical electric field

$$\vec{E}_0 = (E_x^0, E_y^0),$$

the electric field ( $\vec{E}$ ) at the surface of the conducting medium is given by

$$\vec{E}(x, y, 0) = \mathbf{C} \vec{E}_0. \quad (5.27)$$

The tensor,  $\mathbf{C}$ , now termed the channelling tensor is

$$\mathbf{C}_i(x, y, 0) = \begin{pmatrix} \frac{3\sigma_1}{\sigma_2 + 2\sigma_1} & 0 \\ 0 & \frac{3\sigma_1}{\sigma_2 + 2\sigma_1} \end{pmatrix} \quad (5.28)$$

inside the inhomogeneity and

$$\mathbf{C}_e(x, y, 0) = \begin{pmatrix} 1 + P \frac{(2x^2 - y^2)}{r^5} & \frac{P3xy}{r^5} \\ \frac{P3xy}{r^5} & 1 + P \frac{(2y^2 - x^2)}{r^5} \end{pmatrix} \quad (5.29)$$

outside the hemisphere.

The assumption that no primary vertical electric field impinges on the hemisphere is reasonable, unless the body is very near another structure. The electric field in the conducting medium must be zero at the surface of the insulator and (except possibly near an inhomogeneity) the near-surface electric field has very little vertical component.

At this point, it is interesting to note some comparisons to the conclusions of Berdichevsky and Dmitriev (1976). Inside the hemisphere, the channelling tensor has the form

$$\mathbf{C} = g \begin{pmatrix} 1 & 0 \\ 0 & 1 \end{pmatrix} \quad (5.30)$$

and thus the regional (1 or 2-D) electric fields are scaled by a uniform factor,  $g$ , independent of frequency ("static shift"). Outside the hemisphere along the principal axes of the 2D structure (or the measurement axes if regional structure 1D), the channelling tensor has the form of an anisotropy operator as in the Berdichevsky and Dmitriev conclusions.

$$\mathbf{C} = g \begin{pmatrix} 1 + s_1 & 0 \\ 0 & 1 + s_2 \end{pmatrix} \quad (5.31)$$

Once again the regional electric fields are scaled or shifted independent of frequency but by different factors. A quite different form from (5.31) however is found along the lines  $|x| = |y|$ , outside the distorting body. Here

$$\mathbf{C} = \begin{pmatrix} 1 + \frac{P}{2^{5/2}|x|^3} & \frac{3P}{2^{5/2}|x|^3} \\ \frac{3P}{2^{5/2}|x|^3} & 1 + \frac{P}{2^{5/2}|x|^3} \end{pmatrix} \quad (5.32)$$

which can be written in the form

$$\mathbf{C} = g \begin{pmatrix} 1 & e \\ e & 1 \end{pmatrix}. \quad (5.33)$$

The channelling tensor has the form of an elastic strain tensor where the shearing strains are equal and non-zero. This form of the channelling tensor will henceforth be called a *shear* tensor. The resulting components of the electric field are now linear combinations of the primary electric field components. That is

$$E_x = g(E_x^0 + eE_y^0) \quad \text{and} \quad E_y = g(eE_x^0 + E_y^0).$$

It is now possible to make an important conclusion with regard to the distortion operator,  $\mathbf{C}$ . If one examines the distortion operator at locations

which are not on the symmetry axes of the distorting body or the applied primary field,  $\mathbf{C}$  is in general more than an anisotropy operator. It essentially has the effect of distorting the polarization of the electric field from that of the primary electric field, by taking linear combinations of the components of the latter. Thus the need for a decomposition of the impedance tensor which can unmix the components.

A channelling tensor  $\mathbf{D}$ , for the distortion of the magnetic field, can also be defined. Equations A2.4 and A2.6 give the anomalous horizontal magnetic field at an arbitrary field point, due to a uniform electric source field in the  $x$ -direction. By similar calculations for a uniform source field in the  $y$ -direction, it can be shown that the anomalous magnetic fields tangential to the surface  $z_0 = 0$  and on that surface can be expressed as

$$\vec{H}_h^a(x_0, y_0, 0) = \begin{pmatrix} -\gamma & \alpha \\ -\alpha & \gamma \end{pmatrix} \vec{E}_0 = \mathbf{D}\vec{E}_0. \quad (5.34)$$

$\vec{E}_0$  is again an arbitrary uniform and horizontal primary source field. In the region of the hemisphere where this anomalous magnetic field is most significant,  $\alpha$  is much greater than  $\gamma$  and  $\alpha$  has the order of magnitude of  $\sigma_1 R$  (A2.26).

If an inhomogeneity did not have the symmetry of the hemisphere, the representation of anomalous magnetic field as the result of a real, frequency-independent operator,  $\mathbf{D}$ , acting on the primary electric field (5.34) would still be correct. Except, in this case, there could be as many as four independent elements in  $\mathbf{D}$ . When the effect of the magnetic distortion operator  $\mathbf{D}$  is significant, one would still expect the diagonal components of  $\mathbf{D}$  to be significantly smaller than the off-diagonal components. In general, one expects  $\mathbf{D}$  to have two significantly non-zero real parameters.

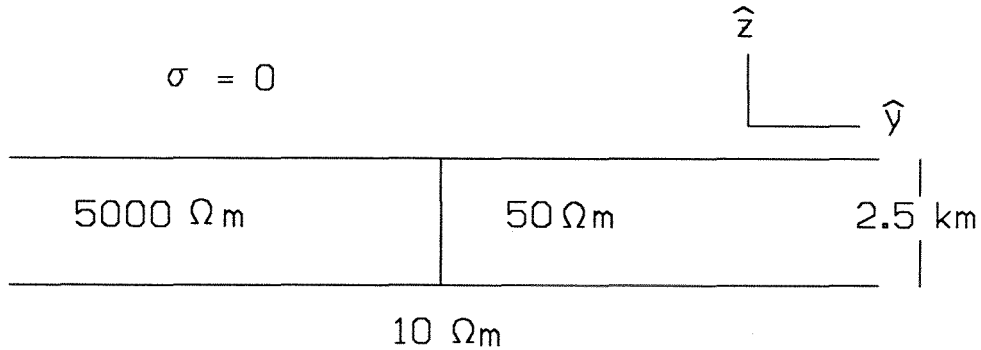


**Figure 5.3:** The regional or two-dimensional conductivity structure with coordinate system.

### 5.2.3 Effects on Magnetotelluric Interpretation

To extend this illustration to include the effects of small-scale inhomogeneities on both magnetotelluric interpretation and the model for the impedance tensor, consider a simple earth model (Figure 5.3).

The model consists of two uniformly conducting, semi-infinite slabs overlying a half-space. The two-dimensional structure together with the MT assumption of a plane wave source field has two decoupled electromagnetic solutions often called the E- and H-Polarizations as discussed in previous chapters of this thesis. That is

$$\vec{E}_0 = \begin{pmatrix} 0 & Z_{\parallel} \\ -Z_{\perp} & 0 \end{pmatrix} \vec{H}_0 = \mathbf{Z}_2 \vec{H}_0 \quad (5.35)$$

if the measurement axes are parallel and perpendicular to the principal axes of the two-dimensional structure. In the E-Polarization, the electric field,  $E_x$ , is parallel to the contact and thus the impedance (the ratio of  $E$  over  $H$ ) is termed  $Z_{\parallel}$ . In the H-Polarization mode the electric field,  $E_y$ , is perpendicular to the contact and thus the impedance is  $Z_{\perp}$ .

In this simple earth model is embedded a conducting hemisphere (Figure 5.4) about 1 km. to the left of the contact. In such a geological setting, it is the 2-D structure which is generally required, and the small-scale inhomogeneity is

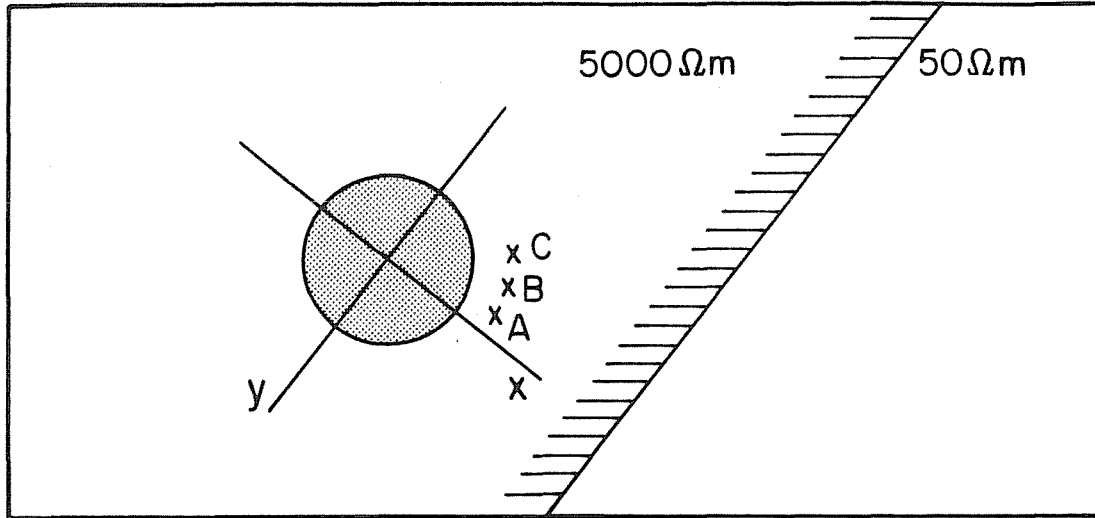


**Figure 5.4:** Plan view of regional structure with embedded hemisphere. The figure is schematic and not to scale. The radius of the hemisphere is 30m, the measuring sites (A,B,C) are just outside the body and the hemisphere is almost 1 km from the two-dimensional contact which separates the two semi-infinite slabs.

of little or no interest.

At the frequencies utilized in this example, the radius of the hemisphere (30 m) is small with respect to the relevant skin-depths. The body is sufficiently removed from the fault to ensure that the primary electric fields (due to the two-dimensional structure) are uniform over the extent of the hemisphere. Due to the small relative size of the hemisphere one can neglect, except as a minor effect, any induced secondary fields produced by the small inhomogeneity. Therefore, the earlier model of simple electrostatic distortion by the hemisphere when excited by a uniform primary electric field, is appropriate. That is

$$\vec{E} = C\vec{E}_0 \quad (5.36a)$$

$$\begin{aligned} \vec{H} &= \vec{H}_0 + D\vec{E}_0 \\ &= (\mathbf{I} + D Z_2) \vec{H}_0 \end{aligned} \quad (5.36b)$$

since  $\vec{E}_0 = Z_2 \vec{H}_0$ . Thus

$$\vec{E} = C Z_2 \vec{H}_0 \quad (5.37a)$$

$$= \mathbf{Z} \vec{H} \quad (5.37b)$$

$$= \mathbf{Z} (\mathbf{I} + \mathbf{D} \mathbf{Z}_2) \vec{H}_0. \quad (5.37c)$$

from (5.36). Therefore,

$$\mathbf{Z} = \mathbf{C} \mathbf{Z}_2 (\mathbf{I} + \mathbf{D} \mathbf{Z}_2)^{-1} \quad (5.38a)$$

$$= \mathbf{C} \mathbf{Z}_2 \left[ \mathbf{I} + \begin{pmatrix} -\gamma & \alpha \\ -\alpha & \gamma \end{pmatrix} \mathbf{Z}_2 \right]^{-1} \quad (5.38b)$$

using (5.34).

The effects of the magnetic field distortion  $\mathbf{D}$  are strongest near the inhomogeneity and at higher frequencies. The components of  $\mathbf{D}$ ,  $\alpha$  and  $\gamma$  are geometrical terms and are independent of frequency. Thus, at sufficiently high frequencies the components of  $\mathbf{D} \mathbf{Z}_2$  have magnitude (A2.26)

$$\sigma_h R \sqrt{\mu_0 \omega \rho_e} \approx \sqrt{\mu_0 \omega \sigma_h R^2} \quad (5.39)$$

where  $\sigma_h$  is the host conductivity in which the body is embedded and  $\rho_e$  is the effective resistivity of the 2-D structure at the frequency under consideration. Assuming  $\rho_e \approx \rho_h$  for simplicity, then

$$\sqrt{\mu_0 \omega \sigma_h R^2} \approx .0012 \sqrt{\nu}$$

where  $\nu$  is the cyclical frequency. For frequencies less than  $10^4$  Hz

$$\sqrt{\mu_0 \omega \sigma_h R^2} \ll 1$$

and thus the effects on the magnetic field can be neglected. If the typical scale length of the surface inhomogeneities and the average surface conductivity are known, then (5.39) can be used to estimate the importance of the static or galvanic effects on the magnetic field.

As well,

$$\sqrt{\mu_0 \omega \sigma_e R^2} \rightarrow 0 \quad \text{as} \quad \nu \rightarrow 0 \quad (5.40)$$

where  $\sigma_e$  is the effective or apparent conductivity of the host as frequency decreases. Therefore, utilizing (5.38)

$$\mathbf{Z} \approx \mathbf{C} \mathbf{Z}_2 [\mathbf{I} - \mathbf{D} \mathbf{Z}_2] \quad (5.41a)$$

$$= \mathbf{C} [\mathbf{I} - \mathbf{Z}_2 \mathbf{D}] \mathbf{Z}_2 \quad (5.41b)$$

$$\approx \mathbf{C} \mathbf{Z}_2. \quad (5.41c)$$

And finally

$$\vec{E} = \mathbf{C} \mathbf{Z}_2 \vec{H}_0 \approx \mathbf{Z} \vec{H} \quad (5.42)$$

neglecting second order terms in  $\mathbf{Z}_2$ . In other words  $\mathbf{C} \mathbf{Z}_2$  is, asymptotically in  $\omega$ , an estimate of the true impedance tensor,  $\mathbf{Z}$ .

Again, the above relation is true, only if the measurement axes are the principal axes of the two-dimensional (regional) structure. In general, the strike of any two-dimensional structure is not known and the measurement axes are not those of the principal axes of the two-dimensional structure. Therefore

$$\vec{E} = \mathbf{R}(\theta) \mathbf{C} \mathbf{Z}_2 \mathbf{R}^t(\theta) \vec{H} \quad (5.43)$$

where  $\mathbf{R}(\theta)$  is a rotation from the principal axes to the measurement axes and  $\mathbf{R}^t$  is the transpose and inverse of the rotation tensor. Thus, the measured impedance tensor,  $\mathbf{Z}_m$ , has the form

$$\mathbf{Z}_m = \mathbf{R} \mathbf{C} \mathbf{Z}_0 \mathbf{R}^t \quad (5.44)$$

under the assumption of (5.42).

The conventional method for interpreting the measured impedance tensor is however

$$\mathbf{Z}_m = \mathbf{R} \begin{pmatrix} s_1 & 0 \\ 0 & s_2 \end{pmatrix} \mathbf{Z}_2 \mathbf{R}^t. \quad (5.45)$$

In other words, it is assumed that the principal impedances,  $(Z_{\parallel}, Z_{\perp})$ , can be obtained by rotating the impedance tensor to an off-diagonal form ( diagonal elements zero) and extracting the principal impedances albeit scaled by real

factors ( $s_1, s_2$ ) or “statically shifted”. Since the data includes noise, stable implementation of this method requires rotating the impedance tensor,  $\mathbf{Z}' = \mathbf{R} \mathbf{Z}_m \mathbf{R}^t$ , such that the sum of the square of magnitudes of the diagonal elements is a minimum. That is (Swift, 1967)

$$|Z'_{xx}|^2 + |Z'_{yy}|^2$$

is minimized in a least squares sense. The equations for this can be found in almost any thesis on MT ( *e.g.* Flores, 1986, Cavaliere, 1987). With the help of the simple numerical example presented here, and the previous solution for the electrostatic distortion by a hemisphere, let us investigate the effects of small-scale surface inhomogeneities on the conventional interpretation.

The standard method of presenting impedance data,  $Z(\omega)$ , is via apparent resistivities,  $\rho_a$  and phases,  $\phi_a$ , as a function of frequency. That is, from the 1-D analog

$$Z(\omega) = \sqrt{\mu_0 \omega \rho_a(\omega)} e^{i\phi_a(\omega)} \quad (5.46)$$

where  $\mu_0$  is the magnetic permeability of free-space and  $\omega$  is the angular frequency of the data. First, let us examine the regional or two-dimensional impedance tensor  $\mathbf{Z}_2$  (Figure 5.5) . The electric and magnetic fields as a function of frequency were first determined by a two-dimensional modelling program developed at M.I.T. (Madden and Thompson 1965) for the two polarizations, (E and H). The H-Polarization solutions were verified by the quasi-analytic solution which was presented earlier in Chapter 3. The impedance tensor,  $\mathbf{Z}_2$  is then determined by (5.41c). In Figure 5.5 the off-diagonal elements, ( $Z_{\parallel}, Z_{\perp}$ ), of the regional impedance tensor are presented in the form of apparent resistivities and phases as functions of period.

To include the effects of the hemisphere, it is now simply a matter of determining the channelling tensor,  $\mathbf{C}$  at the site required (5.28, 5.29) and then operating on the regional or primary electric fields,  $\vec{E}_0$ , with the calculated channelling tensor. Thus the required measured impedance tensor is determined,

$$\vec{E} = \mathbf{C} \vec{E}_0 = \mathbf{C} \mathbf{Z}_2 \vec{H}_0 = \mathbf{Z}_m \vec{H}_0. \quad (5.47)$$

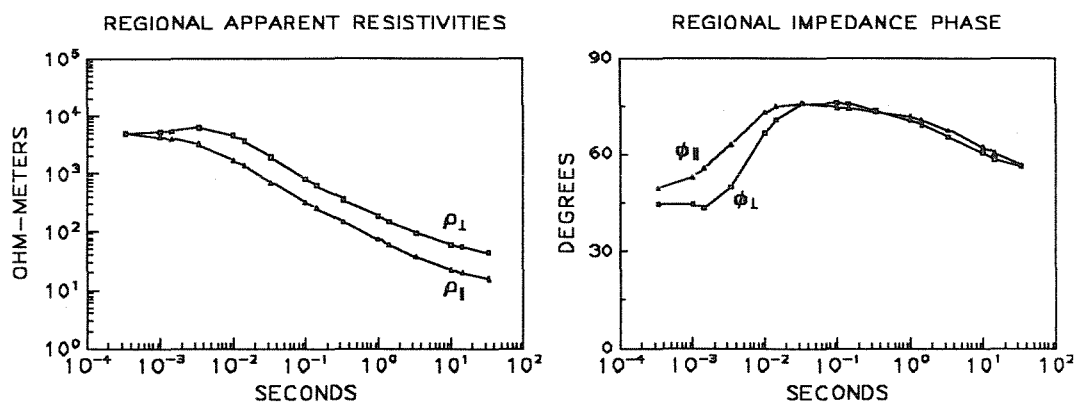


**Figure 5.5:** Two-Dimensional Impedances: This figure presents the two-dimensional parallel and perpendicular apparent resistivities at a position about one kilometer from the vertical contact.

For simplicity, the measuring axes are the principal axes of the two-dimensional structure.  $Z_m$  at measurement site C (Figure 5.4) is presented in Figure 5.6 where each component of the impedance tensor is shown as a function of period.

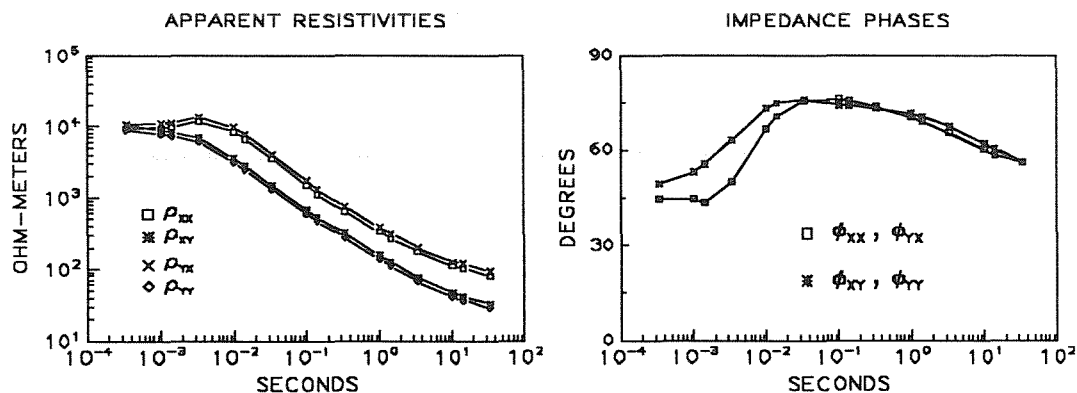


**Figure 5.6:** The Raw Impedance Data: The raw impedance information,  $Z_m$ , at site C in the form of apparent resistivities and phases, if the measurement axes were those of the two-dimensional structure.

It is now possible to examine exactly how the presence of the distorting hemisphere affects the conventional two-dimensional decomposition. Compare Figures 5.5 which presents the two-dimensional regional impedances with Fig-

ure 5.6 which presents the the elements of the resulting impedance at Site C (Figure 5.4). Note that the measured impedance tensor in the presence of the inhomogeneity no longer has only off-diagonal elements. This is so even when the measuring axes are those of the two-dimensional structure. The components  $Z_{xy}$  and  $Z_{yy}$  of  $\mathbf{Z}_m$  have the form of  $Z_{\parallel}$  although scaled by different real coefficients. Similarly,  $Z_{xx}$  and  $Z_{yx}$  have the form of  $Z_{\perp}$ .

The next question asked is “What result or interpretation is obtained when the raw impedance,  $\mathbf{Z}_m$  is rotated to fit an off-diagonal form in a least squares sense?”. In other words, if the impedance tensor,  $\mathbf{Z}_m$  is assumed to be decomposed in the form of Equation (5.3) what values will be obtained for  $Z_{\parallel}$  and  $\mathbf{Z}_{\perp}$  and what relevance will they have to the true 2-D principal impedances?

The answer to the above question for site C are shown in Figure 5.7. Two additional parameters of this interpretation, *skew index* and root mean error of fit are shown in Figure 5.8. The skew (Swift, 1967), defined as

$$\text{skew} = \frac{|Z'_{xx} + Z'_{yy}|}{|Z'_{yx} + Z'_{xy}|} \quad (5.48)$$

is invariant with  $\theta$ . It is exactly zero for two-dimensional structures in the absence of noise. Otherwise, it has the magnitude of the noise to signal ratio in 2-D structures. The root mean square relative error of fit  $\epsilon$  is given by

$$\epsilon^2 = \frac{\sum_{i=1}^2 \sum_{j=1}^2 |\hat{Z}_{ij} - Z_{ij}|^2}{\sum_{i=1}^2 \sum_{j=1}^2 |Z_{ij}|^2} \quad (5.49)$$

where  $Z_{ij}$  and  $\hat{Z}_{ij}$  are the measured and modeled impedance tensor elements respectively. The rms error parameter,  $\epsilon$ , should be small compared with unity if the model of the impedance tensor is adequate. Here, of course, the model of the impedance tensor is that of (5.3). This parameter ( $\epsilon$ ), to verify the decomposition of the impedance tensor, is not generally used. However this thesis will use it extensively.

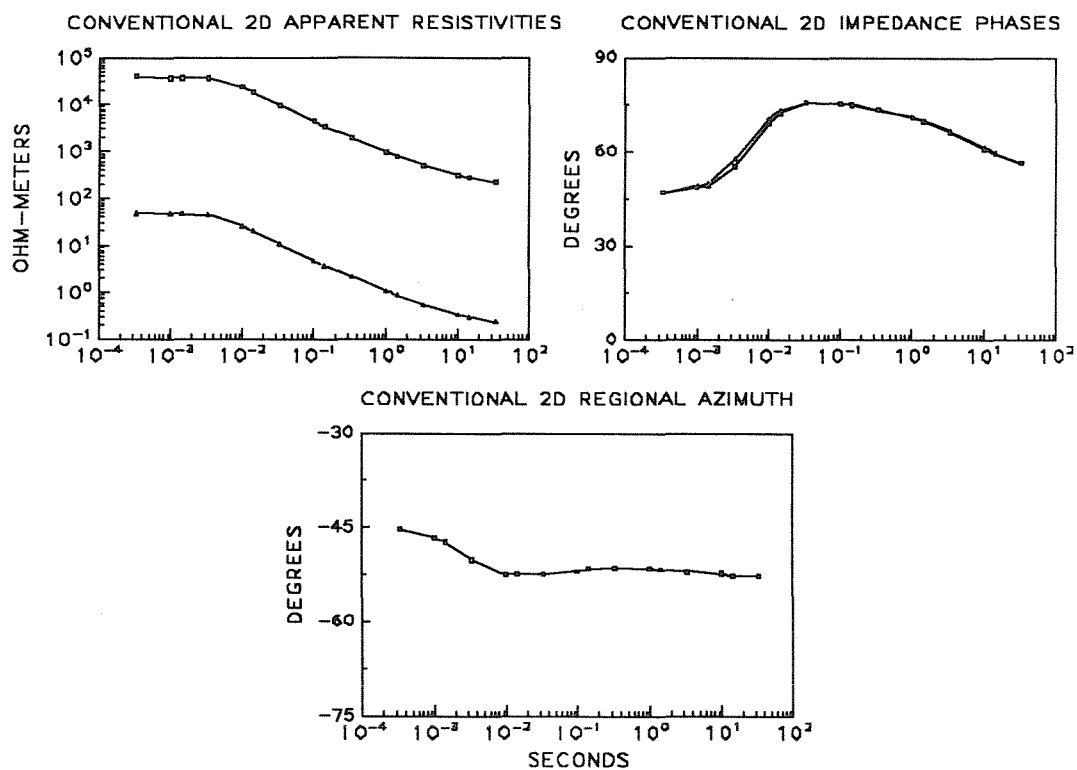


**Figure 5.7:** SITE C - CONVENTIONAL INTERPRETATION: Site C is at 45 degrees to the axes of the 2-D structure and is just outside the channelling body. Included in the figure are conventional apparent resistivities and phases as well as the conventional 2-D regional azimuth or strike angle.

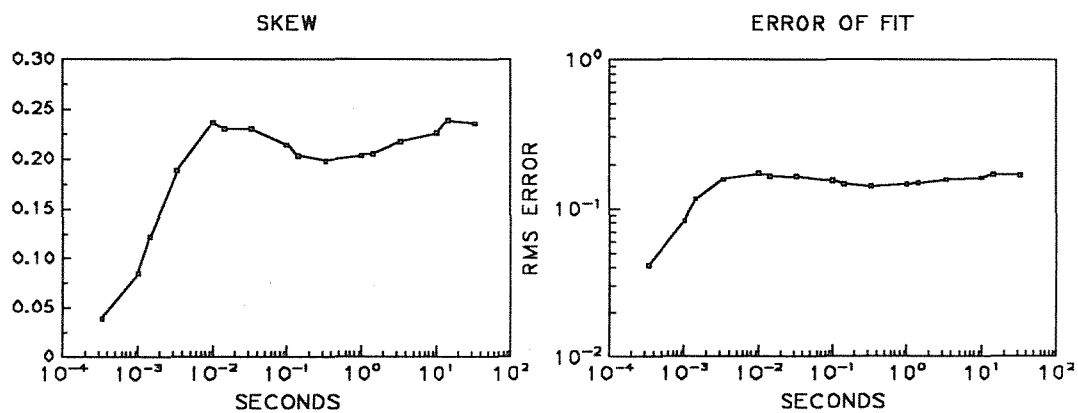


**Figure 5.8:** Three-dimensional indicators for conventional decomposition:

There are a number of interesting results evident from these figures ( 5.7 and 5.8 ). The most obvious features to be noted are in the comparisons of  $\rho_a$  and  $\phi_a$  to the 2-D undistorted principal impedances (Fig. 5.5 ). The principal impedances of  $\mathbf{Z}_m$  have the form neither of  $\mathbf{Z}_{\parallel}$  nor  $\mathbf{Z}_{\perp}$  but rather are mixtures of them. This result is most evident in the phases, but can also be seen in the apparent resistivities at short periods. In fact, conventional wisdom would interpret these results as a 1-D environment with "static shift". This mixing of the principal 2-D impedances is due to the blending of the components of the primary electric field as discussed in section 5.2.2. Note that the conventional method produces an erroneous regional strike (Figure 5.7). The correct regional strike for this orientation of the measuring axes is zero since the measurement axes were taken to be parallel and perpendicular to strike. In fact the Swift method produces an azimuth of about  $51^\circ$  at long periods decreasing to  $45^\circ$  at small periods. It is important to compare the conventional azimuth to the polarization of the total electric field at the measurement site. At Site C the channelling tensor is purely a shear tensor (5.33). At high frequencies, the power in the primary or regional components of electric field are in a ratio of 1-1 over random polarizations of the source field. At high frequencies, the regional response is essentially one-dimensional and therefore the average primary magnetic field  $\vec{H}_0$  is parallel to (1, 1). Some simple calculations show that the direction of the local field at high frequencies at site C is  $45^\circ$ . Similarly, at long periods it can be shown that the local strike (local electric field azimuth) is  $47^\circ$ . That is, it appears that the conventional method tends to pick out the direction of the local current, not the regional current.

The effects of noise on the results of the comparisons of Figures 5.5 and 5.7 can be simulated by adding random error to the calculated data,  $\mathbf{Z}_m$ . If this is done, there are no significant variations in these results. In fact, the estimated principal phases from the mean impedance tensor fall within the error bars of each other and thus the phase curves appear to have no 2-D characteristics.

Turn now to the 3-D indicators (Figure 5.8), skew and the error parameter ( $\epsilon$ ). Skew is often used by MT interpreters as an indicator of three-dimensionality. The skew in this case is small, less than .25 and usually less than .2. In the 2-D case with noise present, the skew is the relative magnitude of the noise. Thus, especially at long periods a skew of about .2 might not be significantly above the noise level. Note that the skew at low periods is very small, ( $< .1$ ). The root mean square error of fit varies from 4% at small periods to about 20% at long periods. The addition of random error to the data will increase the rms error slightly. In the presence of only signal noise, the rms parameter will be the noise to signal ratio. The inference remains that the 2-D or Swift decomposition produces parameters which fit the data adequately although the conceptual model interpretation (1-D with "static shift") is very incorrect.

Thus mixing of principal 2-D impedances, and the resulting wrong interpretations which occur with the presence of the small inhomogeneity are dependent on the position of measuring site with respect to the hemisphere (Figure 5.9). Site C, the one shown already, is in fact very nearly the worst case. Site A is  $15^\circ$  off that principal axes which is perpendicular to the strike while Site B and Site C are  $30^\circ$  and  $45^\circ$  off, respectively. Recall that exactly on the principal axes the effect of the channelling operator, and thus the inhomogeneity on the regional electric fields, is one purely of anisotropy. At such sites, in the absence of any anomalous magnetic field, the 2-D principal impedances will be scaled by real numbers independently of frequency, but not mixed. That is, the principal impedances of  $Z_m$  will have the same frequency dependent behaviour and the phases will be completely unaltered. However, as the measurement site is moved off the principal axes of the body, the components of the primary or regional electric fields are increasingly mixed. This suggests that at some sites the principal impedances will be mixed until they are indistinguishable.

These results are clearly seen in Figure 5.9. The phases for Site A are essentially the phases of the principal impedances, and the apparent resistivities

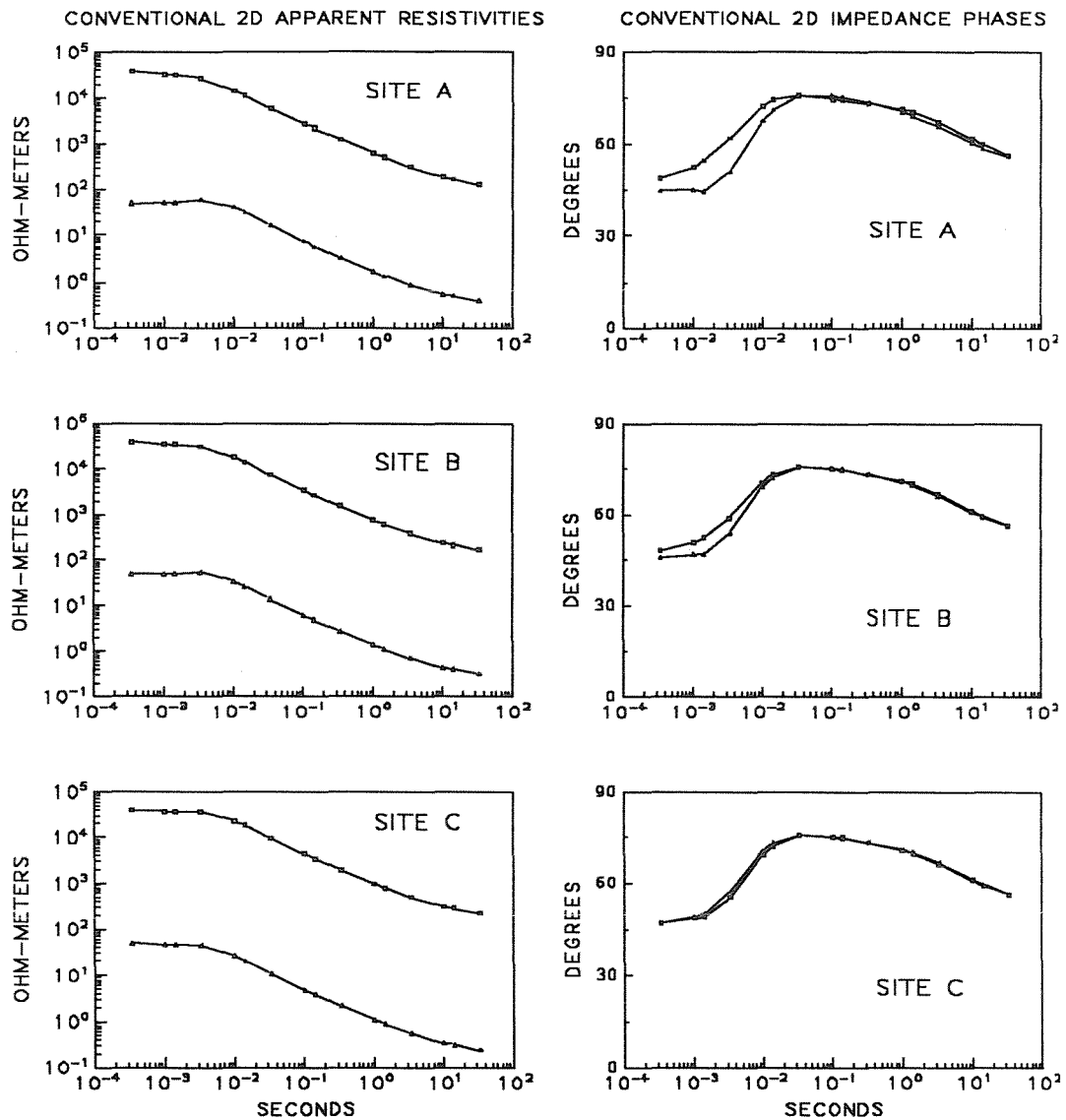


**Figure 5.9:** MIXING OF PRINCIPAL IMPEDANCES AS A FUNCTION OF POSITION: The channelling tensor will mix the principal impedances and this mixing is dependent on position.

still retain the same shape of  $\rho_{\parallel}$  and  $\rho_{\perp}$ , although they have been multiplied by a scaling factor (anisotropy). However, farther from the principal axes at Site B, the principal impedances are no longer as distinguishable. Finally, at Site C the phases are almost identical and the apparent resistivities have almost the

same shape but are scaled differently. In summary, Site A (Figure 5.4) does not simulate a 1-D environment with “static shift” but Site C truly does.

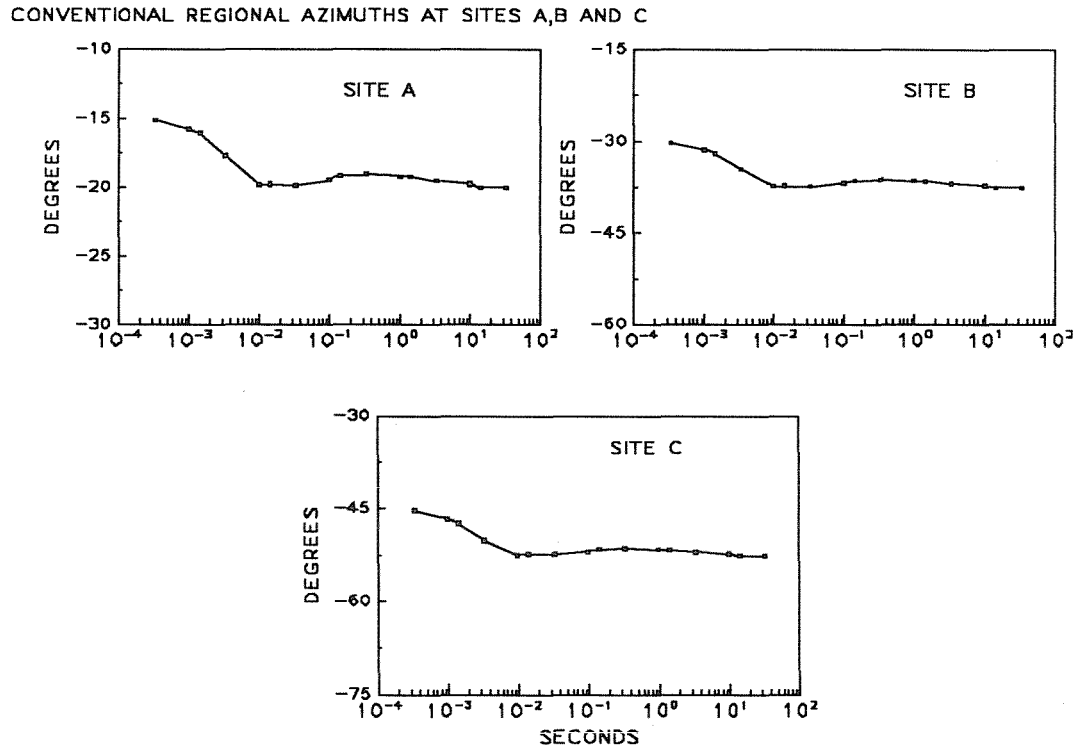


**FIGURE 5.10:** CONVENTIONAL AZIMUTHS: The conventionally calculated regional azimuths at sites A, B and C.

Figure 5.10 indicates the variation in the regional azimuth by the conventional method at the three sites. Again, they indicate that the conventional method determines an azimuth very close to the local electric current polarization. (The negative azimuths in the figure are due to an opposite sign convention for a rotation.) At short periods where the response is essentially 1-D, the conventional method determines exactly the local azimuth. As the period increases the conventional azimuth is consistently close to, but not exactly equal to the local azimuth.

#### 5.2.4 Distortion Effects in a One-Dimensional Environment:

An examination of the effect of the distorting hemisphere in a simple one-dimensional environment also illustrates some interesting results.

The estimated principal impedances from the conventional method can be expressed as

$$\hat{Z}_{\perp} = \alpha_2 + \sqrt{\alpha_2^2 + \det | \mathbf{Z}_m |} \quad (5.50)$$

and

$$\hat{Z}_{\parallel} = \frac{\det | \mathbf{Z}_m |}{\hat{Z}_{\perp}} \quad (5.51)$$

where in a 1D environment with only galvanic electric distortion

$$\det | \mathbf{Z}_m | = \det | \mathbf{C} | \det | \mathbf{Z}_2 | = Z_0^2 \det | \mathbf{C} | \quad (5.52)$$

$$\alpha_2 = \frac{Z_0}{2} (C_{11} + C_{22}) \quad (5.53)$$

where  $Z_0$  is the correct regional one-dimensional impedance.

$$\hat{Z}_{\perp} = Z_0 \left[ \left( \frac{C_{11} + C_{22}}{2} \right) + \left( \frac{C_{11} - C_{22}}{2} \right) \sqrt{1 + \frac{4C_{21}C_{12}}{(C_{11} - C_{22})^2}} \right] = \beta Z_0 \quad (5.54)$$

where  $\beta$  is real and

$$\hat{Z}_{\parallel} = \frac{Z_0}{\beta} \quad (5.55)$$

If the effect of the inhomogeneity is entirely a galvanic effect on the electric fields, the conventional interpretation in a one-dimensional environment does indeed produce purely a “static shift” of the principal impedances, with no phase distortion. The conventional method can however produce an erroneous result for a regional strike. Here since a one-dimensional regional environment is considered one would expect no consistent regional strike as the data is examined frequency by frequency. If there are local distorting bodies present, the conventional method will produce a consistent regional strike which closely follows the local electric polarization. This can be seen in the higher frequencies in

our synthetic model where the regional response is essentially one-dimensional. The effect of the local distorting body on the conventional strike in a one-dimensional regional environment will be discussed again in the next chapter. Referring to the 2-D illustration, the interpretation of Figure 5.7 could as well be that of a 1-D environment with a local distorting body.

Now consider the effect of the anomalous magnetic field. Recall that the anomalous magnetic field can be expressed as the result of a linear operation upon the primary electric fields (5.34) and thus (5.41)

$$\mathbf{Z}_m = \mathbf{C}[\mathbf{I} - \mathbf{Z}_0 \mathbf{D}] \mathbf{Z}_0 = \mathbf{F} \mathbf{Z}_0 \quad (5.56).$$

in the measurement coordinate system.

$$\hat{Z}_{\perp} = Z_0 \left[ \left( \frac{F_{11} + F_{22}}{2} \right) + \left( \frac{F_{11} - F_{22}}{2} \right) \sqrt{1 + \frac{4F_{21}F_{12}}{(F_{11} - F_{22})^2}} \right] = \beta Z_0 \quad (5.57)$$

Since the elements of  $\mathbf{F}$  are complex, if the anomalous magnetic field is significant then  $\beta$  will have a significant imaginary part and there is a shift or distortion in both the phases and the amplitudes of the estimated impedance elements. If the parameter  $\sqrt{\mu_0 \omega \sigma_h R^2}$  (5.39) is of order .1, for example, then  $\beta$  will have a complex phase of about  $6^\circ$  and thus the phase distortion would be about  $6^\circ$ . The variation in the real parts of the distortion operator ( $\mathbf{C}[\mathbf{I} - \mathbf{Z}_0 \mathbf{D}]$ ) will be small with respect to the case of no anomalous magnetic field and thus the presence of the anomalous magnetic field will cause very little additional distortion of the apparent resistivities. In the case of the hemisphere scatterer, these shifts in the phases of the two estimated principal impedances would be equal. However, if the body were elongated the frequency independent shifts in the phases would be unequal and there would result a split in the phases of the two estimated impedances as well as the apparent resistivities.

The effect on the phases of a small imaginary part in the distortion operator leads one to ask if there are other effects which can affect the phases. Consider the effects both of signal noise and local induction in the inhomogeneity. Let us assume the induction in the small body is weak and thus there

is little interaction between the inductive and galvanic responses (McNeill *et al* 1984, Walker 1988). Therefore, the total electric field can be approximately expressed

$$\vec{E} = \mathbf{C}\vec{E}_0 + \vec{E}_s + \vec{\eta}_e. \quad (5.58)$$

$\vec{E}_s$  is the secondary electric field produced by induction and  $\vec{\eta}_e$  is the noise in the electric field. The secondary induced electric field can be approximated by

$$i\omega \mathbf{G}\vec{H}_0 \quad (5.59)$$

since the primary time-varying magnetic field will be the principal cause of the induced electric field. The relation (5.59), of course, does not consider any induced surface horizontal electric fields by the primary vertical magnetic field.

Assuming the galvanic distortion of the electric fields is the only first-order effect, write (5.41, 5.59)

$$\vec{E} = [\mathbf{C} - \mathbf{C}\mathbf{Z}_2\mathbf{D} + i\omega \mathbf{G}\mathbf{Z}_2^{-1} + \eta\mathbf{Z}_2^{-1}] \mathbf{Z}_2\vec{H} \quad (5.60)$$

for a regional structure which has at most two-dimensionality. Therefore, the distortion operator now has three contributors to its imaginary part.

The distortion operator in (5.60) now contains four parts due to galvanic distortion of the electric fields, electrostatic magnetic effects, induced secondary electric effects and noise. If the distorting body is small the galvanic electric distortion operator  $\mathbf{C}$  will have the most significant effect followed in importance by the electrostatic magnetic effect  $\mathbf{C}\mathbf{Z}_2\mathbf{D}$ .

### 5.3 Summary of the Effects of Small-Scale Surface Inhomogeneities

The analysis has shown the way in which local inhomogeneities render invalid an otherwise valid parameterization which is based on a 2-D model of the impedance tensor. With this decomposition the apparent principal impedances of a 2-D locally distorted tensor become linear combinations or mixtures of the true regional 2-D impedances. As well, an erroneous regional strike is obtained.

Even if the regional structure is one-dimensional, the presence of an anomalous electrostatic magnetic field can alter the phases produced by the conventional method from the true one-dimensional impedance phases. This effect combined with static (*i.e.* galvanic) distortions of the estimated apparent resistivities can hide the essentially one-dimensional nature of the regional structure. The presence of weak induction and signal noise will further accentuate this effect on the phases. Also in the 1-D case (where no regional strike is defined) the conventional method can erroneously produce what appears to be a well defined strike.

With the aid of the above analyses one may now address more generally the decomposition or parameterization of the impedance tensor in the presence of three-dimensional inhomogeneities. Examine the representation of the impedance tensor contained in equation (5.60) for a two-dimensional regional conductivity structure with three-dimensional galvanic electric and magnetic distortion and weak induction. Here

$$\mathbf{Z}_m = \mathbf{R} [ \mathbf{C} - \mathbf{C} \mathbf{Z}_2 \mathbf{D} + i\omega \mathbf{G} \mathbf{Z}_2^{-1} + \eta \mathbf{Z}_2^{-1} ] \mathbf{Z}_2 \mathbf{R}^t. \quad (5.61)$$

The operator,  $\mathbf{C}$  can contain four real parameters. (That four independent parameters are required, in general, will be shown in the following chapter.) To first order, as discussed previously,  $\mathbf{D}$  can contain two real parameters, while  $\mathbf{R}$  contains one and  $\mathbf{G}$  can contain at least two parameters. The regional impedance  $\mathbf{Z}_2$  contains up to two complex or four real parameters. Thus, in total, the factorization of  $\mathbf{Z}_m$  (5.61) can contain up to 14 real parameters related to the physical model. The impedance tensor at a single frequency, however, contains but eight real data. Some of these 14 parameters are however frequency-independent. If a solution to this problem is possible, at all, it must involve examining data at multiple frequencies to determine those parameters which are frequency-independent. Determining the frequency-independent parameters from a multiple-frequency data set has two desirable results. Firstly, the number of parameters to be determined become less than the number of data and secondly, the local effects become separated from the regional effects.

This approach is based on a specific physical model, and utilizes the simplifications provided by the physics of that model. This is a distinctly different approach from the decompositions of Eggers, 1982, Spitz, 1985, LaTorraca *et al* 1986 and Yee and Paulson 1986 which are based on purely mathematical aspects of the impedance tensor. They obtain eight parameters from the eight data at each frequency. They do not attempt to separate local from regional effects.

The next chapter bases a decomposition method on this model (5.61) on the assumption that it is desirable and possible to separate local from regional effects.

## CHAPTER 6

# A DECOMPOSITION OF THE MAGNETOTELLURIC IMPEDANCE TENSOR WHICH IS USEFUL IN THE PRESENCE OF CURRENT DISTORTION

### 6.1 Introduction

Experimental magnetotelluric impedance tensors very rarely have the form of an ideal two-dimensional impedance tensor. There will not always exist a rotation of the coordinate axes such that the diagonal elements of the impedance tensor are both zero. This can be due to the presence of any combination of three factors: data errors in the case of one- or two-dimensional induction, large three-dimensional bodies with significant inductive responses, and one- or two-dimensional induction coupled with the effects of telluric distortion. Historically, it has been assumed that data errors are the primary cause of this non-conformity. Therefore, the standard procedure has been to rotate the horizontal coordinate axes so that the measured impedance tensor fits the ideal two-dimensional form as closely as possible. The measure of goodness of fit has usually been a least squares norm (*e.g.* Swift, 1967). The method has been used because of the relative simplicity of calculating such two-dimensional inductive responses.

On many occasions when the large-scale conductivity structure is approximately one or two-dimensional, the magnetotelluric impedance tensor is the result of local galvanic distortion of electric currents which are due to induction in the regional conductivity structure. In recent years, with improvements in data quality, there has been a consensus within the magnetotelluric community that this distortion is the most significant problem in obtaining the Earth's regional or large-scale conductivity structure from measured impedance data. If distortion is present, the measured impedance tensor will not, in general, be close in

any sense to a two-dimensional impedance tensor. Even though the inductive behaviour is at most two-dimensional, the impedance tensor which results will have three dimensional behaviour as indicated by such parameters as skew and the error of fit to a two-dimensional tensor. As illustrated in the preceding chapter, procedures for rotating the impedance tensor to fit a two-dimensional form (*e.g.* minimizing the mean square modulus of the diagonal elements) do not generally recover the correct two-dimensional induction parameters. The directions of the principal axes of induction will not be determined correctly nor will these methods recover the correct principal impedances, but rather it can be shown that they obtain linear combinations of them. In recent years, a number of decomposition methods have been proposed, as discussed in the previous chapter, (*e.g.* Eggers, 1982, Yee and Paulson, 1984; Spitz, 1985; Yee, 1985; LaTorraca *et al.*, 1985; Cevallos, 1986; LaTorraca *et al.*, 1986). These decompositions do not make any physical assumptions about the impedance tensor. Thus, their decompositions retain all 8 real parameters in the data as opposed to only 5 parameters which are kept by an idealized two-dimensional tensor model. The advantage of a lack of any physical assumptions is however, also a disadvantage as it fails to take advantage of any physical simplifications which might exist. This difficulty can result in an inability to make inferences about the Earth's actual conductivity from the decomposition parameters where such inference is in fact straightforward. Also, as discussed in Chapter 5, in a general conductivity distribution more than eight physical parameters can be used to describe an impedance tensor. Even in the case of galvanic channelling there are more than eight parameters present. The conclusion from the last chapter is that any decomposition which would like to separate local from regional parameters must be able to consider the frequency-independence of the parameters.

Recently Bahr (1985) has indicated that galvanic channelling does not destroy most of the available information about an underlying two-dimensional inductive process. In this chapter, a physical approach is taken to the decomposition problem in an attempt to produce a decomposition which is physi-

cally interpretable. The approach makes the assumption that the measured impedance tensor is produced by local galvanic (thus frequency independent) distortion of the regionally induced electric currents caused by arbitrary three-dimensional structures. The large-scale structure is assumed to be at most two-dimensional. The effects of the scatterers on the magnetic field are assumed negligible and initially ignored. Later in the chapter the effects of this secondary magnetic field will be considered. A decomposition of the impedance tensor is presented here which separates the effects of current channelling from those of induction as far as is possible without *a priori* knowledge of the three-dimensional inhomogeneities. If the impedance tensor is the result of regional two-dimensional induction coupled with local frequency independent telluric distortion, the method correctly recovers the principal axes of induction and, except for multiplication by frequency independent real constants, the two principal impedances. Also obtained are two distortion parameters, twist and shear, which partially describe the effects of the telluric distortion. If this physical model of the measured impedance tensor is true, these parameters have physical interpretations and there is every possibility that they can be interpreted either intuitively or by numerical modelling. The effects of the anomalous magnetic field produced by the galvanic current distortion are also considered.

Even where the model is not sufficiently valid for all frequencies of the data set, it may be true over limited frequency ranges in the data. This is because the definition of a "regional" scale changes for different frequency ranges. Since the electromagnetic skin-depth will vary by orders of magnitude throughout the frequency range of a normal data set, the importance of various physical factors will change significantly with frequency range. In the true one or two-dimensional cases, the decomposition reduces to the conventional method and therefore in practice may help to clarify the important physical effects as they vary through the frequency range of the data.

The decomposition contains only seven parameters and these are obtained by a least squares fit of the impedance tensor model to the data. The theory

and methodology of the decomposition are given in this chapter along with a discussion of the improvements obtained over the conventional method. The decomposition is applied to the synthetic example of Chapter 5 and examples with real data are also presented. Suggestions for inclusion of static magnetic distortion and weak induction are also included.

## 6.2 The Ideal Distortion Model of the Impedance Tensor

Let us assume that the Earth is essentially flat and has at most a two-dimensional conductivity structure on a large regional scale. This assumption implies that any three-dimensional structures are all inductively very weak. In the principal axes of the two-dimensional structure (*i.e.* one horizontal axis is along the strike of the two-dimensional structure and the vertical axes normal to the earth's surface), the regional horizontal electric field components,  $\mathbf{e}_r$ , and magnetic field components,  $\mathbf{h}_r$ , are linearly related by

$$\mathbf{e}_r = \begin{pmatrix} 0 & a \\ -b & 0 \end{pmatrix} \mathbf{h}_r = Z_2 \mathbf{h}_r. \quad (6.1)$$

$a$  and  $b$  are either  $Z_{\perp}$  or  $Z_{\parallel}$  depending on whether the  $x$ -axis is perpendicular to strike or parallel to the strike of the two-dimensional structure.  $Z_{\perp}$  and  $Z_{\parallel}$  are the impedance elements for the regionally averaged two-dimensional structure.  $Z_{\perp}$  is the impedance associated with the 2D-mode containing only current perpendicular to strike and  $Z_{\parallel}$  is the impedance associated with the mode containing only current parallel to strike. When the total horizontal electric field,  $\mathbf{e}$ , and the total horizontal magnetic field  $\mathbf{h}$  are measured at a point on the surface of the earth, they are modified by local conductivity variations from the regional values. The electric field  $\mathbf{e}$  can be very strongly distorted by charges that accumulate on conductivity gradients or boundaries, as illustrated in Chapter 5. The magnetic field,  $\mathbf{h}$ , however is not disturbed so strongly since it is due to a weighted spatial average of the telluric current density over a much larger volume. Therefore it is possible to make the simplifying assumption that  $\mathbf{h} = \mathbf{h}_r$  (This assumption was discussed more fully in reference to the

analytic illustration in Chapter 5, and will be revisited later in this chapter).  $\mathbf{e}$  must be related to  $\mathbf{e}_r$  by a distortion or channelling tensor  $\mathbf{C}$  which can vary significantly from the the identity matrix. Such a distortion operator is developed for a particular inhomogeneity in Chapter 5. Following Bahr (1985) and Berdichevsky and Dmitriev(1976),among others, the horizontal electric fields can be expressed as

$$\mathbf{e} = \mathbf{C} \mathbf{e}_r = \begin{pmatrix} C_1 & C_2 \\ C_3 & C_4 \end{pmatrix} \mathbf{e}_r \quad (6.2)$$

in the presence of arbitrary small-scale scatterers. Because these distorting structures are assumed to be inductively weak and their effects thus independent of frequency, the elements of  $\mathbf{C}$  can be taken to be real numbers in the transform or frequency domain. In the absence of distortions  $\mathbf{C}$  will obviously reduce to the identity tensor  $\mathbf{I}$ . This physical model corresponds to fundamental model II of Berdichevsky and Dmitriev (1976) for a 3-D surface inhomogeneity, in which  $\mathbf{C}$  is defined as

$$\mathbf{C} = \begin{pmatrix} F_x^{(x)} & F_x^{(y)} \\ F_y^{(x)} & F_y^{(y)} \end{pmatrix}.$$

The conditions of validity for inductively weak (phase-free) distortions of the electric field have been discussed by numerous authors (*e.g.* Berdichevsky and Dmitriev, 1976; Cox *et al*, 1980; Larsen, 1975; Larsen, 1977; Dmitriev and Berdichevsky, 1979; Hermance, 1982; LeMouel and Menvielle, 1982; Jones, 1983; Park *et al*, 1983; Ranganayaki, 1984; Wannamaker *et al*, 1984a and 1984b; Park, 1985; Bahr, 1985), to which the reader is referred.

It may not be evident that four parameters are required to represent a general distortion tensor. Even though the distortion operator,  $\mathbf{C}$  contains four elements, they may not all be independent. To verify that in general this is true, an example is presented in Figure 6.2.1.

Here, a moderately conductive region of overburden (dotted) is shown on an insulating basement (white) which outcrops through the overburden. Inside the central circular region of overburden, there is an elliptical conducting region

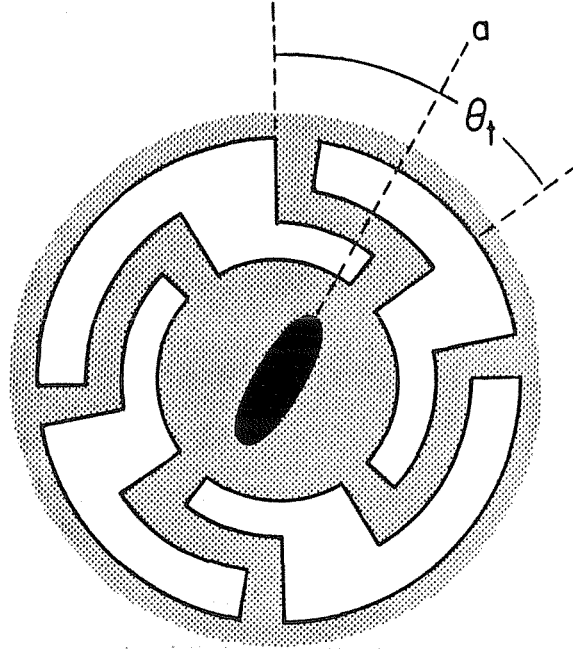


Figure 6.2.1: A synthetic channelling illustration

(black) which represents a swamp. Distortion of the large-scale electric field will be found if measurements are made. In particular, let us analyse this distortion at the centre of the swamp. The regional telluric currents are twisted through an angle  $\theta_t$  due to the presence of the outcrop in the overburden. The elongation and conductivity of the swamp causes a local anisotropy in a coordinate system where the axes are parallel and perpendicular to the direction  $\mathbf{a}$ . The measured electric field at the center of the swamp is therefore related to the regional electric fields by the equation

$$\mathbf{e} = \mathbf{C} \mathbf{e}_r = \mathbf{Q} \Lambda \mathbf{Q}^t \mathbf{T} \mathbf{e}_r \quad (6.3)$$

or more fully

$$\mathbf{C} = \begin{pmatrix} \cos \theta_a & -\sin \theta_a \\ \sin \theta_a & \cos \theta_a \end{pmatrix} \begin{pmatrix} \lambda_1 & 0 \\ 0 & \lambda_2 \end{pmatrix} \begin{pmatrix} \cos \theta_a & \sin \theta_a \\ -\sin \theta_a & \cos \theta_a \end{pmatrix} \begin{pmatrix} \cos \theta_t & -\sin \theta_t \\ \sin \theta_t & \cos \theta_t \end{pmatrix} \quad (6.4)$$

The operator  $\mathbf{T}$  performs the initial twist,  $\mathbf{Q}$  and its transpose  $\mathbf{Q}^t$  rotate the coordinate system to the principal axes of the swamp, and  $\Lambda$  imposes the

anisotropy caused by the ellipticity and conductivity contrast of the swamp. Clearly, four independent real parameters  $\theta_a$ ,  $\theta_t$ ,  $\lambda_1$  and  $\lambda_2$  are required for this physical situation.

The above decomposition of  $\mathbf{C}$  (6.3) is, however, only instructive. It is not useful in terms of real data without *a priori* knowledge of the nature of the distorting inhomogeneities. In fact, without knowledge of the scatterers and with data at only one frequency, none of its four parameters can be recovered uniquely from a measured impedance tensor. It has been suggested by Bahr (1985) in the case of general galvanic distortion and Zhang *et al* (1987) in the case of two-dimensional galvanic distortion, that it is not necessary to solve explicitly for the elements of  $\mathbf{C}$  to determine information concerning the two-dimensional impedances. However, an explicit decomposition is needed to recover any information and thus it is necessary to study the exact ways in which  $\mathbf{C}$  is indeterminate. This we will proceed to do.

Since

$$\mathbf{e} = \mathbf{C} \mathbf{e}_r$$

and in the principal coordinate system of the regional structure

$$\mathbf{e}_r = \mathbf{Z}_2 \mathbf{h}_r$$

then in this coordinate system

$$\mathbf{e} = \mathbf{C} \mathbf{Z}_2 \mathbf{h}_r \quad (6.5)$$

or in the measuring coordinate system

$$\mathbf{e} = \mathbf{R} \mathbf{C} \mathbf{Z}_2 \mathbf{R}^t \mathbf{h} \quad (6.6a)$$

$$= \mathbf{Z}_m \mathbf{h}. \quad (6.6b)$$

Here,  $\mathbf{Z}_m$  is the actual measured impedance tensor.  $\mathbf{Z}_2$  is the regional two-dimensional impedance tensor expressed in its principal coordinate system (i.e. it has the form of  $\mathbf{Z}_2$  in equation 6.1).  $\mathbf{C}$  is the distortion tensor, expressed

in the regional inductive principal axes system, and  $\mathbf{R}$  is a rotation matrix which rotates vectors through an angle  $\theta$  to the regional inductive principal axes system from the measurement axes system.

From physical intuition, it is clear that local anisotropy cannot be separated from parallel regional anisotropy without prior knowledge of the distorting inhomogeneities and the regional structure. It is evident therefore, that this decomposition cannot be done uniquely for measured data at a single frequency. There are nine real parameters: a rotation angle  $\theta$ , four distortion tensor elements, and the two complex principal impedances. The nature of the non-uniqueness of the decomposition can be described quite simply. Consider the two transformations

$$\mathbf{Z}'_2 = \mathbf{W} \mathbf{Z}_2 = \begin{pmatrix} w_1 & 0 \\ 0 & w_2 \end{pmatrix} \mathbf{Z}_2 \quad (6.7)$$

and

$$\mathbf{C}' = \mathbf{C} \mathbf{W}^{-1} \quad (6.8)$$

where  $w_1$  and  $w_2$  are non-zero real numbers. The decomposition of the measured impedance data

$$\mathbf{Z}_m = \mathbf{R} \mathbf{C}' \mathbf{Z}'_2 \mathbf{R}^T$$

is also correct if  $\mathbf{Z}_m$  satisfies equation 6.6 since  $\mathbf{C}'$  is still real, and  $\mathbf{Z}'_2$  has the ideal two-dimensional form of equation (6.1). It will be shown moreover that a diagonal matrix such as  $\mathbf{W}$  produces the most general form of non-uniqueness that can be introduced. The conclusion is that the decomposition of equation 6.6a is still not, at present, a very useful one.

The outline above giving the physical basis for the impedance tensor decomposition (which will be given below), should not be taken to suggest that all magnetotelluric impedance data conform to this simple behaviour. The physical basis is introduced only as a guide to a decomposition which is more useful than the rotation of the tensor to its closest two-dimensional form. However, the parameters will be at least approximately interpretable in a much larger

proportion of cases than with the conventional method. As well, the decomposition reduces to the conventional method in just those physical situations when the conventional method is adequate. A more complete representation of the impedance tensor was given in Chapter 5 (5.61). The method described here is motivated by the discussion in the conclusion to Chapter 5, which argues that frequency independent parameters must be determined if a unique parameterization of the impedance tensor is to be obtained.

### 6.3 A Useful Factorization of the Distortion Operator

It is convenient as per Spitz (1985) to introduce a modified form of a set of bases matrices sometimes termed the Pauli spin matrices:

$$\mathbf{I} = \begin{pmatrix} 1 & 0 \\ 0 & 1 \end{pmatrix} \quad \Sigma_1 = \begin{pmatrix} 0 & 1 \\ 1 & 0 \end{pmatrix} \quad (6.9a)$$

$$\Sigma_2 = \begin{pmatrix} 0 & -1 \\ 1 & 0 \end{pmatrix} \quad \Sigma_3 = \begin{pmatrix} 1 & 0 \\ 0 & -1 \end{pmatrix}. \quad (6.9b)$$

This allows any rank 2 tensor  $\mathbf{M}$  to be expanded as a sum

$$\mathbf{M} = \alpha_0 \mathbf{I} + \alpha_1 \Sigma_1 + \alpha_2 \Sigma_2 + \alpha_3 \Sigma_3. \quad (6.10)$$

Again, this is not directly a useful way to decompose  $\mathbf{C}$  because none of the four parameters  $\alpha_i$  can be recovered uniquely from the data. A more useful decomposition is the factorization

$$\mathbf{C} = g \mathbf{T} \mathbf{S} \mathbf{A} \quad (6.11)$$

where  $g$  is a real scalar and the tensor factors  $\mathbf{T}$ ,  $\mathbf{S}$  and  $\mathbf{A}$  are defined by

$$\mathbf{T} = N_2 (\mathbf{I} + t \Sigma_2) \quad (6.12a)$$

$$\mathbf{S} = N_1 (\mathbf{I} + e \Sigma_1) \quad (6.12b)$$

$$\mathbf{A} = N_3 (\mathbf{I} + s \Sigma_3). \quad (6.12c)$$

Physical interpretations of each of these individual operators and the existence and uniqueness of the factorization will be discussed below. The normalizing

factors  $N_i$  are defined for convenience in such a way that  $\mathbf{T}$ ,  $\mathbf{S}$  and  $\mathbf{A}$  individually preserve power (but not isotropy) when applied to an isotropically polarized random electric field. That is, for example,

$$\langle \mathbf{T}\mathbf{x}, \mathbf{T}\mathbf{x} \rangle = \langle \mathbf{x}, \mathbf{x} \rangle, \quad \forall \mathbf{x} \in \mathfrak{R}^2 \quad (6.13).$$

Here, the inner product is the statistical mean over the random polarizations of the vector scalar product of two vectors. The direction of  $\mathbf{T}\mathbf{x}$  is however not that of  $\mathbf{x}$  unless  $t = 0$ . Equation 6.13 holds for the operators  $\mathbf{S}$  and  $\mathbf{A}$ , as well, and thus

$$N_1 = 1/\sqrt{1 + e^2} \quad (6.14a)$$

$$N_2 = 1/\sqrt{1 + t^2} \quad (6.14b)$$

$$N_3 = 1/\sqrt{1 + s^2}. \quad (6.14c)$$

The product  $\mathbf{T}\mathbf{S}\mathbf{A}$ , however, does not necessarily preserve power. The practical purpose of this normalization is to ensure that the elements of  $\mathbf{T}$ ,  $\mathbf{S}$  and  $\mathbf{A}$  remain bounded during any computations. The matrix  $\mathbf{T}$  is made unitary by this normalization and is thus an ordinary rotation matrix.

Physical insight into this factorization can be obtained by examining the effects of each factor in turn on the regional electric field. First let us examine the splitting or anisotropy operator

$$\mathbf{A} = N_3(\mathbf{I} + s\mathbf{\Sigma}_3) = N_3 \begin{pmatrix} 1 + s & 0 \\ 0 & 1 - s \end{pmatrix}. \quad (6.15)$$

Figure 6.3.1 illustrates the effects of the anisotropy or splitting tensor on a family of unit vectors when  $s$  is positive. The top figure is a family of unit vectors uniformly spaced in angle. The bottom figures represent the effect of operating on the family with each of the three operators individually. There is a one-to-one mapping between the set of vectors in the top figure and the set of vectors in each of the bottom figures. The splitting operator stretches the two field components by different factors ( $N_3(1 + s), N_3(1 - s)$ ). This

generates an anisotropy due to the distortions which is added to the anisotropy already existing in the regional induction impedance tensor  $\mathbf{Z}_2$  (recall equation 6.7). This is because the local anisotropy is created along the same axes as the regional anisotropy. Note that electric fields lying along either of the principal axes of the regional structure are *not* changed in direction. Any rank two diagonal matrix and thus any anisotropy operator can be expressed in this form(6.15). This type of distortion is indistinguishable experimentally from the inductive anisotropy except in special circumstances when the anisotropy of  $\mathbf{Z}_2$  is known independently. Recall that in the hemisphere illustration of Chapter 5, that this was the form of the distortion operator at measurement sights inside the hemisphere (5.28) or outside at sights,  $A$  and  $B$  (5.31).

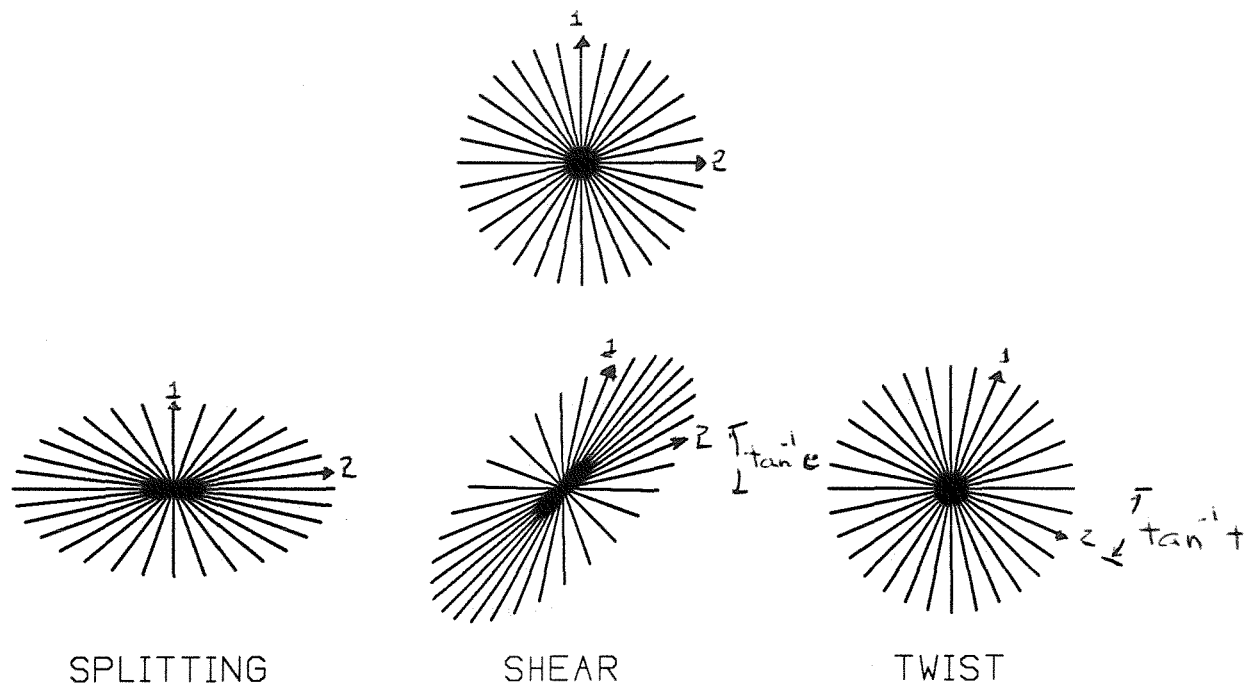


**Figure 6.3.1:** The effects of the anisotropy operator  $\mathbf{A}$ , the shear operator  $\mathbf{S}$  and the twist  $\mathbf{T}$  on a family of unit vectors (top Figure).

Berdichevsky and Dmitriev (1976) have chosen this form for the distortion operator by selection of the measurement location and the symmetries of

the inhomogeneity. This selection of measurement site was unfortunate as it leads to static (frequency independent) scaling of the regional electric fields and thus static shifting of the resulting impedances. This has led to some misunderstanding of the effects of near-surface distorting bodies.

The effect of the twist tensor

$$\mathbf{T} = N_2 (\mathbf{I} + t\boldsymbol{\Sigma}_2) = N_2 \begin{pmatrix} 1 & -t \\ t & 1 \end{pmatrix} \quad (6.16)$$

is simply to rotate the regional electric field vectors through a clockwise angle  $\tan^{-1}t$ . Figure 6.3.1 illustrates again the effect of the twist operator on a family of unit vectors. The twist  $t$  can be characterized by the twist angle  $\phi_t = \tan^{-1}t$ . The inclusion of a twisting effect on the electric fields by the presence of the galvanic scatterers would seem necessary from physical considerations. For the synthetic example of Figure 6.1 such an operator is certainly required to represent the galvanic distortion due to the outcropping basement.

The shear tensor (in analogy to the theory of deformation)

$$\mathbf{S} = N_1 (\mathbf{I} + e\boldsymbol{\Sigma}_1) = N_1 \begin{pmatrix} 1 & e \\ e & 1 \end{pmatrix} \quad (6.17)$$

develops an anisotropy on axes which bisect the regional inductive principal axes. The effect of  $\mathbf{S}$  on a family of unit vectors is shown in Figure 6.3.1 for a positive shear  $e$ . Note that the maximum angular changes in the vector occur when aligned with the principal axes. A vector on the  $x$  axis in the figure is deflected clockwise by an angle  $\tan^{-1}e$ , and a vector along the  $y$  axis counter-clockwise by the same angle. It can therefore be useful to characterize the shear  $e$  by a shear angle  $\phi_e = \tan^{-1}e$ . This may seem at first sight to be an unusual effect and the need for it may not appear intuitively obvious as in the case of the other two operators. However, if one thinks of the gathering of current into a long conducting body this effect may seem more evident. But more theoretically, recall in the illustration of Chapter 5 that for a site (Site C) which is outside the inhomogeneity and 45 degrees from the principal

axes system, the channelling operator  $\mathbf{C}$  has exactly the form of equation 6.16 (5.33).

The real scalar  $g$  performs an overall scaling of the electric fields. This is necessary because the operators  $\mathbf{A}$ ,  $\mathbf{S}$  and  $\mathbf{T}$  have been normalized (16) such that their product is merely proportional to the distortion tensor  $\mathbf{C}$ . We refer to this scalar as the site gain.

One advantage of this factorization of the distortion tensor  $\mathbf{C}$  is now apparent. We know we cannot separate physically the local anisotropic effects from the region without *a priori* knowledge of the conductivity structure. This factorization allows us to include the two anisotropic effects in the mathematical decomposition and therefore remove the non-uniqueness in the model. That is, mathematically, neither  $g$  nor  $\mathbf{A}$  can be separated from  $\mathbf{Z}_2$ , since  $\mathbf{Z}'_2 = g \mathbf{A} \mathbf{Z}_2$  is an equally valid two-dimensional impedance tensor (*i.e.* has zero diagonal elements). In this method we therefore try to determine only  $\mathbf{Z}'_2$  rather than  $\mathbf{Z}_2$ , knowing that the two principal impedances determined in  $\mathbf{Z}'_2$  will have been separately scaled by unknown factors from those of  $\mathbf{Z}_2$ . It is a clear advantage of this factorization of  $\mathbf{C}$  which allows the absorption of the unknown parts of  $\mathbf{C}$  into the regional impedance tensor without destroying the ideal two-dimensional form of that tensor. Previous authors ( Larsen, 1975 and Dmitriev and Berdichevsky, 1976 ) have tried explicit decompositions which include the galvanic distortions. However, these authors assumed the regional structure to be one-dimensional. Thus all anisotropy is due to the local distortions and can therefore be determined. The decomposition presented here can be so adapted if similar information is known about the regional structure. Even for the cases of one-dimensional regional conductivity , the decomposition of Dmitriev and Berdichevsky is, as mentioned previously, inadequate because of its limited application to measurement sites. The decomposition of Larsen is inadequate apart from the limitation due to regional structure, for other reasons which will be discussed below.

The absorption of  $g \mathbf{A}$  into the regional impedance tensor will not greatly

limit our ability to determine the regional impedances. If the telluric distortion is truly frequency independent, as in our original model, this will not alter the shape of the principal apparent resistivity curves as a function of frequency, nor will it change the complex phases of the principal impedances. That is, this method allows us to determine the regional impedances correctly, except for “static shifts”. This is not the case with the conventional method, as discussed in Chapter 5, and it will be illustrated below for more general cases. This is because, in addition to absorbing  $g \mathbf{A}$  into  $\mathbf{Z}_2$ , the conventional method also implicitly absorbs  $\mathbf{T}$  and  $\mathbf{S}$  into  $\mathbf{Z}_2$ . Radically distorting it from an ideal two-dimensional tensor. The problem of the “static shift” is not extreme as any additional information (*e.g.* the near-surface conductivity) allows us to make the correct scaling.

The nature of the physical effects of each factor in the channelling tensor factorization has been discussed. As well, examples of the existence of the shear and anisotropy factors were demonstrated in the analytic distortion illustration of Chapter 5. The presence of the twist operator was indicated in the synthetic example of Figure 6.1. However the question still remains as to whether such a factorization exists for all physical situations of the type we are studying here. Also, it is not clear whether the factorization of the distortion operator by this means is unique or has multiple solutions. These questions are addressed in the following section.

#### 6.4 Uniqueness and Existence of the Factorization

Whether there exists a unique factorization of  $\mathbf{C}$  using real values of  $g$ ,  $t$ ,  $e$  and  $s$  is not obvious for arbitrary  $\mathbf{C}$ . If the factorization is multiplied out explicitly, then

$$\mathbf{C} = \frac{g}{\sqrt{(1+e^2)(1+t^2)(1+s^2)}} \begin{pmatrix} (1+s)(1-te) & (1-s)(e-t) \\ (1+s)(e+t) & (1-s)(1+te) \end{pmatrix}. \quad (6.18)$$

In the case of weak distortions ( $t$ ,  $e$  and  $s$  much less than unity), the factorization can be done very easily. If all second and higher order terms in  $e$ ,  $s$  and  $t$

are neglected, equation 6.18 becomes

$$\mathbf{C} = \begin{pmatrix} C_1 & C_2 \\ C_3 & C_4 \end{pmatrix} \approx g \begin{pmatrix} 1+s & e-t \\ e+t & 1-s \end{pmatrix}. \quad (6.19)$$

From this, the factorization parameters can easily be derived as

$$g \approx \frac{C_1 + C_4}{2} \quad (6.20a)$$

$$e \approx \frac{C_2 + C_3}{C_1 + C_4} \quad (6.20b)$$

$$s \approx \frac{C_1 - C_4}{C_1 + C_4} \quad (6.20c)$$

$$t \approx \frac{C_3 - C_2}{C_1 + C_4}. \quad (6.20d)$$

This is the form (6.19) of the operator utilized by Larsen, 1975. In his work the assumption of a one-dimensional regional conductivity structure allows one to calculate simply the twist, shear, anisotropy and the one-dimensional impedance. The motivation for this form for the distortion operator is not explained by the author. However, its origin can be easily understood. Expanding the present decomposition (6.11) in the Pauli spin bases elements and neglecting all second order and higher terms in the distortion parameters (weak distortion) gives

$$\mathbf{C} \approx g (\mathbf{I} + e\Sigma_1 + t\Sigma_2 + s\Sigma_3).$$

Thus, the distortion parameters are merely scaled Pauli spin coefficients. A decomposition of  $\mathbf{C}$  in this form always exists since the Pauli spin tensors form a basis for an even larger linear space than  $\mathcal{S}$ . The reader may inquire why this form has not been used as Larsen had done ! Such an approach can be made if the regional structure is assumed one-dimensional (Larsen, 1975,1977) but in the 2D case there are too many parameters in the decomposition. This is due to the retention of the local anisotropy.

For stronger distortion, the exact equations (6.18) must be satisfied. It will be shown that for the set  $\mathcal{S}$  of realistic distortion tensors, there always

exists at least one solution to the equations. In general, there exists exactly two solutions.

Recall from equation (16.18)

$$\mathbf{C} = g' \begin{pmatrix} (1+s)(1-te) & (1-s)(e-t) \\ (1+s)(e+t) & (1-s)(1+te) \end{pmatrix}. \quad (16.18a)$$

where  $g'$  now includes the normalizing factors but from here on the prime will be dropped. The set  $\mathcal{S}$  is restricted so that operators of the form

$$\mathbf{C} = \begin{pmatrix} C_1 & 0 \\ C_3 & 0 \end{pmatrix},$$

$$\mathbf{C} = \begin{pmatrix} 0 & C_2 \\ C_3 & 0 \end{pmatrix}$$

and

$$\mathbf{C} = \begin{pmatrix} 0 & C_2 \\ 0 & C_4 \end{pmatrix}$$

are excluded. The fact that these operators are unrealistic is evident from their effect on the unit basis vectors. Such effects cannot exist within the limits of possible earth conductivities since neither perfect conductors nor perfect insulators exist within the crust and upper mantle. The exclusion of these possibilities implies  $s \neq \pm 1$ .

Thus, if  $\mathbf{C} \in \mathcal{S}$ , let

$$\gamma = \frac{C_2}{C_4} = \frac{e-t}{1+te} \quad \text{if } C_4 \neq 0 \quad (6.21)$$

and

$$\beta = \frac{C_3}{C_1} = \frac{e+t}{1-te} \quad \text{if } C_1 \neq 0 \quad (6.22)$$

The special cases where either  $C_1 = 0$  or  $C_4 = 0$  are straightforward and not discussed here. If  $C_1 = C_4 = 0$  then  $\mathbf{C} \notin \mathcal{S}$ . If  $\gamma = \beta$  then there exists only one solution ,

$$t = 0 \quad , \quad e = \gamma = \beta \quad , \quad g = \frac{C_1 + C_4}{2} \quad \text{and} \quad s = \frac{C_1 - C_4}{2g} \quad (6.23)$$

Again if  $\gamma = -\beta$  the only solution is

$$e = 0 \quad , \quad t = -\gamma = \beta \quad , \quad g = \frac{C_1 + C_4}{2} \quad \text{and} \quad s = \frac{C_1 - C_4}{2g} \quad (6.24)$$

However, if  $\gamma \neq \beta$  and  $\gamma \neq -\beta$  then  $e$  and  $t$  satisfy quadratic equations

$$(\gamma + \beta)e^2 + 2e(1 - \gamma\beta) - (\beta + \gamma) = 0 \quad (6.25a)$$

$$(\gamma - \beta)t^2 - 2t(1 + \gamma\beta) - (\gamma - \beta) = 0 \quad (6.25b)$$

which have two real solutions

$$t = \frac{(\gamma\beta + 1) \pm \sqrt{(1 + \gamma^2)(1 + \beta^2)}}{\gamma - \beta} \quad (6.26a)$$

$$e = \frac{(\gamma\beta - 1) \pm \sqrt{(1 + \gamma^2)(1 + \beta^2)}}{\gamma + \beta} \quad (6.26b)$$

We denote the solution for  $t$  with the positive surd as  $t^+$  while  $t^-$  denotes the alternative solution, and similarly for  $e$ . It is easily shown that

$$t^+t^- = -1 \quad \text{and} \quad e^+e^- = -1 \quad (6.27)$$

and the solution sets are therefore

$$(e_1, t_1) = (e^+, t^-) \quad (6.28a)$$

$$(e_2, t_2) = (e^-, t^+). \quad (6.28b)$$

It is also easy to show (6.26) that

$$\gamma\beta = -1 \leftrightarrow t = \pm 1 \quad (6.29a)$$

$$\gamma\beta = +1 \leftrightarrow e = \pm 1. \quad (6.29b)$$

Except for these exceptions, there exists solutions for both  $t, e$  such that each has a solution of magnitude greater than one and a solution with magnitude less than one. To be more specific, it can be shown that if  $(g, t, e, s)$  is a solution to (6.18a) then  $(-gets, -t^{-1}, -e^{-1}, s^{-1})$  is also a solution.

The two solutions cannot always be divided into small (  $|t|, |e| < 1$  ) and large (  $|t|, |e| > 1$  ) distortion solutions. However, if

$$0 \leq |\gamma\beta| \leq 1$$

then

$$|t_2| < |t_1|$$

$$|e_2| < |e_1|$$

and there is a small distortion solution distinct from a large distortion solution. However, if  $|\gamma\beta| > 1$  then the solutions are mixed. That is, there exists one solution which has small shear and large twist and another with small twist and large shear. Note that here small distortion is distinct from the weak distortion case (6.19) previously mentioned.

To solve for the anisotropy factor, equation (16.18a) yields

$$\frac{1+s}{1-s} = \left( \frac{1+te}{1-te} \right) \frac{C_1}{C_4} \quad (6.30)$$

if  $te \neq 1$  and  $C_4 \neq 0$  (The special cases where  $te = 1$  ( $C_1 = 0$ ) and  $C_4 = 0$  are easily obtainable as mentioned above). Equation (6.29) leads to the solutions

$$s_1 = \frac{(C_1 - C_4) + e_1 t_1 (C_1 + C_4)}{(C_1 + C_4) + e_1 t_1 (C_1 - C_4)} \quad (6.31a)$$

and

$$s_2 = \frac{1}{s_1} \quad (6.31b)$$

The small distortion condition  $|\gamma\beta| < 1$  for twist and shear does not necessarily correspond to small  $s$ . However, the size of the anisotropy factor is irrelevant since it can be included into the scaling term  $g$ .

The scaling parameter  $g$  is determined by pre-multiplying  $\mathbf{C}$  by  $\mathbf{S}^{-1} \mathbf{T}^{-1}$ . The inverse of  $\mathbf{T}$  always exists since its determinant is  $1+t^2$  and  $t$  is real. The inverse of  $\mathbf{S}$  exists if  $e \neq \pm 1$ . (This case is considered separately, below.) The resulting matrix  $g \mathbf{A}$  is diagonal and the sum of the diagonal elements yields

$$2g_i = \frac{1}{(1-e_i^2)(1+t_i^2)} [C_1(1+e_i t_i) - C_2(e_i+t_i) - C_3(e_i-t_i) + C_4(1-t_i e_i)] \quad (6.32)$$

where  $i = 1, 2$ . If  $e = \pm 1$  then  $t \neq \pm 1$  (6.28a) and thus (6.18a)

$$g = \frac{C_2}{(s-1)(t \pm 1)}. \quad (6.33)$$

$s \neq 1$  since  $\mathbf{C} \in \mathcal{S}$ .

Thus, in summary there are two solutions (sometimes degenerate) for the decomposition of any physically plausible distortion tensor. If the tensor satisfies the small distortion condition then the solution could be selected by restricting the solutions such that the shear and twist angles have magnitudes less than 45 degrees. We argue that it would be expected that the tensor in a realistic physical environment will satisfy the small distortion condition. This condition implies that the magnitude of the product of the diagonal components of the distortion tensor is larger than the magnitude of the product of the off-diagonal components. This is physically plausible. This restriction allows for a selection of unique parameters from impedance data but does not restrict the method since both solutions can be selected separately, comparisons made and then a choice made by the interpreter as to which is the most likely set of parameters from physical and geological restrictions.

The existence and uniqueness of the factorization can be studied in reference to the synthetic example of the hemisphere inhomogeneity of Chapter 5. Firstly, it can be shown that the channelling tensor (5.28,5.29) is, if the conductivity of the hemisphere is not infinite, always an element of the set  $\mathcal{S}$ . We have, however, restricted ourselves to realistic earth conductivities. On the surface of the conducting media within the hemisphere, the channelling operator is diagonal (5.28). Thus, according to the solution, twist and shear are zero, the solution is unique, and the splitting coefficient  $s$  and the site gain  $g$  are non-zero. In other words, the twist operator  $\mathbf{T}$  and the shear operator  $\mathbf{S}$  are both identity matrices. Some algebra shows that outside the hemisphere, the small channelling condition always holds (*i.e.*  $|\alpha\beta| < 1$ ) if the hemisphere is not infinitely conducting. Thus, we have a unique solution for the channelling factorization if we restrict the twist and shear angles to have magnitude less

that 45 degrees. In the case of Site C (45 degrees to principal axes), the solution results in both  $s$  and  $t$  being zero and thus the channelling factorization is just the site gain  $g$  times a shear operator.

The operators  $\mathbf{T}$ ,  $\mathbf{S}$  and  $\mathbf{A}$  do not necessarily commute. For example,  $\mathbf{T S}$  does not always equal  $\mathbf{S T}$ . The question of the order of the factorization must therefore be addressed. With three factors there are six distinct product factorizations because the factor operators do not commute. However, since the local anisotropy cannot be separated from the regional, there are only two possibilities which are useful

$$\mathbf{C} = g \mathbf{T S A} \quad \text{or} \quad \mathbf{C} = g \mathbf{S T A}. \quad (6.34)$$

The existence and uniqueness of the first has been discussed above. A similar analysis for the second case results in quadratic equations for  $t$  and  $e$  as in the first case. However, the roots of these equations are not always real as in equations 26a and 26b but it is desirable that all factors in  $\mathbf{C}$  be real operators. For this reason the second factorization (6.34) is rejected. From the above considerations, there is only the one possible order of factorization (6.11) from this set of operators ( $\mathbf{S}$ ,  $\mathbf{T}$  and  $\mathbf{A}$ ).

Factorization of the  $\mathbf{C}$  tensor is not our goal, however the above discussion is necessary to establish that the parameters used ( $g, e, t, s$ ) are in fact well defined in the proposed factorization.

## 6.5 The Decomposition of the Impedance Tensor

When the above factorization of the distortion tensor (6.11) is substituted in equation (6.6), the result is

$$\mathbf{Z}_m = \mathbf{R} g \mathbf{T S A Z}_2 \mathbf{R}^t. \quad (6.35)$$

Upon absorbing  $g \mathbf{A}$  into  $\mathbf{Z}_2$  this becomes

$$\mathbf{Z}_m = \mathbf{R T S Z}'_2 \mathbf{R}^t \quad (6.36)$$

where

$$\mathbf{Z}'_2 = g \begin{pmatrix} 0 & (1+s)a \\ -(1-s)b & 0 \end{pmatrix} = \begin{pmatrix} 0 & a' \\ -b' & 0 \end{pmatrix}.$$

It is Equation 6.36 that is the explicit decomposition which is desired. This decomposition has seven real parameters which are:

1 and 2) the scaled real and imaginary parts of the major principal impedance  $a'$  (or equivalently the major apparent resistivity and phase),

3 and 4) the scaled real and imaginary parts of the minor principal impedance  $b'$  (or equivalently the minor apparent resistivity and phase),

5) the azimuth  $\theta$  of the major apparent resistivity,

6) the shear,  $e$  and

7) the twist angle,  $t$ . (An alternative parameter, the local distortion strike or azimuth will be discussed below.)

As discussed previously,  $Z_2$  and  $Z'_2$  are experimentally indistinguishable. Henceforth, the prime on  $Z_2$  will be dropped and it is understood the the resulting principal impedances ( $a', b'$ ) may be scaled by real factors from their true values ( $a, b$ ). Also, it is important to note that if the conductivity structure is truly two-dimensional  $\mathbf{C} = \mathbf{I}$  and (6.36) reduces to the conventional decomposition.

To determine the parameters, a system of equations is developed which relates the data to the model (6.36). The data,  $\mathbf{Z}_m$ , can be represented by a slightly modified set of Pauli spin coefficients (6.10) as

$$\mathbf{Z}_m = \frac{1}{2} (\alpha_0^m \mathbf{I} + \alpha_1^m \Sigma_1 + \alpha_2^m \Sigma_2 + \alpha_3^m \Sigma_3) \quad (6.37)$$

where the coefficients are determined from the elements  $Z_{ij}$  of  $\mathbf{Z}_m$  by

$$\alpha_0^m = Z_{11} + Z_{22} \quad (6.38a)$$

$$\alpha_1^m = Z_{12} + Z_{21} \quad (6.38b)$$

$$\alpha_2^m = Z_{21} - Z_{12} \quad (6.38c)$$

$$\alpha_3^m = Z_{11} - Z_{22}. \quad (6.38d)$$

Multiplying out the decomposition in equation (6.36) and expressing it in the form of equation 6.37, yields, after some algebra, the model coefficients  $\alpha_i$  in terms of the decomposition parameters

$$\alpha_0 = t\sigma + e\delta \quad (6.39a)$$

$$\alpha_1 = (\delta - e\sigma)\cos 2\theta - (t\delta + e\sigma)\sin 2\theta \quad (6.39b)$$

$$\alpha_2 = -\sigma + e\delta \quad (6.39c)$$

$$\alpha_3 = -(t\delta + e\sigma)\cos 2\theta - (\delta - e\sigma)\sin 2\theta. \quad (6.39d)$$

In the above equations (6.39)

$$\sigma = a + b \quad \text{and} \quad \delta = a - b \quad (6.40)$$

are used for the sum of the principal impedances and their difference. The problem now posed is to find the set of parameters  $(\sigma, \delta, e, t, \theta)$  and thus the  $\alpha_i$  which best fits the data parameters,  $\alpha_i^m$ .

The non-linear system of equations (6.39) can be solved analytically for the decomposition parameters if the  $\alpha_i$  are obtained from a tensor of the form (6.36). The proof is not included here. There are however multiple solutions. First of all, there is a  $\theta + n\pi$  uncertainty in the solution for  $\theta$ . This is reflected, physically, in the fact that if  $\theta$  is the regional strike then  $\theta + \pi$  is an equally good value for strike. We therefore restrict  $\theta$  such that  $0 \leq \theta < \pi$ . With this restriction there are still four solutions due to two multiplicities. The first has been discussed and is due to the two solutions for the channelling tensor. The remaining cause of the multiple solutions can be verified by simply noting that if  $(e, t, \sigma, \delta, \theta)$  is a solution of (6.39), then so also is  $(-e, t, \sigma, -\delta, \theta + \frac{\pi}{2})$ . There is no physical significance to the two different solutions for the following reasons. For a regional 2-D structure an azimuth of  $\theta$  or  $\theta + \frac{\pi}{2}$  are both equivalent. In these two cases the sums ( $\sigma$ ) of the principal 2-D impedances are equal whereas the differences ( $\delta$ ) of the principal impedances are the negative of each other. With some analyses it can be shown that: in a rotated coordinate frame (i.e. the azimuth is  $\theta + \frac{\pi}{2}$ ), a twist of ( $t$ ) and a shear of ( $-e$ ) result in the same effect

on any regional electric field, as would a twist ( $t$ ) and a shear ( $e$ ) in the original coordinate frame. The 90 degree ambiguity in  $\theta$  can therefore be resolved by adopting either the convention that  $|a| > |b|$ , so that  $a$  is the major principal apparent resistivity, and  $\theta$  is the azimuth of the electric fields associated with it; or that the azimuth lies between 0 and 90 degrees. The latter has been adopted. Thus, in summary, by restricting  $0 \leq \theta < \frac{\pi}{2}$  and  $\phi_e, \phi_t \leq \frac{\pi}{4}$  there is a unique analytic solution to (6.39).

Although there exists an unique analytic solution to (6.39), within the restricted space of solutions, the data parameters  $\alpha_i^m$  may not have a channelling decomposition solution. This may be true even if the distortion model is a good estimate of the measured impedance tensor. Such possibilities were considered in Chapter 5 (5.61). Solution of these eight real equations for the seven decomposition parameters can be achieved by a least squares fitting procedure. In other words,  $(e, t, \sigma, \delta, \theta)$  are found such that the functional

$$F(e, t, \sigma, \delta, \theta) = \sum_i \Re(\alpha_i - \alpha_i^m)^2 + \Im(\alpha_i - \alpha_i^m)^2 \quad (6.41)$$

is a minimum. This requires good data since the conventional method, in fitting only five parameters, is more stable with respect to data errors. If data are not of sufficient quality to determine all the desired seven parameters, the solution is *not* to return to the conventional method and compute the wrong quantities accurately; it is to obtain better data, or restrict operations to regions where distortion is unimportant.

To illustrate some points concerning the decomposition we will now apply the method to the analytic illustration of Chapter 5 at Site C. This will also provide an opportunity to verify and discuss various aspects of the computer software which has been developed to utilize this decomposition. Recall, that at Site C the distortion operator has the form

$$\mathbf{C} = g \begin{pmatrix} 1 & e \\ e & 1 \end{pmatrix}.$$

Since  $g$  is absorbed into the regional impedance tensor  $\mathbf{Z}_2$  we would expect to recover the correct impedance phases (Figure 6.5.1), the correct apparent

resistivities scaled in this case by equal factors, a zero twist angle (Figure 6.5.2) and a frequency independent non-zero shear angle. Here the measured impedance tensor was produced for a system in which the measuring axes are parallel to the regional principal axes. Thus we expect a zero regional strike (Figure 6.5.1) due to the bounds placed on the strike as discussed above ( $0 \leq \theta < \frac{\pi}{2}$ ).

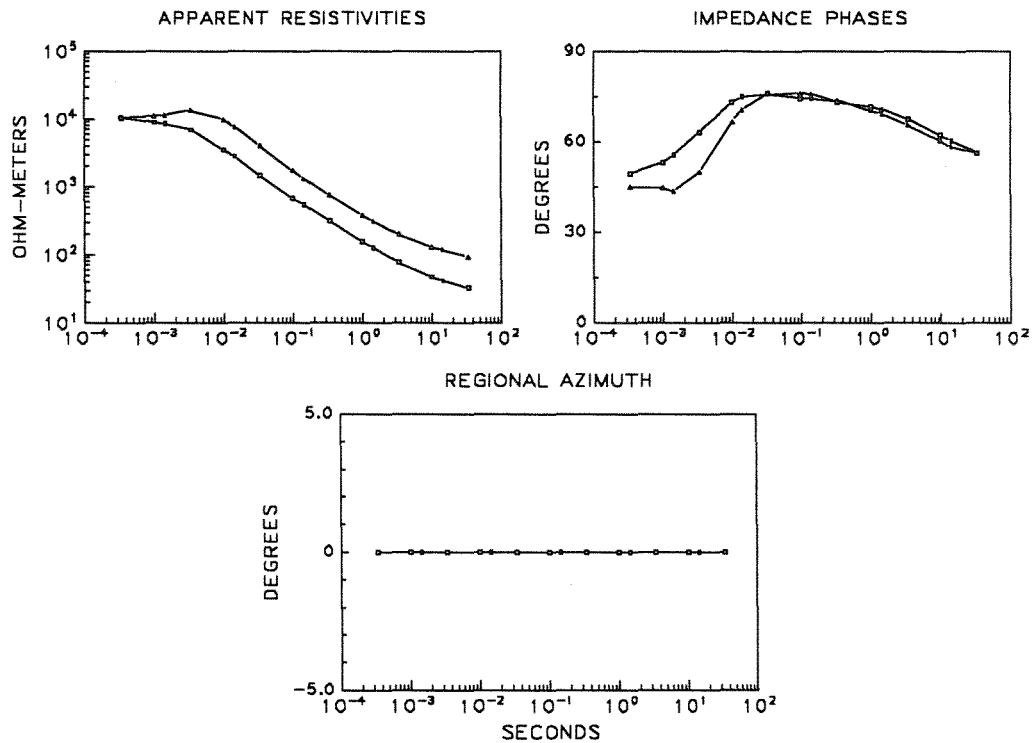


**Figure 6.5.1:** The channelling decomposition principal impedances and regional strike at Site C.

From Figure 6.5.1 we see the program has recovered all the correct information.

The value of the recovered shear ( $\approx 43$  degrees) can be verified by solving for the shear angle with the solution presented earlier in this chapter. As well, the value of the "static shift" parameter  $g$  can also be determined and checked. The channelling or local strike parameter included on this figure (6.5.2) will be discussed below.

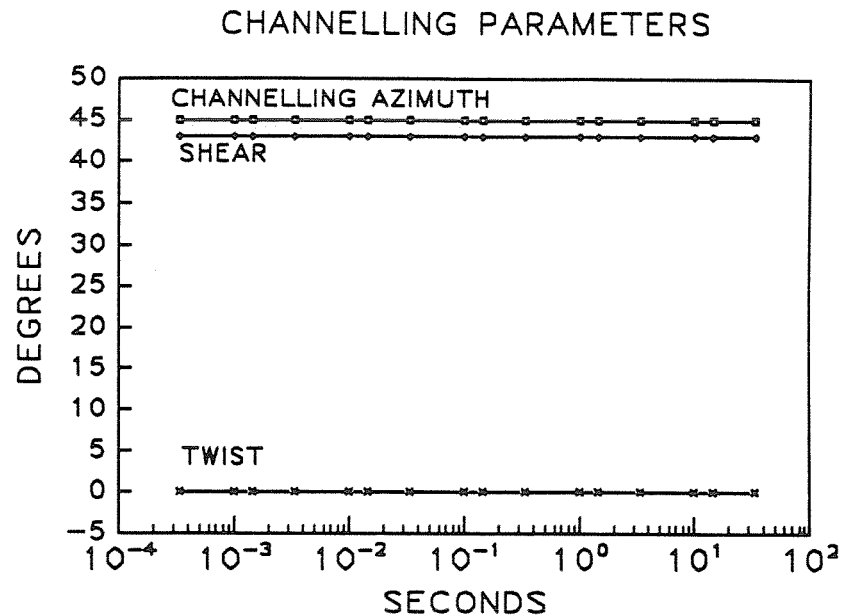


**Figure 6.5.2:** The distortion parameters; twist angle, shear angle and local or channelling strike.

For these figures, the conventional solution for the decomposition of the impedance tensor was used as a starting estimate for the least squares inversion. Various other starting points were also used, including the analytic solution, to verify that the solution was independent of the initial guess. The numerical algorithm for obtaining the decomposition parameters has at its root a NAG functional minimization routine. The routine requires the analytic expression for the functional and its Jacobian but utilizes finite-difference estimates for the Hessian. The algorithm is extremely fast for a system of this size. The inversion at site C for the complete spectrum and the creation of output files for plotting requires significantly less than one minute cpu time on a microVAX. Therefore, computer costs will not be a significant concern. The stability of the inversion in the presence of noise was also tested with this analytic model by adding random Gaussian noise to the analytically created impedance tensor. The error analysis for the parameters will be discussed below when the method

is used on actual experimental data. The analytic model also allowed testing of the software's ability to obtain the correct regional strike, if the impedance tensor is rotated to other measurement axes. The computer routines were also tested with the other two sites, A and B. All the above tests were successful, as expected since the impedance tensor data fitted the distortion physical model, but the tests allowed for effective software debugging.

## 6.6 A Comparison of Interpretation Methods

This section contains some comparisons of the method which has been presented here with more conventional interpretation techniques. To make these comparisons we will assume that the impedance data are due principally to galvanic distortion of the electric fields arising from a large-scale conductivity structure which is at most two-dimensional with negligible magnetic field distortion. That is, we assume

$$\mathbf{Z}_m = \mathbf{R} \mathbf{C} \mathbf{Z}_2 \mathbf{R}^t \quad (6.6)$$

is a good representation of the impedance tensor. This form for the impedance tensor is clearly correct if the three-dimensional inhomogeneities are sufficiently small.

In magnetotellurics, one of the most commonly used indicators of three-dimensionality is skew. Skew was defined by Swift (1967) as

$$|\Gamma| = \left| -\frac{\alpha_0}{\alpha_2} \right|. \quad (6.42)$$

If the only three-dimensional effects are galvanic then (6.39)

$$\Gamma = \frac{t\sigma + e\delta}{\sigma - e\delta}. \quad (6.43)$$

in terms of the decomposition parameters developed here. Thus, it is clear that even when the induction is two dimensional, the skew can be non-zero and a function of frequency, if distortions are present. There are two extreme cases

which are worth noting. If the impedance tensor  $\mathbf{Z}_2$  recovered by the new decomposition is isotropic (*i.e.* the net effect of the distortion anisotropy and the inductive anisotropy is nil or  $a' = b'$ ), then  $\delta$  is zero and

$$\Gamma = t = \tan \phi_t. \quad (6.44)$$

As an example; Site C in the hemisphere illustration (Chapter 5) with a one-dimensional regional structure would have such a response, as there is no local anisotropy. However, at this site there is also no twist and therefore the skew would be zero. The phases and apparent resistivities would appear one-dimensional. There would be no signs, whatsoever, of current distortion effects even though the apparent resistivities would both be “static shifted” from the true values. If the anisotropy of  $\mathbf{Z}_2$  is extreme (*i.e.*  $|a| \gg |b|$ ) then  $\delta \approx \sigma$ . In these cases

$$\Gamma = \frac{t + e}{1 - et} = \tan(\phi_t + \phi_e), \quad (6.45)$$

using the double angle formula for tangent. We are prompted to define a skew angle  $\gamma$  as  $\tan^{-1}\Gamma$  (note that this is to be distinguished from skew angles defined by LaTorraca *et al*, 1985, and Eggers, 1982). Here, the skew angle is an approximate estimate of the magnitudes of the twist and shear angles. Therefore data can be rejected, conventionally, on the basis of a large skew when induction is not three dimensional in nature. The new decomposition proposed above will permit the use of such data.

The skew for Site C is presented in Figure 6.6.1. Note that for higher frequencies, where the regional response is approximately one-dimensional (Figure 5.5), the skew is very small. The twist is almost zero at this site as is expected from equation (6.43). At longer periods, the major impedance has the same phase as the minor and dominates in magnitude by approximately 5 : 2. Thus, from equation (6.43) we would expect the skew to be a fraction ( $\approx \frac{3e}{7}$ ) of the shear.

The conventional method of recovering the principal impedances and the inductive strike is to minimize (Swift, 1967; Sims and Bostick, 1969)

$$|Z_{xx}|^2 + |Z_{yy}|^2$$

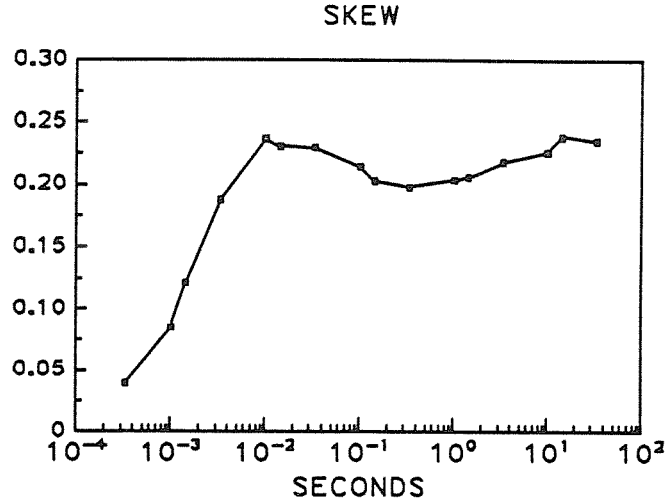


Figure 6.6.1: The skew at Site C of the hemisphere illustration.

as a function of coordinate rotation angle  $\theta'$ . This is equivalent to minimizing  $|\alpha_3(\theta')|^2$  (Spitz, 1985, Sims and Bostick, 1969) as a function of the chosen real coordinate rotation angle  $\theta'$ . In terms of this decomposition we wish to minimize the magnitude of

$$\alpha_3(\theta') = -(t\delta + e\sigma) \cos 2(\theta - \theta') - (\delta - e\sigma) \sin 2(\theta - \theta'). \quad (6.46)$$

If only local anisotropy is present then

$$\alpha_3(\theta') = -\delta \sin 2(\theta - \theta')$$

and the correct regional strike is recovered. However, it is evident from equation (6.46) that minimizing  $|\alpha_3|^2$  with respect to  $\theta'$  will not yield for  $\theta'$  the true inductive strike  $\theta$  if shear or twist distortion is present. This can be demonstrated by the same two limiting cases which we discussed above in terms of skew. In the case where  $\mathbf{Z}_2$  is highly anisotropic which implies ( $\delta \approx \sigma$ ) then  $\alpha_3$  can be made zero by choosing

$$\theta' = \theta + \frac{1}{2} \tan^{-1} \left( \frac{t+e}{1-et} \right) = \theta + \frac{1}{2} \gamma \quad (6.47)$$

if  $e$  and  $t$  are not both zero. The recovered azimuth differs from the principal inductive strike by half the skew angle. The implication of this case is that the azimuth errors of the conventional method can be of the same order of magnitude as the skew angle. In the isotropic case ( $\delta \approx 0$ ),  $\alpha_3$  can be made zero by choosing

$$\theta' = \theta - \frac{1}{2} \tan^{-1} \left( \frac{1}{t} \right) = \theta \pm \frac{\pi}{4} + \frac{1}{2} \phi_t \quad (6.48)$$

if  $t$  is not zero.

The effects of the galvanic distortions can again be illustrated by the analytic distortion model at Site C. For this site, the twist is zero and the shear non-zero. Therefore, at high frequencies, the principal impedances of  $\mathbf{Z}_2$  are essentially zero and thus  $\alpha_3$  can be made zero by

$$\theta' = \theta \pm \frac{\pi}{4} \approx \pm \phi_e = \pm \gamma \quad (6.49)$$

as illustrated in Figure 5.7. At longer periods where  $\frac{\sigma}{\delta}$  is real

$$\theta' = \pm \frac{\pi}{2} + \frac{1}{2} \tan^{-1} \left( \frac{e\sigma}{\delta} \right). \quad (6.50)$$

Thus as can be seen in Figure 5.7

$$\theta' \approx -\frac{\pi}{2} + \frac{1}{2} \tan^{-1} \left( \frac{7}{2} e \right).$$

In Chapter 5 we discussed the effects of local distortion on the conventional method of obtaining the principal impedances. The conclusion there was that the distortion caused the conventional method to produce estimates of the principal impedances which were in fact linear combinations of the true principal impedances. Let us now pursue this subject further with the use of some special cases. For the special case of high anisotropy, what principal impedances will be recovered? We would like to obtain real scalar multiples of  $a(\omega)$  and  $b(\omega)$ , where  $b(\omega) \ll a(\omega)$ . Some algebra shows that the impedances recovered by the conventional method,  $a'$  and  $b'$ , are in fact

$$a'(\omega) \approx a(\omega) \left[ \frac{(1 - et)(1 + \cos\gamma) + (e + t)\sin\gamma}{2} \right] \quad (6.51a)$$

and

$$b'(\omega) \approx a(\omega) \left[ \frac{(1 - et)(1 - \cos\gamma) - (e + t)\sin\gamma}{2} \right]. \quad (6.51b)$$

The major principal impedance is recovered correctly, except for a scaling factor which will be frequency independent if the model is valid. However, the minor principal impedance is not recovered correctly at all. What we obtain is the major principal impedance multiplied by some other scaling factor. The temptation (on seeing such a result for the two principal impedances) would be to conclude that one-dimensional induction (modified by distortions in some unspecified way) was occurring, and thus to attempt to fit the impedance curves with a one-dimensional inductive model. Of course this would be incorrect. The regional azimuth as given by equation (6.47) would however be disturbing for the interpreter making this conclusion.

Another special case is that of weak distortion ( $e$ ,  $t$  and  $s$  all much less than unity) in an approximately isotropic Earth on a regional scale. Thus, terms of second and third order in  $e$ ,  $t$  and  $\delta/\sigma$  can be neglected in (6.39) with the resulting equations;

$$\alpha_0 \approx t\sigma \quad (6.52a)$$

$$\alpha_1 \approx \delta\cos 2\theta - e\sigma\sin 2\theta \quad (6.52b)$$

$$\alpha_2 \approx -\sigma \quad (6.52c)$$

$$\alpha_3 \approx -e\sigma\cos 2\theta - \delta\sin 2\theta \quad (6.52d)$$

Remember that if the splitting term  $s$  is non-zero then  $\delta$  and  $\sigma$  are modified from their true values. Note that if the shear  $e$  is zero,  $|\alpha_3(\theta')|^2$  is minimized by  $\theta' = \theta$ , and the conventional method will recover the correct inductive strike no matter what the twist is. The conventional method also recovers the correct principal impedances in this case (except for the usual static shifts due to the local anisotropy). Note that the skew  $|\alpha_0/\alpha_2| = t$  depends only on the twist and not at all on the shear, whereas it is the shear which determines whether the conventional method is correct. This illustrates a case in which the conventional method gives the right answers even when the skew is non-zero.

However, the conventional method can be significantly incorrect in this case when the skew is zero ( $t = 0$ ) and the shear is non-zero.

The effective one dimensional impedances (Berdichevsky and Dmitriev, 1976; Ranganayaki, 1984); such as half the difference of the off-diagonal elements of  $\mathbf{Z}_m$  (the Berdichevsky impedance) and the square root of the determinant of  $\mathbf{Z}_m$ , must be examined in the light of the channelling model. The use of these effective impedances does not correspond to a belief that the Earth is layered; they are convenient condensations of the information in the measured impedance tensor to forms which hopefully can be modelled. They are thought to be less affected by noise and stationary telluric distortions. In suitable cases, they also have the property of reflecting to some extent a horizontally averaged regional inductive structure. In the absence of distortions, the Berdichevsky impedance is preferable, since its errors of estimation are lower. Where distortions are present, however, the Berdichevsky impedance is no longer simply the arithmetic mean of the two principal impedances, but an unknown linear combination of them, and as such, cannot be modeled. For example, in the regional principal axes system the Berdichevsky impedance is given by

$$Z_{\text{eff}} = C_{11}a + C_{22}b$$

where  $a$  and  $b$  are the regional principal impedances and  $C_{11}$  and  $C_{22}$  are the diagonal elements of the distortion tensor. The determinantal impedance, on the other hand, is in any rotated coordinate system

$$Z_{\text{Det}} = \det | \mathbf{C} | \det | \mathbf{Z}_2 |$$

and as such is unaffected by galvanic distortion, except for multiplication by a frequency independent scalar. This would appear to contradict a result of Berdichevsky and Dmitriev (1976), though it does not. They showed that the trace impedance was less distorted than the determinantal impedance, when measured outside a vertical elliptically cylindrical inhomogeneity. However, the measurement location was on an axis of symmetry where the shear and twist

would be zero (5.9). The advantages of the determinantal impedance lie in its avoidance of effects due to shear and twist.

As mentioned previously, there have been previous studies (Berdichevsky and Dmitriev, 1976, Bahr, 1985, Zhang *et al*, 1987) of the extraction of information from the impedance tensor in the presence of galvanic distortion. We have already discussed the early work by Dmitriev and Berdichevsky and its limitations (Chapter 5). Zhang *et al* (1987) have applied the same physical ideas as Bahr (1985) to the special case where the distortion structure is two-dimensional in nature. What is meant by a two-dimensional distortion structure? This is a structure infinite in one dimension which is superimposed on a regional inductive structure and is sufficiently small in the remaining two-dimensions to cause only a galvanic or charge effect on the region response. In such a situation the channelling tensor is symmetric and as such has only *three* independent parameters and the distortion can then be corrected. This is not a useful consideration in terms of the major problem of near-surface small-scale inhomogeneities. However, they examine in detail the case where the distortion is very strong. For comparison, we examine the strong distortion case (not necessarily two-dimensional) with the decomposition proposed here. Consider the net effect of the tensor  $\mathbf{T} \mathbf{S}$  on the regional electric fields produced by  $\mathbf{Z}_2 \mathbf{h}$ . If the distortion is strong ( $|e|$  approaching unity),  $\mathbf{S}$  highly polarizes the electric field along an azimuth of  $\pi/4$  with respect to the principal inductive coordinate system (or  $-\pi/4$  if the shear is negative). The twist tensor  $\mathbf{T}$  then rotates this axis of polarization by the twist angle. In the measurement coordinates, the final azimuth of the strong local electric field polarization direction is then

$$\theta_l = \theta + \phi_t \pm \frac{\pi}{4}. \quad (6.53)$$

As a decomposition parameter in place of the twist, (as it contains all the information about the twist) it describes more directly the distortion structure. The above result (6.52) can be derived rigorously by using the result of Zhang *et al* (1987) for the form of a two dimensional distortion tensor.

It is instructive to compare the channelling strike (6.53) parameter to the

regional strike  $\theta'$  in light of the inferences from the hemisphere illustration. In these examples, some simple algebra indicated that the conventional strike closely followed the local telluric direction. In physical terms, it seems plausible that a decomposition which attempts to find the best two-dimensional form for an impedance which is the ratio of horizontal electric to magnetic fields would choose the local electric direction. As examples, we can compare the local strike  $\theta_l$  to the conventional azimuth for the limiting illustrations of this chapter. For the highly anisotropic case with strong shear ( $e \approx 1$ ) equation (6.47) gives

$$\theta' = \theta + \frac{1}{2} \left( \frac{\pi}{4} + \phi_t \right).$$

Therefore, the local strike and the conventional azimuth differ by  $(\frac{\phi_e + \phi_t}{2})$ . In the approximate isotropic case, equation (6.48) shows that the local and conventional strike differ by only a half the twist angle. For Site C of the hemisphere example, the two strikes are almost identical at high frequencies (except for the 90 degree ambiguity). For low frequencies, the local strike parameter is 45 degrees, whereas the conventional azimuth (6.50 or Figure 5.7) is approximately -53 degrees and (except for the 90 degree ambiguity) is essentially equivalent. The channelling or local strike parameter and the actual local electric field azimuth can be calculated for Sites A and B and compared with similar results. It appears that for strong channelling the local electric field direction, the local strike parameter and the conventional azimuth are not independent.

### 6.7 Indicators of Three Dimensional Induction, Parameter Error Estimation and Methodology

The assumption of three-dimensional distortion acting on two dimensional induction will not be true in all cases. It is therefore, important to be able to see when the model of galvanic distortion of two-dimensional induction is not an adequate model. Skew, the conventional estimate of three-dimensionality, is not a suitable indicator for this purpose as discussed in the previous section.

There are two ways in which deviations from the ideal distortion model can be detected. These methods, discussed below, must be used in conjunction with each other within the framework of an interpretation methodology.

For a single frequency, the distortion model leads to a decomposition with only seven real parameters and therefore cannot exactly fit all possible impedance tensors. In general, the impedance tensor needs eight real parameters to describe it. The remaining parameter can be expressed as the root mean square relative error of fit  $\epsilon$  of the channeling decomposition which is given by

$$\epsilon^2 = \frac{\sum_{i=1}^2 \sum_{j=1}^2 |\hat{Z}_{ij} - Z_{ij}|^2}{\sum_{i=1}^2 \sum_{j=1}^2 |Z_{ij}|^2} \quad (6.54)$$

where  $Z_{ij}$  and  $\hat{Z}_{ij}$  are the measured and modeled impedance tensor elements respectively. That is,  $\hat{\mathbf{Z}}$  is the estimated impedance tensor from this decomposition model. The root mean error of fit for the conventional model can also be determined (5.3). The error parameter  $\epsilon$  should be small compared with unity, if the particular model for the impedance tensor is correct. It can be calculated at every frequency, and thus can be used to define frequency ranges in which the ideal distortion model is significantly in error. Only one degree of freedom is associated with this sum of residual errors.  $\epsilon$  is therefore also a direct estimate of the data error in each measured impedance tensor element, if all deviations from the ideal distortion model are attributed to data errors. Note that non-zero estimated values for  $\epsilon$  may not be significant if data errors are taken into account.

The second method for detecting deviations from the ideal distortion model is to examine the frequency dependence of the distortion parameters. If the ideal distortion model is a realistic model in a range of frequencies, these parameters will be approximately independent of frequency in that range. In practise, a structure which acts as part of the regional inductive structure at high frequencies, may act as a frequency independent distortion structure at

much lower frequencies. It is necessary to determine the reliability of the hypothesis of frequency independent distortion. Even if the model is correct, we would expect the distortion parameters to vary with frequency due to errors in the data. If the distortion parameters are truly frequency independent it should be possible to decompose the entire data set with fewer degrees of freedom without dramatically increasing the error of fit. This reduction in degrees of freedom is due to constraining the distortion parameters to be frequency independent. The method used here for studying these factors was to determine a minimum in an error surface for the entire data set

$$E = \sum_{i=1}^N \epsilon_i^2 \quad (6.55)$$

when the distortion parameters were constrained to be frequency independent. The sum is over all  $N$  frequencies in the data set. The minimum summed error for constrained decomposition (frequency independent distortion parameters) is then compared with the error for the unconstrained decomposition. If the constrained minimum is not significantly different from the unconstrained minimum with respect to data errors, this is taken as support of the model hypothesis. In opposite terms, if the data set cannot be decomposed with frequency independent distortion parameters such that there is no significant increase in the summed rms error, then the hypothesis of the galvanic distortion model must be rejected. It is important to note that if the distortion parameters are constrained to be independent of frequency throughout the entire frequency range then the total number of parameters used is increased by only two over the conventional method. That is, the channelling decomposition requires  $5N + 2$  parameters for  $N$  frequencies while the conventional method requires  $5N$ . The details of this methodology are discussed further in an example with real data presented below.

If the unconstrained decomposition does not give relatively frequency independent distortion parameters, then the process described would not be of value. However, in this case, we suggest the decomposition remains of sig-

nificant use. Analyses and comparison of the traditional two-dimensional decomposition and the distortion decomposition presented here can indicate the physical regime present, i.e. two-dimensional induction, two-dimensional induction with current distortion or full three-dimensional induction.

It is also necessary to obtain error bars on the decomposition parameters to determine the reliability of the parameter values. In the data set used below, actual realizations of the impedance tensors were available as well as the estimate of the mean impedance tensor. Error ranges for the parameters were obtained by using the scatter in the parameter over the ensemble of impedance estimates for each period. These ensembles were used to obtain an estimate of the true mean impedance tensor which in turn was used to obtain the decomposition parameters. The error bars show the range of values left after discarding the outlying third of the ensemble and thus correspond to  $\pm 1$  standard deviations.

This decomposition method has been applied to other data (not presented here) where individual impedance estimates were not available. However, in these cases estimates of the standard deviation of the impedance elements were available. From the given estimates of the statistics of the impedance tensor, any number of realizations of the impedance tensor could be calculated. The resulting ensemble of estimates were then used in the same manner as discussed above to obtain parameter ranges.

## 6.8 An Example with Experimental Data

The data are long period data obtained in 1985 at a site near Racine Lake (Figure 6.8.1) on the Canadian Shield in northern Ontario, about 30 km north of the town of Chapleau. The data set is expected to have relatively large errors and was chosen for this reason, to test the robustness of the method. The upper crustal rocks are granitic and have resistivities of the order of  $10^4$  ohm-meters. The topographic relief of a few tens of meters is extensively but erratically covered with glacial debris ranging from clays (resistivity of the order of 10

ohm-meters) to gravels and sands (resistivity of the order of  $10^3$  ohm-meters). The likelihood of strong distortion is high with a length scale of the order of a kilometre. A more complete discussion of the geology is available in Cavaliere (1987).

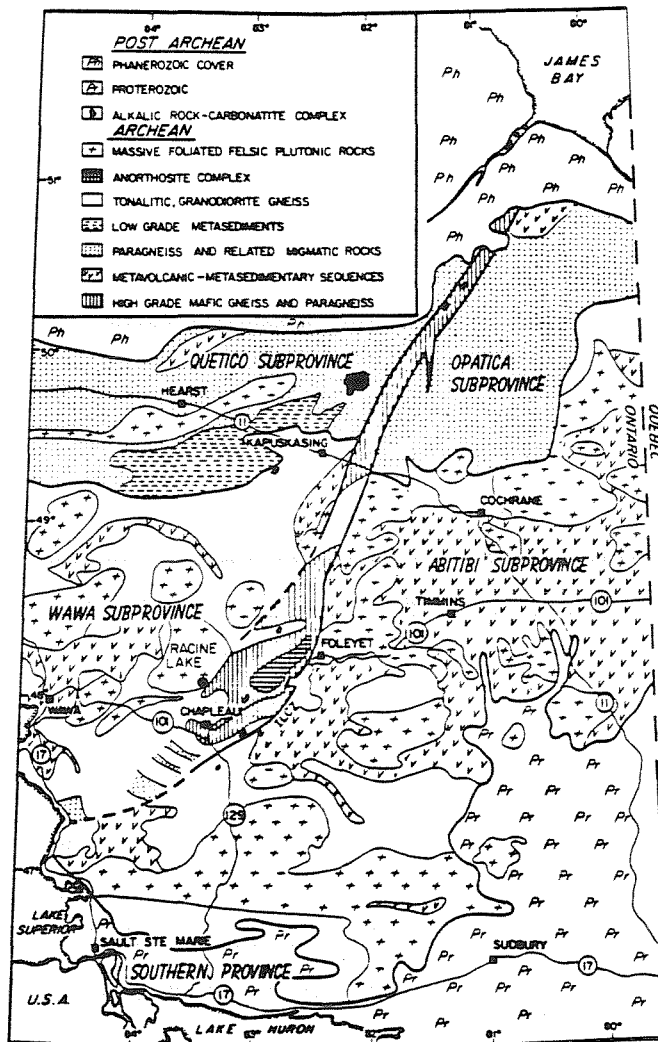


Figure 6.8.1: The Kapuskasing region

Whether the conductivity structure is one-dimensional on a large-scale is of some importance (Cavaliere, 1987). The discussion to follow is not primarily

intended to be a re-interpretation based on the new factorization. It is intended to demonstrate various aspects of the decomposition, the methodology of its application and comparisons made in previous sections to the conventional method. The bandwidth of the data set was larger than presented here. However, the higher frequency data is not as easily interpreted by this decomposition method. A possible cause, is the fact that the noise in the high frequency data here is significantly greater than for low frequencies. This demonstrates a practical aspect of the decomposition which was mentioned previously. The model cannot be expected to fit universally over the full bandwidth of the data which will often span 7 full decades in period. The electromagnetic skin-depth will vary many orders of magnitude through the full spectrum and the physical cause of the secondary electric and magnetic fields will therefore necessarily change throughout the spectrum.

The distortion decomposition was first obtained without any constraints on the distortion parameters. The resulting induction parameters from the conventional method and the new decomposition are compared in Figure 6.8.2 along with the rms error of fit (6.54). Figure 6.8.3 contains the distortion parameters, twist and shear, obtained by the new decomposition.

There are three specific pieces of evidence in these results which suggest the channelling decomposition is appropriate. On examination of Figure 6.8.3, it is observed that the distortion parameter shear is essentially frequency independent without it having been constrained. Secondly, the error of fit,  $\epsilon$ , of the new decomposition is 0.05 or smaller at all frequencies and typically about 0.02. Whereas, the conventional errors ranged as high as 0.4 with the conventional skew ranging (Figure 6.6.5) to 0.4. The error of fit for the new decomposition is improved by an order of magnitude over the conventional method. Thirdly, the local strike (shown in the small figure which contains the new decomposition azimuth) is very close to the conventional regional azimuth. That such results occur in the galvanic distortion regime was discussed in a previous section. However, in opposition to an hypothesis of galvanic dis-

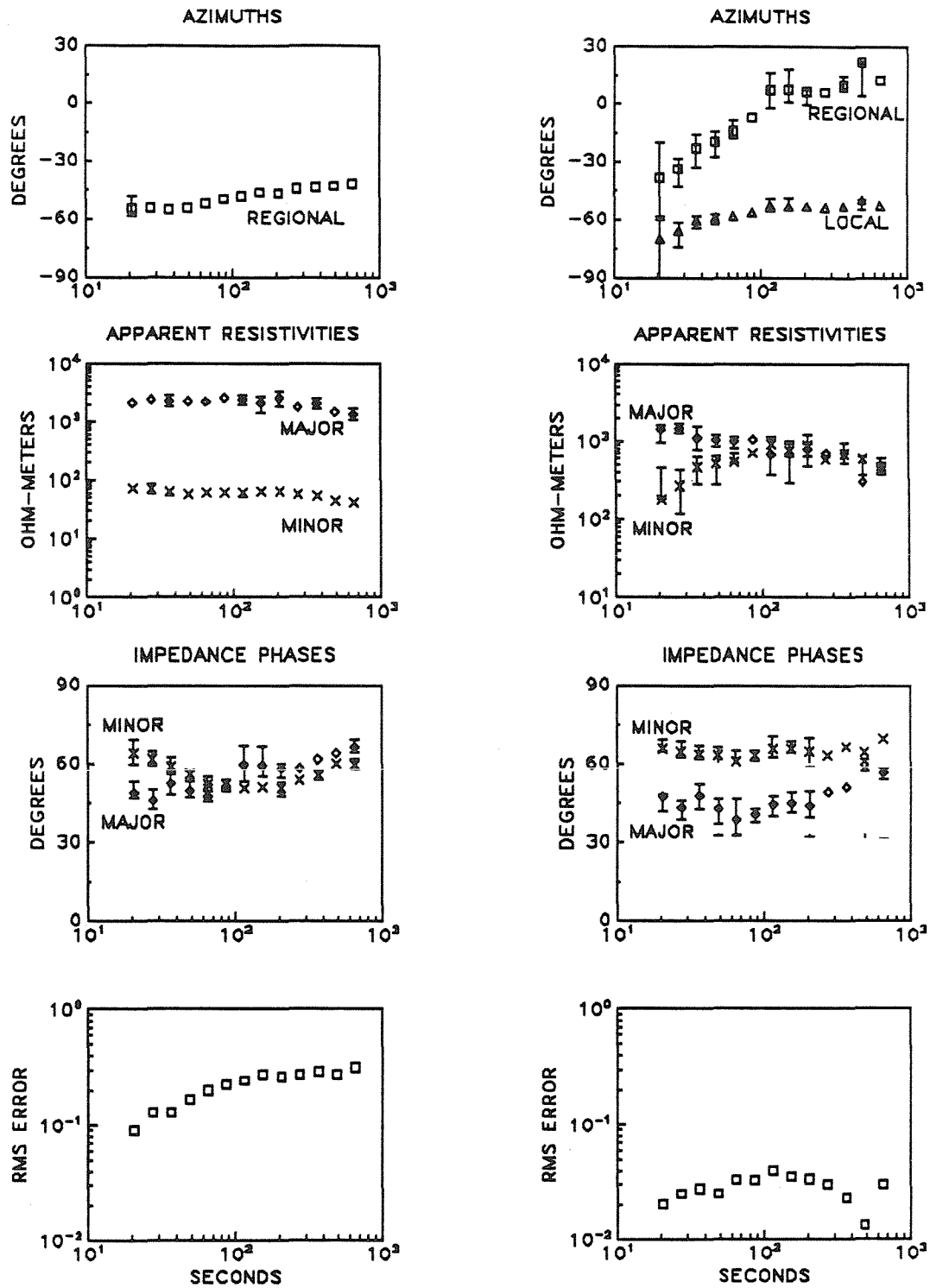
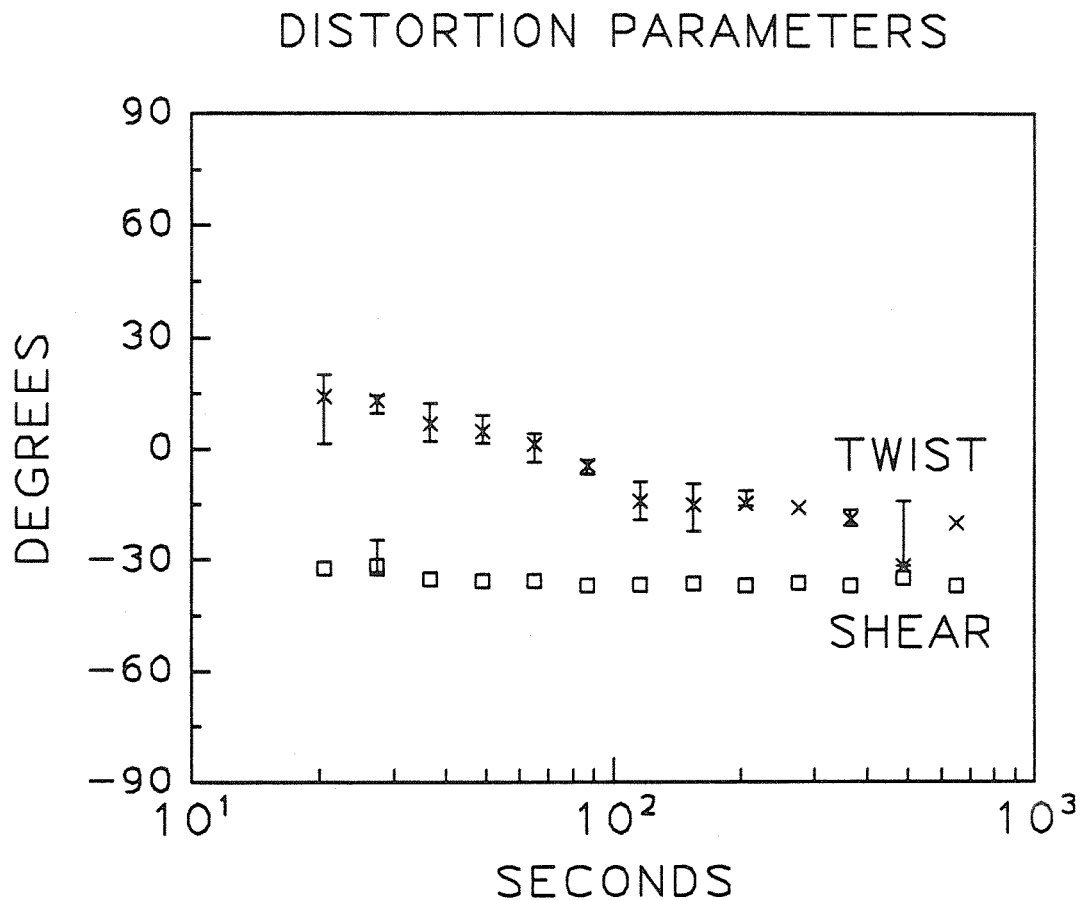


Figure 6.8.2: Comparison of parameters by different methods. The left column contains graphs of the parameters, inductive strike, apparent resistivities, impedance phases and error of fit by the conventional technique. The right column contains the same information for the new technique with the distortion parameters unconstrained. The right column also includes the new channelling parameter, local strike.

tortion, there is the presence in these results of a frequency dependent twist. However, it should be noted that, if the regional azimuth varies slowly with frequency, the local electric current direction may not do the same when there are significant distortion bodies present. Thus, if the local strike is to remain essentially independent of frequency, the twist must vary in an opposite sense from the variation in regional azimuth. This is because, as a rotation operator, the twist angle is given in reference to the regional principal axes system. It can be noted from figures 6.8.2 and 6.8.3 that the twist does indeed vary in somewhat the opposite sense from the regional azimuth.



**Figure 6.8.3:** The distortion parameters (twist and shear ) in degrees for the interpretation given by Figure 6.8.2.

The conventional apparent resistivities are very flat over this period range and appear to be “static shifts” of each other. This result combined with the similarity in the major and minor impedance phases would suggest conventionally, a one-dimensional regional conductivity structure with unknown “static shift”. Three problems arise with this interpretation. First, there appears to be a consistent regional azimuth ranging from about -55 to -45 degrees. There should be no stable azimuth in a one-dimensional regime. Secondly, the error of fit for the two-dimensional model of the impedance tensor is extremely high. The noise in this data is not expected to exceed ten percent. Thirdly, the skew (Figure 6.8.3) is significantly non-zero except at shorter periods.

The apparent resistivities are much more isotropic with the new decomposition (Fig. 6.8.2) than with the conventional method, although they still may contain an unknown splitting. By the conventional method the major apparent resistivity has the same shape as the minor. However, the minor apparent resistivity for this new method has a different form, especially in the high frequencies, than either apparent resistivities by the conventional method. Also, the two impedance phases are significantly different from each other for the new decomposition. In general, the new results are different from those of the conventional method.

The presence of large shear in the channelling decomposition suggests that galvanic distortion has a significant effect and the anisotropy of 30:1 in the conventional method could be the result of this distortion. It is not clear whether the conventional minor resistivity was significantly contaminated by the major resistivity; however this is suggested by the fact that the new method recovers the same shape for the major resistivity but a different shape for the minor resistivity.

The new inductive strike azimuth differs considerably from the old, and varies much more with frequency. The local electric fields seem to have a direction of polarization, namely the apparent local strike or azimuth (which is relatively independent of frequency) as shown on Figure 6.8.2. It now seems

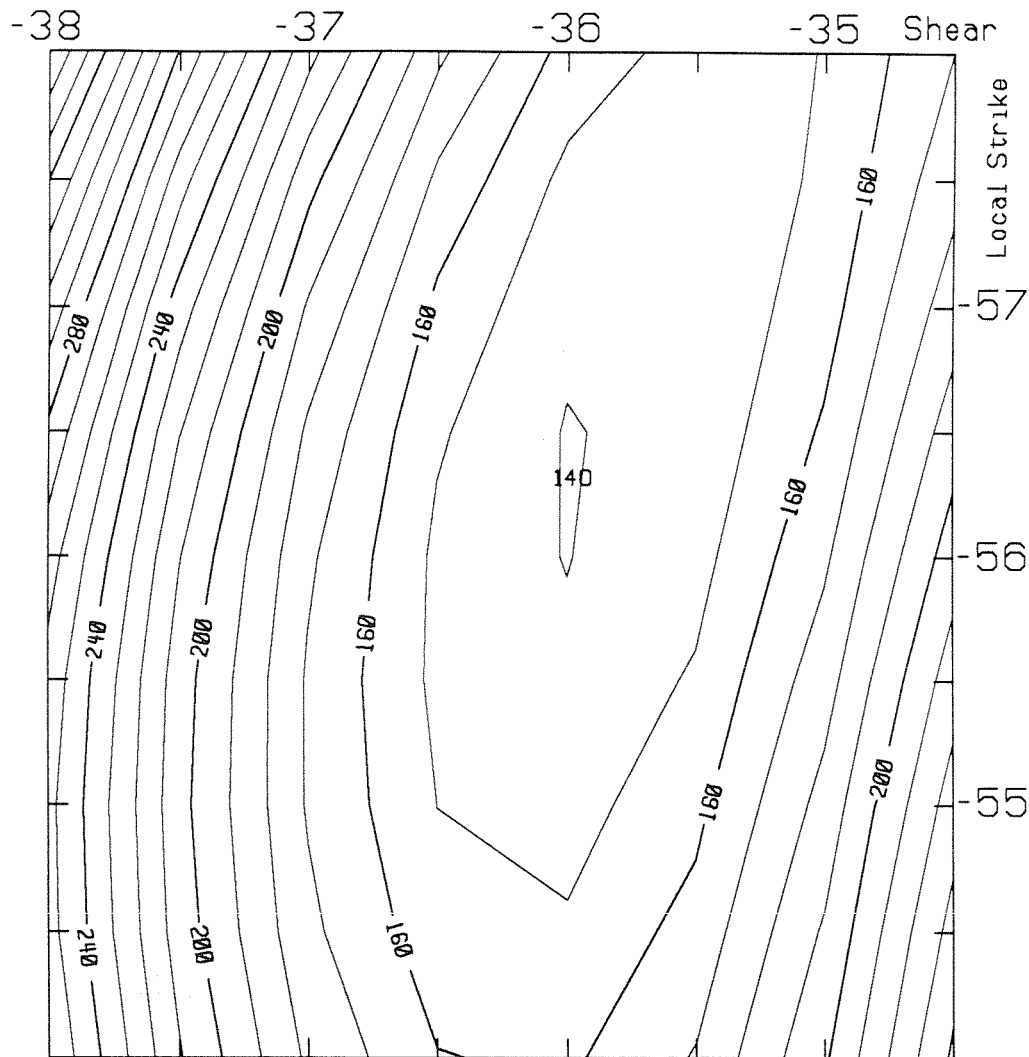
clear that the inductive strike recovered by the conventional method is wrong as a result of domination by distortion effects; note the near coincidence of the conventional strike and the local strike on Figure 6.8.2.

### 6.8.1 Constrained Decompositions

The model for the decomposition dictates that the local distortion parameters be independent of frequency. As required by the physical model underlying the decomposition, the distortion parameters shear and local strike ( $e, \theta_l$ ) are relatively independent of frequency as seen from Figures 6.8.2 and 6.8.3. This decomposition gave a data set error (6.55) as discussed previously of 0.0009 (the average over frequencies of the square of the rms error). The next stage in the methodology is to investigate whether the distortion parameters are actually independent of frequency and whether the observed variations in the distortion parameters in Figures 6.8.2 and 6.8.3 are due slight inadequacies in the model. The shear in Figure 6.8.3 is almost frequency independent as is the local strike in Figure 6.8.2. If we assume *a priori* that the shear and distortion strike are independent of period and constrain them to be so in a least squares fit, the average error of the fit of the decomposition increases to 0.0014. This is a minimum when shear and distortion azimuth are constrained to be independent of period. The increase is not significant with respect to errors in the data and thus supports the model hypothesis.

Figure 6.8.4 contains a contour of the error surface (error as a function of  $e$  and  $\theta_l$ ) for the entire data set, when the local strike and the shear are constrained to be frequency independent. The contour figure shows a clear valley in the surface in parameter space centered on a shear of -36 degrees and a local strike of -56.5 degrees.

Figure 6.8.5 is a comparison of induction parameters between the unconstrained decomposition (left column) and the constrained decomposition (right column). Figure 6.8.6 gives the shear and twist for the constrained solution with the classical skew-angle for comparison. The first item to note from Fig-



0.1

E-06

**Figure 6.8.4:** Contour plot of error surface height for constrained shear and local strike. The bounds on local strike are -58 to -54 degrees and those on shear -38 to -34.5 degrees. The actual errors have been multiplied by  $10^5$  for this presentation.

ure 6.8.5 is that a constrained interpretation does not produce a significantly larger error of fit. The increase in the error of fit is not significant within the data error levels. With the unconstrained decomposition, the data was solved for 7 parameters at each of the 13 periods in the data set meaning a total of 91 parameters were used for the entire data set. The conventional method requires

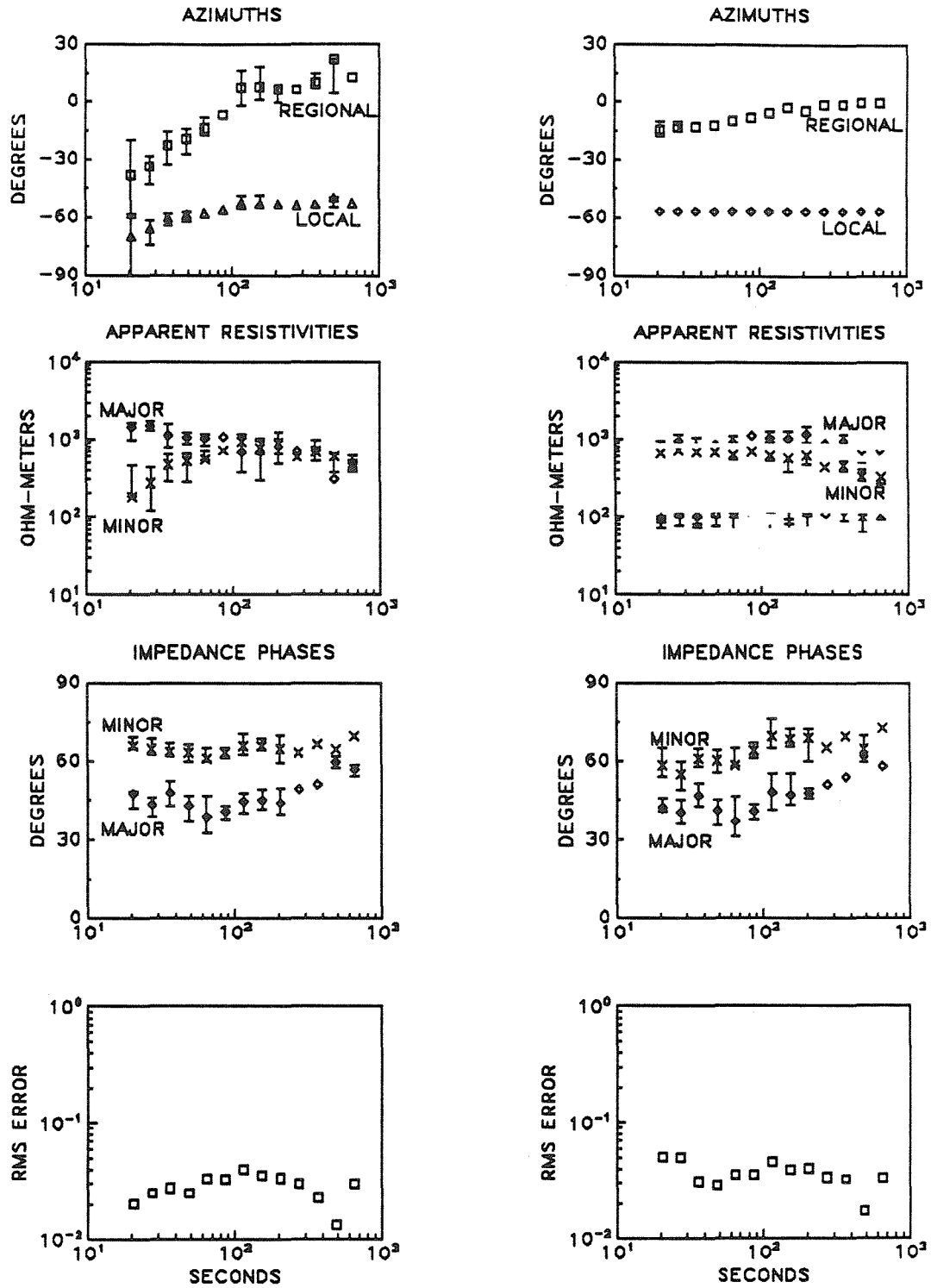


Figure 6.8.5: Comparison of parameters for frequency independent distortion versus non-constrained distortion. Right column contains parameters for a decomposition constrained to have frequency independent shear and local azimuth.

only 65 parameters and thus necessarily we would expect a smaller error of fit for the channelling decomposition which uses 91 parameters. However, for the constrained decomposition here 5 parameters were used per period plus 2 parameters for the frequency independent shear and local azimuth. This results in a total of only 67 parameters being used for the entire data set. As seen in Figure 6.8.5, there is still almost an order of magnitude smaller error for the channelling decomposition with only two more total parameters than used for the conventional parametrization.

The resulting regional azimuth for the constrained decomposition is significantly modified (Fig. 6.8.5) and is now much less variable through the spectrum. The major apparent resistivity and impedance phase are virtually unaltered from the unconstrained case and the minor impedance is only slightly altered from the unconstrained case. The twist still varies in an opposite sense to the regional strike. Note that for a constrained local strike, twist is no longer an independent parameter but depends entirely on local strike and regional azimuth.

Of what significance are these latter results? First, a frequency independent distortion inversion is possible for the data set thus providing some confirmation for the application of the distortion decomposition. Careful study of the results of Figures 6.8.5 and 6.8.6 reveals further information. Examination of the resulting regional azimuth with the conventional regional azimuth shows that the two are different by approximately  $-\frac{\pi}{4} + \frac{1}{2}\phi_t$ . This is the expected result for an approximately net isotropic earth. By a net isotropic earth, it is meant that the combined regional and local anisotropy produce an approximate isotropy. This is evident in Figure 6.8.5 where the apparent resistivities are almost equivalent. It is not yet clear whether there is local anisotropy or whether the regional structure is approximately isotropic.

At lower periods, Figure 6.8.6 reveals that the twist is almost zero. Can a zero twist and approximate net isotropy produce the splitting observed in the convention method (Figure 6.8.2)? A study of the relevant equations shows

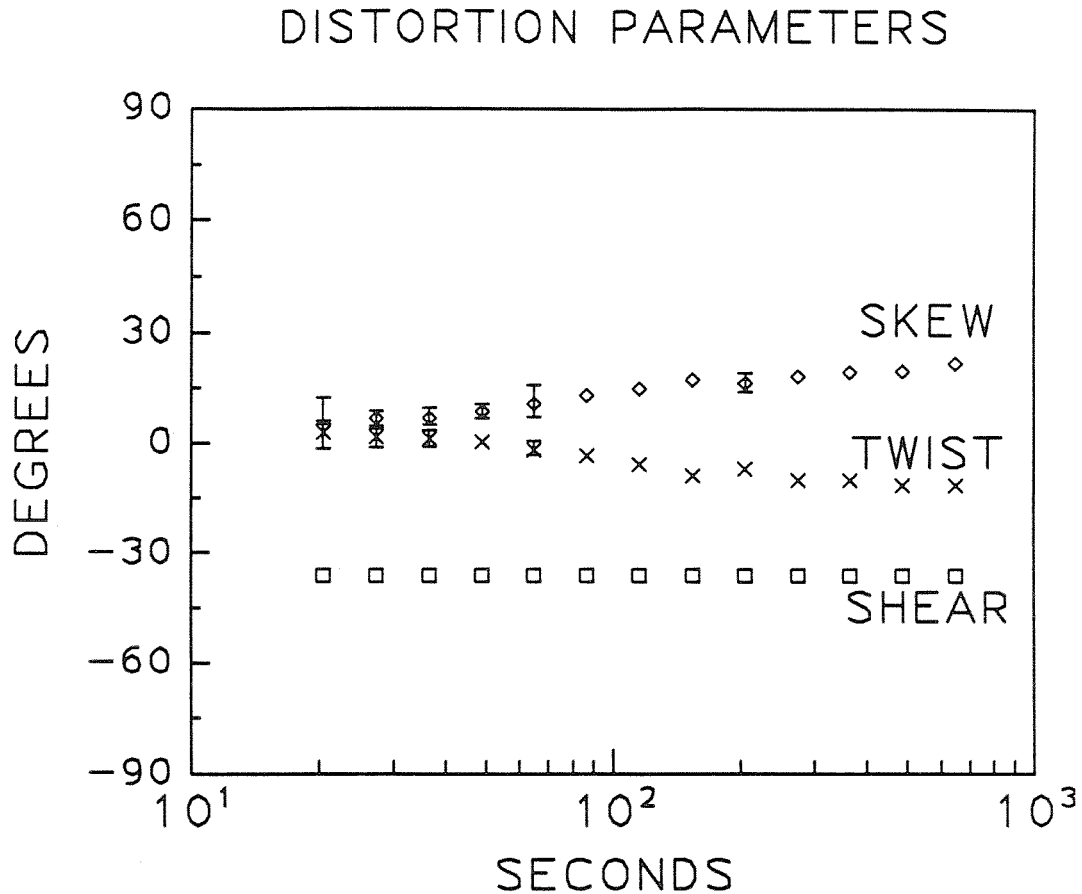


**Figure 6.8.6:** Distortion parameters ( twist and shear ) for the decomposition of Figure 6.8.5 (right column). The conventional three-dimensional indicator, skew, is included for comparison.

that the answer is no, but a small twist and a non-zero shear can produce such a splitting. However, Figure 6.8.6 reveals that the constrained decomposition produced a twist which is dependent upon frequency. Recall that the last constrained decomposition fixed the local strike but if there is no true regional azimuth (one-dimensional), then the regional azimuth and twist can vary in opposite senses such that the sum is constant.

What would the result be if the regional azimuth were constrained to be zero which implies no true regional azimuth and at the same time the shear and twist were also constrained to be independent of frequency? If the large-

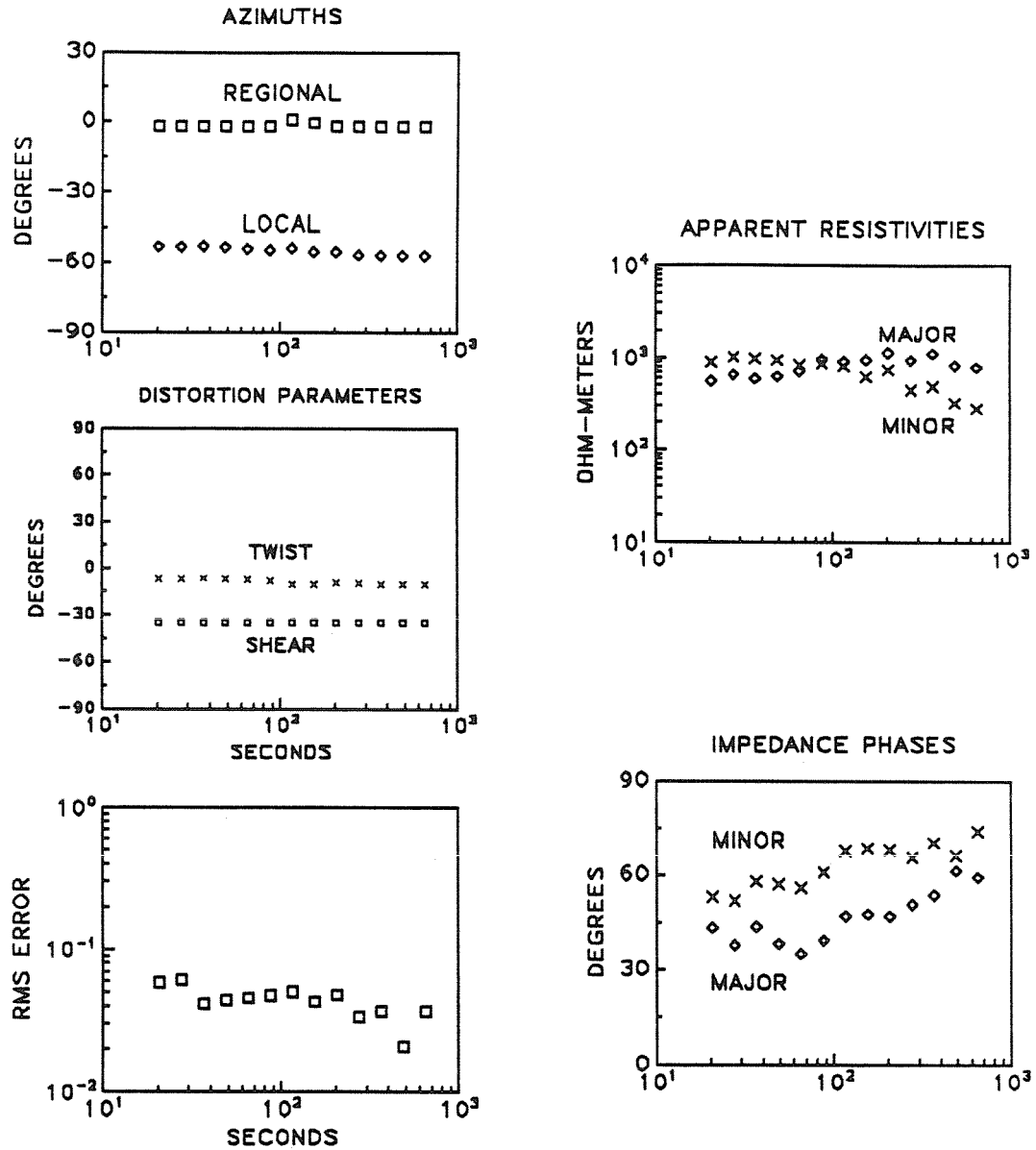


Figure 6.8.7: The decomposition parameters when shear, twist and regional azimuth are constrained.

scale structure is truly one-dimensional this set of constraints should produce an equally valid interpretation. This set of constraints is investigated in Figure 6.8.7. There is very little increase in the error of fit from the unconstrained decomposition. The number of free parameters used for the entire data set is

now less than the number used for the conventional decomposition. However, the error of fit, as seen by comparing Figure 6.8.7 to 6.8.2, is still almost an order of magnitude smaller.

Twist, shear and local azimuth are now essentially frequency independent as is the regional azimuth. There are only slight variations in the impedances from the previous constrained decomposition (Fig. 6.8.5). The large-scale structure can be interpreted as one-dimensional at these periods. Since there is no regional strike, restricting the twist and shear to have magnitude less than one, forces the method to determine values for these parameters with respect to the measurement axes.

There is a significant problem with the interpretation in Figure 6.8.7. If the regional structure is truly one-dimensional, the impedance phases should not be so different. However, other physical factors may be present and causing these phase differences. In the previous chapter, I analysed not only the galvanic distortion of the electric field but also the effects on the impedance tensor of noise, weak induction, and the anomalous magnetic field produced by galvanic distortions of the electric field.

The effect of noise in the data set can be studied by adding random noise to an analytic model such as used in Chapter 5. There is a variation in the magnitude of the apparent resistivities but not a significant variation as the log of the apparent resistivities are plotted. There can however be a significant effects on the impedance phases due to noise. Weak induction, if present, will mainly cause variations in the impedance phases, as well (Chapter 5). The third factor to be considered is the effect on the magnetic field of the galvanically distorted currents. This effect produces a magnetic field out of phase with the primary magnetic field.

As shown in Chapter 5, the anomalous magnetic field due to electrostatic distortions of the electric field can be represented as a distortion operator upon

the primary electric field. To first order, this can be expressed as

$$\vec{H}_a = \mathbf{D}\vec{E}_0 = \begin{pmatrix} 0 & \alpha \\ -\beta & 0 \end{pmatrix} \vec{E}_0 \quad (6.56)$$

where  $\vec{H}_a$  is the anomalous magnetic field caused by galvanic distortion of the primary electric field,  $\vec{E}_0$ . If galvanic distortions are the only effect, the measured impedance tensor can be factored as

$$\mathbf{Z} = \mathbf{C}(\mathbf{I} - \mathbf{D} \mathbf{Z}_0) \mathbf{Z}_0. \quad (6.57)$$

This effect, as discussed in Chapter 5, can cause a shift in the estimated impedance phases from the true regional impedances phases. If the distorting body is elongated,  $\alpha$  and  $\beta$  are not equal and there would be unequal shifts in the two impedance phases. As a result, a splitting of phases would occur even in a one-dimensional regional structure.

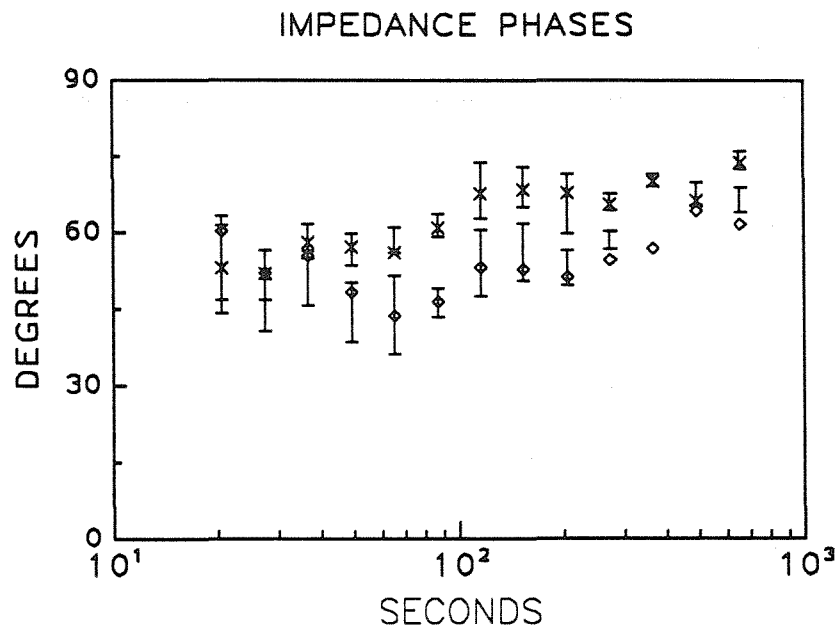


Figure 6.8.8: Impedance phase corrections for the effect on the anomalous field of the static electric distortions.

Figure 6.8.8 is an example of the regional impedance phases of Figure 6.8.7 corrected for the magnetic effects of an hypothesized elongated distorting body. The purpose of this example is not to model the actual body causing the electrostatic distortion but merely to suggest that such electrostatic effects on the magnetic field can account for a significant portion of the phase differences seen in Figure 6.8.7. The phase corrections are based on a model of a highly conducting distorting body of length  $L = 2$  km and width  $R = 120$  meters. The host conductivity ( $\sigma_h$ ) was taken to be  $10^4 \Omega m$  and the apparent one-dimensional resistivity at these periods was assumed to be  $400 \Omega m$ . The magnitude of the anomalous magnetic field,  $h_a$ , was approximated from current channelling considerations (Cheesman, 1985) and the Biot-Savart Law as

$$h_a = \frac{\sigma_h 4L^2}{R} e_r \quad (6.58)$$

where  $e_r$  is the regional electric field. (6.58) is then used to determine the magnetic distortion operator,  $\mathbf{D}$ . The effects on the impedance phases are then removed via (6.57).

Figure 6.8.8 indicates that much of the apparent two-dimensionality in the impedance phases of Figure 6.8.7 can be accounted for by electrostatic effects on the magnetic field due to the surface distorting bodies. However, the lack of one-dimensionality in the impedance phases (Fig. 6.8.7) may actually be a combination of all three causes discussed above (*i.e.* noise, secondary induction, electrostatic magnetic field effects). This suggests an extension of the method proposed herein to obtain the two magnetic distortion parameters  $\alpha$  and  $\beta$ . These parameters could not be recovered at each frequency as there would then be more parameters than data. This is not a limitation, however, as the parameters  $e$ ,  $t$ ,  $\alpha$  and  $\beta$  should be frequency independent and therefore it should be possible to recover  $5N + 4$  parameters over a data set of  $N$  periods.

## 6.9 Interpretation and Modelling

The above discussion is primarily concerned with the problem of obtaining the decomposition parameters from experimental data. But, what if it is desired to compute them for a theoretical model? Calculating the impedance tensor under the ideal distortion assumption is much simpler than performing full three-dimensional induction calculations, and is described partially by Berdichevsky and Dmitriev (1976). A regional two-dimensional structure is postulated, and the azimuth and principal impedances calculated using one of the currently available two-dimensional induction programs. The distortion tensor  $\mathbf{C}$  of the inductively weak distortion structure near a given location can then be modeled by assuming the application of the regional telluric currents to it. This is essentially equivalent to the problem of modeling DC resistivity measurements, with somewhat different boundary conditions imposed by the regional telluric currents than are imposed by currents injected into the Earth by electrodes. It is worth noting that the distortion tensor of a structure can be computed without any knowledge of the regional inductive response as has been done in Chapter 5. The final computation of twist and shear, however, does require knowledge of the regional inductive strike direction, as twist and shear are not intrinsic parameters of the structure but rather descriptions of what the structure does to electric currents arriving from a particular direction. Flores and Edwards (1985) and Flores (1986) have described a program for modeling channeled magnetotelluric responses in this way, modeling the distortion structure as a collection of thin conductive plates, although the results are not presented in terms of the distortion parameters derived in this paper, but rather as complete impedance tensors. This is an example where it would be very useful for workers in numerical methods to describe their results in terms of the decomposition parameters described here. Interpreters of experimental data could therefore use the numerical results to gain insights into their own experimental results.

If sufficiently detailed spatial magnetotelluric coverage of local distortion

structure is available, it should be possible to infer something about its structure by mapping the shear and twist angles at only a single (low) frequency. The regional inductive impedances are irrelevant to this interpretation.

### 6.10 Summary

This chapter presents an explicit decomposition of the impedance tensor, the parameters of which separately represent the determinate distortion effects, the indeterminate distortion effects, and two-dimensional inductive effects. Because the class of magnetotelluric responses described by the distortion model is much larger than that described by ideal two-dimensional induction, the recovered principal impedances and inductive strikes should be physically meaningful in a much larger proportion of experimental cases. Even in cases where the physical system does not conform exactly to the simple distortion model, this decomposition can still offer a useful way to present and compare both real and synthetic magnetotelluric data for three dimensional structures.

## CHAPTER 7

### CONCLUSIONS

The primary contribution of this thesis has been in providing a greater understanding of the effects of small-scale, near-surface inhomogeneities and how to account for these effects. In chapter 5 an analytic model was used to study the effects of small-scale 3D inhomogeneities on regional electromagnetic fields. It was shown that a small scatterer causes the horizontal components of the measured electric field to be position-dependent mixtures of the regional electric field components. This result is in opposition to the frequency-independent scaling of the components ("static shift") which is often considered to be the effect of such inhomogeneities. The analytic model in conjunction with a two-dimensional computer modelling program showed that the conventional decomposition technique produces incorrect regional strikes and impedance parameters which are position-dependent mixtures of the true regional impedances. The analytic model was also used to describe the electrostatic distortion of the magnetic field and then how such scatterers can distort the measured impedance phases purely through frequency independent scattering. In the one-dimensional case, it is shown how the presence of a small surface scatterer can produce a well defined but erroneous regional strike with the conventional 2D decomposition method.

When small 3D inhomogeneities cause only frequency-independent scattering effects, a factorization of the impedance tensor is developed which describes the influence of the different physical effects on the measured impedance data. Specifically, in the case of a 2-D regional structure it allows the separation of local scattering effects from the regional effects. A decomposition method is described, the physical basis of which is an extension of the ideas used by Bahr (1985). This decomposition method allows a) for a standard interpretable data presentation b) easy formulation of fitting methods c) the

investigation of uniqueness d) it incorporates a large set of physical models e) provides the concept for extension to additional physical models. The concept for this parametrization is entirely different from the concept of obtaining eight parameters from the impedance tensor at each frequency. The latter type of parameterization will always mix local and regional effects when both are present. The concept behind the decomposition developed in this thesis enables incorporation of data at multiple frequencies and detection of frequency-independent parameters to obtain a parameterization which separates local 3-D effects from regional 2-D effects.

In chapter 6, the most significant effect of small-scale, near-surface inhomogeneities was addressed; that of galvanic or frequency-independent distortion of the horizontal electric fields. Here, it is assumed that the impedance tensor is due to the response of a regional structure which is at most two-dimensional but coupled with small-scale, three-dimensional, static distortion of the electric fields. This method recovers the correct regional strike and “static-shifts” of the true two-dimensional impedances. That is, the recovered impedances are the true impedances but multiplied by frequency-independent, real constants. Some information on the three-dimensional structure is obtained via two distortion parameters termed twist and shear which describe the local galvanic electric field distortion. Software was developed to determine the decomposition parameters (strike, impedances and distortion parameters) from the impedance data. Error bounds on the parameters can also be produced. Software was developed to study model parameters and model fits when the distortion parameters (twist and shear) are constrained to be independent of frequency. It was demonstrated mathematically and by modelling studies that the method could, in fact, recover all possible information on the regional structure as well as useful information on the distorting bodies. The method was then applied to actual experimental data. Due to the low frequency of the data and the general high resistivity of the upper crust in the area where the data was gathered, it is expected that the data is due primarily to one-dimensional induction coupled with static effects due to the near surface complexity. The entire area

contains small surface structures of relatively high conductivity and thus static distortions of the electric fields were expected. Application of the decomposition obtained a model of the structure which is consistent both with the data and a 1-D structure at depth modified by small-scale surface inhomogeneities. These results cannot be obtained by any method yet developed.

The decomposition method, as well as providing a useful parametrization when the Earth can be modelled by 1-D or 2-D large-scale structure coupled with 3D small-scale local structure, provides the beginnings of a useful method which can incorporate an even more comprehensive model. This model being that for the factorization of Chapter 5 (a 2D regional structure with 3D galvanic and weak induction effects). It is believed that any useful parametrization of impedance data must be approached in, at least, a similar manner as is begun here. For the concept introduced and partly developed in this thesis provides a means of determining those parameters which are frequency-independent. The determination of these parameters over multiple frequencies reduces the number of model parameters to be less than the number of data. Thus allowing for the determination of useful and unique parameters for interpretation.

Chapter 3 provided the H-polarization solution to two conducting, semi-infinite slabs underlain by a half-space of arbitrary conductivity for any frequency of excitation. Previous solutions to this problem had been restricted to unphysical basement conductivities (zero or infinity) and very low frequency approximations. The solution is exactly correct at the Earth's surface where MT measurements are made and approximately correct elsewhere. The source of the error is shown and estimates for the error are given. Comparisons to numerical solutions are given to corroborate the solution and to show the limitations of one commonly used numerical method.

One of the major areas of investigation in the magnetotelluric community is the theoretical study of the inversion of MT data for one-dimensional structures. In light of the amount of effort spent on this research it was felt it was important to understand completely the effects of one-dimensional structures.

It is commonly accepted in magnetotellurics, that if the conductivity is only a function of depth, it is the spatially averaged conductivity which is sampled. Chapter 2 investigated more precisely to what extent this is true. The investigation determines the effects on the surface impedance of a conducting layer whose spatially averaged conductivity is uniform but which has variations from this average conductivity which are only functions of depth. These variations are, however, over distances much smaller than a skin-depth. It was found that there can be some significant differences in the measured impedances from those produced by structures which are entirely uniform but which have the same spatial average conductivity. These results are most significant in the impedance phase where the variations between the uniform and fine-bedding model are as much as ten degrees. The effects were most pronounced at higher average conductivities, with large contrasts in the conductivities of the beds and when the variations correlate over larger distances.

Chapter 4 was a study in the effects of a complex medium consisting of multiple inhomogeneities. The model is that of an infinite sequence of resistive or conducting two-dimensional dikes of equal depth embedded in a host. It is presently thought that correct sampling of the surface electric field can solve the problem of near-surface structure. This model provided a means of investigating these suppositions. The results of this chapter conclude that even in such an extreme case of complex inhomogeneities, magnetotellurics can correctly determine a correct bulk resistivity and a correct thicknesses for such an inhomogeneous layer when the electric field is sampled correctly. However, the results also show that long electrode spacings for determination of the electric fields will not always solve the problems of near-surface structure even in two-dimensional cases. Incorrect sampling with long electrodes spacing can produce just as erroneous results as short spacing. The studies also show that the presence of resistive dikes in a more conducting host can produce false conducting layers if the impedance curves are interpreted only one-dimensionally.

## REFERENCES

- Aki, K and Richards, P.G., 1980. *Quantitative Seismology, Theory and Methods, Vol. II*, W.H. Freeman and Company, San Francisco
- Bahr, K., 1985, Magnetotellurische Messung des Elektrischen Widerstandes der Erdkruste und des Oberen Mantels in Gebieten mit Localen und Regionalen Leitfähigkeitsanomalien, Doctoral thesis, Gottingen.
- Bailey, R.C., 1977. Electromagnetic induction over the edge of a perfectly conducting ocean: the H-polarization case, *Geophys. J. R. astr. Soc.*, **48**, 385-392.
- Berdichevsky, M.N., and Dmitriev, V.I., 1976, Basic principles of interpretation of magnetotelluric curves, *in* *Geoelectric and geothermal studies*: A. Adam, Ed., Akademi Kiado, 165-221.
- Bostick, F. X., 1986, Electromagnetic Array Profiling (EMAP) *presented at* Fifty-sixth Annual Meeting, Society of Exploration Geophysicists, Houston.
- Brewitt-Taylor, C.R. and Weaver, J.T., 1976, On the finite difference solution of two-dimensional induction problems: *Geophys. J. R. astr. Soc.* **47**, 375-396.
- Cagniard, L., 1953, Basic theory of the magneto-telluric method of geophysical prospecting, *Geophysics*, **18**, 605-635.
- Cavaliere, T.C., 1987, A magnetotelluric investigation of the Kapuskasing structural zone: implications for the nature of the lower crust: M.Sc. thesis, University of Toronto.
- Cevallos, C., 1986, Magnetotelluric interpretation - another approach: PhD thesis, Macquarie University, Sydney, Australia.

- Cheesman, S.J., 1985: The Effect of Current Channelling in Square Plates with Applications to MMR: M.Sc. thesis, University of Toronto.
- Cox, C.S., Filloux, J.H., Gough, D.I., Larsen, J.C., Poehls, K.A., von Herzen, R. P., and Winter, R., 1980, Atlantic lithosphere sounding, *J. Geomag. Geoelect.*, **32**, SI 13-32.
- Dawson, T.W. and Weaver, J.T., 1979, H-polarization induction in two thin half-sheets: *Geophys. J. R. astr. Soc.* **56**, 419-438.
- Dmitriev, V.I. and Berdichevsky, M.N., 1979, The fundamental model of magnetotelluric sounding: *Proc. Inst. Elect. and Electron. Eng. Trans.*, **67**, 1034-1044.
- Eggers, D.E., 1982, An eigenstate formulation of the magnetotelluric impedance tensor: *Geophysics*, **47**, 1204-1214.
- d'Erceville, I and Kunetz, G., 1962, Some observations regarding naturally occurring electromagnetic fields in applied geophysics: *Geophysics*, **27**, 651
- Flores, C. and Edwards, R.N., 1985, Approximate calculation of low-frequency magnetotelluric responses using a multiple plate model: *presented at Fifty-fifth Annual Meeting, Society of Exploration Geophysicists, Washington, October 6 - 10.*
- Flores, C.F., 1986, Electromagnetic induction studies over the Meager Creek Geothermal Area, British Columbia: PhD thesis, Univ. of Toronto.
- Gamble, T.D. *et al*, 1979, Magnetotellurics with a remote magnetic reference, *Geophysics*, **44**, 53-68.
- Groom, R.W. and , Bailey, R.C., 1987, A Decomposition of the magnetotelluric impedance tensor that is useful in the presence of distortions. *presented at Fifty-seventh Annual Meeting, Society of Exploration Geophysicists, New Orleans.*
- Hermance, J.F., 1982, The asymptotic response of three-dimensional basin offsets to magnetotelluric fields at long periods: the effects of current chan-

- nelling: *Geophysics* **47**, 1562-1573.
- Grant, F.S. and West, G.F., 1965, *Interpretation theory in Applied Geophysics*, McGraw-Hill, New York.
- Jones, A.G., 1983, The problem of current channelling: A critical review: *Geophys. Surveys*, **6**, 79-122.
- Jones, A.G., 1986, On Static-Shift of Magnetotelluric Data and Its Solution in a Sedimentary Basis Environment: *presented at Eighth Workshop on Electromagnetic Induction in the Earth and Moon*, Neuchatel, 1986,
- Jones, F.W. and Price, A.T., 1970. The perturbations of alternating geomagnetic fields by conductivity anomalies: *Geophys. J.R. astr. Soc.* **20** pp. 317-334.
- Kao, D.W. and Rankin, D., 1977, Enhancement of signal-to-noise ratio in magnetotelluric data: *Geophysics* **42**, 103-110
- Larsen, J.C., 1975, Low frequency (0.1-6.0 cpd) Electromagnetic Study of Deep Mantle Electrical Conductivity Beneath the Hawaiian Islands: *Geophys. J. R. astr. Soc.*, **43**, 17-46
- Larsen, J.C., 1977, Removal of local surface conductivity effects from low frequency mantle response curves: *Acta Geodaet. Geophys. Mont*, **12**, 183-186.
- LaTorraca, G.A., Madden, T.R., and Korringa, J., 1985, An analysis of the magnetotelluric impedance for three-dimensional conductivity structures: *presented at Fifty-fifth Annual Meeting, Society of Exploration Geophysicists*, Washington, October 6 - 10.
- LaTorraca, G.A., Madden, T.R., and Korringa, J., 1986, An analysis of the magnetotelluric impedance for three-dimensional conductivity structures, *Geophysics* **51**, 1819-1829.
- Lee, H., 1975, On the computational aspects of magnetometric resistivity and its application to the mapping of a sink: PhD thesis, University of Toronto.
- LeMouel, J.L. and Menvielle, M., 1982, Geomagnetic variation anomalies and

- deflection of telluric currents, *Geophys. J. R. astr. Soc.* **68**, 575-587.
- Madden, T. and Nelson, P., 1964, A defense of Cagniard's magnetotelluric method: *Geophys. Lab. ONR Proj.* NR-371-401, MIT, Cambridge, Mass..
- Madden, T.R. and Thompson, W., 1965. Low frequency electromagnetic oscillations of the earth-ionosphere cavity: *Reviews of Geophysics* **3**, pp. 211-254.
- McNeill, J.D., Edwards, R.N. and Levy, G.M., Approximate calculations of the transient electromagnetic response from buried conductors in a conductive half-space: *Geophysics* **49**, 918-924.
- Migaux, L., 1946, A new method of applied geophysics: prospecting by telluric currents: *Annales Geophysique*, **2**, 131-146.
- Morse, P.M. and Feshbach, H., 1953, *Methods of Theoretical Physics*, McGraw-Hill Book Company, Toronto.
- Neves, A.S. 1957. The magnetotelluric method in two-dimensional structures. Ph.D. thesis, MIT.
- Oldenburg, D.W., Whittall, K.P., and Parker, R.L., 1984, Inversion of ocean bottom magnetotelluric data revisited: *J. Geophys. Res.*, **89**, 1829-1833.
- Papoulis, A., 1968. *Random Variables and Stochastic Processes*, McGraw Hill Inc., Toronto.
- Park, S.K., Orange, A.S., and Madden, T.R., 1983, Effects of three-dimensional structure on magnetotelluric sounding curves: *Geophysics*, **48**, 1402-1405.
- Park, S.K., 1985, Distortion of magnetotelluric sounding curves by three-dimensional structures: *Geophysics*, **50**, 785-797.
- Parker, R. L., 1968, Electromagnetic induction in a thin strip: *Geophys. J.* **14**, 487-495.
- Parker, R. L., 1980, The inverse problem of electromagnetic induction: Existence and construction of solution based on incomplete data: *J. Geophys. Res.*, **85**, 4421-4428.

- Price, 1962. The theory of magnetotelluric fields when the source field is considered: *J. Geophys. Res.* **67**, pp. 1907-1918.
- Ranganayaki, R.P., 1984, An interpretive analysis of magnetotelluric data: *Geophysics*, **49**, 1730-1748.
- Rankin, D., 1962, The Magneto telluric effect on a dike: *Geophysics* **27**, 666-676.
- Schmucker, U., 1970. Anomalies of geomagnetic variation in the South-Western United States: *Bull. Scripps Init. Ocean.*, Univ. of Calif., San Diego **13** pp. 165.
- Schmucker, U., 1986, A regional quasi-anisotropy in West Germany, *presented at Eighth Workshop on Electromagnetic Induction in the Earth and Moon*, Neuchatel, 1986.
- Sims, W.E. *et al*, 1971, Estimation of magnetotelluric impedance tensor elements from measured data: *Geophysics* **36**, 938-942.
- Sims, W.E. and Bostick, F.X. Jr., 1969, Methods of magnetotelluric analysis: Res. Lab. tech. rep. no. 58, Univ. of Texas, Austin.
- Spitz, S., 1985, The magnetotelluric impedance tensor properties with respect to rotations, *Geophysics* **50**, 1610-1617.
- Swift, C.M., Jr., 1967, A magnetotelluric investigation of an electrical conductivity anomaly in the southwestern United States: PhD Thesis, Mass. Inst. of Tech.
- Tikonov, A.V. 1950. Determination of the electrical characteristics of the deep strata of the Earth's crust: *Dokl. Akad. Nauk.*, U.S.S.R. **75** pp. 295-297.
- Van Kampen, N.G., 1975. *Stochastic Differential Equations, Lect. 1-3*, in *Fundamental Problems in Statistical Mechanics III*, editor E.G.D. Cohen, North-Holland Publishing Company, Amsterdam.
- Wait, J.R. 1954. On the relationship between telluric currents and the Earth's magnetic field: *Geophysics* **19** pp. 281-289.
- Wait, J.R. and Spies, K.P., 1974. Magneto-Telluric Fields for a Segmented Overburden: *J. Geomag. Geoelectr.* **26** pp. 449-458.

- Wannamaker, P.E., Hohmann, G.W., and San Filippo, W.A., 1984a, Electro-magnetic modeling of three-dimensional bodies in layered earths using integral equations: *Geophysics*, **49**, 60-74.
- Wannamaker, P.E., Hohmann, G.W., and Ward, S.H., 1984b, Magnetotelluric responses of three-dimensional bodies in layered earths: *Geophysics*, **49**, 1517-1533.
- Ward, S.H., 1967, *Mining Geophysics 2*, edited by the SEG Mining Geophysics Vol. Edit Committee.
- Weaver, J.T., 1963, The electromagnetic field within a discontinuous conductor with reference to geomagnetic micropulsations near a coast-line. *Canad. J. Phys.* **41**, 484-495
- Weidelt, P., 1971, The electromagnetic induction in two thin half-sheets: *Zeitschrift für Geophysik* **37**, 649-665.
- Weidelt, P., 1972, The inverse problem of geomagnetic induction: half-sheets: *Zeitschrift für Geophysik* **38**, 257-289.
- Yee, E. and Paulson, K.V., 1984, A structural representation for the magnetotelluric impedance tensor: *presented at Annual Meeting, Canadian Geophysical Union, Halifax, May 29 - June 1.*
- Yee, E., 1985, The magnetotelluric impedance tensor - its reconstruction and analysis, Ph.D. thesis, University of Saskatchewan, Saskatoon.
- Yee, E. and Paulson, K.V., 1986, A canonical decomposition for the magnetotelluric tensor. *submitted to Geophysics*, August, 1986.
- Zhang, P., Roberts, R.G., and Pedersen, L.B., 1987, Magnetotelluric strike rules: *Geophysics*, **51**, 267-278.

## APPENDIX 1

### A PROPAGATOR MATRIX METHOD FOR ONE-DIMENSIONAL FORWARD MODELLING

#### A1.1 The Propagator Matrix

We assume the conductivity is given by

$$\sigma = \begin{cases} 0, & z < 0 \\ f(z), & z > 0 \end{cases} \quad (\text{A1.1})$$

and the source field is uniform and propagating vertically. The magnetic permeability,  $\mu_0$ , is assumed to be that of free space.

In a layer of thickness  $a$  and uniform conductivity  $\sigma_a$ , the electromagnetic fields can be expressed as

$$\vec{E} = E\hat{x} = Ae^{-\alpha_a z} + Be^{\alpha_a z}\hat{x} \quad (\text{A1.2a})$$

$$\vec{H} = H\hat{y} = \frac{-1}{i\mu_0\omega} \frac{\partial E}{\partial z}\hat{y} \quad (\text{A1.2b})$$

where  $\alpha_a = \sqrt{i\mu_0\omega\sigma_a}$ . A linear relationship exists between the electromagnetic fields at the bottom of the layer  $\begin{pmatrix} E_0 \\ H_0 \end{pmatrix}$  and fields at the top of the layer  $\begin{pmatrix} E_1 \\ H_1 \end{pmatrix}$ .

$$\begin{pmatrix} E_1 \\ H_1 \end{pmatrix} = \mathbf{T}_a(\alpha_a, a) \begin{pmatrix} E_0 \\ H_0 \end{pmatrix} \quad (\text{A1.3})$$

This relationship (A1.3) can be derived by utilizing (A1.2) with the boundary conditions that tangential electric and magnetic fields are continuous across conductivity contrasts. The propagator matrix  $\mathbf{T}$  is given by

$$\mathbf{T}_a(\alpha_a, a) = \begin{pmatrix} \cosh \alpha_a a & \frac{i\omega\mu_0}{\alpha_a} \sinh \alpha_a a \\ \frac{\alpha_a}{i\mu_0\omega} \sinh \alpha_a a & \cosh \alpha_a a \end{pmatrix}. \quad (\text{A1.4})$$

This formulation enables one to stably and quickly step through multiple layers even if the individual layers are very thin. For example, consider two layers of conductivities  $\sigma_a, \sigma_b$  and thicknesses  $a, b$ . The fields at the top of the two layers (doublet) are given by

$$\begin{pmatrix} E_2 \\ H_2 \end{pmatrix} = \mathbf{T}_a(\alpha_b b) \mathbf{T}_b(\alpha_a, a) \begin{pmatrix} E_0 \\ H_0 \end{pmatrix} = \mathbf{T}(\alpha_b, \alpha_a; b, a) \begin{pmatrix} E_0 \\ H_0 \end{pmatrix} \quad (\text{A1.5})$$

(A1.5) is used in Chapter 2 for a model of fine bedding which consists of a stack of doublets, one upon the other.

### A1.2 Eigenvector , Eigenvalue Expansion

The eigenvalues of the doublet propagator matrix  $\mathbf{T}(\alpha_b, \alpha_a; b, a)$  (A1.5) can be shown to be

$$\lambda_{1,2} = \beta \pm \sqrt{\beta^2 - 1} \quad (\text{A1.6})$$

where

$$\beta = \cosh \alpha_a a \cosh \alpha_b b + \frac{\sigma_a + \sigma_b}{2\sqrt{\sigma_a \sigma_b}} \sinh \alpha_a \alpha_b. \quad (\text{A1.7})$$

The eigenvectors of  $\mathbf{T}$  are therefore given by

$$\psi_1 = \begin{pmatrix} \frac{T_{12}}{\lambda_1 - T_{11}} \\ 1 \end{pmatrix}, \quad \psi_2 = \begin{pmatrix} 1 \\ \frac{T_{21}}{\lambda_2 - T_{22}} \end{pmatrix}. \quad (\text{A1.8})$$

where  $T_{ij}$  is the  $ij$  element of  $\mathbf{T}$ .

The linear transformation

$$\mathcal{T} : \mathcal{V} \rightarrow \mathcal{M} \quad (\text{A1.9})$$

which is represented by the matrix  $\mathbf{T}$  can be shown to have a zero dimensional kernel. That is

$$\text{Ker}(\mathcal{T}) = \{x : \mathcal{T}x = 0\} = \begin{pmatrix} 0 \\ 0 \end{pmatrix}. \quad (\text{A1.10})$$

It is easy to show that the determinant of  $\mathbf{T}$  is

$$\|\mathbf{T}\| = 1. \quad (\text{A1.11})$$

and thus the rank of  $\mathbf{T}$  is 2 and the dimension of the kernel must be zero. Thus the domain space is the range space or

$$\mathcal{M} = \mathcal{V}$$

and thus the eigenvectors  $\{\psi_1, \psi_2\}$  are a basis for  $\mathcal{V}$  over the complex numbers.

Expanding the fields at the bottom of the doublet in the eigenvector basis

$$\begin{pmatrix} E_0 \\ H_0 \end{pmatrix} = \eta_1 \psi_1 + \eta_2 \psi_2 \quad (\text{A1.12})$$

allows one to determine the fields at the top simply as

$$\mathbf{T} \begin{pmatrix} E_0 \\ H_0 \end{pmatrix} = \eta_1 \mathbf{T}\psi_1 + \eta_2 \mathbf{T}\psi_2 = \eta_1 \lambda_1 \psi_1 + \eta_2 \lambda_2 \psi_2 = \begin{pmatrix} E_2 \\ H_2 \end{pmatrix}. \quad (\text{A1.13})$$

This method allows one to determine the solution for many doublets, for arbitrarily fine structure, quickly and accurately. Since, for  $n$  such doublets, the fields at the top of the stack of doublets are given by

$$\begin{pmatrix} E \\ H \end{pmatrix} = \mathbf{T}^n \begin{pmatrix} E_0 \\ H_0 \end{pmatrix} = \eta_1 \lambda_1^n \psi_1 + \eta_2 \lambda_2^n \psi_2 \quad (\text{A1.14})$$

This method can be readily adapted to other characterizations of fine layering other than the repeating doublet model discussed above.



## APPENDIX 2

### THE MAGNETIC FIELD OF A CONDUCTING HEMISPHERE

In section 5.2.1, the problem of determining the effects of a uniformly conducting hemisphere (Figure 5. ) which is embedded in a homogeneous half-space and excited by a uniform static electric field was introduced. As discussed in that section, the total electric field in the conducting half-space ( $z \leq 0$ ) for a primary field,  $E_0 \hat{x}$ , is

$$\vec{E}_i(x, y, z) = E_0 \left( \frac{3\sigma_1}{\sigma_2 + 2\sigma_1}, 0, 0 \right) \quad (A2.1)$$

within the hemisphere ( $r \leq R$ ). Outside the hemisphere ( $r \geq R$ )

$$\vec{E}_e(x, y, z) = \left( E_0 + P \frac{(2x^2 - y^2)}{r^5}, \frac{P3xy}{r^5}, \frac{P3xz}{r^5} \right). \quad (A2.2)$$

Here,  $r^2 = x^2 + y^2 + z^2$ ,  $P = \left( \frac{\sigma_2 - \sigma_1}{\sigma_2 + 2\sigma_1} \right) E_0 R^3$  is the induced dipole moment of the hemisphere and  $R$  is the radius of the hemisphere.

The effect of the hemisphere on the horizontal magnetic field is to be investigated. The source of this anomalous electrostatic magnetic field is the anomalous current density,  $\vec{J}_a$ , within the conducting half-space. The anomalous magnetic field at a field point is therefore given by the Biot-Savart Law as

$$\vec{H}_a(x_0, y_0, z_0) = \frac{1}{4\pi} \int \frac{\vec{J}_a(x, y, z) \times \hat{r}}{r^2} dV \quad (A2.3)$$

where  $\vec{r} = r\hat{r}$  is the vector from  $\vec{J}_a dV$  to the field point  $(x_0, y_0, z_0)$  and the integral is over the half-space  $z < 0$ .

The anomalous current density within the hemisphere, given by

$$\vec{J}_a = \sigma_2 \vec{E} - \sigma_1 \vec{E}_0,$$

is constant as

$$\vec{J}_a = \frac{2\sigma_1(\sigma_2 - \sigma_1)}{\sigma_2 + 2\sigma_1} E_0 \hat{x}.$$

The contribution,  $\vec{H}_H$ , due to the anomalous currents in the hemisphere is given by

$$\vec{H}_H(x_0, y_0, z_0) = \frac{2\sigma_1(\sigma_2 - \sigma_1) E_0}{\sigma_2 + 2\sigma_1} \frac{1}{4\pi} \int_{V_H} \frac{\hat{x} \times \hat{r}}{r^2} dV \quad (A2.4)$$

where  $V_H$  is the volume of the hemisphere. There is no x-component to this vector field and therefore the horizontal anomalous magnetic component,  $H_H^y$ , of this vector field is

$$\vec{H}_H^y(x_0, y_0, z_0) = \frac{2\sigma_1(\sigma_2 - \sigma_1) E_0}{\sigma_2 + 2\sigma_1} \frac{1}{4\pi} \int_{V_H} \frac{z - z_0}{[(x - x_0)^2 + (y - y_0)^2 + (z - z_0)^2]^{\frac{3}{2}}} dV \hat{y} \quad (A2.5).$$

To determine the magnetic field due to the anomalous current outside the hemisphere we utilize a vector identity (Lee, 1975).

$$\begin{aligned} \frac{\vec{J}_a(x, y, z) \times \hat{r}}{r^2} &= \nabla_0 \left( \frac{1}{r} \right) \times \vec{J}_a(x, y, z) = \nabla_0 \times \left( \frac{\vec{J}_a}{r} \right) \\ &= \frac{\nabla \times \vec{J}_a(x, y, z)}{r} - \nabla \times \left( \frac{\vec{J}_a(x, y, z)}{r} \right) \end{aligned}$$

where again  $\hat{r} = \frac{\vec{r}}{r}$  is the unit vector pointing from the source point  $(x, y, z)$  to the field point  $(x_0, y_0, z_0)$ ,  $\nabla_0$  is an operator with respect to the field points and  $\nabla$  is an operator with respect to source points. However, outside the hemisphere since the fields are static

$$\nabla \times \vec{J}_a(x, y, z) = \sigma_1 \nabla \times \vec{E}_a(x, y, z) = 0.$$

Therefore the magnetic field due to the anomalous currents outside the hemisphere,  $\vec{H}_e$  is given by

$$\begin{aligned} \vec{H}_e(x_0, y_0, z_0) &= \frac{-1}{4\pi} \int_V \nabla \times \left( \frac{\vec{J}_a(x, y, z)}{r} \right) dV \\ &= \frac{1}{4\pi} \int_{S_1 \cup S_2} \frac{\vec{J}_a(x, y, z)}{r} \times \vec{d}\vec{a} \quad (A2.6) \end{aligned}$$

utilizing a volume-to-surface integral transformation. The vector  $\vec{da}$  has magnitude  $da$  and is in the direction of the outward normal to the surface. The surface integral is over two surfaces

$$S_1 = \{(x, y, z) | z = 0, \sqrt{x^2 + y^2} > R\} \quad (A2.7a)$$

$$S_2 = \{(x, y, z) | z \leq 0, \sqrt{x^2 + y^2 + z^2} = R\}. \quad (A2.7b)$$

On  $S_2$ ,  $\vec{da}$  is normal to the hemisphere and points towards the origin. Thus

$$\begin{aligned} \vec{J}_a \times \vec{da} &= \frac{\sigma_1 P}{R^5} (2x^2 - y^2, 3xy, 3xz) \times \frac{-da}{R} (x, y, z) \\ &= \frac{-\sigma_1 P da}{R^6} [0, z(x^2 + y^2), -y(x^2 + y^2)]. \end{aligned}$$

Again there is no contribution to the x-component of  $\vec{H}_a$ . Consider a spherical coordinate system, where on the hemisphere

$$\begin{aligned} z &= R \cos \theta, & \frac{\pi}{2} &\leq \theta \leq \pi \\ x &= R \cos \phi \sin \theta & 0 &\leq \phi \leq 2\pi \\ y &= R \sin \phi \sin \theta, \\ da &= R^2 \sin \theta d\theta d\phi. \end{aligned}$$

Thus the horizontal component of  $\vec{H}_e$  due to the surface integral over  $S_2$ ,  $\vec{H}_e^2$ , is given by

$$\vec{H}_e^2(x_0, y_0, z_0) = \frac{-\sigma_1 P}{4\pi R} \int_0^{2\pi} \int_{\frac{\pi}{2}}^{\pi} \frac{\cos \theta \sin^3 \theta}{r(\theta, \phi)} d\theta d\phi \hat{y}, \quad (A2.8)$$

where  $r^2(\theta, \phi) = R^2 + r_0^2 - 2r_0 R (\cos \theta \cos \theta_0 + \cos(\phi - \phi_0) \sin \theta \sin \theta_0)$ .

For the surface  $S_1$ :

$$\begin{aligned} \vec{J}_a \times \vec{da} &= \sigma_1 \vec{E}_a \times da(0, 0, 1) \\ &= \sigma_1 da (E_y^a, -E_x^a, 0) \end{aligned}$$

Thus the contribution to the magnetic field from  $S_1$ ,  $\vec{H}_e^1$  is

$$\begin{aligned}
 \vec{H}_e^1(x_0, y_0, z_0) &= \frac{\sigma_1}{4\pi} \int_{S_1} \frac{E_y^a(x, y, 0)\hat{\mathbf{x}} - E_x^a(x, y, 0)\hat{\mathbf{y}}}{r} da \\
 &= \frac{\sigma_1 P}{4\pi} \left[ \int_R^\infty \frac{1}{\rho^2} \left( \int_0^{2\pi} \frac{3\cos\phi\sin\phi}{r} d\phi \hat{\mathbf{x}} - \int_0^{2\pi} \frac{2\cos^2\phi - \sin^2\phi}{r} d\phi \hat{\mathbf{y}} \right) d\rho \right]
 \end{aligned} \tag{A2.9}$$

where  $r^2(\theta, \phi) = \rho^2 + r_0^2 - 2r_0\rho(\cos(\phi - \phi_0)\sin\theta_0)$  and  $\rho^2 = x^2 + y^2$ .

The total horizontal magnetic field,  $\vec{H}_h^a$ , is therefore from Equations A2.4 and A2.6

$$\vec{H}_h^a = \vec{H}_H^y + \vec{H}_e^2 + \vec{H}_e^1. \tag{A2.10}$$

The y-component,  $H_y^a$ , is (A2.5, A2.8, A2.9)

$$H_y^a \hat{\mathbf{y}} = \vec{H}_H^y + \vec{H}_e^2 - \frac{\sigma_1 P}{4\pi} \int_R^\infty \frac{1}{\rho^2} \int_0^{2\pi} \frac{3\cos^2\phi - 1}{r} d\phi d\rho \hat{\mathbf{y}} \tag{A2.11}$$

and the x-component,  $H_x^a$  (A2.9)

$$H_x^a \hat{\mathbf{x}} = \frac{\sigma_1 P}{4\pi} \int_R^\infty \frac{1}{\rho^2} \int_0^{2\pi} \frac{3\cos\phi\sin\phi}{r} d\phi d\rho \hat{\mathbf{x}}. \tag{A2.12}$$

We would like to determine these integral relations at the surface of the conducting media ( $z_0 = 0$ ). In general, it is difficult to evaluate the integrals analytically. However, at the origin it is possible to integrate analytically. It is also possible to evaluate the order of magnitude of the contributions.

Let

$$\beta = \frac{\sigma_1(\sigma_2 - \sigma_1)}{\sigma_2 + 2\sigma_1} E_0.$$

At the surface of the conducting media

$$\vec{H}_H^y(x_0, y_0, 0) = \frac{\beta}{2\pi} \int_{V_H} \frac{z}{r^3} dV \hat{\mathbf{y}} \tag{A2.13}$$

where in the spherical coordinate system  $r^2 = r_s^2 + r_0^2 - 2r_0r_s\cos(\phi - \phi_0)\sin\theta$ ,  $r_s^2 = x^2 + y^2 + z^2$  and  $r_0^2 = x_0^2 + y_0^2$ . Therefore, at the origin

$$\vec{H}_H^y(0,0,0) = \frac{\beta}{2\pi} \int_0^{2\pi} \int_{\frac{\pi}{2}}^{\pi} \int_0^R \sin\theta \cos\theta dr_s d\theta d\phi \vec{y} = -\frac{\beta R}{2} \vec{y} \quad (A2.14)$$

and thus for a measuring position inside the hemisphere

$$\vec{H}_H^y(x_0, y_0, 0) = -O\left(\frac{\beta R}{2}\right) \vec{y}. \quad (A2.15)$$

Outside the hemisphere,  $\frac{r_s}{r_0} < 1$  and

$$r \approx r_0 \left( 1 - \frac{r_s}{r_0} \cos(\phi - \phi_0) \sin\theta + O\left(\frac{r_s}{r_0}\right)^2 \right).$$

Therefore

$$\begin{aligned} H_H^y(x_0, y_0, 0) &= \frac{\beta}{2\pi} \left\{ \frac{1}{r_0^3} \int_{V_H} r_s^3 \cos\theta \sin\theta dr_s d\theta d\phi + O\left[\left(\frac{R}{r_0}\right)^5 \pi R\right] \right\} \\ &= -\frac{\beta R}{8} \left(\frac{R}{r_0}\right)^3 + O\left[\left(\frac{R}{r_0}\right)^5 \beta R\right] \end{aligned} \quad (A2.16)$$

since

$$\int_0^{2\pi} \cos(\phi - \phi_0) d\phi = 0$$

and

$$\int_0^{2\pi} \cos^2(\phi - \phi_0) d\phi = \pi.$$

Again, at the surface of the conducting media

$$\vec{H}_e^2(x_0, y_0, 0) = -\frac{\beta R^2}{2\pi} \int_0^{2\pi} \int_{\frac{\pi}{2}}^{\pi} \frac{\cos\theta \sin^3\theta}{r} d\theta d\phi \vec{y}$$

where now  $r^2 = R^2 + r_0^2 - 2r_0 R \cos(\phi - \phi_0) \sin\theta$ . Outside the hemisphere,  $\left(\frac{R}{r_0}\right) < 1$ . Thus

$$\begin{aligned} |\vec{H}_e^2|(x_0, y_0, 0) &= -\frac{\beta R^2}{4\pi} \int_0^{2\pi} \int_{\frac{\pi}{2}}^{\pi} \frac{\cos\theta \sin^3\theta}{r_0} \left( 1 + \frac{R}{r_0} \cos(\phi - \phi_0) \sin\theta \right) d\theta d\phi + O\left[\left(\frac{R}{r_0}\right)^3 R\beta\right] \\ &= -\frac{\beta R^2}{4\pi} \left(\frac{2\pi}{r_0}\right) \int_{\frac{\pi}{2}}^{\pi} \cos\theta \sin^3\theta d\theta + O\left[\left(\frac{R}{r_0}\right)^3 R\beta\right] \\ &= \frac{\beta R}{8} \left(\frac{R}{r_0}\right) + O\left[\left(\frac{R}{r_0}\right)^3 R\beta\right]. \end{aligned} \quad (A2.17)$$

Inside the hemisphere,  $\left(\frac{R}{r_0}\right) > 1$ . Thus

$$\begin{aligned} |\vec{H}_e^2|(x_0, y_0, 0) &= -\frac{\beta R^2}{4\pi} \int_0^{2\pi} \int_{\frac{\pi}{2}}^{\pi} \frac{\cos\theta \sin^3\theta}{R} \left(1 + \frac{r_0}{R} \cos(\phi - \phi_0) \sin\theta\right) d\theta d\phi + O\left[\left(\frac{r_0}{R}\right)^2 \beta R\right] \\ &= -\frac{\beta R^2}{4\pi} \left(\frac{2\pi}{R}\right) \int_{\frac{\pi}{2}}^{\pi} \cos\theta \sin^3\theta d\theta + O\left[\left(\frac{r_0}{R}\right)^2 \beta R\right] \end{aligned}$$

and

$$\vec{H}_e^2(x_0, y_0, 0) = \frac{\beta R}{8} + O\left[\left(\frac{r_0}{R}\right)^2 \beta R\right] \vec{y}. \quad (\text{A2.18})$$

At the origin, therefore,

$$\vec{H}_e^2(0, 0, 0) = \frac{\beta R}{8} \vec{y}. \quad (\text{A2.19})$$

The y-component of  $\vec{H}_e^1$ ,  $\vec{H}_y^1$  is given by

$$\vec{H}_y^1(x_0, y_0, 0) = -\frac{\beta R^3}{4\pi} \int_R^\infty \frac{1}{\rho^2} \int_0^{2\pi} \frac{2\cos^2\phi - \sin^2\phi}{r} d\phi d\rho \vec{y} \quad (\text{A2.20})$$

where  $r^2 = \rho^2 + r_0^2 - 2\rho r_0 \cos(\phi - \phi_0)$  and  $\rho^2 = x^2 + y^2$ . At a measuring position inside the hemisphere  $\left(\frac{r_0}{\rho} < 1\right)$

$$\begin{aligned} \vec{H}_y^1(x_0, y_0, 0) &= -\frac{\beta R^3}{4\pi} \int_R^\infty \frac{1}{\rho^3} \int_0^{2\pi} 2\cos^2\phi - \sin^2\phi d\phi d\rho \vec{y} + O\left[\beta R \left(\frac{r_0}{R}\right)^2\right] \vec{y} \\ &= \left\{ -\frac{\beta R}{8} + O\left[\beta R \left(\frac{r_0}{R}\right)^2\right] \right\} \vec{y} \end{aligned} \quad (\text{A2.21})$$

since

$$\int_0^{2\pi} \cos(\phi - \phi_0) \cos^2\phi = 0$$

and

$$\int_0^{2\pi} \cos(\phi - \phi_0) \sin^2\phi = 0.$$

Therefore at the origin

$$\vec{H}_y^1(0, 0, 0) = -\frac{\beta R}{8} \vec{y}. \quad (\text{A2.22})$$

The x-component of  $\vec{H}_e^1$ ,  $\vec{H}_x^1$ , is the only contribution to the x-component of the magnetic field and is given, for a position on the surface, by

$$\vec{H}_x^1(x_0, y_0, 0) = \frac{\beta R^3}{4\pi} \int_R^\infty \frac{1}{\rho^2} \int_0^{2\pi} \frac{3\cos\phi \sin\phi}{r} d\phi d\rho \hat{x}.$$

For a measuring position within the hemisphere,

$$\frac{1}{r} = \frac{1}{\rho} \left( 1 + \left( \frac{r_0}{\rho} \right) \cos(\phi - \phi_0) - \frac{1}{2} \left( \frac{r_0}{\rho} \right)^2 [1 + \cos^2(\phi - \phi_0)] + O \left( \frac{r_0}{\rho} \right)^3 \right).$$

Since

$$\int_0^{2\pi} \cos\phi \sin\phi d\phi = 0$$

and

$$\int_0^{2\pi} \cos(\phi - \phi_0) \cos\phi \sin\phi d\phi = 0$$

$$\vec{H}_x^1(x_0, y_0, 0) = \frac{-3\beta R}{128} \left( \frac{r_0}{R} \right)^2 \sin(2\theta_0) \vec{x} + O \left[ \beta R \left( \frac{r_0}{R} \right)^3 \right] \vec{x}. \quad (\text{A2.23})$$

Therefore at the origin

$$\vec{H}_x^1(0, 0, 0) = 0. \quad (\text{A2.24})$$

Combining equations A2.14, A2.19, A2.22 and A2.24 we obtain the total magnetic field at the origin as

$$\vec{H}_a(0, 0, 0) = \frac{-\beta R}{2} \vec{y}. \quad (\text{A2.25})$$

Inside the hemisphere

$$\vec{H}_e^2(x_0, y_0, 0) + \vec{H}_y^1(x_0, y_0, 0) = O \left[ \beta R \left( \frac{r_0}{R} \right)^2 \right] \vec{y}$$

and thus on the surface inside the hemisphere ( $\frac{r_0}{R} < 1$ )

$$\begin{aligned} \vec{H}_a(x_0, y_0, 0) &\approx \frac{-\beta R}{2} \vec{y} - \frac{3\beta R}{128} \left( \frac{r_0}{R} \right)^2 \sin 2\theta_0 \vec{x} \\ &\approx -\frac{\sigma_1(\sigma_2 - \sigma_1) E_0 R}{\sigma_2 + 2\sigma_1} \frac{E_0 R}{2} \vec{y} \end{aligned} \quad (\text{A2.26a})$$

$$= O(\sigma_1 E_0 R) \vec{y} \quad [\sigma_1 \not\approx \sigma_2] \quad (\text{A2.26b})$$

If the conductivity of host and inhomogeneity are sufficiently similar the effect of the anomalous magnetic field is certainly insignificant.

There are two important conclusions to be obtained here for the main body of the thesis. One is that if the conductivity of the hemisphere is sufficiently

different from that of the host space then the anomalous horizontal magnetic field due to the hemisphere is of the order of  $(\sigma_1 E_0 R)$  in the region of the hemisphere. The anomalous magnetic field will fall off away from the hemisphere and will be of less significance. The second conclusion is that the direction of the anomalous magnetic field is primarily in a direction perpendicular to the exciting electric field.

## APPENDIX 3

### OTHER DECOMPOSITIONS

#### A3.1 Bahr's Channelling Decomposition (1985)

As mentioned earlier Bahr utilized the model for the effects of electric distortion;

$$\mathbf{Z}_m = \mathbf{R} \mathbf{C} \mathbf{Z}_2 \mathbf{R}^t = \mathbf{R} \begin{pmatrix} c_{11} & c_{12} \\ c_{21} & c_{22} \end{pmatrix} \begin{pmatrix} 0 & Z_{\perp} \\ -Z_{\parallel} & 0 \end{pmatrix} \mathbf{R}^t \quad (\text{A3.1a})$$

$$= \mathbf{R} \begin{pmatrix} -c_{12}Z_{\parallel} & c_{11}Z_{\perp} \\ -c_{22}Z_{\parallel} & c_{21}Z_{\perp} \end{pmatrix} \mathbf{R}^t \quad (\text{A3.1b})$$

where  $\mathbf{R}$  is a rotation through  $\theta$  degrees to the measurement axes system from the regional axes system. Bahr derives an analytic solution for the rotation azimuth in this case

$$\tan\theta'_{1,2} = \pm \sqrt{\frac{B+C}{B-C} + \left(\frac{A}{B-C}\right)^2} - \frac{A}{B-C} \quad (\text{A3.2})$$

where

$$A = [\alpha_0, \alpha_3] - [\alpha_1, \alpha_2] \quad (\text{A3.3a})$$

$$B = [\alpha_0, \alpha_1] + [\alpha_3, \alpha_2] \quad (\text{A3.3b})$$

$$C = [\alpha_0, \alpha_1] + [\alpha_3, \alpha_2]. \quad (\text{A3.3c})$$

$\alpha_1$  are defined by equations (6.38).

The product  $[z_1, z_2]$  is similar to an inner product and is defined as

$$[z_1, z_2] = \Re(z_1)\Im(z_2) - \Im(z_1)\Re(z_2) \quad (\text{A3.4})$$

but is not an inner product since

$$[z_1, z_2] = -[z_2, z_1] \neq [z_2, z_1].$$

Bahr states and this can be shown with the aid of equations (6.39) that under the assumption of equation (A3.1),

$$C = 0$$

and therefore (A3.2) reduces to

$$\tan\theta'_{1,2} = \pm \sqrt{1 + \left(\frac{A}{B}\right)^2} - \frac{A}{B}. \quad (\text{A3.5})$$

Utilizing equations (6.39) it can be shown that

$$B = -(1 - e^2)(1 + t^2)\sin 2\theta[\sigma, \delta] \quad (\text{A3.6a})$$

$$A = -(1 - e^2)(1 + t^2)\cos 2\theta[\sigma, \delta] \quad (\text{A3.6b})$$

using the parameters of the decomposition presented in this thesis. In terms of equation (A3.1),

$$\sigma = Z_{\perp} + Z_{\parallel} \quad (\text{A3.7a})$$

$$\delta = Z_{\perp} - Z_{\parallel}. \quad (\text{A3.7b})$$

Therefore, if  $B \neq 0$ ,

$$\frac{A}{B} = \frac{1}{\tan 2\theta} \quad (\text{A3.8})$$

and

$$\theta' = \theta \quad \text{or} \quad \theta' = \theta + \frac{\pi}{2};$$

verifying Bahr's results.

Bahr's results for the regional strike are analytically correct if the impedance tensor is solely the result of electric distortion of two-dimensionally induced electric currents. The method is unstable, however. Practically, the physics of (A3.1) will at best be only approximately correct and therefore

$$B = -(1 - e^2)(1 + t^2)\sin 2\theta[\sigma, \delta] + \epsilon_B \quad (\text{A3.9})$$

where  $\epsilon_B$  is the error in  $B$ . In three cases, the estimation of  $B$  is unstable

$$1) \quad e \approx 1 \quad (A3.10a)$$

$$2) \quad \phi_{\parallel} \approx \phi_{\perp} \quad (A3.10b)$$

$$3) \quad \sin 2\theta \approx 0 \quad (A3.10c).$$

Case 1 was encountered in the analytic example of Chapter 5. For, if Site C is very close to the edge of the hemisphere but outside,  $e \approx 1$ . In the second case when the phases of the two regional impedances are approximately equal. This will obviously be true in the one-dimensional case but it is possible to have a two-dimensional structure which has equal phases at some frequencies. Recall, the two-dimensional model of Chapter 5 at long periods. The third case is obvious. If the measurement axes happen to be aligned parallel to regional axes then the calculation of  $B$  would be unstable. For those knowledgeable with this procedure, this may not appear to be a significant problem. We will return to this problem, however.

The object of this method proposed by Bahr is to rotate the impedance tensor to the form

$$\mathbf{Z} = \begin{pmatrix} -c_{12}Z_{\parallel} & c_{11}Z_{\perp} \\ -c_{22}Z_{\parallel} & c_{21}Z_{\perp} \end{pmatrix}. \quad (A3.11)$$

In other words, the impedance tensor is rotated until the elements in each row have the same complex phase. Thus, the impedance phases can be extracted with the scaled apparent resistivities. The method would be correct except in the above mentioned three cases if it were not for the presence of noise. It is clear from the arguments of chapters 5 and 6, that

$$c_{12}, c_{21} < c_{11}, c_{22} \quad (A3.12).$$

If the off-diagonal components of the distortion tensor are very much less than the diagonal components, it may be impossible to judge, in the presence of noise, whether the components of a row have the same phase. In the one-dimensional case, no rotation is necessary and the impedance tensor elements

should all have the same phase. This again may not be clear, in the presence of noise. The obvious conclusion is that the method, although analytically a correct method for recovering the two-dimensional impedance phases, requires close examination by the investigator. Each impedance tensor must be examined closely and possibly each estimate of the mean impedance tensor must be examined thus making the method unsuitable in many instances. There is no way to recover frequency independent parameters and thus constrain parameterization frequency by frequency. The method does however justify the physical approach made in this this thesis.

### A3.2 The Eigenstate Formulation of Eggers (1982)

Eggers defines impedance tensor eigenstates by

$$\vec{E}^i = \Lambda^i \vec{H}^i, \quad i = 1, 2 \quad (\text{A3.13})$$

such that

$$\vec{E}^i \cdot \vec{H}^i = 0, \quad i = 1, 2. \quad (\text{A3.14})$$

As Eggers states

$$\Lambda^i = \begin{pmatrix} 0 & \lambda^i \\ -\lambda^i & 0 \end{pmatrix}, \quad (\text{A3.15})$$

for (A3.13,A3.14) to be true for all non-zero  $\vec{H}^i$ . We wish, of course, for the eigenstates to be related by the impedance tensor in question; therefore

$$\vec{E}^i = \mathbf{Z} \vec{H}^i = \Lambda^i \vec{H}^i, \quad i = 1, 2 \quad (\text{A3.16})$$

which yields an eigenvalue problem

$$(\mathbf{Z} - \Lambda^i) \vec{H}^i = 0 \quad i = 1, 2. \quad (\text{A3.17})$$

The eigenvalues of (A3.17) are four of the parameters of Eggers decomposition

$$\lambda^\pm = \frac{-\alpha_2}{2} \pm \frac{1}{2} \sqrt{\alpha_2^2 - 4 \det | \mathbf{Z} |} \quad (\text{A3.18})$$

in the Pauli spin coefficients used in this the thesis (6.38). It is interesting to determine these eigenvalues of  $\mathbf{Z}$  in terms of the channelling decomposition. Using equations (6.38) and (6.39)

$$\lambda^{\pm} = \frac{-\alpha_2}{2} \pm \frac{1}{2} \sqrt{\alpha_2^2 - (\sigma^2 - \delta^2)(1 - e^2)(1 + t^2)} \quad (\text{A3.19})$$

where  $\sigma$  and  $\delta$  are given by (A3.7) and

$$\alpha_2 = -\sigma + et\delta. \quad (\text{A3.20})$$

Thus, we see that the eigenvalues are mixes of the two-dimensional impedances and this mixing is dependent upon the channelling parameters  $e$  and  $t$ .

Eggers' decomposition is an eight parameter decomposition of each individual impedance tensor. He obtains the remaining four parameters by first determining the magnetic eigenvectors of (A3.17) and then then the electric eigenvectors via (A3.13);

$$\vec{E}^{\pm} = \begin{pmatrix} \frac{\alpha_0 + \alpha_3}{2} \\ \frac{\alpha_1 + \alpha_2}{2} + \lambda^{\mp} \end{pmatrix} = \begin{pmatrix} E_x^{\pm} \\ E_y^{\pm} \end{pmatrix}. \quad (\text{A3.21})$$

From these equations (A3.21) Eggers derives an the orientation of the major axis of the electric eigenvector polarization ellipses;

$$\tan 2\psi^{\pm} = \frac{2\text{Re}(E_x^{\pm} \overline{E_y^{\pm}})}{|E_x^{\pm}|^2 - |E_y^{\pm}|^2} \quad (\text{A3.22})$$

and the ellipticities of the electric eigenvector polarization ellipses via

$$\xi^{\pm} = \frac{1 - r^{\pm}}{1 + r^{\pm}} \quad (\text{A3.23})$$

where

$$r^{\pm} = \frac{|E_x^2 + E_y^2|}{|E_x|^2 + |E_y|^2 - 2\text{Im}(E_x \overline{E_y})}. \quad (\text{A3.24})$$

In (A3.24) the  $\pm$  was inferred with respect to the components of the electric eigenvectors. In (A3.22) and (A3.24) the overbar means complex conjugate.

In general, it is difficult to determine what information these remaining parameters  $(\psi^\pm, \xi^\pm)$  have with regard to the distortion model. However, there are two simple informative cases. First, let us consider Site C of Chapter 5 but in a one-dimensional regional environment. The distortion operator is given by (5.33). For this simple case

$$t = \delta = \sin(2\theta) = 0 \quad (\text{A3.25a})$$

$$\sigma = 2Z_0 \quad (\text{A3.25b})$$

where  $Z_0$  is the one-dimensional impedance. Therefore (A3.19)

$$\lambda^\pm = Z_0(1 \pm e) \quad (\text{A3.26})$$

and using (6.39) and (A3.21,A3.25)

$$\vec{E}^\pm = eZ_0 \begin{pmatrix} -1 \\ \mp 1 \end{pmatrix}. \quad (\text{A3.27})$$

Therefore, since (A3.27)

$$(E_x^\pm)^2 = (E_y^\pm)^2 \quad (\text{A3.28a})$$

$$|E_x^\pm|^2 = |E_y^\pm|^2 \quad (\text{A3.28b})$$

$$E_x^\pm \overline{E}_y^\pm = \pm e^2 |Z_0|^2 \quad (\text{A3.28c})$$

from (A3.22)

$$\tan 2\psi^\pm = \infty \quad (\text{A3.29})$$

and

$$r^\pm = 1. \quad (\text{A3.30})$$

Therefore, the orientations of both electric eigenvectors is that of the azimuth of the local electric current, *i.e.*

$$\psi^\pm = \frac{\pi}{4} \pm \frac{\pi}{2} \quad (\text{A3.31})$$

and both eigenvectors are linearly polarized *i.e.*

$$\xi^\pm = 0. \quad (\text{A3.32})$$

The second simple case is the one-dimensional regional structure with zero shear. Such a case arises in the synthetic example of Chapter 6 (Figure 6.2.1) in the center of the swamp if the host structure is one-dimensional.

$$e = \delta = \sin(2\theta) = 0 \quad (\text{A3.34a})$$

$$\sigma = 2Z_0 \quad (\text{A3.34b})$$

where again  $Z_0$  is the one-dimensional impedance. Again, from (A3.19)

$$\lambda^\pm = Z_0(1 \pm it) \quad (\text{A3.35})$$

and using (6.39,A3.21,A3.34);

$$\vec{E}^\pm = tZ_0 \begin{pmatrix} 1 \\ \mp i \end{pmatrix}. \quad (\text{A3.36})$$

Therefore, in this case (A3.36)

$$(E_x^\pm)^2 = -(E_y^\pm)^2 = Z_0^2 t^2 \quad (\text{A3.37a})$$

$$|E_x^\pm|^2 = |E_y^\pm|^2 = |Z_0|^2 t^2 \quad (\text{A3.37})$$

$$E_x^\pm \overline{E}_y^\pm = \pm i |E_x^\pm|^2. \quad (\text{A3.37c})$$

The orientations of the polarization ellipses are undefined since

$$\tan 2\psi^\pm = \frac{0}{0} \quad (\text{A3.38})$$

and

$$r^\pm = 0 \quad \text{or} \quad \frac{0}{0}. \quad (\text{A3.39})$$

Thus is one case the ellipticity is 1 and in the other it is undefined.

This decomposition of Eggers is limited from two points of view. As can be seen from (A3.19) the eigenvalues  $\lambda^\pm$  are mixtures of the regional impedances and as such are no more useful than the conventional (2D rotation) estimates for determining the 2-D parameters. Problems with the electric eigenvector ellipse orientation and ellipticity are evident from the simple examples. There is no means to extend this methodology to separate the galvanic from inductive 3D effects which it would seem necessary to perform geological interpretations.

